

1D/2D modelling suite for integral water solutions

# SOBEK SUITE

**Deltares systems**



Hydrodynamics

Technical Reference Manual



# **SOBEK 3**

**Hydrodynamics**

**Technical Reference Manual**

**SOBEK in Delta Shell**

Version: 3.0.1  
Revision: 41932

14 September 2015

## **SOBEK 3, Technical Reference Manual**

### **Published and printed by:**

Deltares  
Boussinesqweg 1  
2629 HV Delft  
P.O. 177  
2600 MH Delft  
The Netherlands

telephone: +31 88 335 82 73  
fax: +31 88 335 85 82  
e-mail: [info@deltares.nl](mailto:info@deltares.nl)  
www: <https://www.deltares.nl>

### **For sales contact:**

telephone: +31 88 335 81 88  
fax: +31 88 335 81 11  
e-mail: [sales@deltaressystem.nl](mailto:sales@deltaressystem.nl)  
www: <http://www.deltaressystem.nl>

### **For support contact:**

telephone: +31 88 335 81 00  
fax: +31 88 335 81 11  
e-mail: [support@deltaressystem.nl](mailto:support@deltaressystem.nl)  
www: <http://www.deltaressystem.nl>

Copyright © 2015 Deltares

All rights reserved. No part of this document may be reproduced in any form by print, photo print, photo copy, microfilm or any other means, without written permission from the publisher: Deltares.

## Contents

<b>1</b>	<b>Conceptual description</b>	<b>1</b>
1.1	Hydrodynamics 1DFLOW	1
1.1.1	Hydrodynamic definitions	1
1.1.1.1	Datum	2
1.1.1.2	Bed level	2
1.1.1.3	Water depth	3
1.1.1.4	Water level	3
1.1.1.5	Flow area	4
1.1.1.6	Storage area	4
1.1.1.7	Wetted area	4
1.1.1.8	Wetted perimeter	5
1.1.1.9	Flow velocity	5
1.1.1.10	Velocity	6
1.1.1.11	Hydraulic radius	6
1.1.2	Model equations	6
1.1.2.1	Continuity equation (1D)	7
1.1.2.2	Momentum equation (1D)	7
1.1.2.3	Transport equation for salinity	8
1.1.3	Inertia	8
1.1.4	Convection	8
1.1.5	Convection (1D)	9
1.1.6	Water level gradient	9
1.1.7	Wind friction	9
1.1.8	Initial conditions	10
1.1.9	Boundary	10
1.1.10	Discharge	11
1.1.11	Lateral discharges	11
1.1.11.1	Incorporating Lateral discharges in the Continuity Equation	12
1.1.11.2	Options for Assigning Lateral Discharges to h-calculation point(s)	12
1.1.11.3	Examples of Lateral Discharges	13
1.1.11.4	Area Based Point Lateral Flow	13
1.1.11.5	Pipe with infiltration (having a lateral diffusive discharge option)	14
1.1.12	Bed friction	16
1.1.12.1	Bos-Bijkerk	17
1.1.12.2	Chézy	17
1.1.12.3	Manning	18
1.1.12.4	Nikuradse	18
1.1.12.5	Strickler	19
1.1.12.6	White-Colebrook	19
1.1.13	Froude number	19
1.1.14	Boussinesq	20
1.1.15	Accuracy	22
1.1.16	Structures	22
1.1.16.1	Advanced weir	23
1.1.16.2	Bridge	25
1.1.16.3	Compound structure	28
1.1.16.4	Culvert	28
1.1.16.5	Database structure	31
1.1.16.6	General structure	32
1.1.16.7	Inverted siphon	36



1.1.16.8	Orifice	40
1.1.16.9	Pump station and Internal Pump station	41
1.1.16.10	External Pump station	46
1.1.16.11	River Pump	51
1.1.16.12	River Weir	56
1.1.16.13	Siphon	58
1.1.16.14	Universal Weir	61
1.1.16.15	Vertical obstacle friction	64
1.1.16.16	Weir	64
1.1.17	Staggered grid; $h$ - and $u$ -calculation points at different locations	66
1.1.18	Construction of the numerical bathymetry on basis of user-defined cross-sections	66
1.1.18.1	The Y-Z type of profiles	67
1.1.18.2	All cross-section types except for the Y-Z type of profiles	67
1.1.19	Method of interpolating between user-defined cross-sections	68
1.1.19.1	Method of Interpolating between Round cross-sections and between Egg-shape cross-sections	68
1.1.19.2	Method of Interpolating between Open Vertical Segmented Y-Z profiles and between Asymmetrical Trapezium profiles	68
1.1.19.3	Method of Interpolating between Cross-sections not being a Round, Egg-shape, Open Vertical Segmented Y-Z profile or Asymmetrical Trapezium profile	68
1.1.20	Methods for computing conveyance	69
1.1.20.1	Tabulated lumped conveyance approach	69
1.1.20.2	Vertically segmented conveyance approach	70
1.1.21	Drying/flooding	76
1.1.22	Free board	76
1.1.23	Ground layer	76
1.1.24	Measurement station	77
1.1.25	Network	78
1.1.25.1	Reach	78
1.1.25.2	Reach length	79
1.1.25.3	Reach segment	80
1.1.25.4	Connection node	80
1.1.26	Reference level	81
1.1.27	Robustness	81
1.1.28	Sediment transport capacity	82
1.1.29	Simulation output parameters at reach segments	83
1.1.30	Time step reductions during the simulation	84
1.1.31	Slope	85
1.1.32	Stationary computation	86
1.1.33	Summer dike	86
1.1.34	Super-critical flow	89
1.1.35	Surface level	89
<b>2</b>	<b>Conceptual description (1D2D)</b>	<b>91</b>
2.1	Hydrodynamics Overland 2DFLOW	91
2.1.1	Introduction	91
2.1.2	Lateral horizontal 1D-2D coupling	95
2.1.2.1	Properties	99
2.1.3	Lateral horizontal 1D-2D coupling — the details	99
2.1.3.1	1D and 2D flow modeling	100
2.1.3.2	Embedded lateral horizontal 1D-2D coupling	104
2.1.3.3	Lateral horizontal 1D-2D coupling with strict model separation	105

2.1.3.4	Analysis of the lateral horizontal 1D-2D coupling . . . . .	114
2.1.3.5	Properties of the horizontal 1D-2D coupling . . . . .	121
<b>3</b>	<b>Numerical concepts (1D)</b>	<b>123</b>
3.1	Staggered grid . . . . .	123
3.2	Computational grid and definitions . . . . .	124
3.3	Upwinding . . . . .	126
3.4	Time integration . . . . .	126
3.4.1	Time integration of the continuity equation . . . . .	126
3.4.2	Time integration of the momentum equation . . . . .	128
3.4.3	Time integration of the combined continuity and momentum equation . . . . .	130
3.4.4	Numerical method for the transport equation . . . . .	131
3.4.5	Open boundary conditions for the transport equation . . . . .	131
3.4.5.1	Thatcher Harleman time lag . . . . .	132
3.4.5.2	Density . . . . .	133
3.4.5.3	Dispersion coefficient . . . . .	133
3.4.5.4	Salinity intrusion and baroclinic term . . . . .	134
<b>4</b>	<b>Numerical concepts (1D2D)</b>	<b>137</b>
4.1	1D-2D coupling . . . . .	137
4.1.1	General . . . . .	137
4.1.2	Optimization of the coupling parameters . . . . .	138
4.1.3	Implementation of the 1D-to-2D coupling into the 2D system of equations . . . . .	141
4.1.4	Implementation of the 2D-to-1D coupling into the 1D system of equations . . . . .	142
4.2	Incorporation of boundary conditions in SOBEK . . . . .	143
4.3	Interface requirements for SOBEK and D-Flow FM . . . . .	144
	<b>References</b>	<b>147</b>





## List of Figures

1.1	Definition of model datum	2
1.2	Definition of bed level	2
1.3	Definition of water depth $d = h - z_b$	3
1.4	Definition of water level	3
1.5	Definiton of flow area ( $A_f$ ) and storage area ( $A_s$ )	4
1.6	Wetted perimeter	5
1.7	Wetted perimeter for the main channel	5
1.8	Computation of hydraulic radius	6
1.9	Wetted perimeter for the main channel (Subdivision in main channel and flood-plains only in SOBEK-River)	6
1.10	Wind direction	10
1.11	Diffuse lateral discharge	11
1.12	Lateral discharges, point and line source	12
1.13	Pipe with Infiltration, a drainage pipe located in a trench	14
1.14	Pipe with infiltration: definition of variables	15
1.15	Definition of energy and water level	23
1.16	Pillar bridge	26
1.17	A suspension bridge with abutments	27
1.18	Fixed bed bridge	27
1.19	Soil bed bridge	27
1.20	Side view of a culvert	28
1.21	Good modelling practice, Culvert, Inverted Siphon and Siphon	31
1.22	General structure, side view	32
1.23	General structure, top view	32
1.24	Drowned gate flow	33
1.25	Drowned weir-flow	34
1.26	Side view of an inverted siphon	37
1.27	Good modelling practice, Culvert, Inverted Siphon and Siphon	39
1.28	Orifice	40
1.29	Pump station with positive pump direction and two pump stages	42
1.30	Pump station with negative pump direction and two pump stages	43
1.31	External pump station with pump direction IN and two pump stages	47
1.32	External pump station with pump direction OUT and two pump stages	47
1.33	River pump with Upward control and start-level above stop-level	52
1.34	River pump with Upward control and stop-level above start-level	53
1.35	River pump with Downward control and start-level above stop-level	53
1.36	River pump with Downward control and stop-level above start-level	54
1.37	Free and drowned weir flow	56
1.38	Drowned flow reduction curves	58
1.39	Siphon	58
1.40	Good modelling practice, Culvert, Inverted Siphon and Siphon	61
1.41	Weir profile of a Universal weir, division in rectangular and triangular weir sections	62
1.42	Weir	64
1.43	Staggered grid, $h$ - and $u$ -calculation points at different locations	66
1.44	Construction of numerical bathymetry for Y-Z profiles	67
1.45	Construction of numerical bathymetry other than Y-Z profiles	67
1.46	Concept of the lumped conveyance approach	69
1.47	Example of constructed vertical segments in a Y-Z profile	70
1.48	Definition sketch of a vertical segment, considered in computing conveyance for a Y-Z profile and an Asymmetrical Trapezium cross-section	72
1.49	Free board	76



1.50	Ground layer in circular cross section . . . . .	77
1.51	Network . . . . .	78
1.52	Reach length in model network . . . . .	79
1.53	Reach segment . . . . .	80
1.54	Connection nodes . . . . .	81
1.55	Definition of reference level . . . . .	81
1.56	Summer dike option, available in a river profile . . . . .	87
1.57	Flow area behind the summer dike as function of local water levels. . . . .	88
1.58	Total area behind the summer dike as function of local water levels. . . . .	90
2.1	The proposed 1D-2D modeling with horizontal coupling. . . . .	94
2.2	Example of a D-Flow FM grid with sufficient resolution across channels to capture the details in that direction. . . . .	94
2.3	Principle of the lateral horizontal 1D-2D coupling, where 2D modeled areas lie next to the 1D modeled waterways. The two red horizontal two-sided arrows indicate the couplings that independently model the flow across two separate waterway banks. That flow exchange, (usually) not modeled in detail, occurs in the strips along the banks left and right of the waterway indicated by the green braces. For clarity, the size of the dikes and the free-surface variation across the dike at the left interface have been exaggerated in the figure. Lateral discharge per unit length from 2D domain to 1D domain $q_{2D-1D}$ is a function of the water levels $\zeta_{2D,I}$ and $\zeta_{1D}$ of those domains at the interface. Because of mass conservation, lateral discharge per unit length in the other direction $q_{1D-2D}$ equals $-q_{2D-1D}$ . . . . .	96
2.4	Principle of the embedded lateral horizontal 1D-2D coupling, more or less applying and solving flow equations across the 1D-2D interface. . . . .	97
2.5	Principle of the lateral horizontal 1D-2D coupling with strict model separation, using separate models for the 2D and the 1D areas coupled at the interfaces by coupling conditions. . . . .	97
2.6	Behavior of normal-mode solutions of (2.31) for 3 different tangential modes $k\Delta y$ (solid, dashed and dotted lines) and 3 different values of $CFL_{2D} = CFL_{2D,x} = CFL_{2D,y}$ (red, blue and green lines). . . . .	119
3.1	Staggered grid for unsteady channel flow . . . . .	123
3.2	Staggered flow grid . . . . .	124
3.3	Figure: Illustration of memory effect for open boundary . . . . .	133
3.4	Salt wedge . . . . .	134
4.1	Predicted reduction factor per 1D-2D iteration as a function of dimensionless wave number $k\Delta x_I$ for several ratios between channel width $W$ and normal 2D grid size $\Delta x_{u,I}$ and several CFL-values, taking all CFL numbers equal ( $CFL_{1D} = CFL_{2D,s} = CFL_{2D,n} = CFL$ ). . . . .	141
4.2	workflow of coupled time step computation. . . . .	145

## List of Tables

1.3	Example of switch-on-levels and switch-off-levels at the suction-side and the delivery-side of a pump station . . . . .	46
1.4	Example of switch-on-levels and switch-off-levels at the suction-side and the delivery-side of an external pump station . . . . .	50
1.5	Flow-Pump station covers the options of a River pump with respect to the pump direction . . . . .	56
1.6	Crest shape and coefficients for simple weir structure (default values) . . . . .	57
2.1	Estimation of the properties of the vertical 1D-2D coupling versus the horizontal 1D-2D coupling. . . . .	93
3.1	Overview on the equation solved for the two different grid elements of a staggered grid and the corresponding output parameters . . . . .	123



# 1 Conceptual description

In this section, we will present in detail the governing equations. Below an overview of the symbols that are used in the equations is presented.

## List of Symbols

Symbol	Units	Meaning
$A_f$	$m^2$	Cross sectional flow area
$A_R$	$m^2$	Rainfall runoff area
$A_s$	$m^2$	Cross sectional storage area
$A_t$	$m^2$	Cross sectional total area (i.e. $A_f + A_s$ )
$A_z$	$m^2$	Surface area
$C$	$m^{1/2}/s$	Chézy coefficient
$C_d$	-	Drag coefficient
$C_{wind}$	-	The wind friction coefficient.
$f_d$	-	Global design factor for overall extreme high or low load (rain-fall)
$g$	$m/s^2$	Acceleration due to gravity ( $\approx 9.81$ )
$h$	$m$	Water level
$i_R$	$mm/s$	Intensity of rainfall
$i_s$	$mm/s$	Intensity of seepage
$O$	$m$	Wetted perimeter
$q_{lat}$	$m^2/s$	Lateral discharge per unit length
$Q$	$m^3/s$	Discharge
$R$	$m$	Hydraulic radius
$t$	$s$	Time
$w_f$	$m$	Cross sectional width at water level
$x, y$	$m$	Cartesian coordinates
$\phi_{wind}$	$deg$	Angle between the wind direction and the local channel direction
$\rho_w$	$kg/m^3$	Water density
$\rho_{air}$	$kg/m^3$	Density of air
$\tau_{wind}$	$N/m^2$	Wind shear stress

## 1.1 Hydrodynamics 1DFLOW

### 1.1.1 Hydrodynamic definitions

### 1.1.1.1 Datum

The Model datum and reference level both refer to a horizontal plane from which elevations are defined (positive in upward direction and negative in downward direction). By default the model datum and reference level are equal to zero.

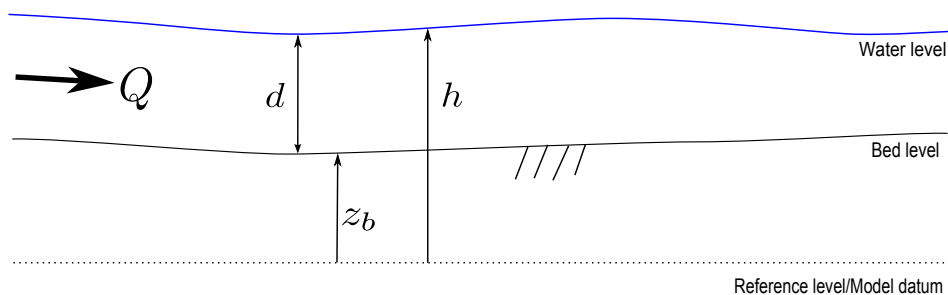


**Figure 1.1:** Definition of model datum



**Note:**

All levels (quantities with a vertical coordinate) in SOBEK are defined with respect to the model datum or reference level.

### 1.1.1.2 Bed level

The bed level is defined as the lowest point in the cross section. In the definition of the cross section an example is given of the interpolation and extrapolation of the bed levels over a reach. The used symbol in the SOBEK-Flow-module is  $z_b$ .

It is given relative to a reference level, for example Mean Sea Level .

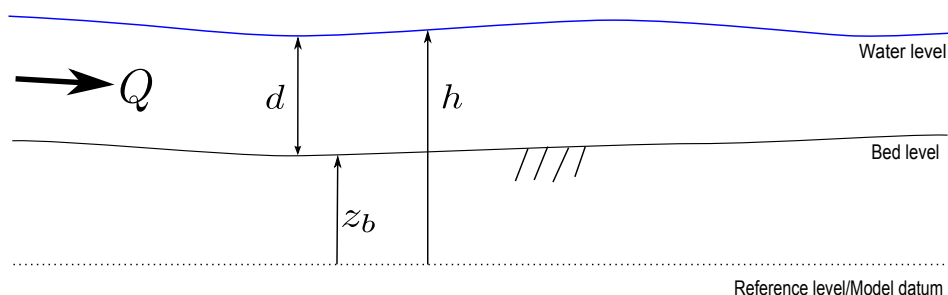


**Figure 1.2:** Definition of bed level

If the water level is lower than the bed level, drying occurs.

### 1.1.1.3 Water depth

In the SOBEK-Flow-module the water depth is the distance between the water level and the bed level. The symbol used for the water depth is  $d$ .

$$d = h - z_b \quad (1.1)$$

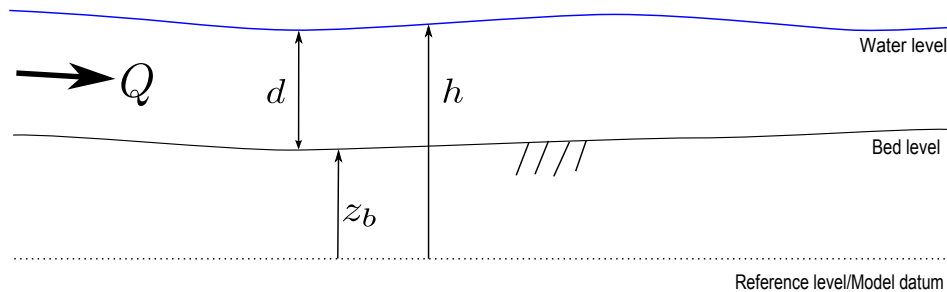


**Figure 1.3:** Definition of water depth  $d = h - z_b$

### 1.1.1.4 Water level

The water level ( $h$ ) is the level of the water surface relative to the reference level or Model datum (= reference level).

In the one-dimensional SOBEK-Flow-module the water level perpendicular to the flow direction is assumed to be horizontal.

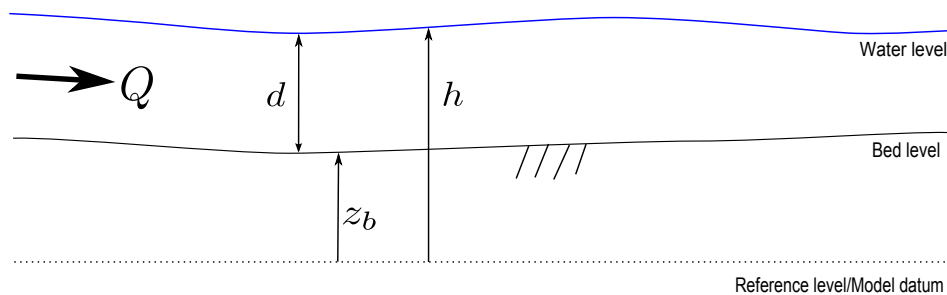


**Figure 1.4:** Definition of water level

The water level together with the discharge form the result of the SOBEK-Flow-module computations. Water levels are calculated at the connection nodes and the  $h$ -calculation points.

**Note:** In each SOBEK-Flow-model, all levels are relative to the reference level



#### 1.1.1.5 Flow area

The flow area  $A_f$  of a cross-section is the area through which water is actually flowing.

In a cross-section, distinction can be made between the flow area and the storage area. In the latter part, water is stored only, see [Figure 1.5](#).

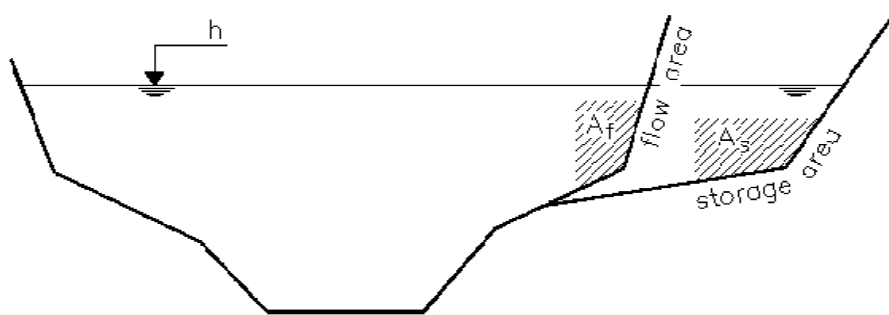


**Figure 1.5:** Definiton of flow area ( $A_f$ ) and storage area ( $A_s$ )

The shape of the cross-section, and the distinction between the flow area and storage area are defined for each cross-section by user input.

#### 1.1.1.6 Storage area

The storage area  $A_s$  of a cross-section is the area in which only water is stored i.e. the non-conveying part of the cross-section.

In a cross-section, distinction can be made between the flow area and the storage area, see [Figure 1.5](#).

The shape of the cross-section, and the distinction between the flow area and storage area is defined for each cross-section by user input.

The total area  $A_t$  is defined as the flow area plus the storage area.

#### 1.1.1.7 Wetted area

The wetted area ( $A_f$  [ $m^2$ ]) is the part of the cross section that is filled with water. See [Figure 1.6](#)



### 1.1.1.8 Wetted perimeter

The wetted perimeter ( $O$  [m]) is the interface between the soil and the flowing water. See [Figure 1.6](#).

In the case of a main channel and one or two floodplains in the cross-section, a wetted perimeter is computed for each section. In that case the water interface between the sections is not included in the wetted perimeter. See also [Figure 1.6](#) and [Figure 1.7](#)

The wetted perimeter is used to compute the hydraulic radius, which is important for the computation of the bed friction.

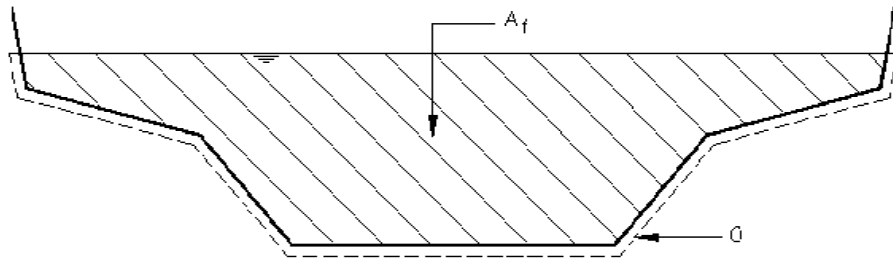


**Figure 1.6:** Wetted perimeter

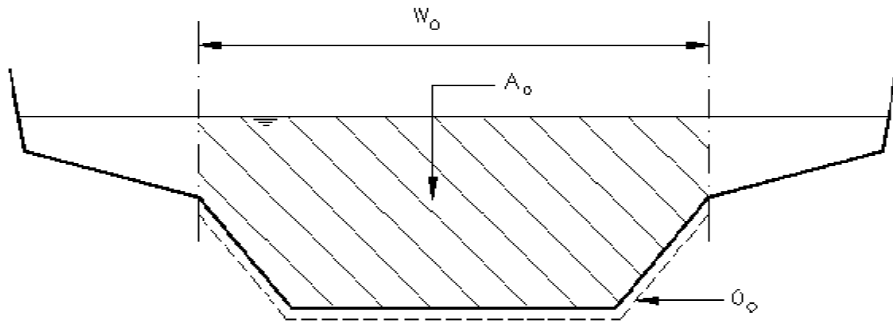


**Figure 1.7:** Wetted perimeter for the main channel

### 1.1.1.9 Flow velocity

The flow velocity ( $u$ ) is defined as the average flow velocity in the flow section of the cross-section. It is by default given in [m/s].

The average flow velocity is derived by dividing the discharge [ $m^3/s$ ] by the flow area [ $m^2$ ]. Output of the overall average flow velocity, the flow velocity in the main channel, the flow velocity in floodplain 1 and the flow velocity in floodplain 2 is possible.

$$u = \frac{Q}{A_f}, \quad u_0 = \frac{Q}{A_0}, \quad u_1 = \frac{Q}{A_1}, \quad u_2 = \frac{Q}{A_2}. \quad (1.2)$$

The indices 0, 1, 2 indicate the main channel, floodplain 1 and floodplain 2 respectively.

### 1.1.1.10 Velocity

The velocity ( $u$ ) is defined as the average flow velocity in the wetted area of the cross section. It is given in [m/s].

$$u = \frac{Q}{A_f} \quad (1.3)$$



**Note:** Discharges and velocities are defined in reach segments, whereas cross sections are defined in  $h$ -calculation points. For the computation of the velocities according to the above formula. The SOBEK-Flow-module uses the upstream cross section

### 1.1.1.11 Hydraulic radius

The hydraulic radius is defined as the wetted area of the cross section divided by the wetted perimeter.

$$R = \frac{A_f}{O} \quad (1.4)$$

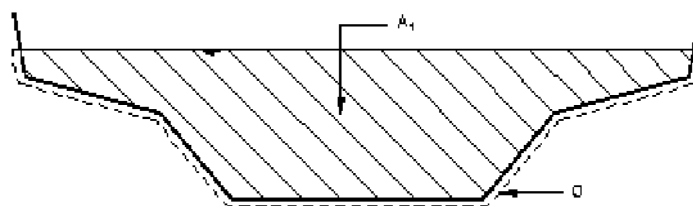
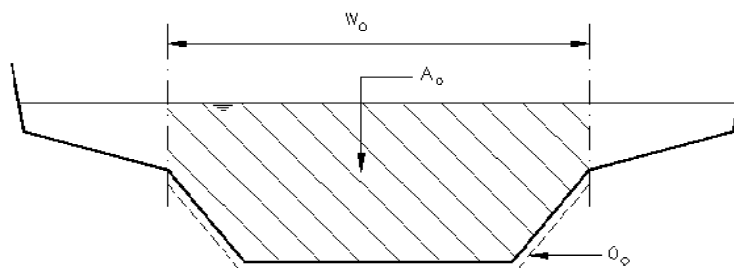


Figure 1 Computation of hydraulic radius

**Figure 1.8:** Computation of hydraulic radius



**Figure 1.9:** Wetted perimeter for the main channel (Subdivision in main channel and floodplains only in SOBEK-River)

## 1.1.2 Model equations

The water flow is computed by solving the complete De Saint Venant equations.

For one dimensional flow (Channel Flow and Sewer Flow modules) the following equations are solved

- ◇ continuity equation 1D
- ◇ momentum equation 1D

For two dimensional flow (Overland Flow module), three equations are solved:

- ◇ continuity equation 2D
- ◇ momentum equation 2D for the  $x$ -direction
- ◇ momentum equation 2D for the  $y$ -direction

These equations are solved numerically using the Delft-scheme.

**Note:** on the 2D equations

As opposed to the shallow water equations, the described equations do not incorporate the turbulent stress terms, accounting for the sub grid transfer of momentum in between grid cells. These terms have been omitted because they are relatively unimportant for flood flow computations, in order to save computational effort.



The wall friction terms have been introduced to account for the added resistance that is caused by vertical obstacles, like houses or trees. The wall friction coefficient is based on the average number and diameter of the obstacles per unit area and the average obstacle drag coefficient ( $C_d$  coefficient).

#### 1.1.2.1 Continuity equation (1D)

The flow in one dimension is described by two equations: the momentum equation and the continuity equation. The continuity equation reads:

$$\frac{\partial A_f}{\partial t} + \frac{\partial Q}{\partial x} = q_{lat} \quad (1.5)$$

#### 1.1.2.2 Momentum equation (1D)

The flow in one dimension is described by two equations: the momentum equation and the continuity equation. The momentum equation reads:

$$\frac{\partial Q}{\partial t} + \frac{\partial}{\partial x} \left( \frac{Q^2}{A_f} \right) + g A_f \frac{\partial h}{\partial x} + \frac{g Q |Q|}{C^2 R A_f} - w_f \frac{\tau_{wind}}{\rho_w} + g A_f \frac{\xi Q |Q|}{L_x} = 0 \quad (1.6)$$

The first term describes the inertia

The second term describes the convection

The third term describes the water level gradient

The fourth term describes the bed friction

The fifth term describes the influence of the wind force

The sixth term describes the influence of extra resistance

where:

$A_f$	Flow area [ $m^2$ ]
$C$	Chezy value [ $m^{1/2}/s$ ]
$g$	Acceleration due to gravity [ $m/s^2$ ]
$h$	Water level [ $m$ ]
$L_x$	Length of Reachsegment, accomodating an Extra Resistance Node [ $m$ ]
$Q$	Discharge [ $m^3/s$ ]
$R$	Hydraulic radius [ $m$ ]

$t$	Time [s]
$w_f$	Water surface width [m]
$x$	Distance along the channel axis [m]
$\rho_w$	Density of fresh water [ $kg/m^3$ ]
$\tau_{wind}$	Wind shear stress [ $N/m^2$ ] (see <a href="#">section 1.1.7</a> )
$\xi$	Extra Resistance coefficient [ $s^2/m^5$ ]

### 1.1.2.3 Transport equation for salinity

Salt transport in estuaries and tidal rivers can be considered as transport of conservative substance in water. The transport of salt is described by an advection-diffusion equation, which is called the transport equation. We remark that in SOBEK temperature cannot be modelled yet. Otherwise, the same transport equation would have been used for temperature as well.

Next to the additional transport equation, density differences have to be accounted for in the momentum equation of the water flow module. The water flow module is therefore coupled with the salt intrusion module by the density and the flow field. The salinity concentration is denoted by  $C$ .

The transport equation for salinity is described by an advection-diffusion equation including source term reads:

$$\frac{\partial A_t C}{\partial t} + \frac{\partial}{\partial x} \left( Q C - A_f D \frac{\partial C}{\partial x} \right) = S_s \quad (1.7)$$

in which

$C$	concentration of salt or chloride, averaged over the total cross-sectional area [ $kg/m^3$ ]
$D$	dispersion coefficient [ $m^2/s$ ]
$S_s$	source term [ $kg/ms$ ]
$Q$	discharge (water) [ $m^3/s$ ]
$A_t$	total cross-sectional area [ $m^2$ ]
$A_f$	flow area [ $m^2$ ]

### 1.1.3 Inertia

The flow in one dimension is described by two equations: the momentum equation and the continuity equation. The first term in the momentum equation is the inertia term:

$$\text{inertia} = \frac{\partial Q}{\partial t} \quad (1.8)$$

$Q$	Discharge [ $m^3/s$ ]
$t$	Time [s]

### 1.1.4 Convection

In the SOBEK-Flow-module an convection term is used to guarantee the conservation of momentum in a reach (between reach segments). The same holds for a connection node when two reaches are connected to this node. In that case the connection nodes could also have been modelled as a  $h$ -calculation point. If there are more than two reaches connected to a connection node the convection term is set to zero.

When a reach has subsections, all subsections have an independent solution for the velocity. The velocity that is used for the conservation of momentum over the reach is the average of the velocities  $u_i$  of the subsections in the cross section.

### 1.1.5 Convection (1D)

The flow in one dimension is described by two equations: the momentum equation and the continuity equation. One of the terms in the momentum equation is the convection term:

$$\text{convection} = \frac{\partial}{\partial x} \left( \frac{Q^2}{A_f} \right) \quad (1.9)$$

$Q$	Discharge [ $m^3/s$ ]
$A_f$	Wetted area [ $m^2$ ]
$x$	Distance [ $m$ ]

### 1.1.6 Water level gradient

The third term in the momentum equation is the water level gradient.

$$\text{water level gradient} = g A_f \frac{\partial h}{\partial x} \quad (1.10)$$

$x$	Distance [ $m$ ]
$A_f$	Wetted area [ $m^2$ ]
$g$	Acceleration due to gravity [ $m/s^2$ ] ( $\approx 9.81$ )
$h$	Water level [ $m$ ] (with respect to the reference level)

This force tries to achieve a flat water surface under influence of the gravitational acceleration. This force together with the bed friction have the greatest effect on the water movements.

### 1.1.7 Wind friction

The wind friction term in the momentum equation is expressed as:

$$\tau_{wind} = -\rho_{air} C_{wind} u_{wind}^2 \cos(\varphi_{wind} - \varphi_{channel}) \quad (1.11)$$

$\tau_{wind}$	Wind shear stress (positive if acting along the positive x-axis of an open channel) [ $N/m^2$ ]
$\rho_{air}$	Density of air, $1.205 \text{ kg}/m^3$
$C_{wind}$	$\alpha_{wind,1} + \alpha_{wind,2} u_{wind}$ , the wind friction coefficient. The used values are:

$$a_{wind,1} = 0.50 \times 10^{-3} \quad [-] \quad (1.12)$$

$$a_{wind,2} = 0.06 \times 10^{-3} \quad [s/m] \quad (1.13)$$

$u_{wind}$	Wind velocity [ $m/s$ ]
$\varphi_{channel}$	Clock-wise angle between the positive $x$ -axis of the 1D open channel and the North (Nautical convention) [degrees]
$\varphi_{wind}$	Clock-wise angle between the wind direction and the North (Nautical convention) [degrees]

The wind direction that is specified in the SOBEK-Flow-module is the direction from which the wind is blowing with respect to the north. So, if the wind is blowing from the north, the wind direction is 0 degrees. Wind from the southeast has a wind direction of 135 degrees.

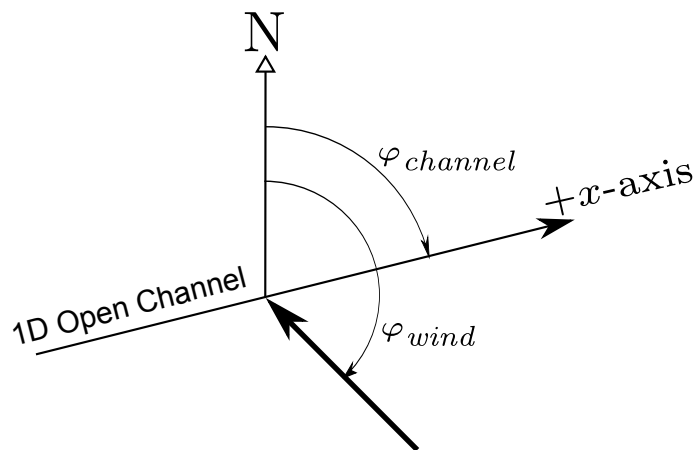


**Figure 1.10:** Wind direction

When a cross section has a top width smaller than 20 *mm* (circular, egg-shaped, or nearly closed tabulated cross section) than the cross section is considered closed. In that case the wind is neglected in the momentum equation

#### 1.1.8 Initial conditions

The initial conditions are the water levels or depths and the discharges at the beginning of the simulation. The initial conditions are defined over a reach (water level and depth at the  $h$ -calculation points, discharges at the reach segments). Therefore the water level that initially should be taken at connection nodes is not strictly defined. This happens when, for example, reach 1 with initial water level 0.5 is connected by a node to reach 2 with initial water level 0.6. In that case the water level at the connection node is set to the lowest value of the connected reaches (0.5). Because the  $h$ -calculation point at the end of reach 1, the connection node and the  $h$ -calculation point at the beginning of reach 2 have the same location, the water levels of these three points are set to 0.5.

#### 1.1.9 Boundary

A boundary can be applied at the locations where the model network ends with a boundary node.

In order to solve the water flow equations (continuity equation and momentum equation), information about the water flow at the model boundaries must be supplied.

At each boundary node, one condition for the water flow must be specified. The following options are available:

- ◇ discharge (constant, tabulated function of time, tabulated function of the water level)
- ◇ water level (constant, tabulated function of time)

Because in the staggered grid, used by SOBEK-Flow-module, the discharges are defined for the reach segments, a discharge boundary is imposed on the first reach segment next to the boundary. Therefore the  $h$ -calculation point just before this first reach segment (first one in a reach) is undefined and will not be taken into consideration during a calculation.

A water level boundary is defined in the first calculation point next to the boundary. This  $h$ -calculation point actually has the same coordinates as the boundary node.

**Note:** In channel flow, usually, the discharge will be specified at boundaries where water is flowing into the model, and the water level where water is flowing out of the model. In both sewer and channel systems a dead end (or beginning) of a reach can be a connection node at the end of a pipe or channel. In contrast to a boundary node, this node has storage.



### 1.1.10 Discharge

The discharge  $Q$  is the amount of water passing a reach segment per unit of time. It is given in  $[m^3/s]$ .

The discharges at the reach segments together with the water levels at the  $h$ -calculation points, form the results of a water flow simulation.

The SOBEK-Flow-module gives a positive discharge when the water flows in positive direction with respect to the defined direction of a reach. If the water is flowing from reach end to reach beginning, the discharge is negative.

### 1.1.11 Lateral discharges

A distinction is to be made between a:

- ◇ **Point lateral discharge:** A point lateral discharge ( $Q_{lat}$ ,  $[m^3/s]$ ) refers to the inflow or outflow of water at a specific point/location in a model schematization.
- ◇ **Diffusive lateral discharge:** A diffusive lateral discharge ( $q_{lat}$ ,  $[m^2/s]$ ) refers to the inflow or outflow of water along a specific reachsegment in a model schematization. A reachsegment is the distance ( $l_i$ ,  $[m]$ ) between two  $h$ -calculation points. A reach may consist of several reachsegments. The total diffusive lateral discharge at a reachsegment equals  $q_{lat} \times l_i$ . A diffusive lateral discharge is uniform distributed along the axis of a reach (see Figure 1.11).

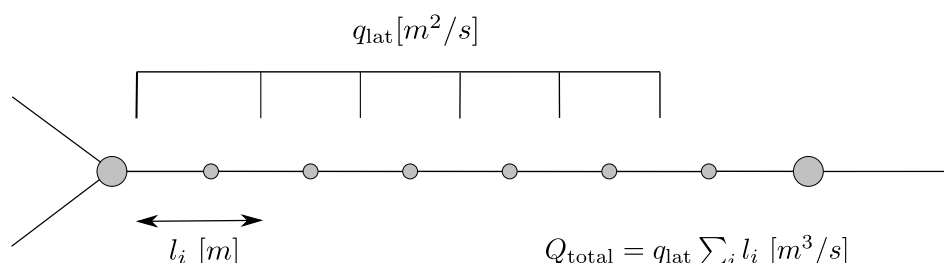


**Figure 1.11:** Diffuse lateral discharge

For both point lateral discharges and diffuse lateral discharges yields that they are assigned to a  $h$ -calculation point(s). More precisely, their lateral inflow or outflow volume is accounted for in the local water balance of such  $h$ -calculation point (e.g. local discretization of the continuity equation, see section 1.1.11.1).

Two options are available for determining to which adjacent  $h$ -calculation point a lateral discharge is assigned (see section 1.1.11.2).

An overview of lateral discharges, available in SOBEK, is given in section 1.1.11.3. In general lateral discharges can be defined as a constant or as a function of time. Exceptions are:

- ◇ The Area Based Point lateral inflow (see section 1.1.11.4)
- ◇ The Pipe with Infiltration (see section 1.1.11.5)

### 1.1.11.1 Incorporating Lateral discharges in the Continuity Equation

Both point lateral discharges and diffusive lateral discharges (see [Figure 1.12](#)) are included in the third term ( $q_{lat}$ ) of the continuity equation (see [Equation 1.14](#)).

$$\frac{\partial A_f}{\partial t} + \frac{\partial Q}{\partial x} = q_{lat} \quad (1.14)$$

$A_f$	Wetted area [ $m^2$ ]
$t$	Time [ $s$ ]
$Q$	Discharge [ $m^3/s$ ]
$x$	Distance [ $m$ ]
$q_{lat}$	Lateral discharge per unit length [ $m^2/s$ ]

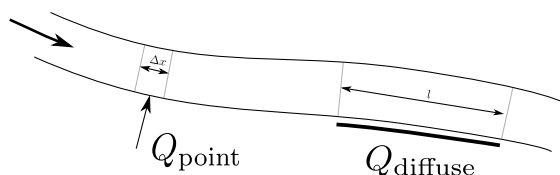


**Figure 1.12:** Lateral discharges:

Point lateral discharge:  $q_{lat} = Q_{point}/\Delta x$ ; and

Diffuse lateral discharge:  $q_{lat} = Q_{diffuse}/l$



**Note:** A large withdrawal of water (negative lateral discharge) can cause problems when the amount of outflowing water is larger than the storage available in a  $h$ -calculation point. As a result negative volumes could be computed in the continuity equation. For that reason the time step is temporarily reduced when the outflowing water volume is larger than half the available volume (safety factor) in the  $h$ -calculation point. The time step is set to a value that allows a withdrawal of half the available volume in one time step. If the time step resulting from this action is smaller than 0.01 second, the lateral withdrawal is set to zero.

### 1.1.11.2 Options for Assigning Lateral Discharges to $h$ -calculation point(s)

Two different *lateral discharge assignment options* are available in Settings (see 1D Flow, Simulation Settings Tab), that determine to which  $h$ -calculation (or water level) point(s) a particular lateral discharge is to be assigned. The two different lateral discharge assignment options are:

**Option 1:** Lateral Assigned to Lowest Water Level Point,

**Option 2:** Lateral Assigned to Nearest Water Level Point.

Hereafter, the consequences of the two different lateral discharge assignment options are discussed for each type of lateral discharge (see [section 1.1.11.3](#)) separately.

#### ◇ Lateral discharge on a Node [ $m^3/s$ ]:

**Irrespective** of the selected lateral discharge assignment option, a lateral discharge on a Node is assigned to its concerning Node (e.g.  $h$ -calculation point, Connection Node or Manhole).

#### ◇ Point-lateral discharge on a Reach [ $m^3/s$ ]:

A point-lateral discharge on a Reach is either assigned to one or equally distributed over both of the  $h$ -calculation points, that are respectively located at the left-side and the right-side of the point-lateral discharge.

- If **option 1** (Lateral Assigned to Lowest Water Level Point) is selected, the point-lateral discharge is assigned to the  $h$ -calculation point having the lowest bed level. If both



calculation points have the same bed level and the point-lateral discharge is located at a  $u$ -velocity point (e.g. centre-point of the two adjacent  $h$ -calculation points), the point-lateral discharge is equally distributed over both adjacent calculation points. Else the point-lateral discharge is assigned to the nearest  $h$ -calculation point.

- If **option 2** (Lateral Assigned to Nearest Water Level Point) is selected and the point-lateral discharge is located at a  $u$ -velocity point (e.g. centre-point of the two adjacent  $h$ -calculation points), the point-lateral discharge is equally distributed over both adjacent  $h$ -calculation points. Else the point-lateral discharge is assigned to the nearest  $h$ -calculation point.
- ◇ Diffusive lateral discharge along a Pipe or Reach [ $m^2/s$ ]:  
A diffusive lateral discharge along a Pipe or Reach is either assigned to one or equally distributed over both of the  $h$ -calculation points, that are respectively located at the beginning and the end of a pipe or reachsegment, receiving a diffusive lateral discharge.
  - If **option 1** (Lateral Assigned to Lowest Water Level Point) is selected, the diffusive lateral discharge is assigned to the  $h$ -calculation point having the lowest bed level. Else the diffusive lateral discharge is equally distributed over both adjacent calculation points.
  - If **option 2** (Lateral Assigned to Nearest Water Level Point) is selected, the diffusive lateral discharge is equally distributed over both adjacent  $h$ -calculation points.

### 1.1.11.3 Examples of Lateral Discharges

Three different types of lateral discharges are discerned:

- 1 Lateral Discharge on a Node [ $m^3/s$ ]:  
Examples of lateral discharges on a Node are:
  - ◇ Point-Lateral Discharge, that is exactly located on a  $h$ -calculation point,
  - ◇ Connection Node with Storage and Lateral Flow,
  - ◇ Manhole with Lateral Flow,
  - ◇ Manhole with Lateral Disch. and Runoff
  - ◇ Manhole with Runoff
  - ◇ Flow - RR Connection on Flow Connection Node.
- 2 Point-Lateral Discharge on a Reach [ $m^3/s$ ]:  
Examples of a point-lateral discharge on a Reach are:
  - ◇ Flow - Lateral Flow Node
  - ◇ Flow - RR Connection on Channel.
- 3 Diffusive Lateral Discharge along a Pipe or Reach [ $m^2/s$ ]:  
Examples of a diffusive lateral discharge along a Pipe or Reach are:
  - ◇ Flow - Pipe with Runoff,
  - ◇ Flow - Dry Weather Pipe,
  - ◇ Flow - Rain Pipe,
  - ◇ Flow - Pipe with Infiltration
  - ◇ Flow - Channel with Lateral Discharge.

### 1.1.11.4 Area Based Point Lateral Flow

Area based Point lateral flow is computed as:

$$Q_{lat} = A(f_d R + S) \quad (1.15)$$

$Q_{lat}$  Lateral discharge [ $m^3/s$ ]

$f_d$	Design factor for area based lateral flow (see ??), a model-wide parameter defined in Settings [—].
$R$	Rainfall [ $m/s$ ].
$A$	The catchment runoff area [ $m^2$ ]
$S$	Seepage (positive, inflow of groundwater) or Infiltration (negative, outflow to groundwater reservoir) [ $m/s$ ].

#### 1.1.11.5 Pipe with infiltration (having a lateral diffusive discharge option)

A pipe with infiltration refers to a drainage pipe fully located inside a trench (see [Figure 1.13](#)). Although the drainage pipe is porous it still can get pressurized. The trench is filled with material (for instance gravel) having a certain porosity.

A pipe with infiltration allows for the exchange of water in the pipe towards the trench (positive sign) and vice versa as well as for the exchange of water in the trench towards the groundwater (negative sign) and vice versa. Hence, a pipe with infiltration can be seen as a pipe having a *diffusive lateral discharge* option (e.g. infiltration of water in the pipe towards the trench and exfiltration of water in the trench towards the pipe). For more information on the infiltration and exfiltration process, reference is made to [Ellis and Bertrand-Krajewski \(2010\)](#), [Rutsch et al. \(2008\)](#) and [Karpf et al. \(2008\)](#).

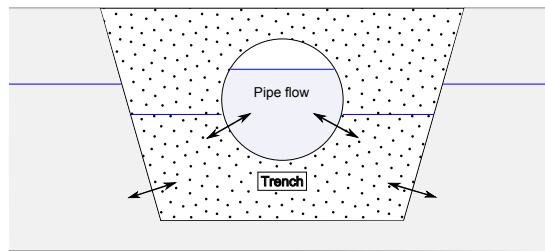


**Figure 1.13:** Pipe with Infiltration (e.g. a drainage pipe located in a trench); Allowing for the exchange of water in the pipe towards the trench (positive sign) and vice versa; Allowing for the exchange of water from the trench towards the groundwater (negative sign) and vice versa

For the computational procedure of a pipe with infiltration yields:

- ◇ The flow (water levels ( $h_p$ , see [Figure 1.14](#)), discharges and velocities) through a pipe with infiltration is computed in exactly the same manner as the flow in any pipe (e.g. by solving the one dimensional depth averaged St.Venant momentum and continuity equations), where the diffusive lateral flow along a pipe with infiltration is taken into account in accordance with the selected lateral discharge assignment option (see [section 1.1.11.2](#)).
- ◇ The exchange of water between the pipe and the trench is computed according to the “**Darcy leakage approach** (see [Rutsch et al. \(2008\)](#) and [Karpf et al. \(2008\)](#))” in which it is assumed that the rate of exchange of water between two media is a function of the resistance at the interface, the interface area and the hydraulic head over the interface. More precisely per meter pipe length (see [Figure 1.14](#)), the rate of exchange of water between the pipe and the trench (e.g. specific discharge  $q_{p \leftrightarrow tr}$ , see [Equation 1.16](#)) depends on the resistance ( $c_{p-tr}$ ), the wetted perimeter ( $P_{p-tr}$ ), the averaged water level in the pipe ( $h_p$ ) and the water level in the trench ( $h_{tr}$ ).
- ◇ Per metre pipe length, the maximum volume of water that can be stored in the trench (e.g. fully saturated trench) equals the cross-sectional area of the trench that is filled with trench material ( $A_{\text{filled with trench material}}$ ) times the porosity of the trench material ( $\phi_{tr}$ , [-]). Once the trench is fully saturated, the water level in the trench ( $h_{tr}$ , see [Figure 1.14](#)) may rise above the top level of the trench ( $z_{tr,top}$ ). In such case, per metre of pipe length an additional

volume of water is stored, that is equal to the top width of the trench ( $W_{tr,top}$ ) times the water depth on the trench ( $= h_{tr} - z_{tr,top}$ ). The top level of the trench is supposed to coincide with the local surface level. Therefore in urban terminology, water depth on the trench is referred to as **water on street**.

- ◇ The exchange of water between the groundwater and the trench per metre pipe length (e.g. specific discharge  $q_{gw \leftrightarrow tr}$ ) is also computed according to the “Darcy leakage approach” (see Equation 1.17).
- ◇ The groundwater reservoir as such is not modelled. The user-defined groundwater levels ( $h_{gw}$ , see Figure 1.14) are used as boundary conditions only.

**Note:** The local surface level is supposed to coincide with the top level of the trench. From a physical point of view, a groundwater level can not rise above the local surface level (see Figure 1.14). Therefore, at the start of a computation it is verified if user-defined ground water levels ( $h_{gw}$ ) are above the top level of the trench ( $z_{tr,top}$ ). If this is the case (e.g. if  $h_{gw} > z_{tr,top}$ ), the computation is terminated with an error message denoting for which “Pipes with Infiltration” yields that groundwater level(s) are above the top level of the trench.



**Note:** The thickness of a possible ground-layer in a pipe does affect the flow through a pipe and is consequently taken into account in determining pipe flow. However, the thickness of a possible ground-layer is neglected in the resistance factor, applied for the interface between pipe and trench. In other words, irrespective of the thickness of a possible ground-layer, the resistance factor applied for the pipe-trench interface equals the user-defined resistance factor ( $c_{p-tr}$ ) (see Equation 1.16).



**Note:** Selecting the option “Impermeable” in the “Permeability of Ground/Soil” scroll-box, available on the “Trench Data” tab (see ??), means that the interface between trench and groundwater is considered to be impermeable (e.g. no exchange of water between trench and groundwater). More precisely, if impermeable is selected Equation 1.17 is not considered in the computational procedure.

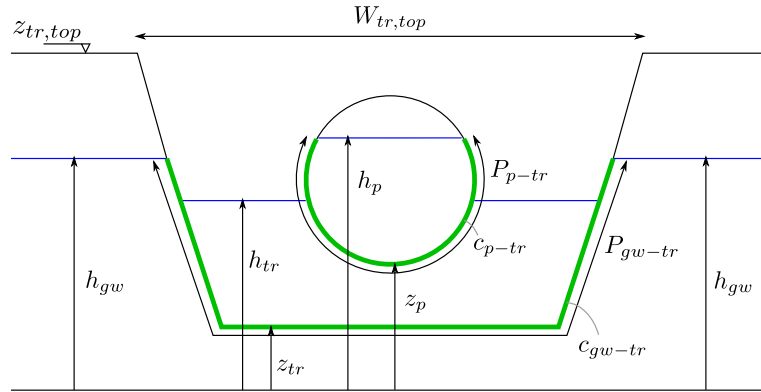


**Figure 1.14:** Pipe with infiltration: definition of variables

The specific discharge ( $q_{p \leftrightarrow tr}$ ) between the pipe and the trench (see Figure 1.14) per metre pipe length is computed according to the “Darcy leakage approach” as follows:

$$q_{p \leftrightarrow tr} = \begin{cases} 0 & \text{if } h_p \leq z_p \text{ and } h_{tr} \leq z_p \\ P_{p-tr}(h_p - z_p)/c_{p-tr} & \text{if } h_p > z_p \text{ and } h_{tr} \leq z_p \\ P_{p-tr}(h_p - h_{tr})/c_{p-tr} & \text{if } h_p > z_p \text{ and } h_{tr} > z_p \end{cases} \quad (1.16)$$

$c_{p-tr}$  resistance factor of the interface between pipe and trench [h].

$h_1$	water level in the pipe (may become pressurized) at the beginning of the pipe (e.g. pipe-side with lowest x-coordinate) [m above datum].
$h_2$	water level in the pipe (may become pressurized) at the end of the pipe (e.g. pipe-side with highest x-coordinate) [m above datum].
$h_p$	averaged water level in the pipe (e.g. $(h_1 + h_2)/2$ , may become pressurized) [m above datum].
$h_{tr}$	water level in the trench [m above datum].
$P_{p-tr}$	wetted perimeter (e.g. length of the interface) between pipe and trench [m]. <b>Note:</b> If $h_p \leq z_p$ and $h_{tr} \leq z_p$ , the wetted perimeter equals zero. Else the maximum water level (e.g. $\max(h_p; h_{tr})$ ) determines the length of the wetted perimeter.
$q_{p \leftrightarrow tr}$	specific discharge per metre pipe length between trench and pipe. Positive if water flows from pipe towards the trench [ $m^2/h$ ].
$z_1$	invert level at the beginning of the pipe (e.g. pipe-side with lowest x-coordinate) [m above datum].
$z_2$	invert level at the end of the pipe (e.g. pipe-side with highest x-coordinate) [m above datum].
$z_p$	averaged pipe invert level (e.g. $(z_1 + z_2)/2$ ) [m above datum].

The specific discharge ( $q_{gw \leftrightarrow tr}$ ) between the pipe and the trench (see [Figure 1.14](#)) per metre pipe length is computed according to the “Darcy leakage approach” as follows:

$$q_{gw \leftrightarrow tr} = \begin{cases} 0 & \text{if } h_{tr} \leq z_{tr} \text{ and } h_{gw} \leq z_{tr} \\ P_{gw-tr}(h_{tr} - z_{tr})/c_{gw-tr} & \text{if } h_{tr} > z_{tr} \text{ and } h_{gw} \leq z_{tr} \\ P_{gw-tr}(h_{tr} - h_{gw})/c_{gw-tr} & \text{if } h_{tr} > z_{tr} \text{ and } h_{gw} > z_{tr} \end{cases} \quad (1.17)$$

$c_{gw-tr}$	resistance factor of the interface between groundwater and trench [h].
$h_{gw}$	groundwater level [m above datum].
$h_{tr}$	water level in the trench [m above datum].
$P_{gw-tr}$	wetted perimeter (e.g. length of the interface) between groundwater and trench [m]. <b>Note:</b> If $h_{tr} \leq z_{tr}$ and $h_{gw} \leq z_{tr}$ , the wetted perimeter equals zero. Else the water level ( $h_{pm}$ ) determining the length of the wetted perimeter is computed as $h_{pm} = \max(h_{tr}^*; h_{gw}^*)$ , where: if $h_{tr} \geq z_{tr,top}$ then $h_{tr}^* = z_{tr,top}$ else $h_{tr}^* = h_{tr}$ ; and if $h_{gw} \geq z_{tr,top}$ then $h_{gw}^* = z_{tr,top}$ else $h_{gw}^* = h_{gw}$ .
$q_{gw \leftrightarrow tr}$	specific discharge per metre pipe length between groundwater and trench. Positive if ground water flows into the trench [ $m^2/h$ ].
$z_{tr,top}$	top level of the trench [m above datum]

### 1.1.12 Bed friction

The bed friction is the friction between the flowing water and the channel bed. As such, it exerts a force on the flowing water always in the direction opposite the water flow.

In water courses, this force together with the force caused by earth gravity usually determines the flow conditions: the other forces are far less important.

The fourth term of the momentum equation is the bed-friction term:

$$\text{bed friction} = \frac{gQ|Q|}{C^2RA_f} \quad (1.18)$$

where:

$g$  Acceleration due to gravity [ $m/s^2$ ] ( $\approx 9.81$ )

$Q$	Discharge [ $m^3/s$ ]
$C$	Chézy coefficient [ $m^{1/2}/s$ ]
$R$	Hydraulic radius [ $m$ ]
$A_f$	Wetted area [ $m^2$ ]

**Note:**

If the specified roughness parameter is equal to zero (Chézy=0, Manning=0, etc.), then the bed friction term is not taken into account in the momentum equation.



The following roughness definitions can be used: [Bos-Bijkerk \(1.1.12.1\)](#), [Chézy \(1.1.12.2\)](#), [Manning \(1.1.12.3\)](#), [Nikuradse \(1.1.12.4\)](#), [Strickler \(1.1.12.5\)](#), [White-Colebrook \(1.1.12.6\)](#)

**1.1.12.1 Bos-Bijkerk**

The bed friction formulation according to de Bos-Bijkerk describes the Manning coefficient as a function of the water depth and a parameter. This parameter can be used to shape the function to a certain empirical curve:

$$k_m = \gamma d^{1/3} \quad (1.19)$$

$k_m$	Manning roughness coefficient [ $m^{1/3}/s$ ]
$d$	Water depth [ $m$ ]
$\gamma$	Parameter [ $1/s$ ], normally between 20 and 40

This formula can be rewritten to a formulation for the Chézy coefficient as a function of the water depth

$$C = \gamma d^{1/3} R^{1/6} \quad (1.20)$$

$C$	Chézy coefficient [ $m^{1/2}/s$ ]
$R$	Hydraulic radius [ $m$ ]

For every computational time step the new friction value is calculated according to the Bos-Bijkerk formula and sequentially applied to the hydrodynamics calculations.

**1.1.12.2 Chézy**

The SOBEK-Flow-module uses the Chézy bed friction value in solving the water flow equations.

The following roughness formulations are possible:

- ◇ Chézy coefficient
- ◇ Bos-Bijkerk friction shape parameter  $g$ , resulting in a Chézy value according to:

$$C = \gamma d^{1/3} R^{1/6} \quad (1.21)$$

$d$	Water depth [ $m$ ]
$\gamma$	Parameter [ $1/s$ ], normally between 20 and 40
$C$	Chézy coefficient [ $m^{1/2}/s$ ]
$R$	Hydraulic radius [ $m$ ]

- ◇ White-Colebrook, using the Nikuradse roughness coefficient  $k_n$ , results in a Chézy value according to:

$$C = 18 \cdot 10^{\log \left( \frac{12R}{k_n} \right)} \quad (1.22)$$

- ◇ Manning coefficient,  $n_m$ , resulting in a Chézy coefficient according to:

$$C = \frac{R^{1/6}}{n_m} \quad (1.23)$$

- ◇ Strickler, using the Nikuradse  $k_n$  roughness coefficient, results in a Chézy value according to:

$$C = 25 \left( \frac{R}{k_n} \right)^{1/6} \quad (1.24)$$

- ◇ Strickler, using the Strickler  $k_s$  roughness coefficient, results in a Chézy value according to:

$$C = k_s R^{1/6} \quad (1.25)$$

- ◇ Engelund-like roughness predictor (for main sections of SOBEK-River profiles only) resulting in a Chézy value according to:

$$C = C_{90} \sqrt{\frac{\theta_{90}}{\theta_s}} \quad (1.26)$$

For SOBEK-River, the Chézy, Nikuradse, Manning or Strickler coefficients may be

- ◇ a constant
- ◇ spatially varying
- ◇ a tabulated function of the water level (h) or the total discharge (Q)

Different values or tables are possible for positive as well as negative flow. See also the chapter 1D hydraulic friction concepts for information on the different friction concepts present in the user interface.

### 1.1.12.3 Manning

One of the methods to define the bed roughness is using the Manning coefficient, symbol  $n_m$ . In the SOBEK-Flow-module, the Manning coefficient is used to compute the actual value of the Chézy coefficient, by:

$$C = \frac{R^{1/6}}{n_m} \quad (1.27)$$

$C$	Chézy coefficient [ $m^{1/2}/s$ ]
$R$	Hydraulic radius [ $m$ ]
$n_m$	Manning coefficient [ $s/m^{1/3}$ ]

### 1.1.12.4 Nikuradse

One of the methods to define the bed friction is by entering an equivalent roughness according to Nikuradse, represented by the symbol  $k_n$  [ $m$ ].

Values of  $k_n$  for open channels with bed forms are in the same order of magnitude as the height of the bed forms.

Using this option, the actual value of the Chézy coefficient will be computed according to the White-Colebrook formula.

### 1.1.12.5 Strickler

One of the methods to define the bed roughness is by using the Strickler formula. The actual value of the Chézy coefficient is computed using:

$$C = 25 \left( \frac{R}{k_n} \right)^{1/6} \quad (1.28)$$

or:

$$C = k_s R^{1/6} \quad (1.29)$$

$C$	Chézy coefficient [ $m^{1/2}/s$ ]
$R$	Hydraulic radius [ $m$ ]
$k_s$	Strickler roughness coefficient [ $m^{1/3}/s$ ]

in which  $k_n$  is the Nikuradse equivalent roughness, and  $k_s$  is the Strickler roughness coefficient. You may select either  $k_s$  or  $k_n$  as input value.

The value of the hydraulic radius  $R$  is taken from the last iteration loop.

It is possible to enter the coefficients varying in space and depending on the local flow direction.

### 1.1.12.6 White-Colebrook

One of the methods to define the bed friction is by specifying an equivalent roughness according to Nikuradse. Using this option, the value of the Chézy coefficient will be computed according to the White-Colebrook formula:

$$C = 18 \cdot 10 \log \left( \frac{12R}{k_n} \right) \quad (1.30)$$

$C$	Chézy coefficient
$R$	Hydraulic radius
$k_n$	Nikuradse equivalent roughness

**Note:**

Actually, this formula is a simplification of the complete White-Colebrook formula.



### 1.1.13 Froude number

The Froude number is defined by  $u/c$ , with  $u$  the average flow velocity and  $c$  the wave celerity.

Herein is  $c$  as follows:

$$c = \sqrt{\frac{gA_f}{W_f}} \quad (1.31)$$

Thus

$$\text{Froude number} = \frac{u}{\sqrt{gA_f/W_f}} \quad (1.32)$$

$u$	Velocity ( $u = Q/A_f$ ) [m/s]
-----	--------------------------------

$g$	Acceleration due to gravity [ $m/s^2$ ] ( $\approx 9.81$ )
$A_f$	Wetted area [ $m^2$ ]
$W_f$	Flow width [ $m$ ]

**Remarks:**

- ◇ When the Froude number is less than 1, the flow is sub-critical, when it is larger than 1, the flow is super-critical
- ◇ Transitions from sub-critical to super-critical flow causes an hydraulic jump.

**1.1.14 Boussinesq**

The Boussinesq coefficient is a parameter in the momentum equation for the water flow. It accounts for the non-uniform velocity distribution in a cross-section.

The Boussinesq constant  $\alpha_B$  is added to the convective term:

$$\frac{\partial}{\partial x} \left( \alpha_B \frac{Q^2}{A_f} \right) \quad (1.33)$$

The definition of the coefficient is:

$$\alpha_B = \frac{A_f}{Q^2} \int_0^{W_f} \frac{q(y)^2}{d(y)} dy \quad (1.34)$$

The constant of Boussinesq is computed by SOBEK. The computation is based upon the Engelund approach ([Engelund and Hansen, 1967](#)). In this approach the water level gradient and bed-friction term are assumed to be an order of magnitude larger than the other terms in the momentum equation. The resulting equation is:

$$g A_f \frac{\partial h}{\partial x} = \frac{g Q^2}{C^2 R A_f} \quad (1.35)$$

in which locally a constant water level gradient is assumed. In an arbitrary cross-section the discharge can be expressed as:

$$Q = \int_0^{W_f} C(y) d(y) \sqrt{R(y) \frac{\partial h}{\partial x}} dy \quad (1.36)$$

in which  $d$  is the water depth. Furthermore, it is assumed that the water level and water level slope are the same for main and floodplains. Combining [Equation 1.35](#) and [Equation 1.36](#) leads to a more accurate estimate of the C  zy coefficient based upon the average of the local C  zy coefficients.

$$C = \frac{1}{A_f \sqrt{R}} \int_0^{W_f} C(y) d(y) \sqrt{R(y)} dy \quad (1.37)$$

Now [Equation 1.34](#) gives combined with [Equation 1.35](#) and [Equation 1.36](#) the following expression for the Boussinesq coefficient:

$$\alpha_B = \frac{1}{A_f R C^2} \int_0^{W_f} C^2(y) d(y) R(y) dy \quad (1.38)$$



Cross-sections in SOBEK may be divided in two or three parts. So the following three options are available.

**option 1:**

The cross-section is not divided into sections with different roughness (only a main channel is present). This gives for the Boussinesq coefficient:

$$\alpha_B = 1 \quad (1.39)$$

**option 2:**

The cross-section is divided into two sections with different roughness for the modeling of, for example, a cross-section with a main channel and a floodplain. During a computation this gives two possibilities:

**possibility 1:**

Actual water flow is in the main channel only:

$$\alpha_B = 1 \quad (1.40)$$

**possibility 2:**

Actual water flow is in the main channel and the floodplain:

$$\alpha_B = \frac{C_0^2 A_{f0} R_0 + C_1^2 A_{f1} R_1}{C^2 R A_f} \quad (1.41)$$

The indices 0 and 1 respectively indicate the main channel and floodplain.

**option 3:**

The cross-section is divided into three sections with different roughness (main channel, floodplain 1 and floodplain 2). During a computation this gives three possibilities:

**possibility 1:**

Actual water flow is in the main channel only:

$$\alpha_B = 1 \quad (1.42)$$

**possibility 2:**

Actual water flow is in the main channel and floodplain 1:

$$\alpha_B = \frac{C_0^2 A_{f0} R_0 + C_1^2 A_{f1} R_1}{C^2 R A_f(h)} \quad (1.43)$$

The indices 0 and 1 respectively indicate the main channel and floodplain.

**possibility 3:**

Water is actually flowing in all sections, main channel, floodplain 1 and floodplain 2:

$$\alpha_B = \frac{C_0^2 A_{f0} R_0 + C_1^2 A_{f1} R_1 + C_2^2 A_{f2} R_2}{C^2 R A_f} \quad (1.44)$$

The indices 0, 1 and 2 respectively indicate the main channel, floodplain 1 and floodplain 2.

### 1.1.15 Accuracy

Whether you are measuring in a prototype, studying water flow in a scale model or modelling with a software system, you should always make some considerations about the accuracy of your activities and of the results of your study.

As for the results of a mathematical model study, the following elements play a role in establishing the overall accuracy:

- ◇ The reliability of the available data describing the prototype;
- ◇ The accuracy of the available data describing the prototype;
- ◇ The violation of certain assumptions underlying the mathematical modelling concept being used;
- ◇ The experience and skill of the modeller(s);
- ◇ The overall accuracy that is required (perhaps more accurate results could be obtained but the aim of the study may not require such accuracy or due to a lack of time you may have to settle for less);
- ◇ The accuracy of the applied numerical modelling technique.

In general practice the first five items are the most important when you are using a one-dimensional mathematical model for hydrodynamic flow. The numerical accuracy is in that case normally of minor importance.

The SOBEK-Flow-module uses the Delft-scheme to solve the water flow equations. This scheme is developed with robustness as the most important design aspect. It can deal with phenomena such as drying/flooding, super-critical flow and it guarantees a solution for every time step.

The accuracy of the solution depends on the grid size; the smaller the grid sizes, the more accurate the solution is. The time step can be chosen arbitrarily. It is reduced internally when this is necessary to guarantee stability by means of a time step estimation procedure. Obviously small grid sizes result in a network with more elements and therefore in a longer simulation time.

The Delft-scheme is designed to produce a closed water balance.

### 1.1.16 Structures

In the SOBEK-Flow-modules the following structure types are available:

<a href="#">section 1.1.16.1</a>	<a href="#">Advanced weir</a>
<a href="#">section 1.1.16.2</a>	<a href="#">Bridge</a>
<a href="#">section 1.1.16.3</a>	<a href="#">Compound structure</a>
<a href="#">section 1.1.16.4</a>	<a href="#">Culvert</a>
<a href="#">section 1.1.16.5</a>	<a href="#">Database structure</a>
<a href="#">section 1.1.16.6</a>	<a href="#">General structure</a>
<a href="#">section 1.1.16.7</a>	<a href="#">Inverted siphon</a>
<a href="#">section 1.1.16.8</a>	<a href="#">Orifice</a>
<a href="#">section 1.1.16.9</a>	<a href="#">Pump station and Internal Pump station</a>
<a href="#">section 1.1.16.10</a>	<a href="#">External Pump station</a>
<a href="#">section 1.1.16.11</a>	<a href="#">River Pump</a>
<a href="#">section 1.1.16.12</a>	<a href="#">River Weir</a>
<a href="#">section 1.1.16.13</a>	<a href="#">Siphon</a>
<a href="#">section 1.1.16.14</a>	<a href="#">Universal Weir</a>

section 1.1.16.15 Vertical obstacle friction  
 section 1.1.16.16 Weir

The flow through structures is computed based on:

- ◇ Upstream water level or energy level (River weir, Advanced weir and General structure only)
- ◇ Downstream water level or energy level (River weir, Advanced weir and General structure only)
- ◇ Structure dimensions (some can be controlled: i.e. crest level, opening height, pump capacity, opening of valve)
- ◇ A number of user-defined parameters, depending on the structure type (contraction coefficient, reduction factor, etc.).

The discharges and wetted areas that are computed in the structure formulas are imposed in the reach segment where the structure is located. The formulas use the water levels of the  $h$ -calculation points on either side of the reach segment. For the River weir, Advanced weir, General structure, River pump, Database structure and Compound structure yields that SOBEK by default places a computational point 0.5 m upstream and 0.5 m downstream of the structure location. Hence such structure is located in a reach having a default length of 1 m.

**Note:**

The dimensions of the structure do not contribute to the storage in the water system.



### 1.1.16.1 Advanced weir

Please note that the discharge through an Advanced weir is computed on basis of upstream and downstream energy levels. Further on please note that default a computational point is located 0.5 m in front and 0.5 m behind an Advanced weir.

**Notation**

The flow direction can be either positive or negative. A positive flow direction is a flow in the direction that the branches have been specified, i.e. with increasing  $x$ -coordinates. The upstream side, facing the beginning of the reach is denoted by the subscript 1, whereas the downstream location facing the end of the reach is denoted with 2. The subscript  $s$  is used for locations at the sill.

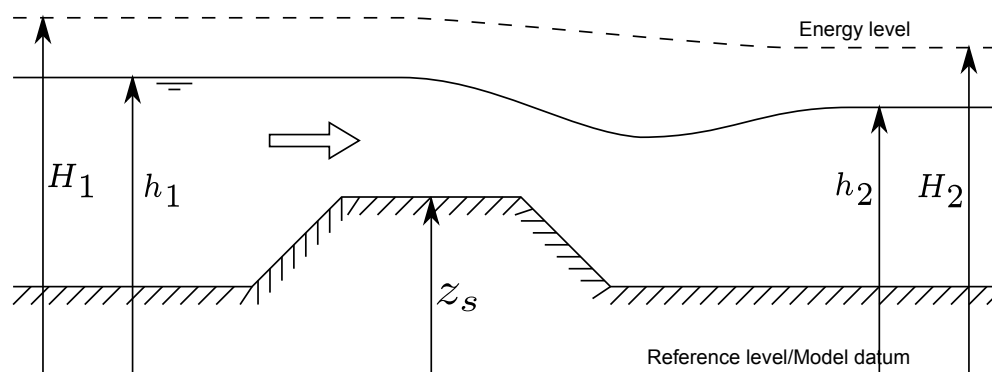


**Figure 1.15:** Definition of energy and water level

The energy level is equal to the water level plus the velocity head ( $u^2/2g$ ). The water depth  $d$  is equal to the water level ( $h$ ) minus the bed level ( $z_b$ ).

The user must enter the following input parameters for this type of hydraulic structure:

- ◇ Level of crest  $Z_s$ ;
- ◇ Total net width  $W_n$ ;
- ◇ Number of piers  $N$ ;
- ◇ Level of upstream face  $P$ ;
- ◇ Design head  $H_0$  of the weir;
- ◇ Pier contraction coefficient  $K_p$ ;
- ◇ Abutment contraction coefficient  $K_a$ .

The following parameters can be controlled by a hydraulic structure controller:

$W_s$  = Width across flow section

$Z_s$  = Crest level of weir

The discharge through the structure is computed with:

$$Q = C_1 C_2 W \sqrt{2g(H_1 - z_s)^3} \quad (1.45)$$

In which  $W$  is the active width and  $C_1$  and  $C_2$  are factors computed in the following way.



**Note:**

if  $h_1 < Z_s$  then  $Q = 0$ .

$$W = W_k - 2(NK_p + K_a)(H_1 - z_s) \quad (1.46)$$

$$C_1 = C_0 C_k \quad (1.47)$$

The value of  $C_0$  is computed depending on the value of the ratio between the upstream face and the design head:

$$\chi = \frac{P}{H_0} \quad (1.48)$$

if  $\chi < 2$  then:

$$C_0 = (0.1256\chi^5 - 1.0178\chi^4 + 3\chi^3 - 3.94\chi^2 + 2.28\chi + 1.66) \frac{\xi}{\sqrt{2g}} \quad (1.49)$$

where  $\xi$  is a correction factor computed with:

$$\xi = -0.052\chi^3 + 0.145\chi^2 - 0.096\chi + 1.01 \quad (1.50)$$

if  $\chi > 2$  then:

$$C_0 = \frac{2.1549008}{\sqrt{2g}} \quad (1.51)$$

The value of  $\chi$  is computed depending on the value of the ratio between the energy level minus the sill level and the design head:

$$\chi_1 = \frac{H_1 - z_s}{H_0} \quad (1.52)$$

if  $\chi_1 < 1.6$  then:

$$C_k = 0.1394\chi_1^3 - 0.416\chi_1^2 + 0.488\chi_1 + 0.785 \quad (1.53)$$

if  $\chi_1 > 1.6$  then:

$$C_k = 1.0718224 \quad (1.54)$$

The value of  $C_t$  is computed depending on the value of the ratio between the energy level minus the downstream water level and the energy level minus the sill level:

$$\chi_2 = \frac{H_1 - h_2}{H_1 - z_s} \quad (1.55)$$

if  $\chi_2 < 0.7$  then:

$$C_t = \sqrt{\left(1 - \frac{(\chi_2 - 0.7)^2}{0.49}\right) + 27(0.7 - \chi_2)^4} \sqrt{\chi_2^3} \quad (1.56)$$

if  $\chi_2 > 0.7$  then:

$$C_t = 1 \quad (1.57)$$

### 1.1.16.2 Bridge

A bridge is one of the structure types that can be included in the SOBEK-Flow-module. The following types of bridges can be modelled:

- ◇ Pillar bridge
- ◇ Abutment bridge
- ◇ Fixed bed bridge
- ◇ Soil bed bridge

The general description of the discharge through a bridge is given by:

$$Q = \mu A_f \sqrt{2g(h_1 - h_2)} \quad (1.58)$$

$Q$	Discharge through bridge [ $m^3/s$ ]
$\mu$	Discharge coefficient derived from loss-coefficients [—]
$A_f$	Wetted area [ $m^2$ ] of flow through bridge at upstream side
$g$	Acceleration due to gravity [ $m/s^2$ ] ( $\approx 9.81$ )
$h_1$	Upstream water level [ $m$ ]
$h_2$	Downstream water level [ $m$ ]

**Note:** For numerical reasons (e.g. validity of structure [Equation 1.58](#)) the discharge coefficient ( $\mu$ ) is limited to a maximum of 1.0. In other words if the discharge coefficient ( $\mu$ ) according to [Equation 1.59](#) (Pillar bridge) or [Equation 1.61](#) (Abutment bridge, Fixed bed bridge or Soil bed bridge) becomes larger than 1.0, the actual applied discharge coefficient in [Equation 1.58](#) is limited to 1.0. This means that for a given discharge, the water level difference over such bridge might be larger than anticipated, when considering the defined friction loss coefficients. In such case it is advised to apply the Extra Resistance Node for modelling this particular bridge. An Extra Resistance Node (see ?? and [section 1.1.2.2](#)) adds additional(extra) resistance to the St. Venant momentum equation. Hence no structure equation is solved at an Extra Resistance Node.



**Pillar bridge**

A pillar bridge has one or more pillars that affect the discharge through the bridge with the following definition for the discharge coefficient ( $\mu$ )

$$\mu = \frac{1}{\sqrt{\xi_y}} \quad (1.59)$$

$\xi_y$  Pillar loss coefficient, defined as

$$\xi_y = \beta \frac{\alpha_y}{A_f} \quad (1.60)$$

$\beta$  Parameter [–] depending on shape of pillar[s] (shape factor). Normally between 0.22 and 1.56

$A_f$  Wetted area [ $m^2$ ] of flow through bridge at upstream side

$\alpha_y$  Area [ $m^2$ ] of wetted part of pillar[s] perpendicular to the flow direction, considered at upstream side

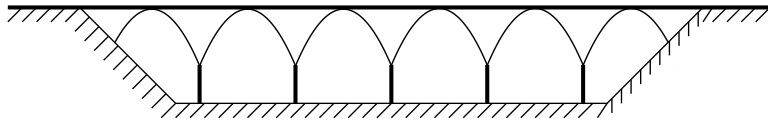


**Figure 1.16:** Pillar bridge



**Note:** For numerical reasons the discharge coefficient ( $\mu$ ) is limited to a maximum of 1.0. For more information, see the note below [Equation 1.58](#).

The plate of the bridge is always so high that it does not effect the flow through the bridge. So the cross section is considered as open.



**Note:**  
Pillar bridges are not allowed in closed cross-sections.

**Abutment bridge**

For the abutment bridge the overall loss coefficient is defined as:

$$\mu = \frac{1}{\sqrt{\xi_i + \xi_f + \xi_o}} \quad (1.61)$$

$\xi_i$  Entrance loss coefficient (in). Constant

$\xi_f$  Friction loss coefficient

$\xi_o$  Exit loss coefficient (out).



**Note:** For numerical reasons the discharge coefficient ( $\mu$ ) is limited to a maximum of 1.0. For more information, see the note below [Equation 1.58](#).

The  $\xi_o$  coefficient is defined as:

$$\xi_o = k \left( 1 - \frac{A_f}{A_{f2}} \right)^2 \quad (1.62)$$

$k$  Constant exit loss coefficient

$A_f$	Wetted area [ $m^2$ ] of flow through bridge at upstream side
$A_{f_2}$	Wetted area [ $m^2$ ] of flow in reach at downstream side of bridge

The  $\xi_f$  coefficient is defined as:

$$\xi_f = \frac{2gL}{C^2 R} \quad (1.63)$$

$g$	Acceleration due to gravity [ $m/s^2$ ] ( $\approx 9.81$ )
$L$	Length of bridge [ $m$ ]
$C$	Chézy coefficient [ $m^{1/2}/s$ ]
$R$	Hydraulic radius [ $m$ ]

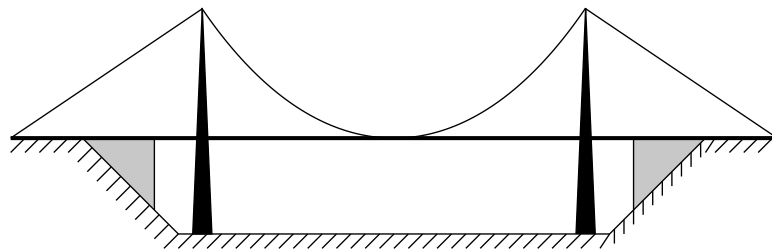


**Figure 1.17:** A suspension bridge with abutments

Here, the plate of the bridge can effect the flow through the bridge. The cross section is closed

**Note:**

The definition of this bridge is similar to the definition of a culvert.



**Fixed bed bridge**

This bridge has the same formulation as the abutment bridge except it has a rectangular profile.



**Figure 1.18:** Fixed bed bridge

**Soil bed bridge**

This bridge has the same formulation as the fixed bed bridge including the rectangular profile. In addition to this it has a ground layer with a different friction formulation. This ground layer can have a zero thickness.

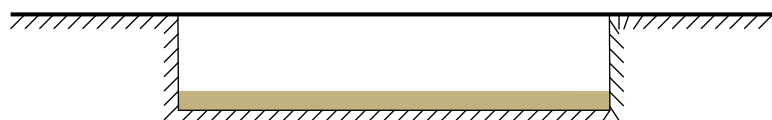


**Figure 1.19:** Soil bed bridge

### 1.1.16.3 Compound structure

A compound structure consists of several hydraulic structures parallel to each other at one location. These hydraulic structures may be of the same type or of different types. Presently following structure types can be placed as a member in a compound structure, viz.: General structure, Database structure, Advanced weir, River weir and River pump.

Please note that a value for structure inertia damping factor can be defined for each individual member of the compound structure.

Each member of the compound structure has its own triggers and controllers.

### 1.1.16.4 Culvert

A culvert is one of the structure types that can be included in the SOBEK-Flow-module. A culvert is an underground structure that normally connects two open channels. The flow through a culvert is affected by its upstream and downstream invert levels, the size and shape of its closed cross section, its ground layer thickness, its entrance loss, its friction loss, its valve loss and its exit loss.

Figure 1.20 shows a side view of a culvert.

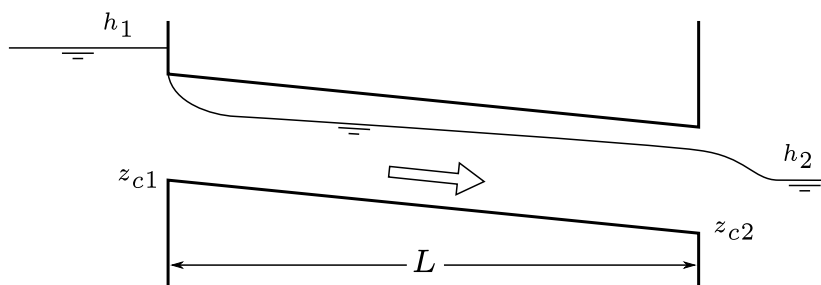


**Figure 1.20:** Side view of a culvert

Two flow conditions can occur:

Free flow when  $h_2 < z_{c2} + d_{c2}$

$$Q = \mu A_{fc} \sqrt{2g(h_1 - (z_{c2} + d_{c2}))} \quad (1.64)$$

Submerged flow when  $h_2 \geq z_{c2} + d_{c2}$ :

$$Q = \mu A_{fc} \sqrt{2g(h_1 - h_2)} \quad (1.65)$$

$Q$	Discharge through culvert [ $m^3/s$ ]
$\mu$	Discharge coefficient, derived from loss-coefficients [—]
$A_{fc}$	Discharge culvert flow area $\min(A_{fc1}, A_{fcgate})$ [ $m^2$ ]
	$A_{fc1}$ : Flow area in the culvert at its upstream side [ $m^2$ ]
	$A_{fcgate}$ : Flow area under the culvert gate [ $m^2$ ]
$g$	Acceleration due to gravity [ $m/s^2$ ] ( $\approx 9.81$ )
$h_1$	Upstream water level [ $m$ ]
$h_2$	Downstream water level [ $m$ ]
$z_{c2}$	Downstream culvert invert level [ $m$ ]
$d_{c2}$	Critical culvert depth at the downstream side, $\sqrt[3]{Q^2/(gT_2^2)}$ [ $m$ ]



$T_2$  Surface width in the culvert at its downstream side [ $m$ ]

For numerical reasons the discharge coefficient ( $\mu$ ) is limited to a maximum of 1.0. The discharge coefficient ( $\mu$ ) is computed as follows:

$$\mu = \frac{1}{\sqrt{\xi_i + \xi_f + \xi_v + \xi_o}} \quad (1.66)$$

$\xi_i$  Entrance loss coefficient [–]  
 $\xi_f$  Friction loss coefficient [–]  
 $\xi_v$  Valve loss coefficient [–]  
 $\xi_o$  Exit loss coefficient [–]

The entrance loss coefficient ( $\xi_i$ ) can be defined as a constant value only.

The friction loss coefficient ( $\xi_f$ ) is computed as follows:

$$\xi_f = \frac{2gL}{C_1^2 R} \quad (1.67)$$

$L$  Length of the culvert [ $m$ ]  
 $C_1$  Chézy coefficient in the culvert at its upstream side [ $m^{1/2}/s$ ]  
 $R$  Hydraulic radius [ $m$ ]  
 If  $h_1 \geq z_{c1} + GHO$ ;  $R = R_{c1}$   
 If  $h_1 < z_{c1} + GHO$ ;  $R = R_{gate}$   
 $GHO$  Gate height opening [ $m$ ]  
 $R_{c1}$  Hydraulic radius in the culvert at its upstream side [ $m$ ]  
 $R_{gate}$  Hydraulic radius based on actual gate height opening [ $m$ ]  
 $z_{c1}$  Upstream culvert invert level [ $m$ ]

The valve loss coefficient ( $\xi_v$ ) can be defined as a constant value or as a function of the ratio of the “Gate height opening” and the “maximum inner culvert height”.

**Note:**

- ◇ In case the valve loss coefficient ( $\xi_v$ ) is not a constant, in computations the actual valve loss coefficient ( $\xi_v$ ) is derived from the user defined table, while using the ratio of the “actual gate height opening and the “actual maximum inner culvert height”.
- ◇ In case the ground layer thickness is greater than zero, both the “actual gate height opening” and the “actual maximum inner culvert height” will differ from the values as defined in the user interface (see next paragraph)

The exit loss coefficient ( $\xi_o$ ) is computed as follows:

Submerged flow ( $h_2 = z_{c2} + d_{c2}$ ):

$$\xi_o = k \left( 1 - \frac{A_{fc}}{A_{fr2}} \right)^2 \quad (1.68)$$

$k$  User defined constant exit loss coefficient [–]  
 $A_{fr2}$  Flow area in the reach, adjacent to the downstream culvert side [ $m^2$ ]  
 $A_{fc}$  Culvert flow area [ $m^2$ ]  
 If  $h_1 \geq z_{c1} + GHO$ ;  $A_{fc} = A_{fcgate}$   
 If  $h_1 < z_{c1} + GHO$ ;  $A_{fc} = A_{fc1}$

$GHO$	Gate height opening [m]
$z_{c1}$	Upstream culvert invert level [m]
$A_{f_{gate}}$	Flow area under the culvert gate [m <sup>2</sup> ]
$A_{f_{c1}}$	Flow area in the culvert at its upstream side [m <sup>2</sup> ]

Free flow ( $h_2 < z_{c2} + d_{c2}$ ):

$$\xi_o = 0 \quad (1.69)$$

### ***Culvert cross-sections, bed friction and ground layer***

For a culvert all available closed cross-section types can be used. In a culvert, a ground layer with constant thickness can be defined. Culvert friction and ground layer friction can be specified, using any of the available bed friction formulations.

Defining a ground layer thickness  $> 0$  implies that in culvert computations:

- ◇ Defined invert levels are raised with the ground layer thickness,
- ◇ Gate height openings are reduced with the ground layer thickness,
- ◇ Maximum inner height of the culvert is reduced with the ground layer thickness,
- ◇ Cross-sectional parameters (such as: flow areas, hydraulic radius and so on) are computed based on a cross-sectional profile, that is reduced by the ground layer thickness.

### ***Culvert, Good modelling practice aspects***

It is advised to avoid that the bed level of a cross-section in front of a Culvert, Inverted Siphon or Siphon is above the ground-layer level (= invert level + ground-layer thickness), since such situation can result in very small computational time-steps (e.g. long required wall-clock times) or even in a termination of the simulation.

This is explained as follows. Consider the situation depicted in [Figure 1.40](#) where the bed level in front of a Culvert (Inverted Siphon or Siphon) is 0.60 m above the ground-layer level. This means that at small upstream water depths, water will be sucked into the culvert (Inverted Siphon or Siphon), resulting in large flow velocities. For the computational time-step ( $\Delta t$ ) yields that  $\Delta t \leq \Delta x / U$ , where  $U$  is the local flow velocity and  $\Delta x$  is distance between two water level computational points (or h-points). At very low discharges even negative water depths may be computed, leading to a termination of the simulation.

The situation explained above can be avoided by making the bed level in front of the Culvert (Inverted Siphon or Siphon) equal to the ground-layer level. In other words by defining a bed level slope from h-point  $h_2$  to  $h_3$  as depicted in [Figure 1.40](#). Providing for the parameter "Maximum Lowering of Cross-section Bed Level at Culvert" a value greater or equal to 0.60 m means that before the computation starts, the bed level at h-point  $h_3$  is set equal to the ground-layer level. In ?? it is shown how to provide a value for parameter "Maximum Lowering of Cross-section Bed Level at Culvert".

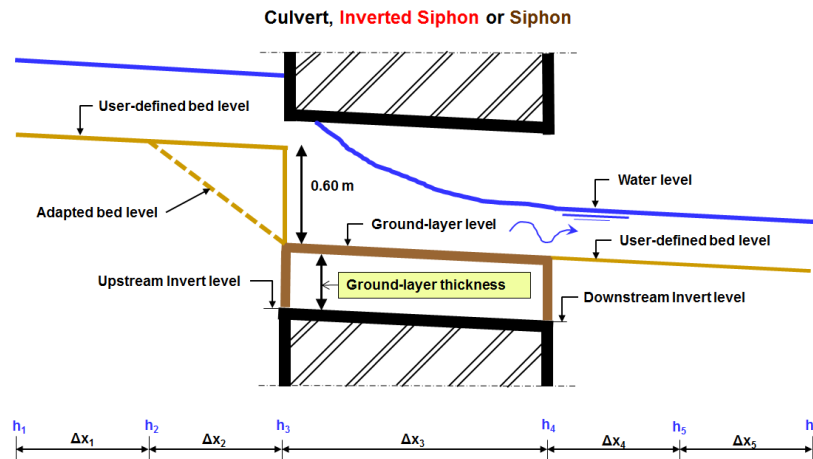


**Figure 1.21:** Good modelling practice, Culvert, Inverted Siphon and Siphon

### 1.1.16.5 Database structure

Please note that default a computational point is located 0.5 *m* before and 0.5 *m* behind a Database structure. In a hydraulic structure the discharge through the structure depends on upstream and downstream water levels and structure parameters that define the dimension of the structure etc. In other words the hydraulic behaviour of a structure can be defined in the structure equation as a relationship between upstream and downstream water level. In the database structure however, this relationship is defined in a tabulated form which is stored in a database. The user has to define this database.

The database consists in fact of a matrix of discharges. At every point of the matrix a discharge ( $Q$ ) is defined as a function of two corresponding water levels: one facing the beginning of the branch ( $h_1$ ) and one facing the end ( $h_2$ ), are defined. There are two ways to define the relation:

- ◇ a function of both water levels  $Q = Q(h_1 - z_s, h_2 - z_s)$ , to be used for structures with relatively high head differences;  $z_s = \text{crest level w.r.t. datum}$
- ◇ a function of the water level and the water level difference  $Q = Q(h_1 - z_s, \Delta h = h_1 - h_2)$ , to be used for structures with relatively small water level differences combined with large water level variations;  $z_s = \text{crest level w.r.t. datum}$

All discharges in a row correspond to the same water level ( $h_1$ ) facing the beginning of the reach segment. All discharges in a column correspond either to the same water level ( $h_2$ ) facing the end of the reach segment or to the water level difference ( $\Delta h = h_1 - h_2$ ). The water levels that are part of the database are defined with respect to a user defined datum.

During a simulation, discharges at any point in the domain of the matrix will be obtained by interpolation. In most cases this will be a linear interpolation in two directions. However when the discharge is requested at a water level that lies within 10 percent of a water level defined in the matrix, cubic interpolation takes place for that water level.

#### Warning:

- ◇ The crest level can be adjusted by a controller. This implies the assumption that the discharge head relation is independent of the level of the crest. This is not completely correct. The user should be aware of this.



### 1.1.16.6 General structure

Please note that default a computational point is located 0.5 m in front and 0.5 m behind a general structure. In the general structure type in sobek weir and gate flow is combined in one structure type. In addition, the general structure gives more freedom in defining the dimensions and the geometry of the hydraulic structure. The geometrical shape is given in [Figure 1.22](#) and [Figure 1.23](#). See ?? for the definition of input parameters. Please note that the discharge through a General structure is computed on basis of upstream and downstream energy levels. Please note as well that a structural inertia damping factor can be defined for each individual General structure.

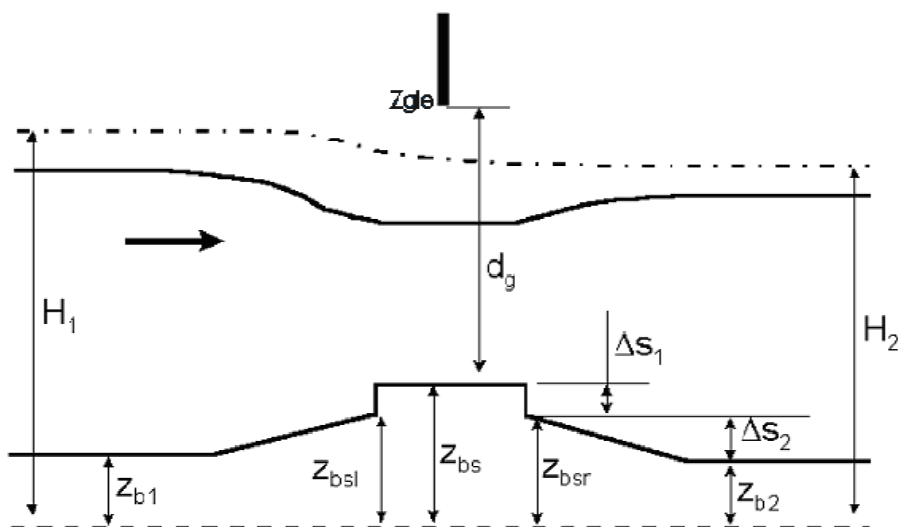


Figure 1.22: General structure, side view

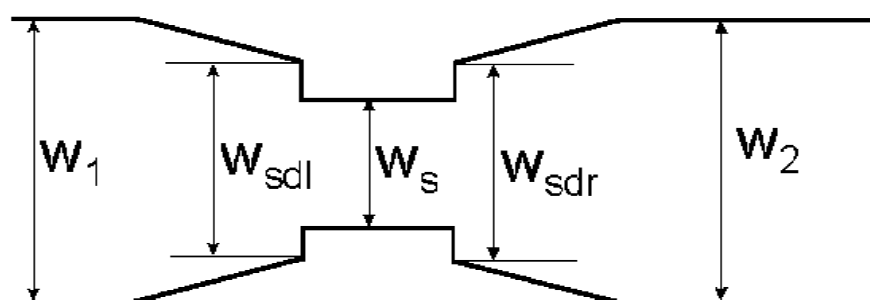


Figure 1.23: General structure, top view

Flow across the general structure can be of the following types: drowned weir flow, free weir flow, drowned gate flow, and free gate flow, depending on the dimensions of the structure and the flow conditions.

When salt intrusion is modelled, the density difference of the water over the structure is incorporated in the impulse balance (this is not the case with the other structure types).

In the solution method for the general structure particular attention has been given to the modelling of the transition between free- and submerged flow.

For this purpose, the water level at the sill ( $d_s$ ) is computed by applying an impulse balance instead of taking it equal to the water level further downstream.

As a result the general structure is especially attractive for those who want to simulate the shifting conditions from free- to submerged gate flow accurately and of course in case of important density-differences over the structure.

### Computation of downstream water level

In case of drowned gate flow or drowned weir flow the water level at the sill or downstream of the gate is required. This level is computed by application of the impulse balance.

◇ drowned gate-flow

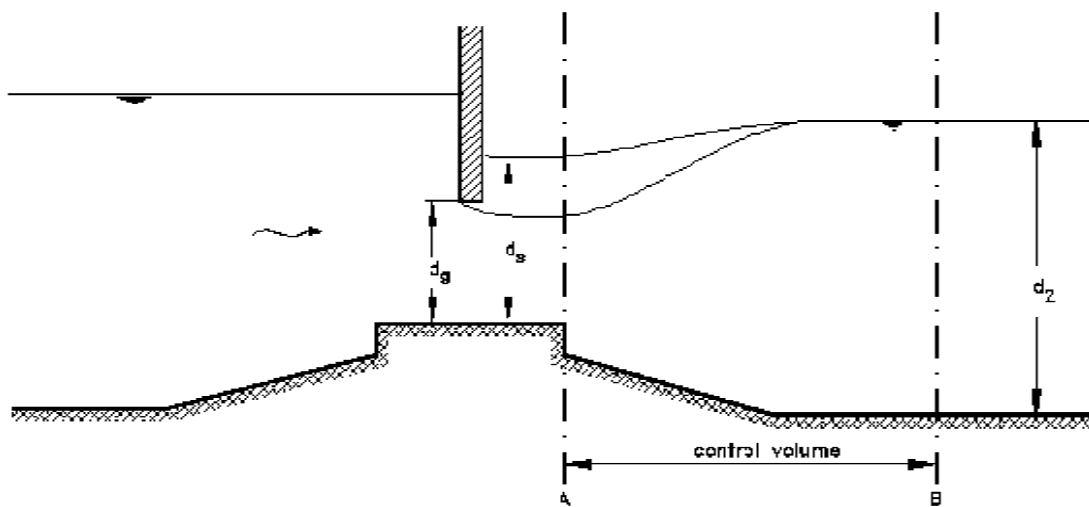


**Figure 1.24:** Drowned gate flow

The water depth  $d_s$  can be described by a second order algebraic equation:

$$A_w d_s^2 + B_w d_s + C_w = 0 \quad (1.70)$$

with:

$$A_g = (1 + \rho^*) \left( \frac{W_{sd}}{3} + \frac{W_2}{6} \right) + (1 - \rho^*) \left( \frac{W_{sd}}{4} + \frac{W_2}{12} \right) \quad (1.71)$$

$$\begin{aligned} B_g = & (1 + \rho^*) \left( (\Delta S_1 + \Delta S_2 - d_2) \left( \frac{W_{sd}}{3} + \frac{W_2}{6} \right) + (2\Delta S_1 + d_2) \frac{W_{sd}}{6} + \right. \\ & \left. (\Delta S_1 + 2d_2) \frac{W_2}{6} \right) + \\ & + (1 - \rho^*) \left( \Delta S_1 \frac{W_{sd}}{3} + (\Delta S_1 + d_2) \frac{W_{sd} + W_2}{6} \right) + \\ & + \frac{4\rho^* c_{gd}^2 \mu_{gd}^2 d_g^2 W_s^2}{W_2 d_2} \left( 1 + \frac{\lambda}{d_2} \right) - 4c_{gd} \mu_{gd} d_g W_s \end{aligned} \quad (1.72)$$

$$\begin{aligned} C_g = & (1 + \rho^*) (\Delta S_1 + \Delta S_2 - d_2) \left( 2\Delta S_1 + d_2 \right) \frac{W_{sd}}{6} + (\Delta S_1 + 2d_2) \frac{W_2}{6} + \\ & + (1 - \rho^*) \left( (\Delta S_1)^2 \frac{W_{sd}}{6} + (\Delta S_1 + d_2) \frac{W_{sd} + W_2}{12} \right) + \\ & - \frac{4\rho^* c_{gd}^2 \mu_{gd}^2 d_g^2 W_s^2 H_{s1}}{W_2 d_2} \left( 1 + \frac{\lambda}{d_2} \right) + 4c_{gd} \mu_{gd} d_g W_s H_{s1} \end{aligned} \quad (1.73)$$

where  $\rho^*$  is given by the expression:

$$\rho^* = \frac{\rho_2}{\rho_1} \quad (1.74)$$

$\lambda$ : extra resistance of general structure can be defined for each general structure separately.

Equation 1.70 leads to:

$$d_s = \frac{-B_g + \sqrt{B_g^2 - 4A_g C_g}}{2A_g} \quad (1.75)$$

◇ drowned weir-flow

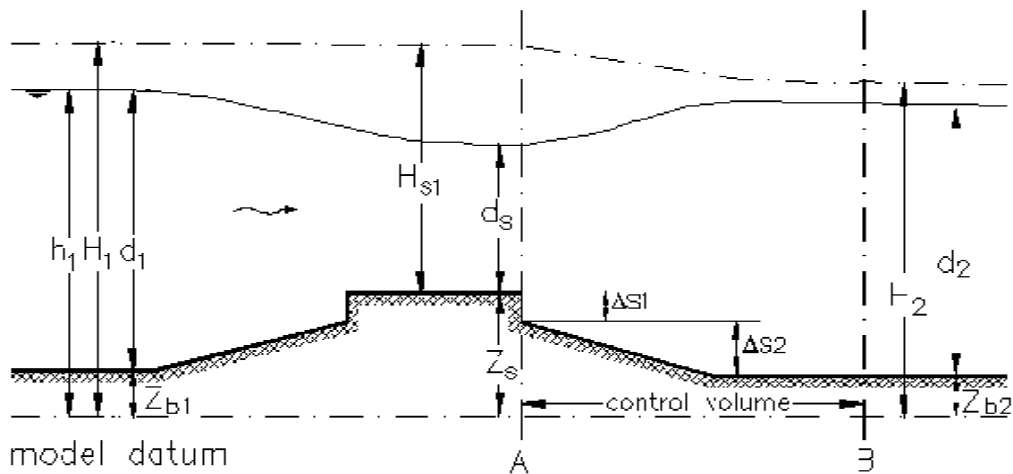


Figure 1.25: Drowned weir-flow

The water depth at the sill  $d_s$  is described by a third order algebraic equation:

$$D_w d_s^3 + A_w d_s^2 + B_w d_s + C_w = 0 \quad (1.76)$$

with:

$$D_w = \frac{4\rho^* c_{wd}^2 W_s^2}{W_2 d_2} \left(1 + \frac{\lambda}{d_2}\right) \quad (1.77)$$

$$A_w = (1 + \rho^*) \left( \frac{W_{sd}}{3} + \frac{W_2}{6} \right) + (1 - \rho^*) \left( \frac{W_{sd}}{4} + \frac{W_2}{12} \right) +$$

$$- \frac{4\rho^* c_{wd}^2 W_s^2 H_{s1}}{W_2 d_2} \left(1 + \frac{\lambda}{d_2}\right) + 4c_{wd} W_s \quad (1.78)$$

$$B_w = (1 + \rho^*) \left( (\Delta S_1 + \Delta S_2 - d_2) \left( \frac{W_{sd}}{3} + \frac{W_2}{6} \right) + (2\Delta S_1 + d_2) \frac{W_{sd}}{6} + \right.$$

$$\left. (\Delta S_1 + 2d_2) W_2 \frac{W_2}{6} \right) +$$

$$+ (1 - \rho^*) \left( \Delta S_1 \frac{W_{fd}}{3} + (\Delta S_1 + d_2) \frac{W_{fd} + W_2}{6} \right) + 4C_{wd} W_s H_{s1} \quad (1.79)$$

$$C_w = (1 + \rho^*) (\Delta S_1 + \Delta S_2 - d_2) \left( (2\Delta S_1 + d_2) \frac{W_{sd}}{6} + (\Delta S_1 + 2d_2) \frac{W_2}{6} \right) +$$

$$+ (1 - \rho^*) \left( (\Delta S_1)^2 \frac{W_{sd}}{6} + (\Delta S_1 + d_2) \frac{W_{sd} + W_2}{12} \right) \quad (1.80)$$

A direct method is applied to calculate  $d_s$  from equation [Equation 1.76](#).

### Discharge equations

The following discharge equations are applied during the computations.

◇ Free gate flow:

$$u_s = \mu_{gf} c_{gf} \sqrt{2g(H_1 - (z_s + \mu_{gf} d_g))} \quad (1.81)$$

$$A_f = W_s d_g \quad (1.82)$$

$$Q = u_s A_f = \mu_{gf} c_{gf} W_s d_g \sqrt{2g(H_1 - (z_s + \mu_{gf} d_g))} \quad (1.83)$$

◇ Drowned gate flow:

$$u_s = \mu_{gd} c_{gd} \sqrt{2g(H_1 - (z_s + d_s))} \quad (1.84)$$

$$A_f = W_s d_g \quad (1.85)$$

$$Q = u_s A_f = \mu_{gd} c_{gd} W_s d_g \sqrt{2g(H_1 - (z_s + d_s))} \quad (1.86)$$

$$(1.87)$$

◇ Free weir flow:

$$u_s = c_{wf} \sqrt{\frac{2}{3}g(H_1 - z_s)} \quad (1.88)$$

$$A_f = W_s \frac{2}{3}(H_1 - z_s) \quad (1.89)$$

$$Q = u_s A_f = c_{wf} W_s \frac{2}{3} \sqrt{\frac{2}{3}g(H_1 - z_s)^{3/2}} \quad (1.90)$$

◇ Drowned weir flow:

$$u_s = c_{wd} \sqrt{2g(H_1 - (z_s + d_s))} \quad (1.91)$$

$$A_f = W_s d_s \quad (1.92)$$

$$Q = u_s A_f = c_{wd} W_s d_s \sqrt{2g(H_1 - (z_s + d_s))} \quad (1.93)$$

where:

$\mu_{gf}$	contraction coefficient for free gate flow
$\mu_{gd}$	contraction coefficient for drowned gate flow ( $\mu_{gd} = \mu_{gf}$ )
$c_{gf}$	correction coefficient for free gate flow
$c_{gd}$	correction coefficient for drowned gate flow
$c_{wf}$	correction coefficient for free weir flow
$c_{wd}$	correction coefficient for drowned weir flow



**Note:**

The contraction coefficient has a maximum value  $\mu = 1.0$ . In case the user specifies a higher value, a warning will be generated

#### Criteria for flow types

First it is assumed that it is weir flow. Then the water level at the sill  $d_s$  and the critical depth  $d_c = 2/3(H_1 - z_s)$  are calculated.

The criteria are:

- ◇  $d_s > d_c$  and  $d_g > d_s$  drowned weir flow
- ◇  $d_s < d_c$  and  $d_g > d_s$  free weir flow
- ◇ otherwise gate flow.

In the latter case the water level at the sill  $d_s$  is recalculated using the gate flow conditions. The critical depth  $d_c$  is now defined as  $\mu_{gf} d_g$ .

The criteria are.

- ◇  $d_s > d_c$  drowned gate flow
- ◇  $d_s < d_c$  free gate flow
- ◇  $d_s$  imaginary free gate flow (i.e. downstream water level below crest level)



**Note:**

In case upstream water level is above gate lower edge level, there can still be **drowned weir flow** if  $d_s > d_c$  and  $d_g > d_s$  or **free weir flow** if  $d_s < d_c$  and  $d_g > d_s$ .

#### 1.1.16.7 Inverted siphon

An inverted siphon is one of the structure types, that can be included in the SOBEK-Flow-module. An inverted siphon is a structure that normally connects two open channels, that are separated by a particular infrastructural work (e.g. dike, railroad). The inverted siphon makes an underground connection through such infrastructural work. An inverted siphon is assumed to be fully filled with water at its deepest point. In case this does not yield for your structure, you can consider to use a culvert. The flow through an inverted siphon is affected by its upstream and downstream invert level, the size and shape of its closed cross section, its ground layer thickness, its entrance loss, friction loss, its valve loss, losses due to its bends (bend loss), and its exit loss.



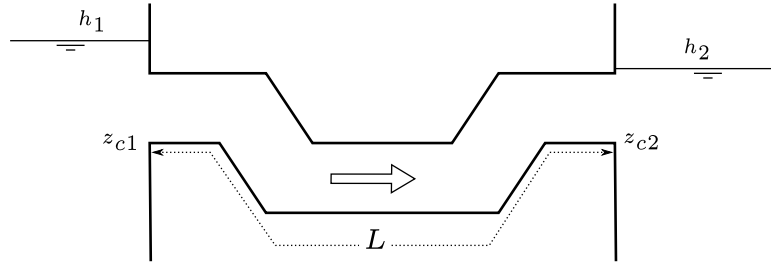


**Figure 1.26:** Side view of an inverted siphon

Two flow conditions can occur:

Free flow when  $h_2 < z_{c2} + d_{c2}$

$$Q = \mu A_{fis} \sqrt{2g(h_1 - (z_{c2} + d_{c2}))} \quad (1.94)$$

Submerged flow when  $h_2 \geq z_{c2} + d_{c2}$ :

$$Q = \mu A_{fis} \sqrt{2g(h_1 - h_2)} \quad (1.95)$$

$Q$	Discharge through inverted siphon [ $m^3/s$ ]
$\mu$	Discharge coefficient, derived from loss-coefficients [—]
$A_{fis}$	Discharge inverted siphon flow area ( $= \min(A_{fcrs}, A_{fisgate})$ ) [ $m^2$ ]
$A_{fcrs}$	Cross-sectional area of the inverted siphon. At its deepest point the inverted siphon is considered to be completely filled with water [ $m^2$ ]
$A_{fisgate}$	Flow area under the inverted siphon gate [ $m^2$ ]
$g$	Acceleration due to gravity [ $m/s^2$ ] ( $\approx 9.81$ )
$h_1$	Upstream water level [ $m$ ]
$h_2$	Downstream water level [ $m$ ]
$z_{c2}$	Downstream inverted siphon invert level [ $m$ ]
$d_{c2}$	Critical inverted siphon depth at the downstream side

$$d_{c2} = \sqrt[3]{Q^2 / (g T_2^2)} \quad [m] \quad (1.96)$$

$T_2$  Surface width in the inverted siphon at its downstream side [ $m$ ]

For numerical reasons the discharge coefficient ( $\mu$ ) is limited to a maximum of 1.0. The discharge coefficient ( $\mu$ ) is computed as follows:

$$\mu = \frac{1}{\sqrt{\xi_i + \xi_f + \xi_v + \xi_b + \xi_o}} \quad (1.97)$$

$\xi_i$	Entrance loss coefficient [—]
$\xi_f$	Friction loss coefficient [—]
$\xi_v$	Valve loss coefficient [—]
$\xi_b$	Bend loss coefficient [—]
$\xi_o$	Exit loss coefficient [—]

The entrance loss coefficient ( $\xi_i$ ) can be defined as a constant value only.

The friction loss coefficient ( $\xi_f$ ) is computed as follows:

$$\xi_f = \frac{2gL}{C^2 R} \quad (1.98)$$

$L$	Length of the inverted siphon [ $m$ ]
$C$	Chézy coefficient for fully water filled inverted siphon [ $m^{1/2}/s$ ]
$R$	Hydraulic radius [ $m$ ] If $GHO < MIISH$ ; $R = R_{gate}$ If $GHO \geq MIISH$ ; $R = R_{inverted\ siphon}$
$GHO$	Gate height opening [ $m$ ]
$MIISH$	Maximum inner inverted siphon height [ $m$ ]
$R_{inverted\ siphon}$	Hydraulic radius based on a fully water filled inverted siphon [ $m$ ]
$R_{gate}$	Hydraulic radius based on actual gate height opening [ $m$ ]

The valve loss coefficient ( $\xi_v$ ) can be defined as a constant value or as a function of the ratio of the “Gate height opening” and the “maximum inner inverted siphon height”.



**Note:**

- ◇ In case the valve loss coefficient ( $\xi_v$ ) is not a constant, in computations the actual valve loss coefficient ( $\xi_v$ ) is derived from the user defined table, while using the ratio of the “actual gate height opening and the “actual maximum inner inverted siphon height”.
- ◇ In case the ground layer thickness is greater than zero, both the “actual gate height opening” and the “actual maximum inner inverted siphon height” will differ from the values as defined in the user interface.

The exit loss coefficient ( $\xi_o$ ) is computed as follows:

Submerged flow ( $h_2 = z_{c2} + d_{c2}$ ):

$$\xi_o = k \left( 1 - \frac{A_{fis}}{A_{fr2}} \right)^2 \quad (1.99)$$

$k$	User defined constant exit loss coefficient [—]
$A_{fr2}$	Flow area in the reach, adjacent to the downstream inverted siphon side [ $m^2$ ]
$A_{fis}$	Inverted siphon flow area [ $m^2$ ] If $GHO \leq MIISH$ ; $A_{fis} = A_{fisgate}$ If $GHO > MIISH$ ; $A_{fis} = A_{inverted\ siphon}$
$GHO$	Gate height opening [ $m$ ]
$MIISH$	Maximum inner inverted siphon height [ $m$ ]
$A_{fisgate}$	Flow area under the inverted siphon gate [ $m^2$ ]
$A_{inverted\ siphon}$	Flow area based on a fully water filled inverted siphon [ $m^2$ ]

Free flow ( $h_2 < z_{c2} + d_{c2}$ ):

$$\xi_o = 0 \quad (1.100)$$

**Inverted siphon cross-sections, bed friction and ground layer:**

For an inverted siphon all available closed cross-section types can be used. In an inverted siphon, a ground layer width constant thickness can be defined. Inverted siphon friction and ground layer friction can be specified, using any of the available bed friction formulations.

Defining a ground layer thickness  $> 0$  implies that in inverted siphon computations:

- ◇ Defined invert levels are raised with the ground layer thickness,
- ◇ Gate height openings are reduced with the ground layer thickness,
- ◇ Maximum inner height of the inverted siphon is reduced with the ground layer thickness,

- ◇ Cross-sectional parameters (such as: flow areas, hydraulic radius and so on) are computed based on a cross-sectional profile, that is reduced by the ground layer thickness.

### ***Inverted Siphon, Good modelling practice aspects***

It is advised to avoid that the bed level of a cross-section in front of a Culvert, Inverted Siphon or Siphon is above the ground-layer level (= invert level + ground-layer thickness), since such situation can result in very small computational time-steps (e.g. long required wall-clock times) or even in a termination of the simulation.

This is explained as follows. Consider the situation depicted in Figure 1.40 where the bed level in front of a Culvert (Inverted Siphon or Siphon) is 0.60 m above the ground-layer level. This means that at small upstream water depths, water will be sucked into the culvert (Inverted Siphon or Siphon), resulting in large flow velocities. For the computational time-step ( $\Delta t$ ) yields that  $\Delta t \leq \Delta x / U$ , where  $U$  is the local flow velocity and  $\Delta x$  is distance between two water level computational points (or h-points). At very low discharges even negative water depths may be computed, leading to a termination of the simulation.

The situation explained above can be avoided by making the bed level in front of the Culvert (Inverted Siphon or Siphon) equal to the ground-layer level. In other words by defining a bed level slope from h-point  $h_2$  to  $h_3$  as depicted in Figure 1.40. Providing for the parameter "Maximum Lowering of Cross-section Bed Level at Culvert" a value greater or equal to 0.60 m means that before the computation starts, the bed level at h-point  $h_3$  is set equal to the ground-layer level. In ?? it is shown how to provide a value for parameter "Maximum Lowering of Cross-section Bed Level at Culvert".

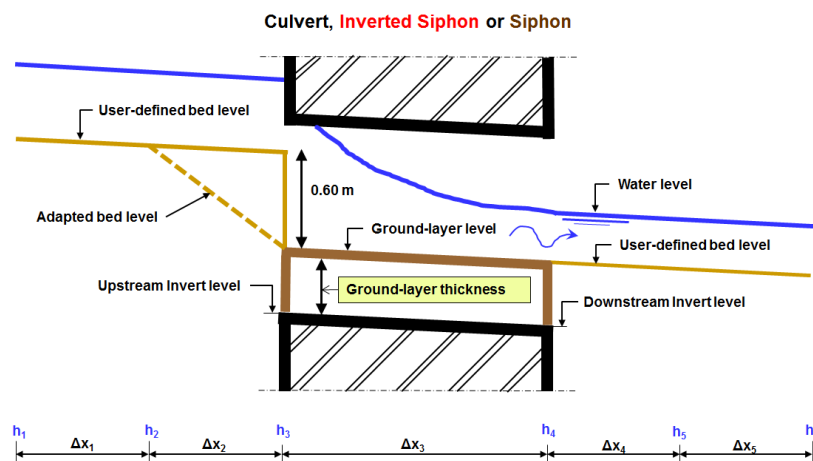


**Figure 1.27:** Good modelling practice, Culvert, Inverted Siphon and Siphon

### 1.1.16.8 Orifice

The geometrical shape of an orifice is given in [Figure 1.28](#). Four different types of orifice flow can be discerned, viz: free weir flow, submerged weir flow, free gate flow and submerged gate flow. No discharge flows through the orifice if its gate is closed, if the upstream water level equals the downstream water level or if both the upstream water level and the downstream water level are below the crest level.

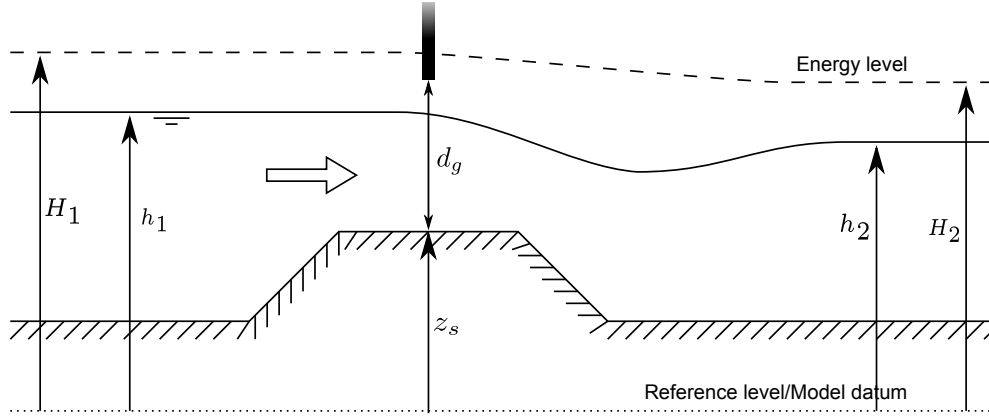


Figure 1.28: Orifice

The following discharge equations are applied:

◇ Free weir flow:

$$A_f = W_s \frac{2}{3} (h_1 - z_s) \quad (1.101)$$

$$Q = c_w W_s \frac{2}{3} \sqrt{\frac{2}{3} g} (h_1 - z_s)^{3/2} \quad (1.102)$$

◇ Submerged weir flow:

$$A_f = W_s \left( h_1 - z_s - \frac{u_s^2}{2g} \right) \quad (1.103)$$

$$Q = c_e c_w W_s \left( h_1 - z_s - \frac{u_s^2}{2g} \right) \sqrt{2g(h_1 - h_2)} \quad (1.104)$$

◇ Free gate flow:

$$A_f = W_s \mu d_g \quad (1.105)$$

$$Q = c_w W_s \mu d_g \sqrt{2g(h_1 - (z_s + \mu d_g))} \quad (1.106)$$

◇ Submerged gate flow:

$$A_f = W_s \mu d_g \quad (1.107)$$

$$Q = c_w W_s \mu d_g \sqrt{2g(h_1 - h_2)} \quad (1.108)$$

$Q$	Discharge across orifice [ $m^3/s$ ]
$A_f$	Flow area [ $m^2$ ]
$\mu$	Contraction coefficient [—] Normally 0.63
$c_w$	Lateral contraction coefficient [—]

$c_e$	Discharge coefficient [—]
$W_s$	Crest width [m]
$d_g$	Opening height [m] (gate lower edge level minus crest level)
$g$	Gravity acceleration [ $m/s^2$ ] ( $\approx 9.81$ )
$h_1$	Upstream water level [m]
$h_2$	Downstream water level [m]
$z_s$	Crest level [m]
$u_s$	Velocity over crest [m/s]

The different formulas are applied when the following conditions are met

◇ Free weir flow:

$$h_1 - z_s < \frac{3}{2}d_g \quad \text{and} \quad h_1 - z_s > 3/2(h_2 - z_s) \quad (1.109)$$

◇ Submerged weir flow:

$$h_1 - z_s < \frac{3}{2}d_g \quad \text{and} \quad h_1 - z_s \leq \frac{3}{2}(h_2 - z_s) \quad (1.110)$$

◇ Free gate flow:

$$h_1 - z_s \geq \frac{3}{2}d_g \quad \text{and} \quad h_2 \leq z_s + d_g \quad (1.111)$$

◇ Submerged gate flow:

$$h_1 - z_s \geq \frac{3}{2}d_g \quad \text{and} \quad h_2 > z_s + d_g \quad (1.112)$$

#### 1.1.16.9 Pump station and Internal Pump station

The functionality of a Pump station and an Internal Pump station is identical. The only difference comprises the fact that:

- ◇ Pump station: A Pump station is located on an open channel reach. The pump discharge is determined using the water levels at the nearest  $h$ -calculation points, respectively located at the upstream-side and downstream-side of the Pump station.
- ◇ Internal Pump station: An Internal Pump station is accommodated in a pipe. The pump discharge is determined using the water levels (or hydrostatic pressure heads) at the upstream side of the pipe and at the downstream side of the pipe.

Here after, both the Pump station and the Internal Pump station are referred to as the Pump station. Please note that:

- ◇ When activated, water is always pumped from the suction-side towards the delivery-side,
- ◇ A Pump station cannot be placed in a compound structure,
- ◇ A Time Controller, Hydraulic controller, a PID controller or an Interval controller can overrule the pump capacity of a Pump station.
- ◇ Pump station output parameters becomes available by checking the Pump Data check-box on the 1DFLOW/Output options/Structures Tab in Settings.

#### Pump direction

- ◇ Positive pump direction means that the pump discharge is flowing in the positive  $x$ -direction along a reach (see [Figure 1.29](#)). Hence, water is pumped in downstream direction towards the pump-side with the highest  $x$ -coordinate.

- ◇ Negative pump direction means that the pump discharge is flowing in the negative  $x$ -direction along a reach (see Figure 1.30). Hence, water is pumped in upstream direction towards the pump-side with the lowest  $x$ -coordinate.

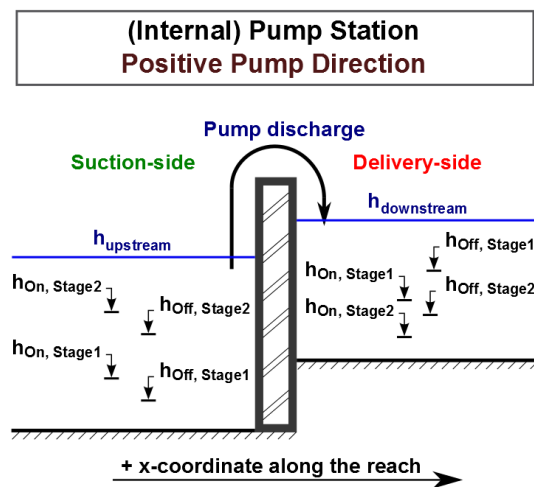


**Figure 1.29:** Pump station with positive pump direction and two pump stages

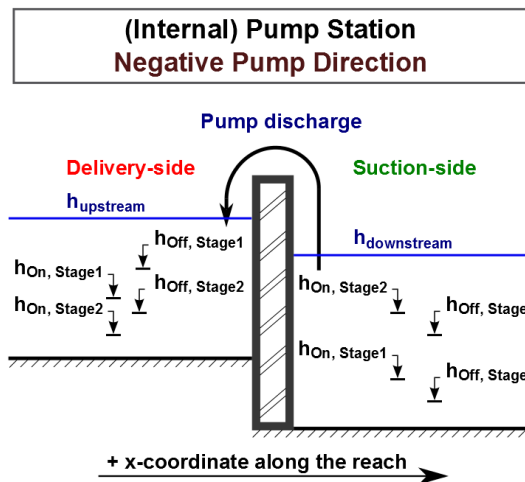


**Figure 1.30:** Pump station with negative pump direction and two pump stages

### Six possible pump stages

A Pump station comprises of one (1) pump only, which can have up to six different pump stages (1, 2, 3, 4, 5 or 6). Each pump stage can have a different pump capacity. At each point-in-time, the pump can be in one (1) particular pump stage only.

### The actual pump stage

The actual pump stage is determined using dead-band triggers, defined either at the suction-side only, at the delivery-side only or both at the suction-side and the delivery-side of the pump. At the beginning of each time-step for all pump stages, the status [On/Off] of their dead-band trigger at the suction-side (if defined) and their dead-band trigger at the delivery-side (if defined) are evaluated. This evaluation is done on basis of actual water levels and the Switch-on and Switch-off levels, defined for the concerning pump stage. For more details, see dead-band trigger algorithm. For more information on how to define Switch-on and Switch-off levels at the suction-side and the delivery-side of the pump, see Conventions for switch-on and switch-off levels. The actual pump stage, applied in the time-step from  $t=t$  to  $t=t+dt$ , is the number of the highest pump stage (1, 2, 3, 4, 5 or 6) that is triggered at  $t=t$ , meaning that all its dead-band triggers have the status [On]. If not any pump stage is triggered, the pump becomes inactive (pump discharge is zero) and the actual pump stage is set to 0. If the pump is overruled by a controller, the actual pump stage is set to -1.

## Controllers

A Time-controller, a Hydraulic-controller, a PID controller or an Interval controller can be assigned to a pump station. A controller is only active in case the pump is triggered in accordance with the Switch-on and Switch-off levels, defined for stage 1. An active controller overrules the pump capacity of the triggered pump stage, while the actual pump stage is set to -1. Please note that capacity reduction factors are applied to the pump capacities set by a controller. Advice: In using a controller at a pump station, define only one (1) pump stage and take care that its dead-band trigger is always [On].

## Capacity reduction table

A capacity reduction table can be defined, which is applied to all pump stages as well as to pump capacities, that are set by a controller. In the capacity reduction table a capacity reduction factor can be given as function of the pump head (e.g. water level at delivery-side minus water level at suction-side). Pump heads (first column) in a capacity reduction table should be in increasing order. Capacity reduction factors should be equal or larger than 0. The pump discharge equals the pump capacity times the capacity reduction factor. If no capacity reduction table is defined in effect a capacity reduction factor equal to 1 is applied. Please note that the pump head at  $t=t$  is used to determine the capacity reduction factor to be applied in the time-step from  $t=t$  to  $t=t+dt$ .

## Pump station output parameters

Pump station output parameters can be viewed in Result in Charts (Pump.his file) by checking the Pump Data check-box on the 1DFLOW/Output options/Structures Tab in Settings. Available pump station output parameters as function of time are:

- ◇ Suction-Side level: Water level at the suction-side of the pump.
- ◇ Delivery-Side level: Water level at the delivery-side of the pump.
- ◇ Pump Head: The water level at the delivery-side of the pump minus the water level at the suction-side of the pump.
- ◇ Actual Pump Stage: Equal to -1 if pump is overruled by a controller; equal to 0 if pump is inactive; or equal to 1, 2, 3, 4, 5 or 6 depending on the actual pump stage that is triggered (see Dead-band triggering algorithm).
- ◇ Pump Capacity: The pump capacity is either defined by its controller; equal to zero if pump is inactive; or equal to the pump capacity defined for the actual pump stage.
- ◇ Reduction Factor: The reduction factor follows from the pump head and the capacity reduction table.
- ◇ Pump Discharge: The pump discharge is equal to the pump capacity times the reduction factor.

## Dead-band triggering algorithm

A distinction is to be made between evaluating the status [On/Off] of dead-band triggers defined at the suction-side of the pump and dead-band triggers defined at the delivery-side of the pump:



### Dead-band triggering at the Suction-side of the pump

Parameters used in determining the status [On/Off] of a suction-side dead-band trigger are  $h_{Suction}$  (water level at the suction-side),  $h_{On,Suction}$  (switch-on-level) and  $h_{Off,Suction}$  (switch-off-level), where  $h_{On,Suction} > h_{Off,Suction}$ . Two booleans are used (e.g.  $S_{On,Suction}$  and  $S_{Off,Suction}$ ):

- ◇ If  $h_{Suction} > h_{On,Suction} \Rightarrow S_{On,Suction} = True; Else S_{On,Suction} = False$
- ◇ If  $h_{Suction} < h_{Off,Suction} \Rightarrow S_{Off,Suction} = True; Else S_{Off,Suction} = False$

If at the start of a computation yields that  $h_{Off,Suction} \leq h_{Suction} \leq h_{On,Suction}$  the dead-band trigger is set [On]. During a computation the dead-band trigger is set [On] or [Off] according to the following rules:

- ◇ If ( $S_{On,Suction} = True$  and  $S_{Off,Suction} = False$ )  $\Rightarrow Trigger = [On]$
- ◇ If ( $S_{On,Suction} = False$  and  $S_{Off,Suction} = True$ )  $\Rightarrow Trigger = [Off]$
- ◇ If ( $S_{On,Suction} = False$  and  $S_{Off,Suction} = False$ )  $\Rightarrow Trigger$  obtains the status determined in the previous computational time step.

### Dead-band triggering at the Delivery-side of the pump

Parameters used in determining the status [On/Off] of a delivery-side dead-band trigger are  $h_{Delivery}$  (water level at the delivery-side),  $h_{On,Delivery}$  (switch-on-level),  $h_{Off,Delivery}$  (switch-off-level), where  $h_{Off,Delivery} > h_{On,Delivery}$ . Two booleans are used (e.g.  $S_{On,Delivery}$  and  $S_{Off,Delivery}$ ):

- ◇ If  $h_{Delivery} < h_{On,Delivery} \Rightarrow S_{On,Delivery} = True; Else S_{On,Delivery} = False$
- ◇ If  $h_{Delivery} > h_{Off,Delivery} \Rightarrow S_{Off,Delivery} = True; Else S_{Off,Delivery} = False$

If at the start of a computation yields that  $h_{On,Delivery} \leq h_{Delivery} \leq h_{Off,Delivery}$  the dead-band trigger is set [On]. During a computation the dead-band trigger is set [On] or [Off] according to the following rules:

- ◇ If ( $S_{On,Delivery} = True$  and  $S_{Off,Delivery} = False$ )  $\Rightarrow Trigger = [On]$
- ◇ If ( $S_{On,Delivery} = False$  and  $S_{Off,Delivery} = True$ )  $\Rightarrow Trigger = [Off]$
- ◇ If ( $S_{On,Delivery} = False$  and  $S_{Off,Delivery} = False$ )  $\Rightarrow Trigger$  obtains the status determined in the previous computational time step

### Conventions for switch-on and switch-off levels

A distinction is to be made between switch-on-levels and switch-off-levels, defined at the suction-side and defined at the delivery-side of the pump (see [Table 1.3](#)).

- ◇ Suction-side: The switch-on level should increase with increasing stage number. For each stage, its switch-off-level should be lower than its switch-on-level. The switch-off-level should increase with increasing stage number.
- ◇ Delivery-side: The switch-on-level should decrease with increasing stage number. For each stage, its switch-off-level should be higher than its switch-on-level. The switch-off-level should decrease with increasing stage number.

**Table 1.3:** Example of switch-on-levels and switch-off-levels at the suction-side and the delivery-side of a pump station

Pump		Suction-side		Delivery-side	
Stage	Capacity	Switch-on-level	Switch-off-level	Switch-on-level	Switch-off-level
$No$	$m^3/s$	$m$	$m$	$m$	$m$
1	0.1	0.80	0.10	0.80	1.90
2	0.2	0.90	0.20	0.70	1.80
3	0.3	1.00	0.30	0.60	1.70
4	0.4	1.10	0.40	0.50	1.60
5	0.5	1.20	0.50	0.40	1.50
6	0.6	1.30	0.60	0.30	1.40

**1.1.16.10 External Pump station**

An External Pump station is located at the end of an open channel reach or at the end of a (closed) pipe. The end of an open channel reach can either have the highest  $x$ -coordinate or an  $x$ -coordinate equal to zero. The same applies for a pipe. The pump discharge is either determined using the boundary water level and the water level at the reach-side of the pump or determined using the boundary water level and the water level (or hydrostatic pressure head) at the pipe-side of the pump. Please note that:

- ◇ When activated, water is always pumped from the suction-side towards the delivery-side.
- ◇ Water can be stored at an External Pump station, for more information see Storage options at an External Pump station.
- ◇ The External Pump station cannot be placed in a compound structure,
- ◇ A Time Controller, Hydraulic controller, a PID controller or an Interval controller can overrule the pump capacity of an External Pump station.
- ◇ External Pump station output parameters becomes available by checking the Pump Data check-box on the 1DFLOW/Output options/Structures Tab in Settings.

**External Pump direction:**

- ◇ Pump direction IN means that (see [Figure 1.31](#)):
  - Water is pumped into the model or flows towards the reach/pipe-side (or upstream-side) of the pump,
  - The pump discharge has a negative sign, this is irrespective of the  $x$ -direction along the reach (or pipe).
- ◇ Pump direction OUT means that (see [Figure 1.32](#)):
  - Water is pumped out off the model or flows towards the boundary-side (or downstream-side) of the pump ,
  - The pump discharge has a positive sign, this is irrespective of the  $x$ -direction along the reach (or pipe).

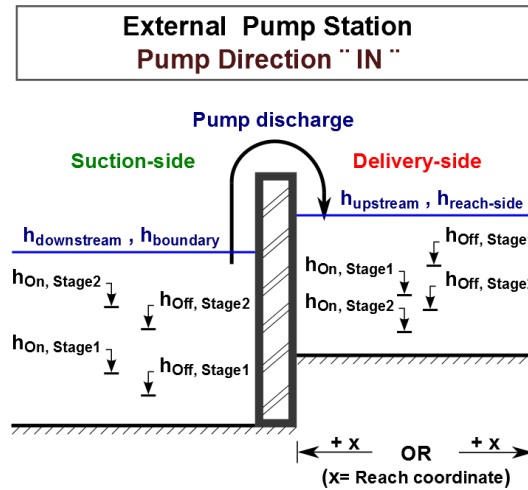


**Figure 1.31:** External pump station with pump direction IN and two pump stages

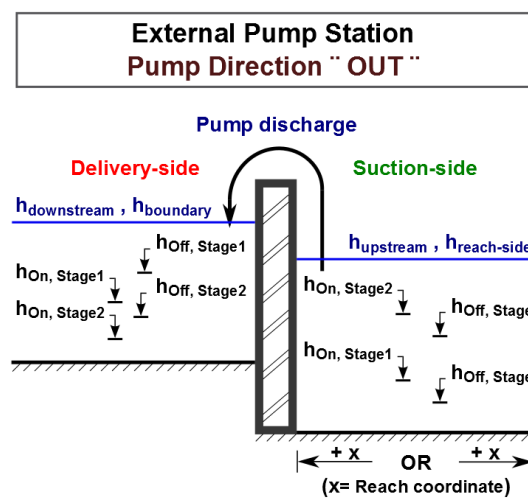


**Figure 1.32:** External pump station with pump direction OUT and two pump stages

**Six possible External Pump stages**

An External Pump station comprises of one (1) pump only, which can have up to six different pump stages (1, 2, 3, 4, 5 or 6). Each pump stage can have a different pump capacity. At each point-in-time, the pump can be in one (1) particular pump stage only.

**The actual pump stage**

The actual pump stage is determined using dead-band triggers, defined either at the suction-side only, at the delivery-side only or both at the suction-side and the delivery-side of the pump. At the beginning of each time-step for all pump stages, the status [On/Off] of their dead-band trigger at the suction-side (if defined) and their dead-band trigger at the delivery-side (if defined) are evaluated. This evaluation is done on basis of actual water levels and the Switch-on and Switch-off levels, defined for the concerning pump stage. For more details, see dead-band trigger algorithm. For more information on how to define Switch-on and Switch-off levels at the suction-side and the delivery-side of the External Pump station, see Conventions for switch-on and switch-off levels. The actual pump stage, applied in the time-step from  $t=t$  to  $t=t+dt$ , is the number of the highest pump stage (1, 2, 3, 4, 5 or 6) that is triggered at  $t=t$ , meaning that all its dead-band triggers have the status [On]. If not any pump stage is triggered, the pump becomes inactive (pump discharge is zero) and the actual pump stage is set to 0. If the pump is overruled by a controller, the actual pump stage is set to -1.

**Controllers**

A Time-controller, a Hydraulic-controller, a PID controller or an Interval controller can be assigned to an External Pump station. A controller is only active in case the pump is triggered in accordance with the Switch-on and Switch-off levels, defined for stage 1. An active controller overrules the pump capacity of the triggered pump stage, while the actual pump stage is set to -1. Please note that capacity reduction factors are applied to the pump capacities set by a controller. Advice: In using a controller at an External Pump station, define only one (1) pump stage and take care that its dead-band trigger is always [On].

**Capacity reduction table**

A capacity reduction table can be defined, which is applied to all pump stages as well as to pump capacities, that are set by a controller. In the capacity reduction table a capacity reduction factor can be given as function of the pump head (e.g. water level at delivery-side minus water level at suction-side). Pump heads (first column) in a capacity reduction table should be in increasing order. Capacity reduction factors should be equal or larger than 0. The pump discharge equals the pump capacity times the capacity reduction factor. If no capacity reduction table is defined in effect a capacity reduction factor equal to 1 is applied. Please note that the pump head at  $t=t$  is used to determine the capacity reduction factor to be applied in the time-step from  $t=t$  to  $t=t+dt$ .

### External Pump station output parameters

External Pump station output parameters can be viewed in Result in Charts (Pump.his file) by checking the Pump Data check-box on the 1DFLOW/Output options/Structures Tab in Settings. Available External pump station output parameters as function of time are:

- ◇ Suction-Side level: Water level at the suction-side of the pump.
- ◇ Delivery-Side level: Water level at the delivery-side of the pump.
- ◇ Pump Head: The water level at the delivery-side of the pump minus the water level at the suction-side of the pump.
- ◇ Actual Pump Stage: Equal to -1 if pump is overruled by a controller; equal to 0 if pump is inactive; or equal to 1, 2, 3, 4, 5 or 6 depending on the actual pump stage that is triggered (see Dead-band triggering algorithm).
- ◇ Pump Capacity: The pump capacity is either defined by its controller; equal to zero if pump is inactive; or equal to the pump capacity defined for the actual pump stage.
- ◇ Reduction Factor: The reduction factor follows from the pump head and the capacity reduction table.
- ◇ Pump Discharge: The pump discharge is equal to the pump capacity times the reduction factor.

### Dead-band triggering algorithm

A distinction is to be made between evaluating the status [On/Off] of dead-band triggers defined at the suction-side of the External Pump station and dead-band triggers defined at the delivery-side of the External Pump station:

#### Dead-band triggering at the Suction-side of the External Pump station:

Parameters used in determining the status [On/Off] of a suction-side dead-band trigger are  $h_{Suction}$  (water level at the suction-side),  $h_{On,Suction}$  (switch-on-level) and  $h_{Off,Suction}$  (switch-off-level), where  $h_{On,Suction} > h_{Off,Suction}$ . Two booleans are used (e.g.  $S_{On,Suction}$  and  $S_{Off,Suction}$ ):

- ◇ If  $h_{Suction} > h_{On,Suction} \Rightarrow S_{On,Suction} = True; Else S_{On,Suction} = False$
- ◇ If  $h_{Suction} < h_{Off,Suction} \Rightarrow S_{Off,Suction} = True; Else S_{Off,Suction} = False$

If at the start of a computation yields that  $h_{Off,Suction} \leq h_{Suction} \leq h_{On,Suction}$  the dead-band trigger is set [On]. During a computation the dead-band trigger is set [On] or [Off] according to the following rules:

- ◇ If ( $S_{On,Suction} = True$  and  $S_{Off,Suction} = False$ )  $\Rightarrow Trigger = [On]$
- ◇ If ( $S_{On,Suction} = False$  and  $S_{Off,Suction} = True$ )  $\Rightarrow Trigger = [Off]$
- ◇ If ( $S_{On,Suction} = False$  and  $S_{Off,Suction} = False$ )  $\Rightarrow Trigger$  obtains the status determined in the previous computational time step.

#### Dead-band triggering at the Delivery-side of the External Pump station:

Parameters used in determining the status [On/Off] of a delivery-side dead-band trigger are  $h_{Delivery}$  (water level at the delivery-side),  $h_{On,Delivery}$  (switch-on-level),  $h_{Off,Delivery}$  (switch-off-level), where  $h_{Off,Delivery} > h_{On,Delivery}$ . Two booleans are used (e.g.  $S_{On,Delivery}$  and  $S_{Off,delivery}$ ):

- ◇ If  $h_{Delivery} < h_{On,Delivery} \Rightarrow S_{On,Delivery} = True$ ; Else  $S_{On,Delivery} = False$
- ◇ If  $h_{Delivery} > h_{Off,Delivery} \Rightarrow S_{Off,Delivery} = True$ ; Else  $S_{Off,Delivery} = False$

If at the start of a computation yields that  $h_{On,Delivery} \leq h_{Delivery} \leq h_{Off,Delivery}$  the dead-band trigger is set [On]. During a computation the dead-band trigger is set [On] or [Off] according to the following rules:

- ◇ If  $(S_{On,Delivery} = True \text{ and } S_{Off,Delivery} = False) \Rightarrow Trigger = [On]$
- ◇ If  $(S_{On,Delivery} = False \text{ and } S_{Off,Delivery} = True) \Rightarrow Trigger = [Off]$
- ◇ If  $(S_{On,Delivery} = False \text{ and } S_{Off,Delivery} = False) \Rightarrow Trigger$  obtains the status determined in the previous computational time step

### Conventions for switch-on and switch-off levels

A distinction is to be made between switch-on-levels and switch-off-levels, defined at the suction-side and defined at the delivery-side of the External Pump station (see [Table 1.4](#)).

- ◇ Suction-side: The switch-on level should increase with increasing stage number. For each stage, its switch-off-level should be lower than its switch-on-level. The switch-off-level should increase with increasing stage number.
- ◇ Delivery-side: The switch-on-level should decrease with increasing stage number. For each stage, its switch-off-level should be higher than its switch-on-level. The switch-off-level should decrease with increasing stage number.

**Table 1.4:** Example of switch-on-levels and switch-off-levels at the suction-side and the delivery-side of an external pump station

Pump		Suction-side		Delivery-side	
Stage	Capacity	Switch-on-level	Switch-off-level	Switch-on-level	Switch-off-level
<i>No</i>	$m^3/s$	<i>m</i>	<i>m</i>	<i>m</i>	<i>m</i>
1	1.1	1.80	1.10	2.80	3.90
2	2.2	1.90	1.20	2.70	3.80
3	3.3	2.00	1.30	2.60	3.70
4	4.4	2.10	1.40	2.50	3.60
5	5.5	2.20	1.50	2.40	3.50
6	6.6	2.30	1.60	2.30	3.40

### Storage options at an External Pump station

Water can be stored at the site, accommodating an external pump station. In SOBEK a distinction is made between water stored below and above a certain design level, hereafter referred to as street level.

- ◇ Below street level: At water levels below street level, water is considered to be stored in a so-called bottom-storage-reservoir.
- ◇ Above street level: For water levels above street level, there are three options:
  - Water is stored in a street-level-reservoir, having a bed level equal to street level and walls that cannot be overtopped;
  - Water cannot be stored (e.g. closed pump station), hence water levels inside the pump station may become pressurized; and
  - Water leaves the external pump station (e.g. loss of water) by flowing towards low lying areas, while the water level inside the pump station is considered to remain at street level.

#### 1.1.16.11 River Pump

The River Pump is to be located on an open channel reach. Please note that:

- ◇ When activated, water is always pumped from the suction-side towards the delivery-side.
- ◇ The River “Pump” can be placed in a compound structure.
- ◇ Controllers cannot be assigned to a River “Pump”,
- ◇ Flow “ $h$ ”-calculation points are default located 0.5 m in front and 0.5 m behind a River “Pump”.
- ◇ River pump output parameters becomes available by checking the Pump Data check-box on the 1DFLOW/Output options/Structures Tab in Settings.

#### Control direction determines location of trigger-water-level ( $h_{trig}$ ) of a River pump:

The control direction of the River pump defines the location of the so-called trigger-water-level ( $h_{trig}$ ):

- ◇ Upward control direction means that the trigger water level ( $h_{trig}$ ) is located upward, e.g. at the pump-side with the lowest  $x$ -coordinate along the reach.
- ◇ Downward control direction means that the trigger water level ( $h_{trig}$ ) is located downward, e.g. at the pump-side with the highest  $x$ -coordinate along the reach.

#### Start-level and stop-level determine location of the suction-side and the delivery-side:

The elevation of the start-level ( $h_{start}$ ) and the elevation of the stop-level ( $h_{stop}$ ) define the location of the suction-side and the delivery-side of a river pump as follows:

- ◇ If start-level is above stop-level: water is pumped away from the trigger-water-level side of the pump (e.g. trigger-water-level side coincides with the suction-side of the pump).
- ◇ If stop-level is above start-level: water is pumped towards the trigger-water-level side of the pump (e.g. trigger-water-level side coincides with the delivery-side of the pump).

**Discharge direction of a River pump:**

The discharge direction of a river pump with respect to the positive  $x$ -direction along the reach is defined by the control direction and the elevations of the start-level and the stop-level. Four different situations can be discerned:

- ◇ Upward control and start-level above stop-level (see [Figure 1.33](#)),
- ◇ Upward control and stop-level above start-level (see [Figure 1.34](#)),
- ◇ Downward control and start-level above stop-level (see [Figure 1.35](#)),
- ◇ Downward control and stop-level below start-level (see [Figure 1.36](#)),

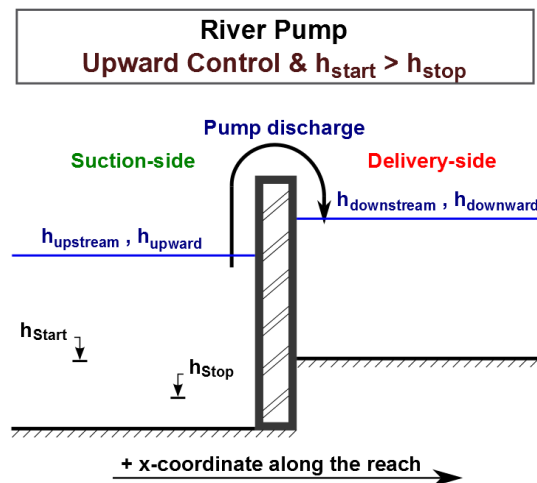


**Figure 1.33:** River pump with Upward control and start-level above stop-level



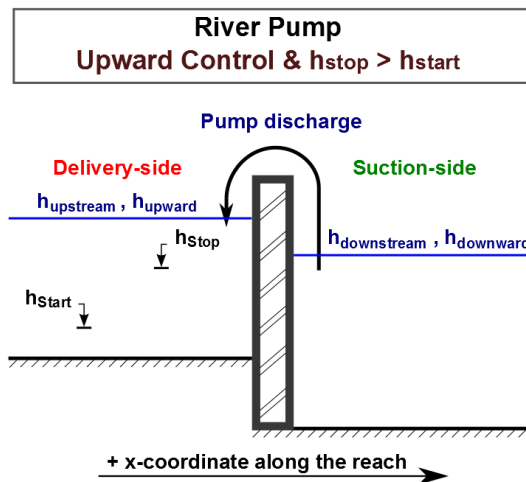


**Figure 1.34:** River pump with Upward control and stop-level above start-level

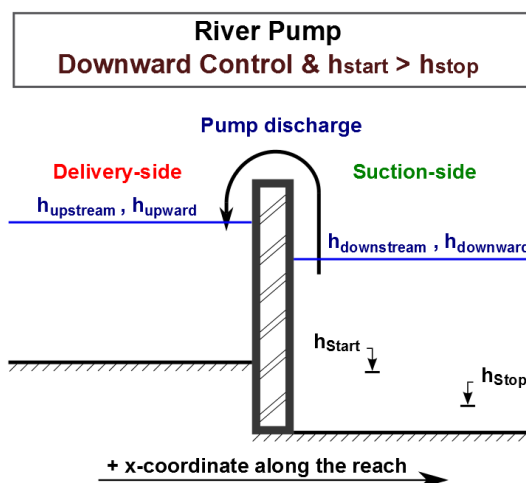


**Figure 1.35:** River pump with Downward control and start-level above stop-level

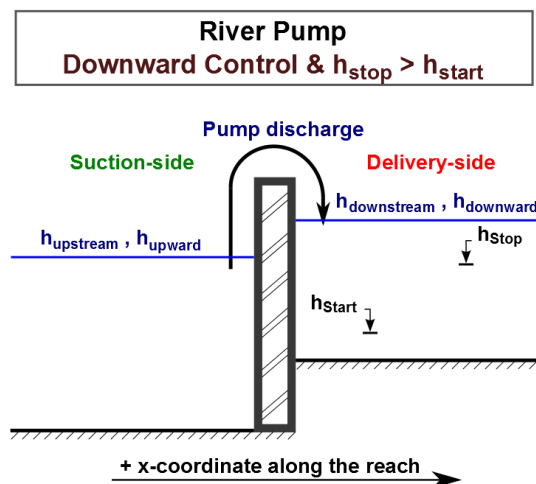


**Figure 1.36:** River pump with Downward control and stop-level above start-level

### River pump stages

A River pump has only one pump stage, hence only one pump capacity can be defined.

### Constant Reduction Factor or Reduction Factor F(Pump Head)

- ◇ **Constant Reduction Factor:** WARNING: This means that irrespective of the pump head, the actual pump capacity always equals the defined pump capacity times the constant reduction factor. Say you defined a pump capacity of  $100 \text{ m}^3/\text{s}$  and constant reduction factor of 0.7. This means that the pump will have a capacity of  $70 (=0.7 \cdot 100) \text{ m}^3/\text{s}$  for both positive and negative pump heads.
- ◇ **Reduction Factor F(Pump Head):** With this option you define a capacity reduction factor as function of the pump head (e.g. water level at the delivery-side minus the water level at the suction-side). The capacity reduction factor may vary between 0 and 1. The first row in the F(Pump Head) table should read 0,1 (pump head, capacity reduction factor). For positive pump-heads, the pump discharge equals the pump capacity times the capacity reduction factor. For negative pump-heads a capacity reduction factor equal to 1 is applied. Please note that the pump head at  $t = t^n$  is used to determine the capacity reduction factor to be applied in the time-step from  $t = t^n$  to  $t = t^n + \Delta t$ .

### River pump output parameters

River pump output parameters can be viewed in Result in Charts (<Pump.his> file) by checking the Pump Data check-box on the 1DFLOW/Output options/Structures Tab in Settings. Available River pump output parameters as function of time are:

- ◇ Suction-Side level: Water level at the suction-side of the pump.
- ◇ Delivery-Side level: Water level at the delivery-side of the pump.
- ◇ Pump Head: The water level at the delivery-side of the pump minus the water level at the suction-side of the pump.
- ◇ Actual Pump Stage: Equal to 0 if pump is inactive; or equal to 1 if the pump is triggered (Please note that a river pump has one pump stage only).
- ◇ Pump Capacity: The pump capacity is either equal to zero if pump is inactive; or equal to its defined pump capacity.
- ◇ Reduction Factor: The reduction factor is either a constant or follows from the F(Pump Head) table
- ◇ Pump Discharge: The pump discharge is equal to the pump capacity times the reduction factor.

### Dead-band triggering algorithm

A dead-band trigger [On/Off] determines if the River Pump should pump (e.g. actual pump stage = 1) or not pump (e.g. pump discharge is zero; actual pump stage = 0). The actual status [On/Off] of the dead-band trigger is determined as follows. Firstly, the value of two Booleans ( $S_{on}$  and  $S_{off}$ ) is determined. In case of triggering at the suction-side of the pump, or in other words if the start-level ( $h_{Start}$ ) is above the stop-level ( $h_{Stop}$ ) yields (see [Figure 1.33](#) and [Figure 1.35](#)):

- ◇ If  $h_{trig} > h_{Start} \Rightarrow S_{on} = True; \quad Else \quad S_{on} = False$
- ◇ If  $h_{trig} < h_{Stop} \Rightarrow S_{off} = True; \quad Else \quad S_{off} = False$

In case of triggering at the delivery-side of the pump, or in other words if the stop-level ( $h_{Stop}$ ) is above the start-level ( $h_{Start}$ ) yields (see [Figure 1.34](#) and [Figure 1.36](#)):

- ◇ If  $h_{trig} < h_{Start} \Rightarrow S_{on} = True; \quad Else \quad S_{on} = False$
- ◇ If  $h_{trig} > h_{Stop} \Rightarrow S_{off} = True; \quad Else \quad S_{off} = False$

If at the start of a computation yields that  $h_{stop} \leq h_{trig} \leq h_{off}$ , the dead-band trigger is set [On]. During a computation the dead-band trigger is set [On] or [Off] according to the following algorithm

- ◇ If ( $S_{on} = True$  and  $S_{off} = False$ )  $\Rightarrow Trigger = [On]$
- ◇ If ( $S_{on} = False$  and  $S_{off} = True$ )  $\Rightarrow Trigger = [Off]$
- ◇ If ( $S_{on} = False$  and  $S_{off} = False$ )  $\Rightarrow Trigger$  obtains the status determined in the previous computational time step

### Comparing a River Pump and a Pump station:

- ◇ From a pump direction point of view the Pump station covers the options available at a River Pump (see [Table 1.5](#)).
- ◇ Advantage of the River Pump over a Pump station is the fact that it can be placed in a compound structure
- ◇ Limitations of the River Pump with respect to the Pump station:
  - No controllers can be assigned,
  - Only one (1) pump stage can be defined,

- Only one (1) dead-band trigger can be defined at a River Pump, hence it is not possible to operate the pump on basis of water levels at both its suction-side and its delivery-side.

**Table 1.5:** Flow-Pump station covers the options of a River pump with respect to the pump direction

River pump		Pump station	
Control Direction	Start-level ( $h_{start}$ ) Stop-level ( $h_{stop}$ )	Pump Direction	Triggering at
Upward	$h_{start} > h_{stop}$	Positive	Suction-side
Upward	$h_{stop} > h_{start}$	Negative	Delivery-side
Downward	$h_{start} > h_{stop}$	Negative	Suction-side
Downward	$h_{stop} > h_{start}$	Positive	Delivery-side

#### 1.1.16.12 River Weir

Please note that discharges are computed on basis of upstream and downstream energy levels. Further on please note that default a computational point is located 0.5 m in front and 0.5 m behind a River weir. A structure inertia damping factor can be defined for each individual River weir.

Two types of flow conditions can occur in the case of weir flow. These are free (modular) flow and drowned (submerged) flow. If high tail water conditions do affect the flow, the weir is said to be drowned. These conditions may then be computed by applying a reduction factor to the modular function, i.e. to the equation applied if the weir or flume is not drowned ([Ackers et al., 1978](#); [Schmidt, 1955](#); [Bos, 1989](#)).

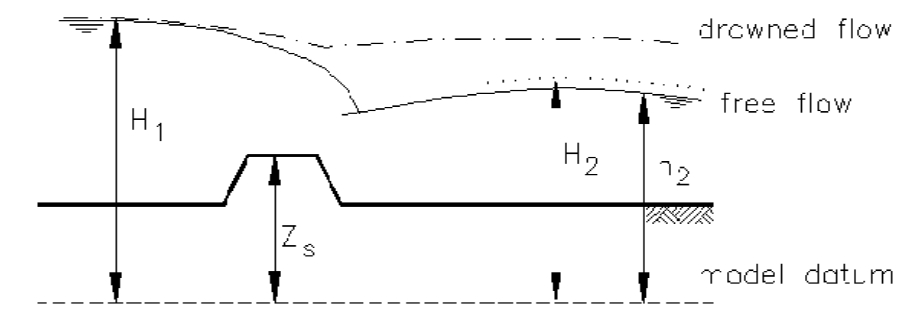


**Figure 1.37:** Free and drowned weir flow

The discharge through the weir is computed with:

$$Q = c_w f W_s \frac{2}{3} \sqrt{\frac{2}{3} g} (H_1 - Z_s)^{3/2} \quad (1.113)$$

in which:

$c_w$       correction coefficient  
 $W_s$       width across flow section  
 $H_1$       upstream energy level

$f_s$  drowned flow reduction factor  
 $Z_s$  crest or sill level of weir

The submergence factor of the weir is defined as:

$$S_f = \frac{H_2 - Z_s}{H_1 - Z_s} \quad (1.114)$$

in which:

$S_f$  submergence factor  
 $H_2$  downstream energy level

If the actual submergence factor exceeds the submergence limit, drowned flow occurs. In all other cases modular flow occurs and a drowned flow reduction factor equal to 1.0 should be applied. The submergence limit depends on the crest shape (see [Table 1.6](#)).

For a weir the user must specify:

- ◇ level of crest or crest height
- ◇ crest width across flow section
- ◇ crest shape (broad, triangular, round, or sharp)

Depending on the crest shape the following parameters are used ([Table 1.6](#)), which can be adjusted by the user:

- ◇ correction coefficient (default see [Table 1.6](#))
- ◇ submergence limit (default see [Table 1.6](#))
- ◇ drowned flow reduction curve (default see [Table 1.6](#))

**Table 1.6:** Crest shape and coefficients for simple weir structure (default values)

Crest shape	Correction coef.	Submergence limit	Reduction curve ( <a href="#">Figure 1.38</a> )
broad	1.0	0.82	1
triangular	1.05	0.67	2
round	1.1	0.3	4
sharp	1.2	0.01	5

#### Notes:

- ◇ If only one flow direction has been specified, the coefficients for that flow direction are used as default coefficients for the other flow direction.
- ◇ The default drowned flow reduction curve depends on the submergence limit.

The drowned flow reduction curve is stored in tabulated format.

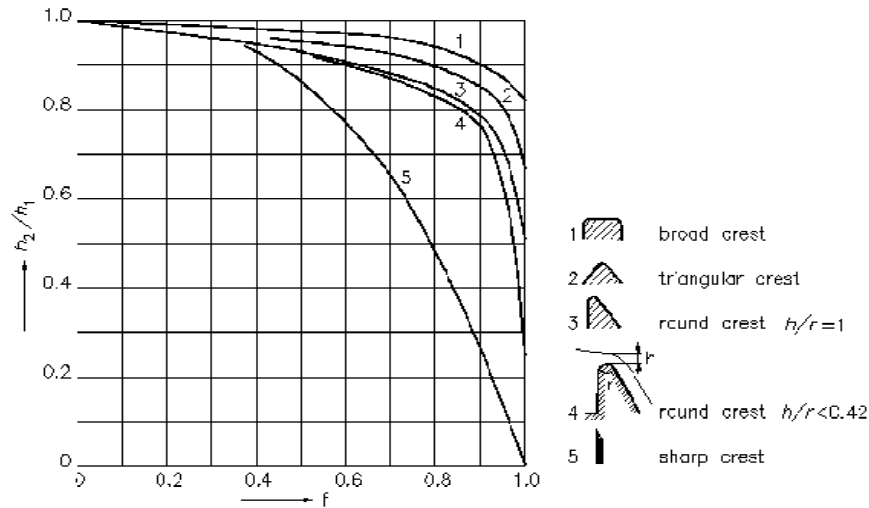


**Figure 1.38:** Drowned flow reduction curves

### 1.1.16.13 Siphon

A siphon (see [Figure 1.39](#)) can only transport water from its upstream defined side to its downstream defined side. **Hence, only positive flow is possible.**

A switch-on-level and a switch-off-level at its downstream side determine if the siphon may or may not discharge water. If the downstream water level drops below the switch-on-level, the siphon start discharging water. If the downstream water level rises above the switch-off-level, the siphon stops discharging water. If the downstream water level is in between the switch-on-level and the switch-off-level (e.g. in between its dead-band), the siphon remains in its present state of operation. In case the downstream water level is in its dead-band at the onstart of a computation, the siphon will start discharging water.

Discharge can only flow through a siphon if its upstream cross-sectional area is fully filled with water, meaning that the upstream water level is above the obvert level (invert level + inner cross-sectional height) of the siphon. If the upstream cross-sectional area is not fully filled with water, air will be contained in the upper part of the siphon, this air will prevent the siphon from discharging water.

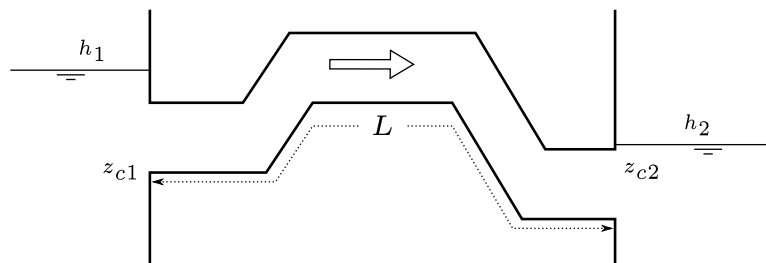


**Figure 1.39:** Siphon

Two flow conditions can occur:

Free flow when  $h_2 < z_{c2} + d_{c2}$

$$Q = \mu A_{fs} \sqrt{2g(h_1 - (z_{c2} + d_{c2}))} \quad (1.115)$$

Submerged flow when  $h_2 \geq z_{c2} + d_{c2}$ :

$$Q = \mu A_{fs} \sqrt{2g(h_1 - h_2)} \quad (1.116)$$

$Q$	Discharge through siphon [ $m^3/s$ ]
$\mu$	Discharge coefficient, derived from loss-coefficients [—]
$A_{fs}$	Discharge siphon flow area ( $= \min(A_{fcrs}, A_{fsgate})$ ) [ $m^2$ ]
$A_{fcrs}$	Cross-sectional area of the siphon. At its highest point the siphon is considered to be completely filled with water [ $m^2$ ]
$A_{fsgate}$	Flow area under the siphon gate [ $m^2$ ]
$g$	Acceleration due to gravity [ $m/s^2$ ] ( $\approx 9.81$ )
$h_1$	Upstream water level [ $m$ ]
$h_2$	Downstream water level [ $m$ ]
$z_{c2}$	Downstream siphon invert level [ $m$ ]
$d_{c2}$	Critical siphon depth at the downstream side

$$d_{c2} = \sqrt[3]{Q^2 / (g T_2^2)} \quad [m] \quad (1.117)$$

$T_2$  Surface width in the siphon at its downstream side [ $m$ ]

For numerical reasons the discharge coefficient ( $\mu$ ) is limited to a maximum of 1.0. The discharge coefficient ( $\mu$ ) is computed as follows:

$$\mu = \frac{1}{\sqrt{\xi_i + \xi_f + \xi_v + \xi_b + \xi_o}} \quad (1.118)$$

$\xi_i$	Entrance loss coefficient [—]
$\xi_f$	Friction loss coefficient [—]
$\xi_v$	Valve loss coefficient [—]
$\xi_b$	Bend loss coefficient [—]
$\xi_o$	Exit loss coefficient [—]

The entrance loss coefficient ( $\xi_i$ ) can be defined as a constant value only.

The friction loss coefficient ( $\xi_f$ ) is computed as follows:

$$\xi_f = \frac{2gL}{C^2 R} \quad (1.119)$$

$L$	Length of the siphon [ $m$ ]
$C$	Chézy coefficient for fully water filled siphon [ $m^{1/2}/s$ ]
$R$	Hydraulic radius [ $m$ ] If $GHO < MIISH$ ; $R = R_{gate}$ If $GHO \geq MIISH$ ; $R = R_{siphon}$
$GHO$	Gate height opening [ $m$ ]
$MIISH$	Maximum inner inverted siphon height [ $m$ ]
$R_{siphon}$	Hydraulic radius based on a fully water filled siphon [ $m$ ]
$R_{gate}$	Hydraulic radius based on actual gate height opening [ $m$ ]

The valve loss coefficient ( $\xi_v$ ) can be defined as a constant value or as a function of the ratio of the “Gate height opening” and the “maximum inner siphon height”.

**Note:**



- ◇ In case the valve loss coefficient ( $\xi_v$ ) is not a constant, in computations the actual valve loss coefficient ( $\xi_v$ ) is derived from the user defined table, while using the ratio of the “actual gate height opening and the “actual maximum inner siphon height”.
- ◇ In case the ground layer thickness is greater than zero, both the “actual gate height opening” and the “actual maximum inner siphon height” will differ from the values as defined in the user interface (see the paragraph “Siphon cross-sections, bed friction and ground layer” below)

The exit loss coefficient ( $\xi_o$ ) is computed as follows:

Submerged flow ( $h_2 = z_{c2} + d_{c2}$ ):

$$\xi_o = k \left( 1 - \frac{A_{fs}}{A_{fr2}} \right)^2 \quad (1.120)$$

$k$	User defined constant exit loss coefficient [–]
$A_{fr2}$	Flow area in the reach, adjacent to the downstream siphon side [ $m^2$ ]
$A_{fis}$	Siphon flow area [ $m^2$ ] If $GHO \leq MISH$ ; $A_{fs} = A_{fsgate}$ If $GHO > MISH$ ; $A_{fs} = A_{siphon}$
GHO	Gate height opening [ $m$ ]
MISH	Maximum inner siphon height [ $m$ ]
$A_{fsgate}$	Flow area under the siphon gate [ $m^2$ ]
$A_{siphon}$	Flow area based on a fully water filled siphon [ $m^2$ ]

Free flow ( $h_2 < z_{c2} + d_{c2}$ ):

$$\xi_o = 0 \quad (1.121)$$

Siphon cross-sections, bed friction and ground layer:

For a siphon all available closed cross-section types can be used. In a siphon, a ground layer with constant thickness can be defined. Siphon friction and ground layer friction can be specified, using any of the available bed friction formulations.

Defining a ground layer thickness  $> 0$  implies that in siphon computations:

- ◇ Defined invert levels are raised with the ground layer thickness,
- ◇ Gate height openings are reduced with the ground layer thickness,
- ◇ Maximum inner height of the siphon is reduced with the ground layer thickness,
- ◇ Cross-sectional parameters (such as: flow areas, hydraulic radius and so on) are computed based on a cross-sectional profile, that is reduced by the ground layer thickness.

***Siphon, Good modelling practice aspects***

It is advised to avoid that the bed level of a cross-section in front of a Culvert, Inverted Siphon or Siphon is above the ground-layer level (= invert level + ground-layer thickness), since such situation can result in very small computational time-steps (e.g. long required wall-clock times)



or even in a termination of the simulation.

This is explained as follows. Consider the situation depicted in Figure 1.40 where the bed level in front of a Culvert (Inverted Siphon or Siphon) is 0.60 m above the ground-layer level. This means that at small upstream water depths, water will be sucked into the culvert (Inverted Siphon or Siphon), resulting in large flow velocities. For the computational time-step ( $\Delta t$ ) yields that  $\Delta t \leq \Delta x/U$ , where  $U$  is the local flow velocity and  $\Delta x$  is distance between two water level computational points (or h-points). At very low discharges even negative water depths may be computed, leading to a termination of the simulation.

The situation explained above can be avoided by making the bed level in front of the Culvert (Inverted Siphon or Siphon) equal to the ground-layer level. In other words by defining a bed level slope from h-point  $h_2$  to  $h_3$  as depicted in Figure 1.40. Providing for the parameter "Maximum Lowering of Cross-section Bed Level at Culvert" a value greater or equal to 0.60 m means that before the computation starts, the bed level at h-point  $h_3$  is set equal to the ground-layer level. In ?? it is shown how to provide a value for parameter "Maximum Lowering of Cross-section Bed Level at Culvert".

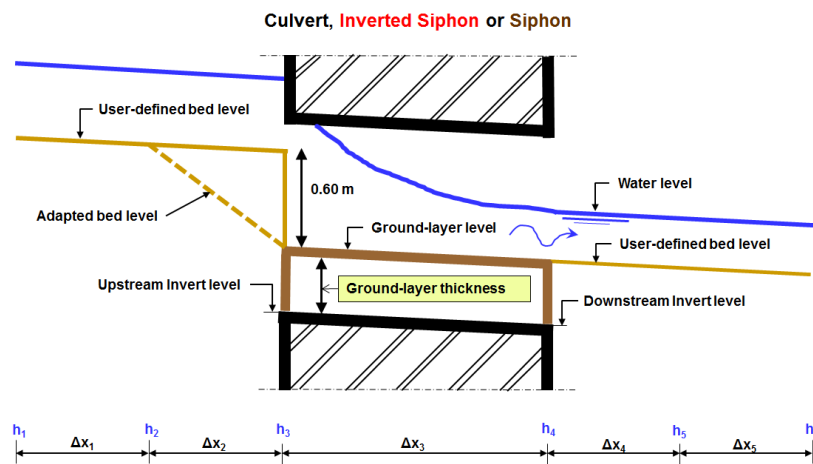
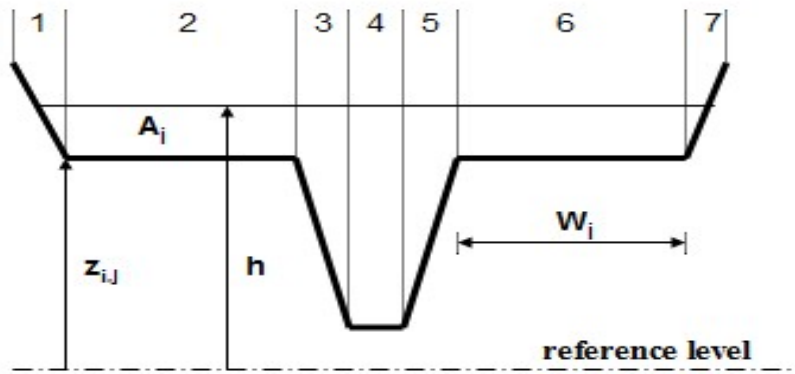


**Figure 1.40:** Good modelling practice, Culvert, Inverted Siphon and Siphon

#### 1.1.16.14 Universal Weir

The weir profile (see Figure 1.41) of a universal weir can be defined as a Y-Z profile or an Asymmetrical trapezium profile. The weir profile of a universal weir is divided into *rectangular weir sections* having a horizontal bed and *triangular weir sections* having a sloping bed. It is assumed that the total discharge over an universal weir is the sum of the discharge over each individual weir section, where rectangular weir sections are considered as a broad-crested weir and a triangular weir sections are considered as (the half of) a broad-crested weir with truncated triangular control section (Bos, 1989).



No.1,3,5,7 are Triangular weir sections

No. 2,4,6 are Rectangular weir sections

$A_i$  = Flow area above section  $i$

$h$  = Water level

$W_i$  = Width of section  $i$

$z_{i,j}$  = Level of weir profile at the  $j^{\text{th}}$  side ( $j = 1$  or  $2$ ) of section  $i$

**Figure 1.41:** Weir profile of a Universal weir, division in rectangular and triangular weir sections

$A_i$	Flow area above section $i$
$h$	Water level
$W_i$	Width of section $i$
$z_{i,j}$	Weir profile level at the $j^{\text{th}}$ side ( $j = 1$ or $2$ ) of section $i$

$$Q = \sum_i^N (u_i A_i) = \sum_i^N Q_i \quad (1.122)$$

where:

$A$	Total flow area above the universal weir [ $m^2$ ]
$A_i$	Flow area above section $i$ [ $m^2$ ]
$N$	Total number of sections $i$ in which the universal weir is subdivided [—]
$Q$	Total discharge over the universal weir [ $m^3/s$ ]
$Q_i$	Discharge over section $i$ [ $m^3/s$ ]
$u_i$	Flow velocity over section $i$ [m/s]
$U_{Structure} = U_{mean}$	Average flow velocity over the universal weir [m/s]

**For rectangular weir sections yields**

$$z_{i1} = z_{i2} \quad \text{crest level of the rectangular weir section}$$

$$m_l \quad \text{modular water-level-based limit} = (h_2 - z_{i1}) / (h_1 - z_{i1}) = 2/3$$

◇ Free rectangular weir flow, i.e.,  $(h_2 - z_{i1})/(h_1 - z_{i1}) \leq 2/3$

$$Q_i = c_e \frac{2}{3} \sqrt{\frac{2}{3}} g W_i (h_1 - z_{i1})^{3/2} \quad (1.123)$$

$$u_i = c_e \sqrt{\frac{2}{3}} g \sqrt{h_1 - z_{i1}} \quad (1.124)$$

$$A_i = \frac{2}{3} W_i (h_1 - z_{i1}) \quad (1.125)$$

◇ Submerged rectangular weir flow, i.e.,  $(h_2 - z_{i1})/(h_1 - z_{i1}) > 2/3$

$$Q_i = c_e W_i (h_2 - z_{i1}) \sqrt{2g(h_1 - h_2)} \quad (1.126)$$

$$u_i = c_e \sqrt{2g(h_1 - h_2)} \quad (1.127)$$

$$A_i = W_i (h_2 - z_{i1}) \quad (1.128)$$

**For triangular weir sections yields**

$z_{i1} \neq z_{i2}$ ;  $\min(z_{i1}, z_{i2})$  is crest level of the triangular weir section

$ml$  modular *water-level-based* limit =  $(h_2 - \min(z_{i1}, z_{i2})) / (h_1 - \min(z_{i1}, z_{i2}))$

If  $(h_1 - \min(z_{i1}, z_{i2})) \leq 1.25|z_{i1} - z_{i2}|$ ;  $ml = 4/5$

If  $(h_1 - \min(z_{i1}, z_{i2})) > 1.25|z_{i1} - z_{i2}|$ ;  $ml = 2/3 + 1/6(|z_{i1} - z_{i2}| / (h_1 - \min(z_{i1}, z_{i2})))$

◇ Free triangular weir flow, i.e.  $(h_2 - \min(z_{i1}, z_{i2})) / (h_1 - \min(z_{i1}, z_{i2})) \leq ml$

$$Q_i = c_e A_i \sqrt{2g(1 - ml)h_1} \quad (1.129)$$

$$u_i = c_e \sqrt{2g(1 - ml)h_1} \quad (1.130)$$

If  $ml(h_1 - \min(z_{i1}, z_{i2})) \leq |z_{i1} - z_{i2}|$

$$A_i = 0.5 (ml(h_1 - \min(z_{i1}, z_{i2})))^2 \frac{1}{|z_{i1} - z_{i2}|} W_i \quad (1.131)$$

If  $ml(h_1 - \min(z_{i1}, z_{i2})) > |z_{i1} - z_{i2}|$

$$A_i = (ml(h_1 - \min(z_{i1}, z_{i2})) - 0.5|z_{i1} - z_{i2}|) W_i \quad (1.132)$$

◇ Submerged triangular weir flow, i.e.  $(h_2 - \min(z_{i1}, z_{i2})) / (h_1 - \min(z_{i1}, z_{i2})) > ml$

$$Q_i = c_e A_i \sqrt{2g(h_1 - h_2)} \quad (1.133)$$

$$u_i = c_e \sqrt{2g(h_1 - h_2)} \quad (1.134)$$

If  $h_2 - \min(z_{i1}, z_{i2}) \leq |z_{i1} - z_{i2}|$

$$A_i = 0.5 (h_2 - \min(z_{i1}, z_{i2}))^2 \frac{1}{|z_{i1} - z_{i2}|} W_i \quad (1.135)$$

If  $h_2 - \min(z_{i1}, z_{i2}) > |z_{i1} - z_{i2}|$

$$A_i = (h_2 - \min(z_{i1}, z_{i2}) - 0.5|z_{i1} - z_{i2}|) W_i \quad (1.136)$$

where:

$c_e$	Discharge coefficient, applicable to all weir sections of the universal weir [—]
$g$	Acceleration due to gravity [ $m/s^2$ ] ( $\approx 9.81$ )
$h_1$	Upstream water level [ $m$ ]
$h_2$	Downstream water level [ $m$ ]
$ml$	$= (h_2 - \min(z_{i1}, z_{i2})) / (h_1 - \min(z_{i1}, z_{i2}))$ <i>water-level-based</i> modular limit [—]; for ratio's of $(h_2 - \min(z_{i1}, z_{i2})) / (h_1 - \min(z_{i1}, z_{i2})) > ml$ , the weir gets drowned.
$W_i$	Width of weir section $i$ [ $m$ ]
$z_{i1}$	Weir profile level at the beginning of weir section $i$ [ $m$ ]
$z_{i2}$	Weir profile level at the end of weir section $i$ [ $m$ ]

#### 1.1.16.15 Vertical obstacle friction

The vertical obstacle friction terms have been introduced to account for the added resistance that is caused by vertical obstacles, like houses or trees. The vertical obstacle friction coefficient is based on the number of obstacles, their diameter and drag coefficient. This spatial coefficient can be prescribed in a ARC-INFO grid file, like the bathymetry.

The vertical obstacle friction coefficient  $a$  is specified as the summation of the product of obstacle width and drag coefficient over the number of obstacles per unit area.

$$a = \frac{1}{A} \sum_{i=1}^N D_i C d_i \quad (1.137)$$

where:

$a$	Vertical obstacle friction coefficient [ $1/m$ ]
$N$	Number of obstacles in unit area [—]
$A$	Unit area [ $m^2$ ]
$D_i$	Diameter of obstacle $i$ [ $m$ ]
$C d_i$	Drag coefficient of obstacle $i$ [—]

For round pillars,  $Cd$  is usually 1.0. In this formulation it is assumed that the obstacle height will always be larger than the waterdepth. In case the obstacles do become submerged, a more advanced option is the Depth-Dependent Vegetation Roughness.

#### 1.1.16.16 Weir

Three types of flow conditions can occur in the case of weir flow. These are free (modular) flow, submerged flow and no flow (water levels below crest level). If high tail water conditions do affect the flow, the weir is said to be submerged.

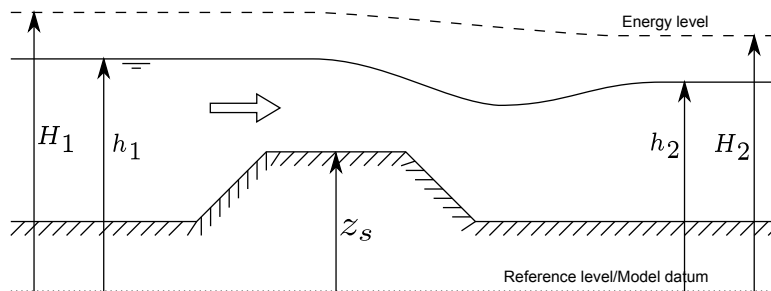


Figure 1.42: Weir

The discharge and wetted area through the weir is computed with the following formulas:

**Free weir flow:**

$$u_s = c_e \sqrt{\frac{2}{3}g} \sqrt{h_1 - z_s} \quad (1.138)$$

$$A_f = c_w W_s \frac{2}{3} (h_1 - z_s) \quad (1.139)$$

$$Q = u_s A_f = c_e c_w W_s \frac{2}{3} \sqrt{\frac{2}{3}g} (h_1 - z_s)^{3/2} \quad (1.140)$$

**Submerged weir flow:**

$$u_s = c_e \sqrt{2g(h_1 - h_2)} \quad (1.141)$$

$$A_f = c_w W_s (h_2 - z_s) \quad (1.142)$$

$$Q = u_s A_f = c_e c_w W_s \sqrt{2g(h_1 - h_2)} (h_2 - z_s) \quad (1.143)$$

$Q$	Discharge across weir [ $m^3/s$ ]
$A_f$	Wetted area [ $m^2$ ]
$c_e$	Discharge coefficient [—]
$c_w$	Lateral contraction coefficient [—]
$W_s$	Crest width [ $m$ ]
$g$	Acceleration due to gravity [ $m/s^2$ ] ( $\approx 9.81$ )
$h_1$	Upstream water level [ $m$ ]
$h_2$	Downstream water level [ $m$ ]
$z_s$	Crest level [ $m$ ]
$u_s$	Velocity over crest [ $m/s$ ]

The different formulas are applied when the following conditions occur

**Free weir flow:**

$$h_1 - z_s > \frac{3}{2}(h_2 - z_s) \quad (1.144)$$

**Submerged weir flow:**

$$h_1 - z_s \leq \frac{3}{2}(h_2 - z_s) \quad (1.145)$$

**Note:**

Broad weirs can cause oscillations, because the discharge calculated with the broad crest move a lot of water at a time step. This large discharge can lower the upstream water level significantly resulting in a discharge with a reverse flow direction at the next time step. The following (rather conservative) rule-of-thumb can be used to avoid oscillations:



$$A_s = \frac{3}{2} W_s \quad (1.146)$$

$A_s$	Storage area upstream of the structure [ $m^2$ ]
$W_s$	Crest width [ $m$ ]

### 1.1.17 Staggered grid; $h$ - and $u$ -calculation points at different locations

A SOBEK-Flow-model consists of a network of reaches connected to each other at connection nodes. The SOBEK-Flow-model uses a staggered grid. On a staggered grid the water level points (e.g.  $h$ -calculation points) and velocity points (e.g.  $u$ -calculation points) are at different locations (see [Figure 1.43](#)). Water levels are computed at the  $h$ -calculation points, while velocities are computed half way between the  $h$ -calculation points, on the so called  $u$ -calculation points. Please note that Connection Nodes and Boundary Nodes are  $h$ -calculation points.

In each reach a number of  $h$ -calculation points can be defined. These  $h$ -calculation points represent the spatial numerical grid used in the simulation. The momentum equation is solved between  $h$ -calculation points, while the continuity equation is solved between the  $u$ -calculation points.

The location of each  $h$ -calculation point should be selected on various criteria:

- ◇ the distance between two neighbouring  $h$ -calculation points should not be too large (for accuracy and proper representation of the physical processes)
- ◇ the distance between two neighbouring  $h$ -calculation points should not be too small because of increasing simulation time. The default minimum distance SOBEK uses during a simulation is 1 meter.
- ◇ the location of the  $h$ -calculation points may be non-equidistant.

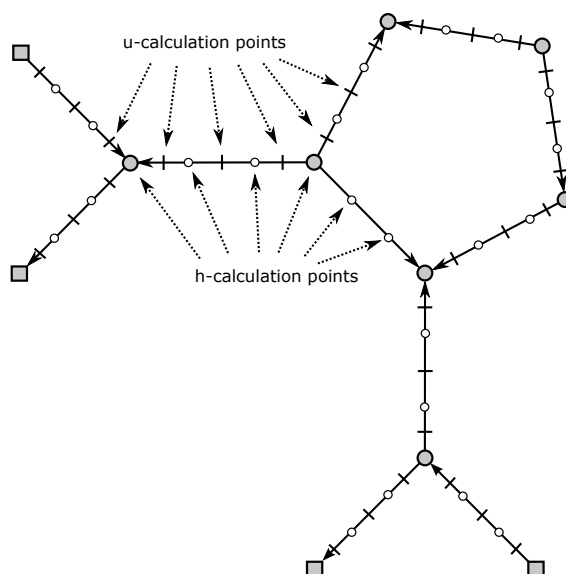


**Figure 1.43:** Staggered grid,  $h$ - and  $u$ -calculation points at different locations

### 1.1.18 Construction of the numerical bathymetry on basis of user-defined cross-sections

Cross-sections (e.g. bathymetrical data) may be defined at arbitrary locations in a model, provided that for each reach at least one cross-section is specified. An overview of the available type of cross-sections is given in ??.

This section explains how the numerical bathymetry of a SOBEK model is constructed on basis of the user-defined cross-sections. With numerical bathymetry is referred to the bathymetrical information, that depending on the cross-section type is available at  $h$ -calculation points only or available at both  $h$ - and  $u$ -calculation points. Water levels and discharges are computed using this numerical bathymetrical information. For more information on  $h$ - and  $u$ -calculation points, reference is made to [section 1.1.17](#).

In constructing the numerical bathymetry a distinction is to be made between"

- ◇ The Y-Z type of profiles (e.g. Open Vertical Segmented Y-Z profile, Asymmetrical Trapezium profile, Open Lumped Y-Z profile and Closed Lumped Y-Z profile).
- ◇ All cross-section types except for the Y-Z type of profiles.


### 1.1.18.1 The Y-Z type of profiles

With the Y-Z type of profiles is referred to the Open Vertical Segmented Y-Z profile, the Asymmetrical Trapezium profile, the Open Lumped Y-Z profile and the Closed Lumped Y-Z profile (for more information, see ??).

For the Y-Z type of profiles yields that numerical bathymetrical information is made available at both  $h$ - and  $u$ -calculation points by interpolating (see [section 1.1.19](#)) between the user-defined cross-sectional profiles. The construction of the numerical bathymetrical information for Y-Z type of profiles is depicted in [Figure 1.44](#).

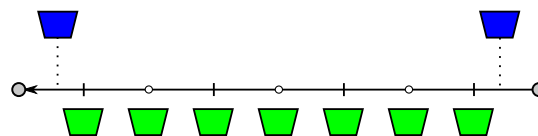


**Figure 1.44:** Construction of the numerical bathymetrical information for Y-Z type of profiles; Blue coloured objects are the user-defined cross-sections; Green coloured objects are the interpolated numerical bathymetrical information; Open circle are  $h$ -calculation points; Small vertical lines are  $u$ -calculation points

**Note:** If only one cross-section is specified for a reach, the bathymetrical information of each  $h$ -calculation point and each  $u$ -calculation point located on this reach will be identical to this specified cross-section. 

### 1.1.18.2 All cross-section types except for the Y-Z type of profiles

With the Y-Z type of profiles is referred to the Open Vertical Segmented Y-Z profile, the Asymmetrical Trapezium profile, the Open Lumped Y-Z profile and the Closed Lumped Y-Z profile (for more information, see ??).

For all cross-section types except for the Y-Z type of profiles yields that numerical bathymetrical information is made available at  $h$ -calculation points only by interpolating (see [section 1.1.19](#)) between user-defined cross-sectional profiles. The construction of the numerical bathymetrical information for all cross-section types except the Y-Z type of profiles is depicted in [Figure 1.45](#).

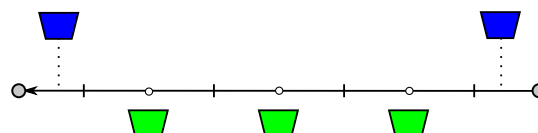


**Figure 1.45:** Construction of the numerical bathymetrical information for all cross-section types except for the Y-Z type of profiles; Blue coloured objects are the user-defined cross-sections; Green coloured objects are the interpolated numerical bathymetrical information; Open circle are  $h$ -calculation points; Small vertical lines are  $u$ -calculation points



**Note:** If only one cross-section is specified for a reach, the numerical bathymetrical information for each  $h$ -calculation point located on this reach will be identical to this specified cross-section.

#### 1.1.19 Method of interpolating between user-defined cross-sections

This section explains the method of interpolating between user-defined cross-sections. An overview of the available type of cross-sections is given in ???. Following distinction between cross-sections types is to be made:

- ◇ Round and Egg-shape (see [section 1.1.19.1](#)).
- ◇ Open Vertical Segmented Y-Z profile and Asymmetrical Trapezium profile (see [section 1.1.19.2](#)).
- ◇ Cross-sections not being a Round, Egg-shape, Open Vertical Segmented Y-Z profile or Asymmetrical Trapezium profile (see [section 1.1.19.3](#)).

##### 1.1.19.1 Method of Interpolating between Round cross-sections and between Egg-shape cross-sections

A Round is specified by an invert level, a diameter and the elevation of a ground-layer surface. Interpolating between two Round cross-sections refers to the linear interpolation along the reach of invert level, diameter and the elevation of the ground-layer surface.

An Egg-shape is specified by an invert level, a height, a width and the elevation of a ground-layer surface. Interpolating between two Egg-shape cross-sections refers to the linear interpolation along the reach of invert level, height, width and the elevation of the ground-layer surface.

##### 1.1.19.2 Method of Interpolating between Open Vertical Segmented Y-Z profiles and between Asymmetrical Trapezium profiles

For both an Open Vertical Segmented Y-Z profile and an Asymmetrical Trapezium profile yields that first from the user-defined cross-sectional information so-called conveyance tables are constructed. In a conveyance table the width, area and conveyance as function of water level are given. Interpolation between two of these type of profile refers to the linear interpolation along the reach of their respective conveyance tables.

##### 1.1.19.3 Method of Interpolating between Cross-sections not being a Round, Egg-shape, Open Vertical Segmented Y-Z profile or Asymmetrical Trapezium profile

For all cross-sections not being a Round, Egg-shape, Open Vertical Segmented Y-Z profile or Asymmetrical Trapezium profile yields that the cross-sectional profile is defined in a Table.

Before interpolation starts it is taken care of that the concerning two cross-sections contain exactly the same vertical spacing for flow and total widths. In this context vertical spacing means the level at which a certain width in one of the two cross-sections is defined minus the bed level (lowest point) of the concerning cross-section. Afterwards, for each vertical spacing the flow width and total width of an intermediate constructed cross-section is determined by linear interpolation along the reach. The ground-layer surface of an intermediate constructed cross-section is determined by linear interpolation along the reach as well.



**Note:** In case of a River profile, the properties of a summer dike (e.g. Flow area, Total area, Dike crest level and Flood plain base level) are linear interpolated along the reach. The same applies for the width of the main section, the width of floodplain 1 and the width of flood plain 2.



**Note:** The height of a cross-section is the maximum level at which a width is defined minus the bed level (lowest point) of this cross-section. For open cross-sectional profiles yields that in case two cross-sections have different heights, the height of the lowest cross-section will be vertically extended with a width equal to the width defined at its maximum level. This is done to obtain in the lowest cross-section exactly the same vertical spacing as in the highest cross-section. Please note that the same procedure is applied for closed cross-sections, with the exception that the width of the lowest cross-section above its obvert level (maximum defined level) becomes equal to zero.



### 1.1.20 Methods for computing conveyance

Conveyance is computed for each  $u$ -calculation point (or velocity calculation point). A  $u$ -calculation point is located in the centre point of its two adjacent  $h$ -calculation points (or water level calculation points). A distinction is to be made between:

- ◇ The tabulated lumped conveyance approach (see [section 1.1.20.1](#)),
- ◇ Analytical formulae for computing lumped conveyance, and
- ◇ The vertically segmented conveyance approach (see [section 1.1.20.2](#)).

The vertically segmented conveyance approach is used for Y-Z profiles and Asymmetrical Trapezium cross-sections only. Analytical formulae for computing lumped conveyance are used for the Egg-shaped cross-section and the Round cross-section. For the remaining cross-section types, the tabulated lumped conveyance approach is used.

#### 1.1.20.1 Tabulated lumped conveyance approach

In the tabulated lumped conveyance approach, it is assumed that there is an uniform flow velocity ( $\bar{U}$ ) in the cross-sectional profile for a given water level (see [Figure 1.46](#)). Hence, it is assumed that differences in flow velocities across the cross-sectional profile can be neglected. This assumption generally does not yield for rivers. Therefore, in modelling rivers Y-Z profiles (or Asymmetrical Trapeziums) are preferred, where conveyance is computed using the vertically segmented conveyance approach (see [section 1.1.20.2](#)).

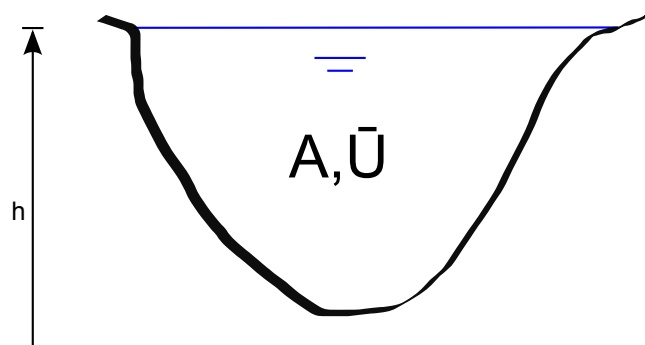


**Figure 1.46:** Concept of the lumped conveyance approach

First an asymmetrical cross-sectional profile as depicted in [Figure 1.46](#) is transferred into a symmetrical cross-sectional profile. Thereafter the tabulated lumped conveyance is computed as:

$$K(h) = A(h)C(h)\sqrt{R(h)} \quad (1.147)$$

where:

$K(h)$	Tabulated lumped conveyance at water level $h$
$A(h)$	Cross-sectional area at water level $h$
$C(h)$	Chézy friction value at water level $h$
$P(h)$	Wetted Perimeter at water level $h$
$R(h)$	Hydraulic radius at water level $h$ ( $R(h) = A(h)/P(h)$ )

If the water level in an open tabulated rises above the highest level in a cross-sectional profile, the tabulated lumped conveyance is computed taking the flow width at this water level equal to the flow width, defined at the highest cross-sectional level.



**Note:** Please note that in case of a River profile, the tabulated lumped conveyance of its main section, floodplain 1 and floodplain 2 are computed separately, and thereafter added to obtain the total tabulated lumped conveyance of a river profile at a particular water level.

### 1.1.20.2 Vertically segmented conveyance approach

The vertically segmented conveyance approach is suited for modelling flow in rivers, since in this approach it is assumed that flow velocities vary across the cross-sectional profile for a given water level. In line with this assumption, the cross-section is divided in vertical segments (see [Figure 1.47](#)).

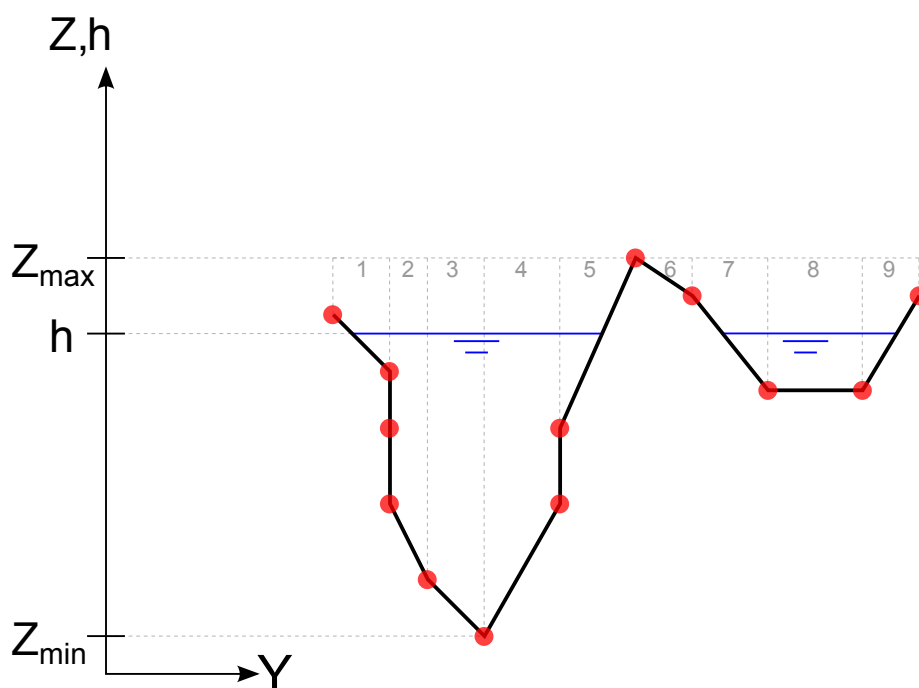


**Figure 1.47:** Example of constructed vertical segments in a Y-Z profile  
 13  $(y_i, z_i)$  points *red dots*  
 9 vertical segments



**Note:** Conveyance table constructed from  $Z_{\min}$  to  $Z_{\max}$ .

A Y-Z profile is defined by a number ( $n$ ) of  $(y_i, z_i)$  points. For the total number ( $n_{seg}$ ) of vertical segments yields:  $n_{seg} = n - a - 1$ , where  $a$  = number of succeeding  $(y_i, z_i)$  points for which  $y_i = y_{i+1}$ . So, *please note* that vertical walls in a Y-Z profile do not induce

a vertical segment. *Moreover*, the length of vertical walls is not considered in computing the conveyance of a Y-Z profile. Omitting vertical walls in computing the conveyance of a Y-Z profile, means that for a canal having a rectangular profile with a small ratio of width and water depth only, substantial difference in discharge capacity can occur if such canal is modelled as a rectangular cross-section (i.e. lumped conveyance approach) or as a rectangle shaped Y-Z profile (i.e. vertically segmented conveyance approach). The surface level of a Y-Z profile is equal to its highest  $(y_i, z_i)$  point. In analogy, the same yields for an Asymmetrical Trapezium cross-section.

The conveyance ( $K_i$ ) of each vertical segment is computed separately (for formulae, see conveyance per vertical segment further below). The conveyance of each inclined vertical segment is determined by solving an integral from  $y_i$  to  $y_{i+1}$ . The advantage of using an integral is that irrespective of the number of user-defined intermediate points, that lie on a straight line between  $(y_0, z_0)$  to  $(y_1, z_1)$ , the same conveyance for the cross-sectional part from  $y_0$  to  $y_1$  is computed. The total conveyance ( $K_{tot}$ ) at a particular water level is the summation of the conveyance of all the vertical segments ( $K_{tot} = \sum K_i$ ).

### Conveyance tables, applied in the vertically segmented conveyance approach

A conveyance table gives the conveyance, flow width and flow area of a cross-section as function of water level. Conveyance tables are used for Y-Z profiles and Asymmetrical Trapeziums only. These conveyance tables are made by a pre-processor before the onstart of a hydrodynamic calculation. In constructing the conveyance table of each user-defined cross-section, it is ensured that the difference in conveyance between two succeeding water levels is less than 1 %. Conveyance tables are used for reducing computational efforts, hence increasing SOBEK's computational performance.

Conveyance tables are made from the bed-level up to the highest  $(y_i, z_i)$  point, irrespective of the actual location of the highest  $(y_i, z_i)$  point within the cross-sectional profile. This implies that no distinction is made between the left and the right embankment height.

Conveyance tables for computational points located in between two user-defined cross-sections are obtained by linear interpolating the conveyance tables, constructed at these two user-defined cross-sections (see also cross-section).

### Extrapolation of conveyance tables

Say the water level ( $h$ ) rises above the highest level ( $n_{\max}$ ) of a conveyance table. In this case the conveyance ( $K_h$ ) at water level ( $h$ ) is computed as

$$K_h = a(h - z_{\min})^b, \quad (1.148)$$

where:  $z_{\min}$  is the lowest level in the cross-sectional profile; and  $a$ ,  $b$  are constants derived from the conveyances at levels  $n_{\max}$  and  $n_{\max} - 1$ .

### Lumped hydraulic output for Y-Z profiles and Asymmetrical Trapezium

As a courtesy at subsection branch output, lumped hydraulic output ( $Q$ ,  $C_{lumped}$ ,  $A_{flow}$ ,  $W_{flow}$  and  $R$ ) are provided for Y-Z profiles and Asymmetrical Trapeziums. The discharge ( $Q$ ) is the discharge through the profile, having a flow area ( $A_{flow}$ ) and flow width ( $W_{flow}$ ). The hydraulic radius ( $R$ ) is computed on basis of  $A_{flow}$  and  $W_{flow}$  assuming a symmetrical profile as function of water level. The latter assumption is made, since different Y-Z profiles may have different shapes, that might have to be interpolated. The lumped Chézy value ( $C_{lumped}$ ) is computed as

$$C_{lumped} = \frac{K}{A_{flow} \sqrt{R}}, \quad (1.149)$$

where  $K$  is the conveyance.

### Conveyance per vertical segment

A vertical segment is defined by two  $(y_0, z_0)$  and  $(y_1, z_1)$  points for which yields that  $y_0$  is not equal to  $y_1$  (see Figure 1.48).

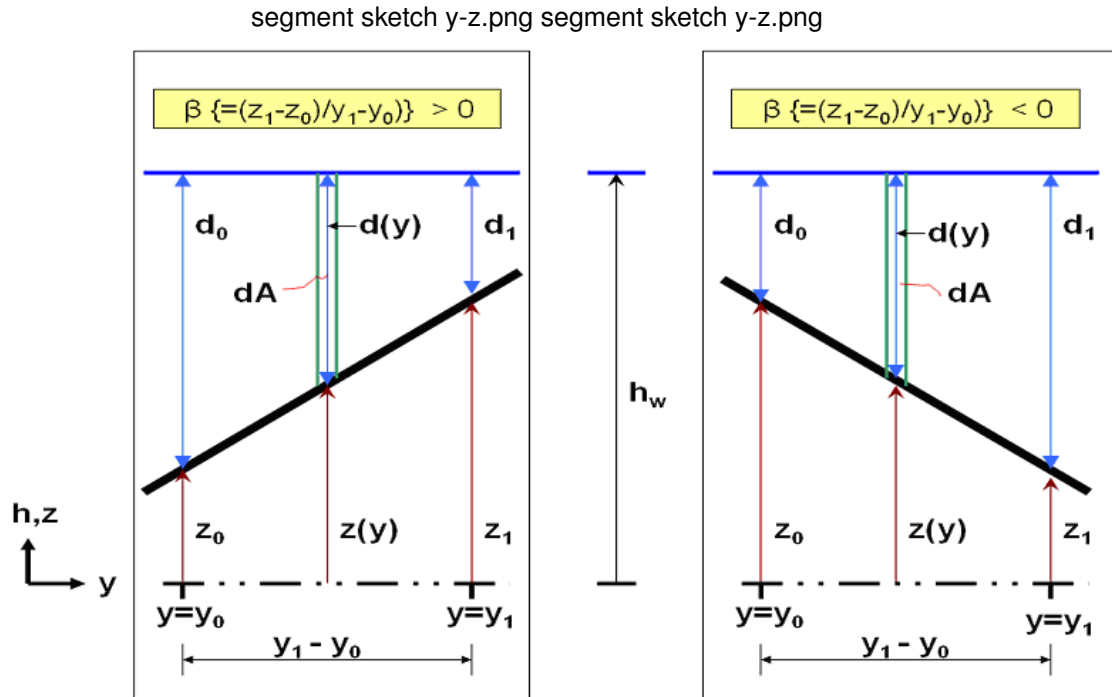


**Figure 1.48:** Definition sketch of a vertical segment, considered in computing conveyance for a Y-Z profile and an Asymmetrical Trapezium cross-section

Hereunder, the conveyance formulae for a vertical segment are given in case of:

- ◇ Chézy roughness,
- ◇ Manning roughness,
- ◇ Strickler ( $k_n$ ) roughness,
- ◇ Strickler ( $k_s$ ) roughness,
- ◇ White-Colebrook ( $k_n$ ) roughness, and
- ◇ Bos&Bijkerk ( $\gamma$ ) roughness.

**Chézy roughness conveyance for a vertical segment (see Figure 1.48):**

```

 $d = \max(d_0, d_1)$ 
if  $d \leq 0$  then
   $k = 0$ 
else
  if  $d < |z_1 - z_0|$  then
    if  $|\beta| \leq 0.01$  then
       $k_1 = \frac{2C}{|\beta|(1+\beta^2)^{1/4}} \left(\frac{d}{2}\right)^{5/2}$ 
    elseif  $|\beta| > 0.01$  then
       $k_2 = \frac{2C}{5|\beta|(1+\beta^2)^{1/4}} d^{5/2}$ 
    elseif  $d \geq |z_1 - z_0|$  then
      if  $|\beta| \leq 0.01$  then
         $k_3 = \frac{C}{(1+\beta^2)^{1/4}} \left(\frac{d_0+d_1}{2}\right)^{3/2} (y_1 - y_0)$ 
      elseif  $|\beta| > 0.01$  then
         $k_4 = \frac{2C}{5|\beta|(1+\beta^2)^{1/4}} \left|d_0^{5/2} - d_1^{5/2}\right|$ 
      endif
    endif
  endif
endif

```

**Manning roughness conveyance for a vertical segment (see [Figure 1.48](#)):**

```

 $d = \max(d_0, d_1)$ 
if  $d \leq 0$  then
   $k = 0$ 
else
  if  $d < |z_1 - z_0|$  then
    if  $|\beta| \leq 0.01$  then
       $k_1 = \frac{2}{n|\beta|(1+\beta^2)^{1/4}} \left(\frac{d}{2}\right)^{8/3}$ 
    elseif  $|\beta| > 0.01$  then
       $k_2 = \frac{3}{8n|\beta|(1+\beta^2)^{1/4}} d^{8/3}$ 
    elseif  $d \geq |z_1 - z_0|$  then
      if  $|\beta| \leq 0.01$  then
         $k_3 = \frac{1}{n(1+\beta^2)^{1/4}} \left(\frac{d_0+d_1}{2}\right)^{5/3} (y_1 - y_0)$ 
      elseif  $|\beta| > 0.01$  then
         $k_4 = \frac{3}{8n|\beta|(1+\beta^2)^{1/4}} \left|d_0^{8/3} - d_1^{8/3}\right|$ 
      endif
    endif
  endif
endif

```

**Strickler ( $k_n$ ) roughness conveyance for a vertical segment (see [Figure 1.48](#)):**

```

 $d = \max(d_0, d_1)$ 
if  $d \leq 0$  then
   $k = 0$ 
else
  if  $d < |z_1 - z_0|$  then
    if  $|\beta| \leq 0.01$  then
       $k_1 = \frac{50k_n^{-1/6}}{|\beta|(1+\beta^2)^{1/4}} \left(\frac{d}{2}\right)^{8/3}$ 

```

```

elseif  $|\beta| > 0.01$  then
     $k_2 = \frac{75k_n^{-1/6}}{8|\beta|(1+\beta^2)^{1/4}} d^{8/3}$ 
elseif  $d \geq |z_1 - z_0|$  then
    if  $|\beta| \leq 0.01$  then
         $k_3 = \frac{25k_n^{-1/6}}{(1+\beta^2)^{1/4}} \left(\frac{d_0+d_1}{2}\right)^{5/3} (y_1 - y_0)$ 
    elseif  $|\beta| > 0.01$  then
         $k_4 = \frac{75k_n^{-1/6}}{8|\beta|(1+\beta^2)^{1/4}} \left| d_0^{8/3} - d_1^{8/3} \right|$ 
    endif
    endif
endif
endif

```

**Strickler ( $k_s$ ) roughness conveyance for a vertical segment (see [Figure 1.48](#)):**

```

 $d = \max(d_0, d_1)$ 
if  $d \leq 0$  then
     $k = 0$ 
else
    if  $d < |z_1 - z_0|$  then
        if  $|\beta| \leq 0.01$  then
             $k_1 = \frac{2k_s}{|\beta|(1+\beta^2)^{1/4}} \left(\frac{d}{2}\right)^{8/3}$ 
        elseif  $|\beta| > 0.01$  then
             $k_2 = \frac{3k_s}{8|\beta|(1+\beta^2)^{1/4}} d^{8/3}$ 
        elseif  $d \geq |z_1 - z_0|$  then
            if  $|\beta| \leq 0.01$  then
                 $k_3 = \frac{k_s}{(1+\beta^2)^{1/4}} \left(\frac{d_0+d_1}{2}\right)^{5/3} (y_1 - y_0)$ 
            elseif  $|\beta| > 0.01$  then
                 $k_4 = \frac{3k_s}{8|\beta|(1+\beta^2)^{1/4}} \left| d_0^{8/3} - d_1^{8/3} \right|$ 
            endif
        endif
    endif
endif
endif

```

**White-Colebrook ( $k_n$ ) roughness conveyance for a vertical segment (see [Figure 1.48](#)):**

```

 $d = \max(d_0, d_1)$ 
 $c_1 = (1 + \beta^2)^{1/4} \ln(10)$ 
 $c_2 = \frac{k_n}{12}$ 
if  $d \leq 0$  then
     $k = 0$ 
else
    if  $d < |z_1 - z_0|$  then
        if  $|\beta| \leq 0.01$  then
            if  $\frac{6d}{k_n} \leq 1.0005$  then
                 $k_1 = \frac{36}{|\beta|(1+\beta^2)^{1/4}} 0.00022 \left(\frac{d}{2}\right)^{5/2}$ 
            else
                 $k_1 = \frac{36}{|\beta|(1+\beta^2)^{1/4}} 10 \log \left\{ \frac{6d}{k_n} \right\} \left(\frac{d}{2}\right)^{5/2}$ 
            endif
        endif
    endif
endif

```

```

elseif  $|\beta| > 0.01$  then
  if  $\frac{d}{c_2} \leq 1.495$  then
     $k_2 = \frac{36}{5|\beta|c_1} d^{5/2} 0.00213$ 
  else
     $k_2 = \frac{36}{5|\beta|c_1} d^{5/2} \left( \ln \left\{ \frac{d}{c_2} \right\} - \frac{2}{5} \right)$ 
  endif
elseif  $d \geq |z_1 - z_0|$  then
  if  $|\beta| \leq 0.01$  then
    if  $\frac{6(d_0+d_1)}{k_n} \leq 1.0005$  then
       $k_3 = \frac{18}{(1+\beta^2)^{1/4}} 0.00022 (y_1 - y_0) \left( \frac{d_0+d_1}{2} \right)^{3/2}$ 
    else
       $k_3 = \frac{18}{(1+\beta^2)^{1/4}} {}^{10}\log \left\{ \frac{6(d_0+d_1)}{k_n} \right\} (y_1 - y_0) \left( \frac{d_0+d_1}{2} \right)^{3/2}$ 
    endif
  elseif  $|\beta| > 0.01$  then
    if  $\frac{d_0}{c_2} \leq 1.495$  and  $\frac{d_1}{c_2} \leq 1.495$  then
       $k_4 = \frac{36}{5|\beta|c_1} \left| d_0^{5/2} 0.00213 - d_1^{5/2} 0.00213 \right|$ 
    elseif  $\frac{d_0}{c_2} \leq 1.495$  and  $\frac{d_1}{c_2} > 1.495$  then
       $k_4 = \frac{36}{5|\beta|c_1} \left| d_0^{5/2} 0.00213 - d_1^{5/2} \left( \ln \left\{ \frac{d_1}{c_2} \right\} - \frac{2}{5} \right) \right|$ 
    elseif  $\frac{d_0}{c_2} > 1.495$  and  $\frac{d_1}{c_2} \leq 1.495$  then
       $k_4 = \frac{36}{5|\beta|c_1} \left| d_0^{5/2} \left( \ln \left\{ \frac{d_0}{c_2} \right\} - \frac{2}{5} \right) - d_1^{5/2} 0.00213 \right|$ 
    else
       $k_4 = \frac{36}{5|\beta|c_1} \left| d_0^{5/2} \left( \ln \left\{ \frac{d_0}{c_2} \right\} - \frac{2}{5} \right) - d_1^{5/2} \left( \ln \left\{ \frac{d_1}{c_2} \right\} - \frac{2}{5} \right) \right|$ 
    endif
  endif
endif
endif
endif

```

**Bos&Bijkerk ( $\gamma$ ) roughness conveyance for a vertical segment (see [Figure 1.48](#)):**

```

 $d = \max(d_0, d_1)$ 
if  $d \leq 0$  then
   $k = 0$ 
else
  if  $d < |z_1 - z_0|$  then
    if  $|\beta| \leq 0.01$  then
       $k_1 = \frac{2\gamma}{|\beta|(1+\beta^2)^{1/4}} \left( \frac{d}{2} \right)^3$ 
    elseif  $|\beta| > 0.01$  then
       $k_2 = \frac{\gamma}{3|\beta|(1+\beta^2)^{1/4}} d^3$ 
    endif
  elseif  $d \geq |z_1 - z_0|$  then
    if  $|\beta| \leq 0.01$  then
       $k_3 = \frac{\gamma}{(1+\beta^2)^{1/4}} \left( \frac{d_0+d_1}{2} \right)^2 (y_1 - y_0)$ 
    elseif  $|\beta| > 0.01$  then
       $k_4 = \frac{\gamma}{3|\beta|(1+\beta^2)^{1/4}} |d_0^3 - d_1^3|$ 
    endif
  endif
endif

```

endif

### 1.1.21 Drying/flooding

When a water level upstream of a reach segment is lower than 5 mm above the bed level of the  $h$ -calculation point at this upstream side, the reach segment is assumed to be dry; the discharge through this reach segment is said to be zero. When a reach segment is dry and upstream or downstream of the segment the water level rises higher than 10 mm above the bed level of the  $h$ -calculation point at that side, the reach segment starts flooding again.

The same deadband is used for the check on drying and flooding of structures. In case of a weir and orifice, the upstream water level is compared to the crest level. In case of culverts, siphons and inverted siphons, the water level is compared to the maximum of the bed level and the bottom of the structure at the upstream side.

### 1.1.22 Free board

Freeboard is the difference between surface level and water level at some location in the system. It is defined from surface level to water level, so the freeboard is positive when the water level is lower than the surface level. When the freeboard is negative, there is a flood at that location.

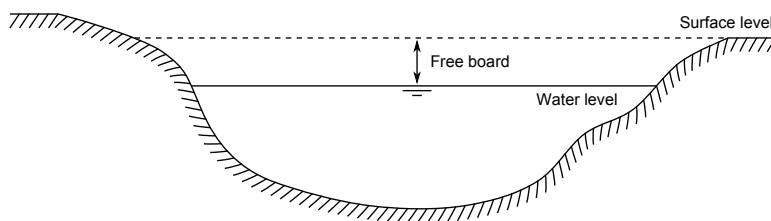


**Figure 1.49:** Free board

### 1.1.23 Ground layer

Except for a Y-Z profile, cross sections can have a fixed horizontal ground layer (or sediment layer). The ground layer level (top level of the ground layer) equals the bottom level (or invert level) plus the ground layer thickness. The part of the cross-section located beneath the ground layer level is omitted in the hydraulic computations. Hence, a ground layer reduces both the wetted area and the wetted perimeter for a given water level. In [Figure 1.50](#) a circular cross section is shown with a ground layer with thickness  $D_{gr}$ .



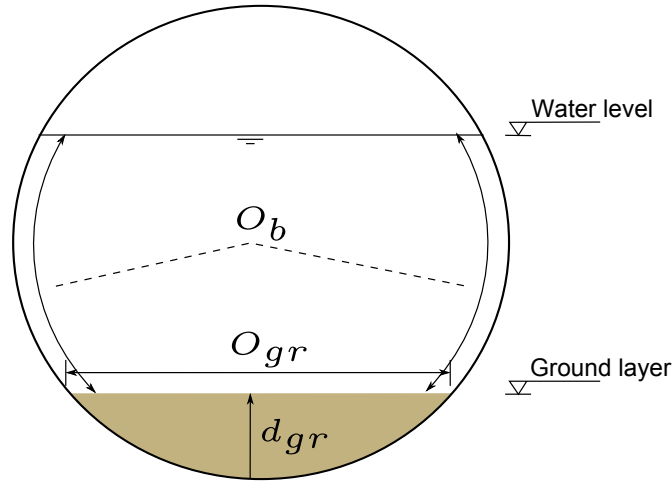


**Figure 1.50:** Ground layer in circular cross section

For a ground layer a friction value can be specified that differs from the bed friction value. The ground layer friction value is applied for the cross-sectional width at the ground layer level only. For the remaining wetted perimeter of the cross-section, the bed friction value is applied. The same friction formulation (i.e. Chézy, Manning etc.) is to be applied for both the ground layer and the remaining wetted perimeter (i.e. the bed) of the cross-sectional profile. The combined friction that is used is computed according to:

$$k_s = \sqrt{\frac{O_b k_{sb}^2 + O_{gr} k_{sgr}^2}{O_b + O_{gr}}} \quad (1.150)$$

$k_s$	Combined Strickler friction value
$k_{sb}$	Strickler bed friction value
$k_{sgr}$	Strickler friction value of the ground layer
$O_b$	Wetted perimeter of the bed
$O_{gr}$	Wetted perimeter of the ground layer

#### 1.1.24 Measurement station

In channel flow a measurement station is placed on a reach. From a measurement station the actual (calculated) value of a water level or a discharge can be retrieved. This value can then be used in an algorithm of a controller.

The water level that a measurement station retrieves is the water level at the nearest calculation point. The retrieved discharge is the discharge at the reach segment where the measurement station is located.

In sewer flow the measurement station can be placed on a connection node or on a reach. Water levels are taken at the nodes, discharges at the reaches.

### 1.1.25 Network

The schematic basis of each model is the network of reaches. These reaches are connected to each other at connection nodes.

One can say that the network of reaches and nodes is the modelled representation of the real geographic data of the modelled area.

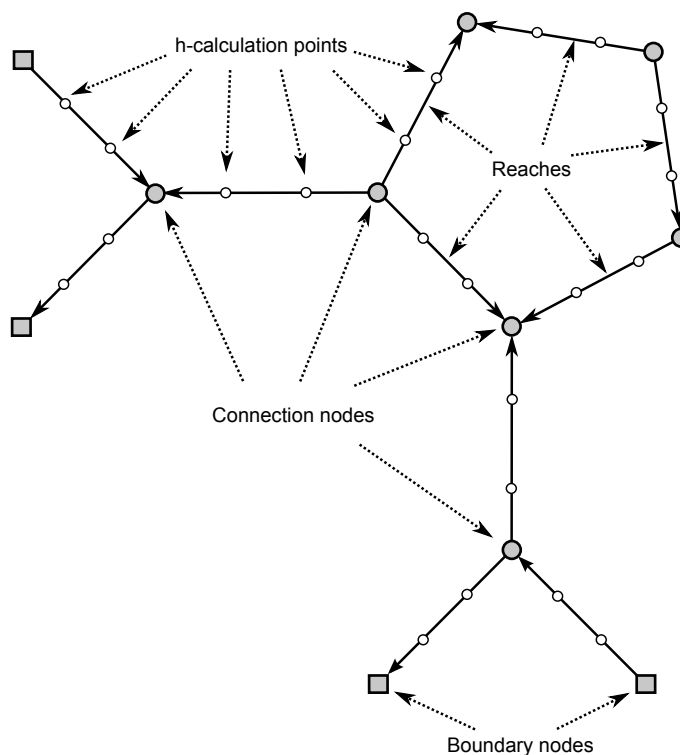


**Figure 1.51: Network**

In the Delft-scheme used by the SOBEK-Flow-module, the network is split up into a staggered grid. The water levels are defined at the connection nodes and the  $h$ -calculation points of this grid, while the discharges are defined at the reach segments.

#### 1.1.25.1 Reach

A reach in a SOBEK-Flow-model is one of the basic elements in the schematisation. A reach connects two nodes, and has the following attributes:

- ◇ Begin node
- ◇ End node
- ◇ Reach length
- ◇ A geographical orientation (used only in case wind friction effect is included in your model).

The direction of the reach (positive  $x$ -direction) is from begin node to end node.

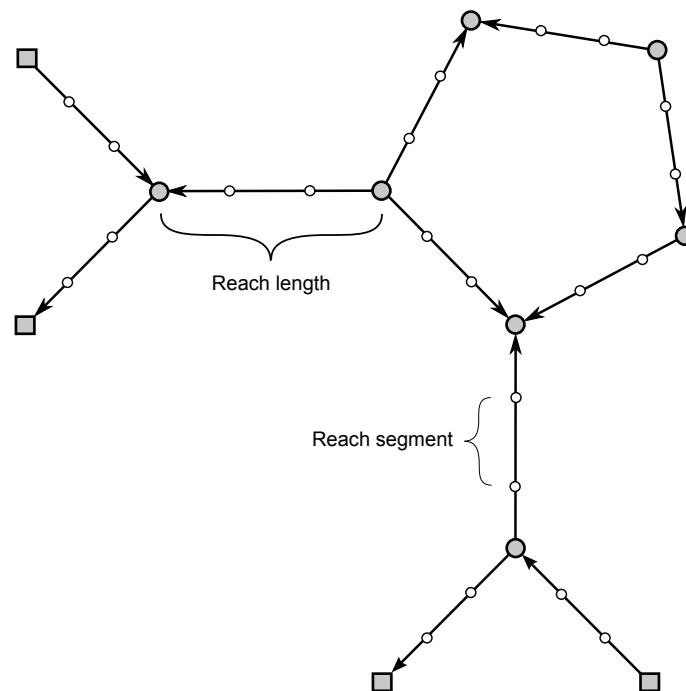


**Figure 1.52:** Reach length in model network

When using channel flow,  $h$ -calculation points can be specified on a reach. If this is done, the reach is split up into reach segments. The numerical simulation will be carried out based on these  $h$ -calculation points and reach segments in a staggered grid. The discharges are calculated at the reach or reach segments. Water levels are calculated at the connection nodes and  $h$ -calculation points.

In case of sewer flow, each reach has a maximum of two  $h$ -calculation points at the beginning and end of that reach. The reach can be interpreted as one reach segment.

### 1.1.25.2 Reach length

In sewer systems the length of a reach is the length from the begin connection node to the end connection node. This length is referred to as the co-ordinate length. In open channel systems, a reach can be made longer than this minimum co-ordinate length, with the use of vector points on the reach. This length is referred to as vector length. With this vector length the actual length of a meandering river or channel can be modelled. If the vector length is defined on a reach, this length is used in the computation of the water flow equations. If this length is not defined, the co-ordinate length is used.

**Note:** The vector length is always equal to or greater than the co-ordinate length



### 1.1.25.3 Reach segment

A SOBEK-Flow-network consists of reaches that are connected in connection nodes. These reaches can be divided by  $h$ -calculation points into segments; the so-called reach segments. The discharges that result from the water flow equations are defined in these reach segments

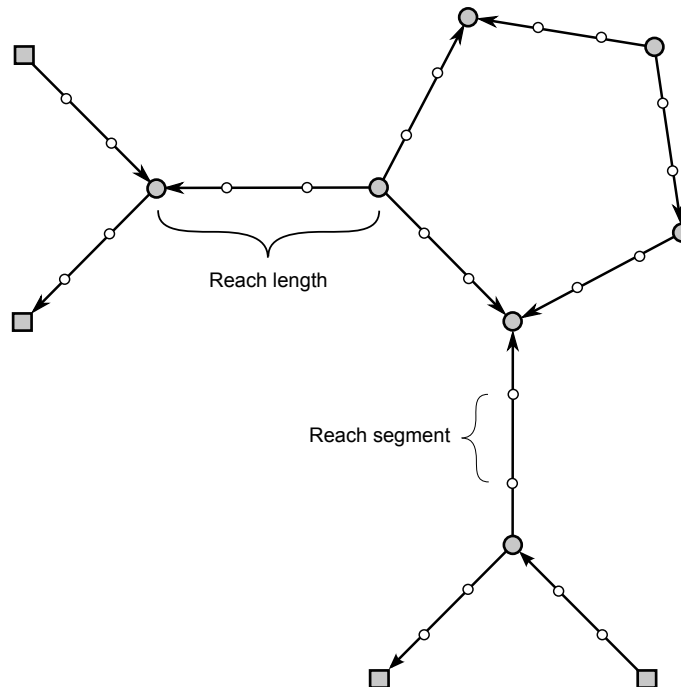


**Figure 1.53:** Reach segment

In sewer networks no  $h$ -calculation points can be used. So each reach consists of one reach segment.

### 1.1.25.4 Connection node

A connection node in a SOBEK-Flow-model is a location where reaches can be joined to other reaches. Water levels are defined at the connection nodes and the  $h$ -calculation points.

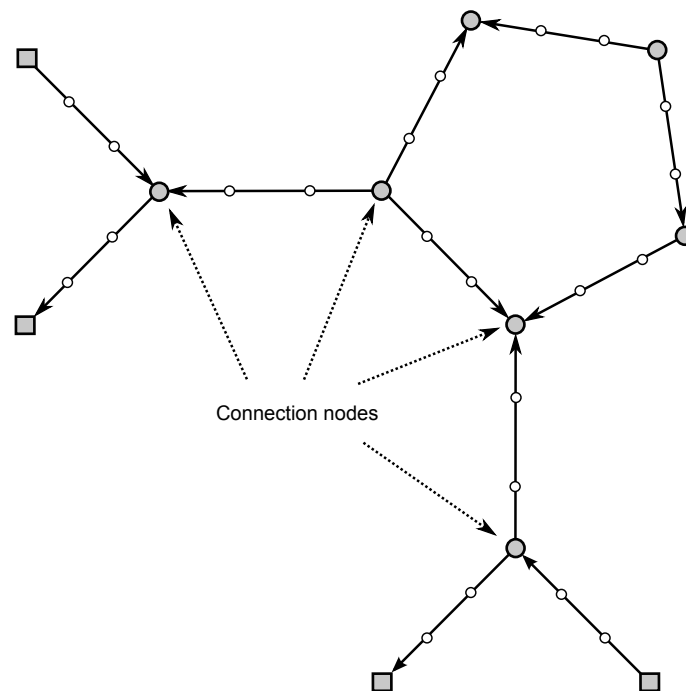


**Figure 1.54:** Connection nodes

**Note:** A node located at the bounds of the model can be a connection node (with storage) or a boundary node (no storage).



### 1.1.26 Reference level

The reference level is the over-all reference level of a model. Normally Mean Sea Level is used.

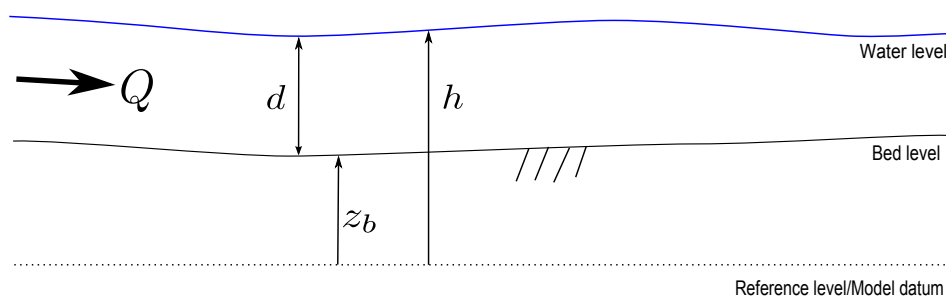


**Figure 1.55:** Definition of reference level

**Note:** All levels (quantities with a vertical co-ordinate) in the SOBEK-Flow-module are defined with respect to the reference level.



### 1.1.27 Robustness

The Delft-scheme is developed with robustness as its most important design aspect. This scheme can deal with phenomena such as drying/flooding, supercritical flow and flow transitions (hydraulic jumps) and guarantees a solution for every time step, though the actual computational time step can be reduced internally under certain flow conditions (large discharges in combination with little storage).

The computational time step reduction is done by a time step estimation procedure before a new time step or at the end of a time step when negative depths are computed. In the latter case the step is repeated with a time step reduced by a factor 2 until a correct solution is achieved.

### 1.1.28 Sediment transport capacity

The SOBEK-Flow-module computes the sediment transport capacity according to the following two formulations.

#### Frijlink

$$T_v = D_{50} \sqrt{g \mu R |S_e|} 5 \exp \left( \frac{-0.27 D_{90}}{\mu R |S_e|} \right) \quad (1.151)$$

$$\mu = \left( \frac{C}{18^{10} \log \left( \frac{12R}{D_{90} + \frac{3\nu}{\sqrt{gR|S_e|}}} \right)} \right)^{3/2} \quad (1.152)$$

$$S_E = \frac{\Delta \left( h + \frac{u^2}{2g} \right)}{\Delta x} \quad (1.153)$$

$T_v$	Sediment transport capacity per $m$ bed width [ $m^2/s$ ]
$\mu$	Bottom roughness factor (ripple factor)
$D_{50}$	Grain diameter at which 50 % of the grains is smaller [ $m$ ]
$D_{90}$	Grain diameter at which 90 % of the grains is smaller [ $m$ ]
$R$	Hydraulic radius [ $m$ ]
$S_e$	Energy slope [—]
$C$	Chézy coefficient [ $m^{1/2}/s$ ]
$\nu$	Kinematic viscosity [ $m^2/s$ ]. Normally $1.002 \times 10^{-6}$
$h$	Water level [ $m$ ]
$u$	Velocity [ $m/s$ ]
$g$	Acceleration due to gravity [ $m/s^2$ ] ( $\approx 9.81$ )
$x$	Length of reach segment [ $m$ ]

#### Van Rijn

$$T_v = 0.053 \frac{T_{gr}^{2.1}}{D_{gr}^{0.3}} \sqrt{(s-1)g} D_{50}^{1.5} \quad (1.154)$$

$$T_{gr} = \frac{u_*^2 - u_{*c}^2}{u_{*c}^2} \text{ if } u_*^2 > u_{*c}^2 \quad (1.155)$$

$$T_{gr} = 0 \text{ if } u_*^2 \leq u_{*c}^2 \quad (1.156)$$

$$u_* = \frac{u \sqrt{g}}{C} \quad (1.157)$$

$$C = 18^{10} \log \left( \frac{12R}{3D_{90}} \right) \quad (1.158)$$

$C$	Chézy coefficient related to bed material
$u$	Average flow velocity [ $m/s$ ]
$u_{*c}$	Critical shear stress velocity according to Shields [ $m/s$ ]

The grain size under water is defined dimensionless by  $D_{gr}$ :


$$D_{gr} = D_{50} \sqrt[3]{\frac{(s-1)g}{\nu^2}} \quad (1.159)$$

$(s-1)$	Relative density
$s$	$s = s/w$
$r_s$	Density of sediment [ $kg/m^3$ ]. Normally 2650 $kg/m^3$
$r_w$	Density of water [ $kg/m^3$ ]. Normally 1000 $kg/m^3$
$\nu$	Kinematic viscosity [ $m^2/s$ ]


The critical shear stress velocity according to Shields  $u_{*c}$  can be found with

$$u_{*c} = \sqrt{\theta_{cr}(s-1)gD_{50}} \quad (1.160)$$

$$\theta_{cr} = \begin{cases} 0.24D_{gr}^{-1} & \text{if } D_{gr} \leq 4 \\ 0.14D_{gr}^{-0.64} & \text{if } 4 < D_{gr} \leq 10 \\ 0.04D_{gr}^{-0.1} & \text{if } 10 < D_{gr} \leq 20 \\ 0.013D_{gr}^{-0.29} & \text{if } 20 < D_{gr} \leq 150 \\ 0.055 & \text{if } D_{gr} > 150 \end{cases} \quad (1.161)$$

**Note:** The sediment transport capacity computed with these formulas is always positive. To give an indication of the direction of the sediment transport in the network, the result is multiplied by the sign of the velocity. 

The mentioned formulas are defined in sediment transport capacity per meter bed width. To arrive at a more comprehensible definition the results are multiplied with a certain characteristic width. For closed cross sections, the maximum width of the profile is taken. For open cross sections the wetted perimeter at a certain level (normally 0.30 m) above the bed level is taken.

**Note:** The parameters that are used in the formulations, like grain diameters, are constant over the whole network 

### 1.1.29 Simulation output parameters at reach segments

For more background information on time step reductions, see section [Time step reductions during the simulation](#). The simulation output parameters available at each reach segment (see option "Simulation Info at the Reach Segments" in the file <flowanal.his> or in Results in Charts and Results in Maps) are:

- ◇ **Time step estimation:** This refers to the number of times that the time step is reduced, since the allowable Courant time step of this reach segment is smaller than the user-defined time step.
- ◇ **No iteration up and No iteration down:** Parameters "No iteration up" and "No iteration down", respectively refer to the number of times that convergence in the Newton iteration process is not satisfied at the water level point with the lowest  $x$ -coordinate ("No iteration up") and the water level point with highest  $x$ -coordinate ("No iteration down") of the reach segment.
- ◇ **Negative depth up and Negative depth down:** Parameters "Negative depth up" and "Negative depth down", respectively refer to the number of times that a time step reduction is needed for avoiding negative depths at the upstream water level point (lowest  $x$ -coordinate) and the downstream water level point (highest  $x$ -coordinate) of the reach segment.

- ◇ **Total:** The number of times that the allowable Courant time step is smaller than the user-defined time step and the number of times that the time step is reduced for either satisfying the convergence condition or for avoiding negative depths.

### 1.1.30 Time step reductions during the simulation

The user can define a time step in the Settings Task block. During the computation this user-defined time step may be reduced for stability reasons (e.g. to prevent the simulation from crashing). SOBEK performs the following checks:

- ◇ At the start ( $t = t^k$ ) of each computational time-step, the allowable Courant time-step is determined. This is done as follows:
  - For each 1D reach segment ( $i$ ) its 1D Courant time step is computed as:

$$\Delta t_i = \sigma \frac{Vol_{i,tot}}{Q_{i,t}} \quad \text{1D Courant} \quad (1.162)$$

where:

$\sigma$	the user-defined value for "maximum flow (1D) and velocity (2D) Courant number" in Settings
$Vol_{i,tot}$	the total volume of water at the upwind (or upstream) water level point
$Q_{i,t^k}$	the discharge at $t = t^k$

Then the 1D reach segment having the smallest 1D Courant time step (e.g. the allowable 1D Courant time step) is determined. The applicable 1D time step at  $t = t^k$  is the minimum of the user-defined time step and the allowable 1D Courant time step. The reach segment with the smallest 1D Courant time step is logged in case its 1D Courant time step is smaller than the user-defined time step.

- The 2D Courant time step for all 2D links in U-direction and for all 2D links in V-direction are respectively computed as:

$$\Delta t = \sigma \frac{\Delta x_m}{U_{m,t^k}} \quad \text{2D Courant, U-direction} \quad (1.163)$$

and

$$\Delta t = \sigma \frac{\Delta y_n}{V_{n,t^k}} \quad \text{2D Courant, V-direction} \quad (1.164)$$

where:

$\sigma$	the user-defined value for "maximum flow (1D) and velocity (2D) Courant number" in Settings
$\Delta x_m$	the grid spacing in $x$ -direction
$\Delta y_n$	the grid spacing in $y$ -direction
$U_{m,t^k}$	the depth-averaged flow velocity in $x$ -direction at $t = t^k$
$V_{n,t^k}$	the depth-average flow velocity in $y$ -direction at $t = t^k$

The allowable 2D Courant time step is the minimum of the 2D Courant time steps of all 2D U-links and 2D V-links. The applicable 2D time step is the minimum of the user-defined time step and the allowable 2D Courant time step.

- In case of a combined 1D-2D hydraulic computation, the applied time step ( $\Delta t$ ) is the minimum of the applicable 1D time step and the applicable 2D time step.
- ◇ In each computational time step (from  $t = t^k$  to  $t = t^k + \Delta t$ ), it is checked that for each water level point yields that the lateral inflow volume is not larger than its volume of water



- at  $t = t^k$ . If this condition is not satisfied, the user defined time step is reduced to such extend that this condition is met. The reduced time step, however, is not made smaller than the user-defined "minimum time step" in Settings.
- ◇ Due to various circumstances (discontinuities in model schematization, unrealistic boundary conditions, etc.), the above determined actual time step ( $\Delta t$ ) may still be too large for finding a valid solution at  $t = t^k + \Delta t$ . Two conditions are to be fulfilled in finding a valid solution:
    - The first condition is that the Newton iteration process converges in terms of water levels and volumes (both computed at water level points). In other words differences in water levels and volumes between the last and previous Newton solution are to be within the user-defined values for "epsilon for water depth" and "epsilon for volume". In Settings, the user can define the "maximum number of Newton iterations". If the convergence condition is not satisfied within the maximum number of Newton iterations, the time step is reduced by a factor 2. If this does not satisfy the convergence condition, the time step is again reduced by a factor 2. The simulation is terminated if a time step smaller than the user-defined "minimum time step" (see Settings) is needed for satisfying the convergence condition. All water level points, that after the maximum number of Newton iterations are conducted, still having a water level convergence error are logged during a computational time step.
    - The second condition is that no negative depths (e.g. water level is below bed level) may occur. Negative depths at a particular water level point may occur if the outflow during a time step is larger than the volume stored at  $t = t^k$ . If negative depths occur, the time step is reduced up to a time step for which yields that the outflow during the reduced time step is smaller than the volume stored at  $t = t^k$  and hence no negative depth occurs. The simulation is terminated if a reduced time step smaller than the user-defined "minimum time step" (see Settings) is needed to avoid negative depths. All water level points for which the time step needs to be reduced in order to avoid negative depths are logged during a computational time step.

**Note:** If a model run requires a lot of computational effort (e.g. an unexpected long simulation time is needed), often a large number of time step reductions during simulation is performed. These time step reductions are needed to find a valid solution and/or to prevent the model from crashing. Defining a smaller calculation time step in Settings may result in shorter simulation times. The reason for this, the smaller user-defined time step allows more moderated intermediate solutions to be found. More moderate solutions reduce the number of circumstances in which the model encounters large discontinuities, which require a considerable amount of time step reductions before finding a valid solution. The final actual time step can be much smaller than the user-defined time step. In other words: A smaller user-defined time step can result in significant less total number of time step reductions leading to a decrease of total computational time. This is because the total required simulation time is directly related to the total number of computational time steps.



### 1.1.31 Slope

In the SOBEK-Flow-module slope can refer to the slope of the water level or the bed slope. If the word "slope" is used without further indication, then it pertains to the slope of the water level in the model. The symbol used is  $i$ :

$$i = \frac{\partial h}{\partial x} \quad (1.165)$$

where

$h$                       Water level [m]

$x$  Distance [m]

For bed slope, the symbol used is  $i_b$ :

Bed slope:

$$i_b = \frac{\partial z_b}{\partial x} \quad (1.166)$$

with  $z_b$  as the bed level.

### 1.1.32 Stationary computation

A stationary computation is performed in the SOBEK-Flow-module by running a non-stationary simulation until a steady state is reached. During this simulation, all time depending parameters, such as lateral and boundary conditions, are set to their initial value and kept constant.

In some cases a steady state cannot be reached, for example, when a pump is switching on and off. In that case the computation stops after 1 000 simulation steps (not time steps, see Time step estimation) and the maximum difference of water level compared to the last time step in the network is given. If this value is low enough (<1 mm for example) the solution can be considered as steady.

The results of a stationary computation can be used as an initial condition for a non-stationary simulation.

### 1.1.33 Summer dike

A flood plain might be separated from a river by means of a small dike, having a crest level lower than the crest level of the main dike (see [Figure 1.56](#)). In the Netherlands large floods usually occur in winter. The main dike and the small dike are, therefore, respectively referred to as the “winter dike” and the “summer dike”.

The presence of a summer dike implies that the cross-sectional profile as measured in situ (see shadowed line in [Figure 1.56](#)) does not increase monotonously with rising water levels. When the water level becomes slightly higher than the crest level of the summer dike, first the area behind the summer dike is to be filled, before water levels can become any higher. This implies a local attenuation of the flood wave at water levels just above the crest level of the summer dike. This hydraulic phenomenon can be modelled using the summer dike option available at a river profile.

In defining a summer dike in a river profile a distinction is to be made between:

#### ◇ The cross-sectional profile

The cross-sectional profile comprises of a “flow area” and a “storage area”, which in [Figure 1.56](#) are respectively located above the blue lines and the black lines. The summation of flow area and storage area is called the “total area”. Both flow area and total area are defined by its width as function of elevation. At each elevation in the cross-sectional profile yields that storage width equals total width minus flow width. Hence, no storage is defined if total width equals flow width. The flow area of the cross-sectional profile can be divided in three separate flow sections, respectively called the (i) main section, (ii) floodplain 1 and (iii) floodplain 2. Each such flow section can have a different roughness value and a different roughness formulation.

#### ◇ The area behind the summer-dike

In analogy with the cross-sectional profile, the “total area behind a summer dike” is divided

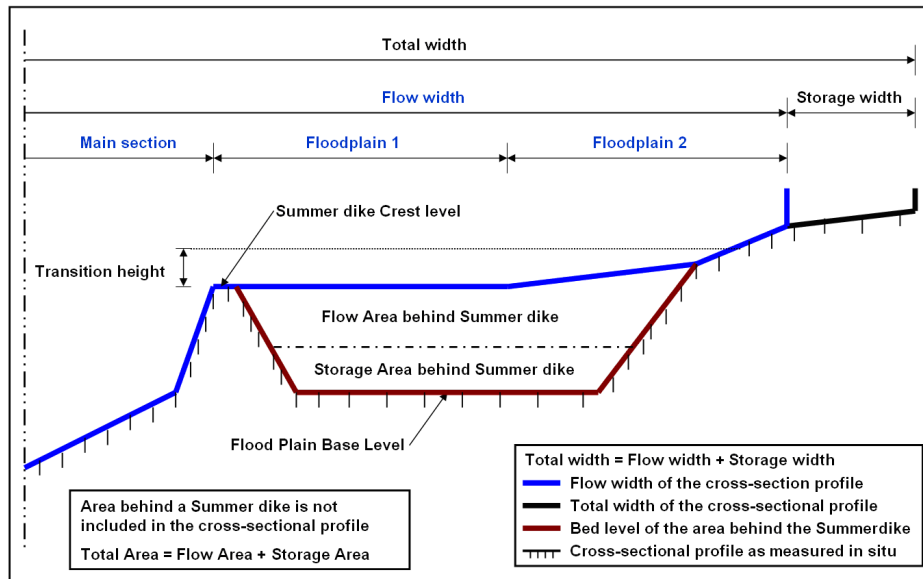


**Figure 1.56:** Summer dike option, available in a river profile

in a “flow area” and a “storage area”. The “Flood Plain Base Level” coincides with the lowest part of the area behind the summer dike (see [Figure 1.56](#)).

**Remark:**

- ◇ Both the cross-sectional profile and the area behind the summer dike should be mutually consistent with the cross-sectional profile as measured in situ (see shadowed line in [Figure 1.56](#)). Hence, both the flow area and the storage area behind the summer dike should not be included in the cross-sectional profile.



The so-called “transition height” is used for avoiding numerical oscillations. More precisely, the transition height ensures that the flow area and storage area behind the summer dike are gradually taken into computation. Transition height for summer dikes is a model-wide parameter, that is defined in the Settings Taskblock (*Edit* button next to 1DFLOW (River); Advanced settings Tab).

Lets consider the following summer dike properties:

- ◇ flood plain base level ( $Z_{\text{base}}$ ) of 2 m,
- ◇ summer dike crest level ( $Z_{\text{sd}}$ ) of 4 m,
- ◇ transition height ( $T$ ) of 0.5 m,
- ◇ storage area behind the summer dike of 200 m<sup>2</sup>,
- ◇ flow area behind the summer dike (ExtraFlowArea) of 50 m<sup>2</sup>, and
- ◇ total area behind the summer dike (ExtraTotalArea) of 250 m<sup>2</sup>.

In explaining how a summer dike is taken into computation, we make a distinction between:

- ◇ The actual value of the (extra) flow area behind the summer dike,
- ◇ The flow velocity applied to the (extra) flow area behind the summer dike, and
- ◇ The actual value of the (extra) total area behind the summer dike.

The actual (extra) flow area is a unique function of the local water level ( $h$ ) in the cross-sectional profile (see [Figure 1.57](#)). More precisely:

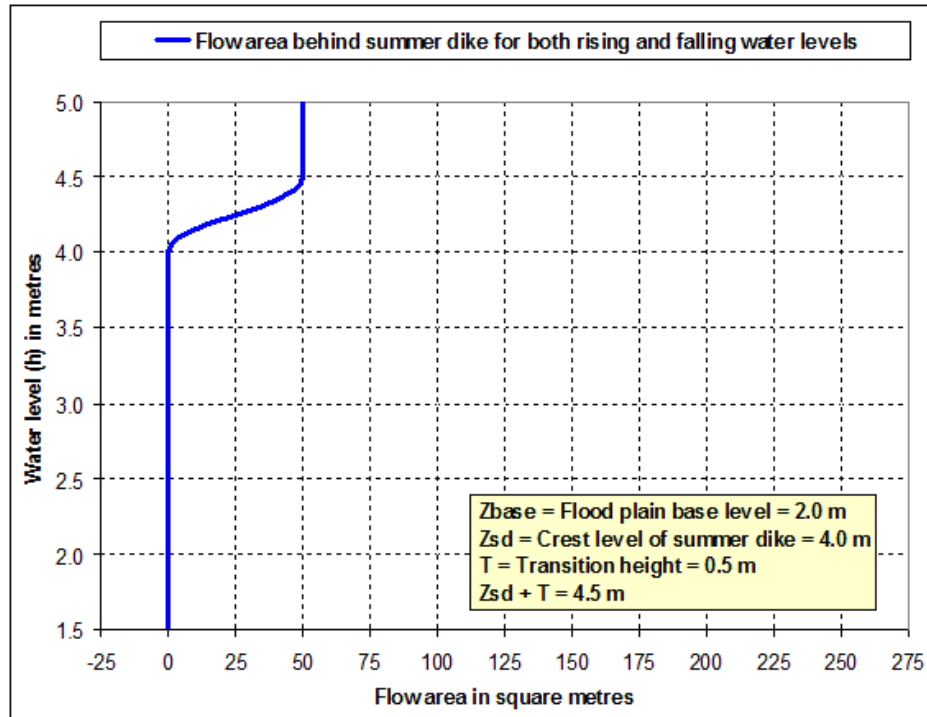


**Figure 1.57:** Flow area behind the summer dike as function of local water levels.

- ◇ If  $h < Z_{sd}$ ; Flow area behind the summer dike is zero.
- ◇ If  $Z_{sd} \leq h \leq Z_{sd} + T$ ; Flow area behind the summer dike varies as a quadratic function of water level ( $h$ ) between zero and ExtraFlowArea ( $= 50 \text{ m}^2$ ).
- ◇ If  $h > Z_{sd} + T$ ; Flow area behind the summer dike is equal to ExtraFlowArea.

The flow velocity applied to the (extra) flow area behind the summer dike is the flow velocity in one of the three available flow sections. Hence, either the flow velocity in the main section, in floodplain 1 or in floodplain 2. The actual flow velocity applied to the (extra) flow area behind the summer dike is determined as follows:

- 1 Default the flow velocity in floodplain 2 is used.
- 2 However, if the wetted area of floodplain 2 becomes less than  $0.4 \text{ m}^2$ , the flow velocity in floodplain 1 is used,
- 3 Furthermore, if the wetted area of floodplain 1 becomes less than  $0.4 \text{ m}^2$ , the flow velocity of the main section is used.



**Remarks:**

- ◇ Please contact Deltares if you like to use a different threshold value (i.e. not  $0.4 \text{ m}^2$ ) for discerning which flow velocity is to be applied to the (extra) flow area behind the summer dike.
- ◇ The flow velocity applied to the (extra) flow area behind the summer dike is computed as follows

$$U_i = C_i \sqrt{R_i S} \quad i \in \{\text{main section, floodplain 1, floodplain 2}\} \quad (1.167)$$

where:

$U_i$	average flow velocity
$C_i$	Chézy coefficient of the flow section
$R_i$	$(A_i + A_{sd})/P_i$ : hydraulic radius of the flow section

$A_i$	wetted area of the flow section
$A_{sd}$	extra flow area behind the summer dike
$P_i$	wetted perimeter of the flow section
$S$	water-level slope

- ◇ The discharge including the (extra) flow area behind the summer dike is computed as follows

$$Q_i = U_i(A_i + A_{sd}) \quad (1.168)$$

Figure 1.58 depicts the actual (extra) total area behind the summer dike as function of the local water level ( $h$ ) in the cross-sectional profile. The (extra) total area behind the summer dike is added to the total area of the cross-sectional profile. There is a hysteresis in the extra total area for water levels varying from flood plain base level ( $Z_{base} = 2.0 \text{ m}$ ) to crest level of summer dike plus transition height ( $Z_{sd} + T = 4.5 \text{ m}$ ). We call line ABC the rising limp and line CA the falling limp of the hysteresis. The so-called “hysteresis flag” determines which limp of the hysteresis is to be followed. In case the hysteresis flag=1 the rising limp of the hysteresis is followed, else the falling limp is followed. At the onstart of a computation yields that the hysteresis flag=1. The actual applied extra total area behind the summer dike is computed as follows:

- 1 If  $h < Z_{base}$ ; Hysteresis flag is set to 1. Total area behind the summer dike is zero.
- 2 If  $Z_{base} \leq h \leq Z_{sd} + T$  and hysteresis flag=1;
  - ◇ For  $Z_{base} \leq h < Z_{sd}$ ; Total area behind the summer dike is zero.
  - ◇ For  $Z_{sd} \leq h \leq Z_{sd} + T$ ; Total area behind the summer dike varies as a quadratic function of water level ( $h$ ) between zero and ExtraTotalArea (= 250 m<sup>2</sup>)
- 3 If  $Z_{base} \leq h \leq Z_{sd} + T$  and hysteresis flag=0; Total area behind the summer dike varies as a quadratic function of water level ( $h$ ) between zero and ExtraTotalArea.
- 4 If  $h > Z_{sd} + T$ ; Hysteresis flag is set to 0. Total area behind the summer dike is equal to ExtraTotalArea.

#### 1.1.34 Super-critical flow

The SOBEK-Flow-module can deal with super-critical flow. The flow in a reach or reach segment is super-critical if the Froude number [–] is higher than 1:

$$\text{Froude} = \frac{u}{\sqrt{gA_f/W_f}} \quad (1.169)$$

$u$	Velocity [m/s]
$g$	Acceleration due to gravity [ $\text{m/s}^2$ ] ( $\approx 9.81$ )
$A_f$	Wetted area [ $\text{m}^2$ ]
$W_f$	Flow width [ $\text{m}$ ]

##### Remarks:

- ◇ When the Froude number is less than 1, the flow is sub-critical.
- ◇ Transitions from super-critical to sub-critical flow causes an hydraulic jump.



#### 1.1.35 Surface level

The surface level is the level of the soil surface i.e. the embankment level of the cross section. When the water level is higher than this level there is a flood. Normally water is stored above this level on a certain storage area. When the water level drops, this storage is emptying back into the reach or node.

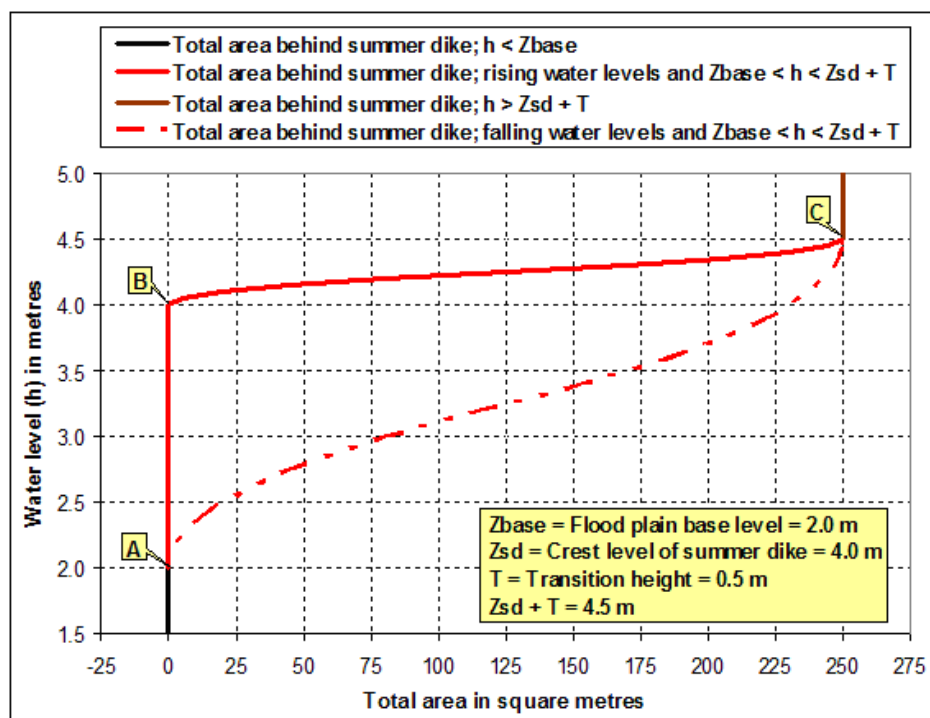


**Figure 1.58:** Total area behind the summer dike as function of local water levels.

## 2 Conceptual description (1D2D)

### 2.1 Hydrodynamics Overland 2DFLOW

#### 2.1.1 Introduction

This section is about the modeling of the lateral coupling between 1D horizontal network flow models (obtained upon averaging over width and depth) and 2D (depth-averaged) horizontal overland flow models in between the network branches, for the modeling of flooding in urban and rural areas:

- ◇ flash flooding (or pluvial flooding);
- ◇ fluvial flooding;
- ◇ coastal flooding;
- ◇ groundwater flooding.

Both the physical modeling of such a lateral coupling and its numerical implementation will be considered.

This section assumes the availability of model components that provide, or that are required to compute, the incoming discharge:

- ◇ rainfall;
- ◇ (upstream) discharges;
- ◇ (tidal) water levels;
- ◇ groundwater fluxes.

The focus lies on the modeling of the response to these discharges by the flow through an urban or rural area with drainage channels and rivers:

- ◇ inundation patterns;
- ◇ (maximum) water levels;
- ◇ local discharges and flow velocities.

Point of departure is to model the flow through networks of channels and rivers by means of efficient 1D shallow-water network models, and to include a 2D shallow-water model for the flow across any urban or rural area when the discharges or water levels are high enough for such an area to flood. This requires couplings between the two models that become active everywhere in the domain where there is a flow from a 1D network to an adjacent 2D area or vice versa.

A 1D network flow description assumes that the flow dynamics in crosswise direction can be neglected, i.e., the effect of any crosswise flow can be ignored and the water level in crosswise direction can be assumed uniform. For example, 2D/3D dynamic effects in (sharp) bends are not taken into account, i.e., their effect on the global flow behavior is assumed negligible.

When a 1D-modeled channel section is flooded, strong crosswise flow may occur, in which case the assumptions of negligible crosswise flow dynamics and uniform crosswise water level may not be valid anymore. If that is the case, then the only solution is to model that stretch of channel 2D or even 3D.

An alternative solution seems to be to model the flow in channel sections 1D for water levels below the flooding level and to apply 2D modeling for the flood flow above the channel's



flooding level when the water level rises above that level.

In this approach a 2D model for the flow in flood plains and other flooded areas lies on top of the 1D channel flow models, with a vertical coupling in between: a *1D-2D modeling with vertical coupling*. This approach poses several problems:

- ◇ Since the water level in crosswise direction is assumed constant in the 1D model and can have a gradient in the 2D model, which water level to use in the 1D model to compute the lengthwise hydrostatic pressure gradient if the 2D layer is active?
- ◇ If the 2D layer is active, crossflow effects are still neglected in the 1D part and therefore only partially included.
- ◇ The flow in lengthwise direction inside the channel and in the flood layer above the channel are not independent. It is not clear how the 1D model and 2D model should be coupled vertically to take this dependency into account properly. Some sort of friction condition between the two layers?
- ◇ The vertical coupling should ensure that the 2D model above the channel bed feels the bed friction. Bed friction is included in the 1D model, but it is not clear how to include it in the 2D model on top of the 1D model. It is also not clear how to include the effect of the flow in the 2D layer in the friction formulation used in the 1D model.

The first two items do not pose a problem if in the, usually small, area covered by the channel network the effect of crossflow momentum can also be neglected in case of flooding. In that case a horizontal coupling between a network of channels modeled 1D and the flood plains between the channels modeled 2D may just as well be considered. This may even be a better approach. Describing the flow in the channels at any water level with one and only one 1D model makes the modeling of this part of the flow problem more transparent and easier to calibrate.

Notice that when a relatively small water layer in flooded areas is present, a flow in the flood plains will cause an at most small crossflow in the channels where the water depth is (much) larger. When the water layer in flooded areas is rather large, the velocity variations and water-level gradients are usually moderate to small. In other words, in both cases the effect of any momentum transport across the channels caused by flooding may generally be expected to be negligible, indicating that a *1D-2D modeling with a horizontal coupling* in between may often be adequate. Obviously, the assumption is only valid if the channels in the 1D network are sufficiently deep. In particular, the applied 1D channel models should *not* include any shallow areas like river flood plains.

Summarizing, there are basically two ways to establish a 1D-2D coupling:



- ◇ **vertical 1D-2D coupling:** the 2D area is defined in the entire domain and lies 'on top of' the 1D network where it coincides with channels and rivers. **Note:** in this approach, *the 1D channels and rivers have limited height*. They end at the bottom of the 2D area, where in vertical direction the 2D area starts.
- ◇ **horizontal 1D-2D coupling:** separate 2D areas are defined in between the branches of the 1D network of channels and rivers (domain decomposition approach). **NOTE:** in this approach, *the 1D channels and rivers have limited width*. They end at the boundaries of the 2D areas, where in horizontal direction the 2D areas start.

Because of the close connection between the 1D model and the 2D model, the shape of the 2D model affects that of the 1D model or vice versa. With the vertical coupling, the 1D model is limited from above; with the horizontal coupling, the boundaries of the 2D models limit the width of the 1D model, or, equivalently, the 1D model determines the position of



the boundaries of the 2D models in between the branches. This is not the case when the 1D model and the 2D model are strictly separated. Seyoum *et al.* (2012) present a vertical coupling by means of the flow through manholes between an otherwise separated 1D sewer network model and 2D overland flow model. Chen *et al.* (2012) and Chen *et al.* (2013) present a horizontal coupling connecting independently designed 1D network models and 2D or 3D shallow-water models through the exchange of information at the boundaries.

An overview<sup>1</sup> of the properties of both types of couplings is presented in Table 2.1. Based on these properties, and on experiences with the vertical coupling technique in SOBEK 2 it was decided to implement a new horizontal coupling for SOBEK 3. **Note:** A question mark has been added to some properties, because the experiences with the new horizontal 1D-2D coupling are of course still limited.



	vertical 1D-2D coupling	horizontal 1D-2D coupling
accurate	—	+
efficient	+	?
robust	+	+?
extendable, easy maintenance	—	+
easy to set up model	+	+
modeling restrictions	+	—
insight in physical modeling	—	+

**Table 2.1:** Estimation of the properties of the vertical 1D-2D coupling versus the horizontal 1D-2D coupling.

Explanation to the properties of the new horizontal 1D-2D coupling:

- ◇ *accuracy* and *insight in physical modeling* is obtained because each 1D-2D interface is a separate weir-type model component that can be set up independently for each 1D channel bank (*no modeling restrictions*);
- ◇ tests have so far shown that the *efficiency* is reasonable; further improvement is possible and probably required;
- ◇ tests have so far shown that the *robustness* is quite good;
- ◇ there are several ways to *extend* the currently implemented 1D-2D coupling; the possibility to use non-matching grids and non-matching time steps at 1D-2D interfaces, to be realized in the future, is particularly interesting because that will improve the efficiency, flexibility and ease of use of the new 1D-2D modeling approach; the algorithm has been set up such that this is fairly easy to realize (*easy maintenance*);
- ◇ the developed preprocessing tools make it *easy to set up a 1D-2D model*.

From here on, the focus of this document will lie on the conceptual description of the horizontal 1D-2D coupling. In section 2.1.2 the technique currently applied in SOBEK 3 is described: a technique based on an explicit coupling between the 1D model (as described in section 1.1) and the 2D model (as described in the D-Flow FM technical reference manual).

**Note:** The 1D network modeling capabilities of D-Flow FM and a technique to couple a 1D D-Flow FM model to a 2D D-Flow FM model are currently also under development for use in future versions.



A horizontal 1D-2D coupling as mentioned above has never been developed. The principle is:

- ◇ a network grid for the 1D channel and river network;

<sup>1</sup> This overview is indicative and for a typical complex 1D-2D application. Depending on the model and the effort spent in its optimization, the comparison of both types of couplings may be different for some of the properties.

- ◇ boundary-fitted (unstructured) grids for the 2D areas in between the branches and in between branches and the domain boundaries;
- ◇ horizontal couplings to connect at the interfaces the solution of the 1D network and the solution of the 2D areas.

An example is shown in Figure 2.1.

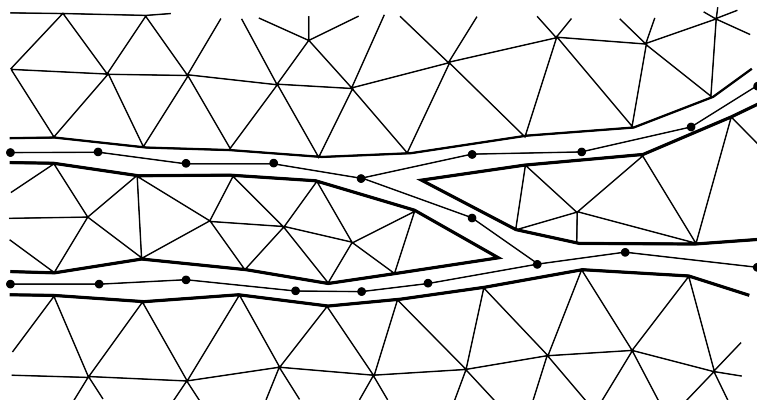


**Figure 2.1:** The proposed 1D-2D modeling with horizontal coupling.

Flooding in urban and rural areas can also be modeled by the use of just a 2D model, provided that a sufficiently high resolution is available locally to capture the details of the flow through the 1D network. An example of a fully 2D D-Flow FM river-overland flow model is given in Figure 2.2.

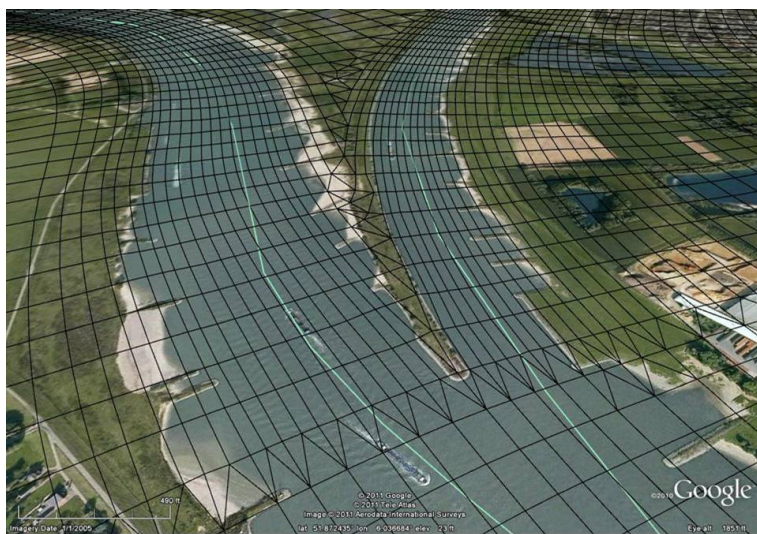


**Figure 2.2:** Example of a D-Flow FM grid with sufficient resolution across channels to capture the details in that direction.

Because of the (much) larger number of grid cells inside the channels, an excessive amount of computational time will then be required to simulate large-scale network flows. Moreover, since in a 2D model the momentum equation in crosswise channel direction is solved as well, a large time-step restriction and hence very long computational times may result, because of the partially explicit nature of the applied numerical scheme in combination with the usually small grid size across channels. This may even be the case when narrow channels are discretized with a single row of long but thin grid cells with high aspect ratio.

The conclusion reads that the large-scale modeling of flooding in urban and rural areas with

just a 2D model is not convenient.

Kim *et al.* (2012) describe a model consisting of a coupling between a hydrological model and a 2D hydrodynamic model using unstructured grids of regular grid cells with refinements in channels. The locally fine grids (also in streamwise direction, which is a waste of resolution in elongated channels) require the use of small time steps. By applying local time stepping the efficiency has been improved by 50–70%. See also, e.g., Bradford and Sanders (2002), Begnudelli *et al.* (2008), Gallegos *et al.* (2009), and Sanders *et al.* (2010).

**Note:** The coupling between 1D and 2D in *longitudinal direction*, i.e., the coupling of 1D models to 2D models at the boundaries of 1D branches and in the direction of the 1D flows in those branches (instead of through 1D lateral discharges along the branches that are normal to the direction of the 1D flows, as in the lateral 1D-2D coupling), is not considered yet in this version. Because an efficient longitudinal 1D-2D coupling can be realized using standard open-boundary formulations, its realization in the future is considered fairly straightforward. With regard to its accuracy, integration of the discharges and averaging of the water levels across the (parts of) the outer 2D cell faces connected to a 1D cross-sectional area suffices for a longitudinal coupling from 2D to 1D. For the longitudinal coupling in the other direction, from 1D to 2D, the average discharge and water level at a 1D coupling boundary need to be distributed across the faces of the 2D grid cells where a 2D domain is connected to an outer 1D channel cross-section. For the discharge a distribution based on the conveyance across the 1D width could be used, but it may also be possible to use the distribution as it is computed at the interface in the 2D domain. These aspects are currently under consideration in the development of a longitudinal horizontal 1D-2D coupling compatible with the lateral horizontal 1D-2D coupling described below.



### 2.1.2 Lateral horizontal 1D-2D coupling

In this approach, 1D network flow models are combined with 2D overland flow models that lie *in between* (and *not* across, as in vertical 1D-2D couplings) the branches, as well as in between branches and the boundaries of the domain. A schematic of this modeling approach is depicted in Figure 2.3.

**Note:** Two ways of horizontal 1D-2D coupling are envisioned: embedded (in future D-Flow FM) and with strict model separation (in SOBEK 3 and presented here).



The principle of the **embedded lateral horizontal 1D-2D coupling** is shown in Figure 2.4.

The principle of the **lateral horizontal 1D-2D coupling with strict model separation** is shown in Figure 2.5.

In the Figures 2.4 and 2.5, the 2D areas are discretized using unstructured grids, but the use of other type of grids may be feasible as well. The figures illustrate that it will generally not be possible to have the 2D grids coincide exactly with the boundaries of the 1D channels. Note, however, that the construction of those boundaries is an approximation anyway and that the gap can be made small compared to the 2D grid size in which case its effect will be negligible.

Description and properties of both horizontal 1D-2D couplings:

- ◇ In D-Flow FM at lateral horizontal 1D-2D interfaces: mass conservation (single discharge  $q_{1D-2D} \equiv q_{2D-1D}$  in Figure 2.4) and a flow link, i.e., some discretized normal momentum equation using the nearest 1D and 2D water level ( $\zeta_{1D}$  and  $\zeta_{2D,i}$  in Figure 2.4) and some distance between them to determine a water-level gradient (not necessarily normal to the interface). If an (explicit) discretization of the convection terms is included (not clear which

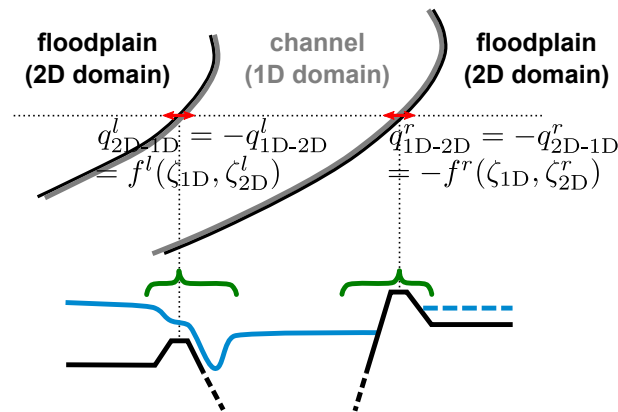


**Figure 2.3:** Principle of the lateral horizontal 1D-2D coupling, where 2D modeled areas lie next to the 1D modeled waterways. The two red horizontal two-sided arrows indicate the couplings that independently model the flow across two separate waterway banks. That flow exchange, (usually) not modeled in detail, occurs in the strips along the banks left and right of the waterway indicated by the green braces. For clarity, the size of the dikes and the free-surface variation across the dike at the left interface have been exaggerated in the figure. Lateral discharge per unit length from 2D domain to 1D domain  $q_{2D-1D}$  is a function of the water levels  $\zeta_{2D,I}$  and  $\zeta_{1D}$  of those domains at the interface. Because of mass conservation, lateral discharge per unit length in the other direction  $q_{1D-2D}$  equals  $-q_{2D-1D}$ .

velocity variables to use here), there may be a severe time-step stability restriction in case of a narrow 1D channel and (hence) small 2D grid cells.

Advantage: fully implicit coupling of water levels.

Disadvantages: not flexible: 1D and 2D grids must match at interface, 1D and 2D time steps must be equal, intertwining of 1D implementation and 2D implementation due to fairly strong coupling between 1D modeled areas and 2D modeled areas (single overall systems of equations for the water levels at each next time level must be constructed).

- ◇ In the coupling technique of SOBEK 3 at lateral horizontal 1D-2D interfaces: mass conservation ( $q_{1D-2D} = q_{2D-1D}$  in Figure 2.5) and a  $q$ - $h$  relation, i.e., a reduced normal momentum equation using the 1D and 2D water level at the interface at the same location ( $\zeta_{1D}$  and  $\zeta_{2D}$  in Figure 2.5). Implicit coupling solved iteratively using explicit updates of flow information crossing the interface.

Advantages: flexible: allows in principle non-matching 1D and 2D grids as well as different 1D and 2D time steps. Because of explicit updates interpolations are feasible and of moderate complexity. Inherent parallelism: due to the explicit update of coupling information across the 1D-2D interfaces, update of the solution per 2D area in independent computations. Strict separation of 1D modeled areas and 2D modeled areas, hence strict separation between 1D implementation and 2D implementation possible, with explicit exchange of information through a generalized implementation of lateral discharges (1D) and boundary conditions (2D).

Disadvantage: requires an iterative solution procedure to be optimized, which is likely to require more advanced 1D lateral discharge implementations and 2D boundary condition implementations especially when going for fast convergence.

The SOBEK 3 lateral horizontal coupling technique works as follows:

- ◇ Discretize the 1D network using a 1D network model. It is important in this step to clearly define the lateral boundaries of the channels, as they define the position of the interfaces between the 1D network and the 2D areas where an overland model will be used.

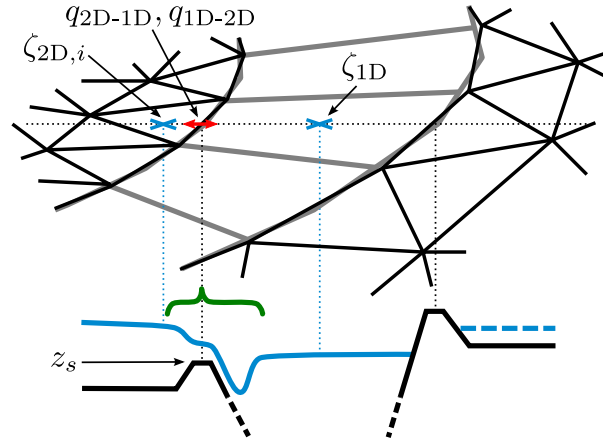


**Figure 2.4:** Principle of the embedded lateral horizontal 1D-2D coupling, more or less applying and solving flow equations across the 1D-2D interface.

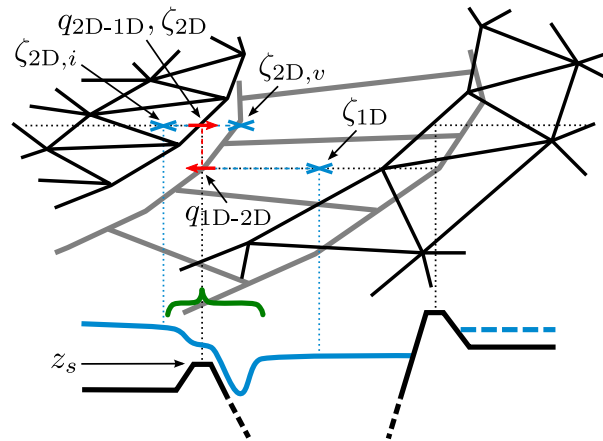


**Figure 2.5:** Principle of the lateral horizontal 1D-2D coupling with strict model separation, using separate models for the 2D and the 1D areas coupled at the interfaces by coupling conditions.

- ◇ Discretize the 2D areas in between the channels of the 1D network model and in between 1D channels and the outer boundaries of the (2D) domain by D-Flow FM-type unstructured grids.

Matching grids at the interfaces (like in the Figures 2.1 and 2.5) is undoubtedly the easiest option to realize. This may require the subdivision of grid cells of the 1D model for cells in which the orientation of the channel segment changes significantly. The subdivision is to ensure a proper representation of curved channel boundaries by the straight cell faces of the 2D grid. It will also require the redesign of the grid of the 1D model in stretches where the 1D grid size varies significantly, to avoid excessively large grid-cell variations in the 2D grid.

Since the coupling between the 1D network model and the 2D overland models will be explicit per iteration per time step (implicit per time step upon convergence), non-matching grids are not much more complicated. With suitable integration/interpolation procedures of discharges and water levels at or near the interfaces (easy to apply because the coupling is explicit), the grids of the 1D network model and the 2D overland models could be designed fully independently. The subdivision of certain 1D grid cells may then still be useful, to avoid a loss of resolution in the case of flow across a 1D channel. This is because information of a 2D model will be integrated if the 1D grid has a coarser resolution at the interface than the 2D grid, while information of the 1D model will be interpolated.

So with a fine-grid 2D model on both sides of a coarse-grid 1D model section, flow details along the interface may get lost when crossing the channel, because the interpolation of 1D model data will not fully restore the details that were present in the 2D solution prior to integration. In fact, the possibility of non-matching grids is mainly useful to avoid that an irregular grid size distribution in the 1D model affects the quality of the grid of the 2D models.

- ◇ Define the couplings between the 1D network model and the 2D overland models, by applying mass conservation across the interfaces (lateral discharge of 1D model equal to discharge at boundary of a 2D model) and by a dynamic condition. The latter describes the discharge through the interface as a function of the water-level slope normal to the interface: a weir-type  $q$ - $h$  relation that depends on dike height, dike shape, that includes resistance terms, etc.
- ◇ Solve the couplings (iteratively, if necessary) by solving alternately per time step the 1D network model and the 2D overland models using an optimized update of coupling information (optimized multiplicative Schwarz, a DD algorithm).

At present, the best procedure seems to be to first do an inexpensive 1D network computation with an optimized combination of the two coupling conditions to determine a first estimate of the lateral discharges at the next time level, using the water levels near the interfaces of the 2D models at the previous time step. Then compute the 2D models with an optimized (non-reflecting or Riemann) combination of the two coupling conditions as boundary condition at the interfaces, using the updated water levels of the 1D model. Repeat those two steps if necessary. The final step is a 1D network computation with imposed lateral discharge, i.e., the discharge at the interface computed in the last executed 2D model runs. This final step is to ensure mass conservation.

**Note:**

- ◇ In the above approach, the assumption is that the 1D channels are narrow enough for the lateral momentum changes across the channel width to be negligible. In case of flooding, the flow (lateral discharge) is simply passed from one bank to the other. Friction losses across the channel banks (due to the presence of levees or dikes) are to be modeled by including them in the  $q$ - $h$  relations applied at the interfaces. Such a modeling is required anyway when using a 2D grid too coarse to capture 'small-scale' features like levees and dikes in detail.
- ◇ As expected, the application of optimized coupling conditions required an extension of the available boundary-condition implementation of D-Flow FM and an extension of the implementation of lateral discharges in SOBEK.
- ◇ Supercritical flow at the interfaces into or out of the 2D areas may require special measures. In the former case, two boundary conditions should normally be applied; in the latter, no boundary conditions should be applied. Some experience is available in changing the number of applied boundary conditions as a function of the flow regime in a 1D shallow-water model.

For the time being the flow at the 2D side of 1D-2D interfaces is assumed to be subcritical. The flow across a 1D-2D interface, however, may be both subcritical and supercritical, i.e., both drowned-weir flow and free-weir flow are supported.



### 2.1.2.1 Properties

Advantages:

- ◇ Modular approach: 1D model and 2D model can be separate codes, loosely connected by the exchange of 'external' data determining the lateral discharges and the boundary values to be applied.

- ◇ Modular approach: independent development of the 1D model and the 2D model remains possible.

**Note:** Of particular interest is the extension of D-Flow FM (and SOBEK) with a more implicit time integration that reduces the current time-step stability restriction. This is expected to improve the efficiency of D-Flow FM (and SOBEK), with at most a marginal loss in accuracy. The latter is especially true if in addition a variable time step will be implemented: small time steps when transient phenomena like flooding are to be modeled; large time steps when the flow is nearly stationary.



- ◇ Modular approach: fully independent design of 1D schematization and all 2D schematizations.

**Note:** This advantage will become fully available when in the future the coupling will be extended to non-matching grids and the use of different 1D and 2D time steps at the interfaces.



- ◇ Inherent parallelism: models of all 2D areas are independent and can be computed in parallel.

Disadvantages:

- ◇ Non-proven technology.

The results obtained so far with the current implementation confirm the feasibility of the method.

- ◇ Several iterations are generally required per time step.

**Note:** Further study and development is required to check and improve the efficiency of this method. For example, it may be possible to combine the 1D-2D coupling iterations with the existing iterative solution procedures that solve for the water level. Further optimization of the 1D-2D iterative solver is also possible.



- ◇ 2D grid generation required per 2D area, which may not be obvious when there are many of such areas.

**Note:** Algorithms have been designed using the D-Flow FM grid generation tools already developed to fully automate this procedure.



### 2.1.3 Lateral horizontal 1D-2D coupling — the details

The flow in the domain is either modeled 1D or it is modeled 2D. The flow is modeled 1D in the branches of the network(s) of channels and rivers. In the areas in between the flow is modeled 2D. A horizontal 1D-2D coupling is applied to connect the 1D and 2D flow models.

The elements to be discerned in the development of a horizontal 1D-2D coupling are:

- ◇ 1D network flow model,
- ◇ 2D flood flow model,
- ◇ horizontal 1D-2D coupling.

The issues to be considered in the coupling are the physical modeling of the coupling (→ the coupling equations) and the numerical implementation of the coupling (→ discretization and solution procedure). Applying the coupling equations is trivial when they are discretized explicitly in time. However, since the 1D and 2D flow models that will be used (SOBEK, D-Flow FM)

are partially implicit in time, the coupling equations must be implemented implicitly in time as well, to avoid a loss in stability and accuracy. In fact, the space and time discretization of the flow models dictates the numerical implementation of the coupling equations. For this reason, the discretization of the flow models as far as relevant for the implementation of the coupling is first presented, following a memo by Kernkamp (Kernkamp (2008)) and the D-Flow FM technical reference manual (Deltares (2014)). Next, two ways of lateral horizontal 1D-2D coupling are presented: the one under development for D-Flow FM (embedded coupling) and the one implemented in SOBEK 3 (coupling with strict model separation).

### 2.1.3.1 1D and 2D flow modeling

The flow in the 2D parts of the domain is modeled by the 2DH shallow-water equations. Because of the numerical implementation that is used both in SOBEK and in D-Flow FM, the 2DH continuity equation and 2DH momentum equation may be written as:

$$\frac{\partial h}{\partial t} + \nabla \cdot (h\mathbf{u}) = 0 , \quad (2.1a)$$

$$\frac{\partial \mathbf{u}}{\partial t} + g\nabla\zeta + b\mathbf{u} = \mathbf{e} , \quad (2.1b)$$

with  $\mathbf{e}$  all terms in the momentum equation that are discretized explicitly (convection, viscosity, Coriolis, wind force) and with  $b\mathbf{u}$  the bottom-friction term in quasi-linear form that is discretized implicitly, where  $b$  is the linearization coefficient (e.g.,  $g|\mathbf{u}|/(C^2h)$ ) that is evaluated explicitly (Picard linearization). Furthermore,  $h = h(\mathbf{x}, t) = \zeta + d$  is the total water depth, with  $\zeta = \zeta(\mathbf{x}, t)$  and  $d = d(\mathbf{x})$  respectively surface elevation and stationary depth relative to a horizontal plane of reference,  $\mathbf{u} = \mathbf{u}(\mathbf{x}, t) = (u, v)^T$  is the horizontal velocity vector, and  $\nabla = (\partial/\partial x, \partial/\partial y)^T$  is the horizontal gradient operator.

The numerical implementation of the 1DH depth- and width-averaged shallow-water equations in SOBEK and D-Flow FM is similar, hence these equations are written similarly:

$$\frac{\partial A}{\partial t} + \frac{\partial(Au)}{\partial x} = q , \quad (2.2a)$$

$$\frac{\partial u}{\partial t} + g\frac{\partial \zeta}{\partial x} + bu = e , \quad (2.2b)$$

with  $A$  the wetted cross-sectional area,  $u$  the average flow velocity over the wetted cross-sectional area in the longitudinal direction  $x$  of the 1D channel, and with  $q$  the incoming lateral discharge per unit length.

Because of the applied staggered-grid technique, momentum equation (2.1b) is discretized per normal velocity component  $u$  that are defined at the cell faces:

$$\frac{u_f^{n+1} - u_f^n}{\Delta t} + \frac{g}{\Delta x_u} (\theta(\zeta_2^{n+1} - \zeta_1^{n+1}) + (1 - \theta)(\zeta_2^n - \zeta_1^n)) + b^n u_f^{n+1} = e^n , \quad (2.3)$$

with  $\zeta_2$  and  $\zeta_1$  the water level at the circumcenter downstream (in positive  $u_f$ -direction) and upstream (in negative  $u_f$ -direction) of the cell face, with  $\Delta x_u$  the distance between these two circumcenters, and with  $\theta$  the parameter that determines the level of implicitness of the terms taken implicitly.

The discretization of (2.2b) has exactly the same form as (2.3).

The mass-conservative finite volume discretization of (2.1a) is written in a generic form that



also represents the discretization of (2.2a):

$$\frac{V_c^{n+1} - V_c^n}{\Delta t} + \sum_{\text{cell faces}} A_f^n s_{c,f} (\theta u_f^{n+1} + (1 - \theta) u_f^n) = \Delta x_q q_c^*, \quad (2.4)$$

with  $V_c = V_c(\zeta_c)$  the water-level dependent volume of water that is contained in a control volume (the grid cells) over which (2.1a) is integrated and subsequently discretized, with the  $A_f$  the surfaces of the *vertical* cell faces (where the velocity unknowns  $u_f$  are located), with  $q_c^*$  the average value over the time step<sup>2</sup> of some incoming lateral discharge per unit length  $q_c$  for the grid cell (mass control volume) under consideration, and with  $\Delta x_q$  the horizontal length of the part of the cell where depth-integrated mass flow  $q_c$  is specified. If both  $\zeta$  and  $d$  are approximated piecewise constant per grid cell, this reads  $V_c = S_\zeta(\zeta_c + d_c)$ , with  $S_\zeta$  the constant *horizontal* surface of the control volume (the surface of a grid cell). In that case the first term in the left-hand side of (2.4) can be written as  $(V_c^{n+1} - V_c^n)/\Delta t = S_\zeta(\zeta_c^{n+1} - \zeta_c^n)/\Delta t$ .

The sum in (2.4) is taken over the mass fluxes through the faces of the grid cell under consideration (the faces of the mass control volume). They are approximated per cell face by the product of the wetted cell-face surface  $A_f = A_f(\zeta)$  and normal velocity  $u_f$ <sup>3</sup>. The direction of the mass flux depends on the direction of  $u_f$  relative to the grid cell (outward or inward) and is taken care of by the switches  $s_{c,f}$  for the faces of the cell:

$$s_{c,f} = \begin{cases} 1 & \text{if } u_f > 0 \text{ is directed } \textit{outward} \text{ of cell } c, \\ -1 & \text{if } u_f > 0 \text{ is directed } \textit{inward} \text{ of cell } c. \end{cases} \quad (2.5)$$

An external discharge  $q_c$  has been added in the right-hand side of (2.4) to have this discretization in a form that can also represent the discretization of 1D continuity equation (2.2a). In that case this reads  $V_c(\zeta) = A_\zeta(\zeta)\Delta x_\zeta$ , with  $A_\zeta$  the water-level dependent wetted cross-sectional area at the location of the  $\zeta$ -point and with  $\Delta x_\zeta$  the length of a 1D control volume, i.e., the distance between two adjacent  $u$ -points where the two mass fluxes in the sum of (2.4) are computed. The generalization to  $\zeta$ -points where several 1D branches are connected to (connection nodes) is straightforward. The  $A_f$  in the 1D mass fluxes are the wetted vertical faces of the 1D mass control volumes that are normal to the channel axis, i.e., the wetted cross-sectional areas at the location of the  $u$ -points.

The discretized time derivative in (2.4) is generally nonlinear in the unknown  $\zeta_c^{n+1}$ , the water level at the cell center/control volume. Its determination therefore requires linearization in combination with an iterative solution procedure:

$$\frac{V_c^{n+1} - V_c^n}{\Delta t} \approx \frac{V_c^{p-1} + (\zeta_c^p - \zeta_c^{p-1})(\partial V/\partial \zeta)^{p-1} - V_c^n}{\Delta t} = \frac{V_c^{p-1} + (\zeta_c^p - \zeta_c^{p-1})S_\zeta^{p-1} - V_c^n}{\Delta t}, \quad (2.6)$$

where the superscripts  $p - 1$  and  $p$  indicate respectively the previous and the next iterative approximation of variables at the next time level  $n + 1$ .

<sup>2</sup>The level of implicitness of  $q_c$  turns out to be irrelevant in the horizontal 1D-2D coupling, hence no  $\theta$ -weighing here.

<sup>3</sup>Please recall that often an upwind approximation is used for the wetted face surface  $A_f$  in (2.4). Since  $A_f$  is evaluated explicitly, the upwind direction is determined by  $u_f^n$  and *not* by the velocity approximation that is actually used per time step, i.e.,  $\theta u_f^{n+1} + (1 - \theta) u_f^n$ . As a result, the evaluation of  $A_f$  may be *downwind* at locations and time steps where the flow normal to a face changes direction. Since this normally occurs at at most a small number of faces while  $u_f$  at these faces will then be small, the destabilizing effect of this downwind discretization is expected to be negligible.

Variable  $S_\zeta$  in (2.6) represents the (*horizontal*) surface of the mass control volume at the free surface. In 1D  $S_\zeta = W_\zeta \Delta x_\zeta$ , with  $W_\zeta = W_\zeta(\zeta_c)$  the channel width at the free surface at the location of the  $\zeta$ -point. In 1D  $S_\zeta$  is a constant per mass control volume if channel width  $W_\zeta$  is constant over the depth. In 2D  $S_\zeta$  is constant per grid cell (and equal to the surface of the grid cell) as soon as the water level is above the shallowest bottom level inside a grid cell, and hence a constant per mass control volume if, as mentioned above, both  $\zeta$  and  $d$  are approximated piecewise constant per grid cell.

Substituting (2.6), (2.4) can be written as (replacing  $u_f^{n+1}$  by  $u_f^p$  and  $q_c^*$  by  $q_c^p$ , since when the  $\zeta_c^{n+1}$  are determined iteratively, the  $u_f^{n+1}$  and  $q_c^*$  are as well):

$$\begin{aligned} & \frac{S_\zeta^{p-1} \zeta_c^p}{\Delta t} + \sum_{\text{cell faces}} A_f^n s_{c,f} \theta u_f^p - \Delta x_q q_c^p \\ &= \frac{S_\zeta^{p-1} \zeta_c^{p-1} - V_c^{p-1}}{\Delta t} + \frac{V_c^n}{\Delta t} - \sum_{\text{cell faces}} A_f^n s_{c,f} (1 - \theta) u_f^n. \end{aligned} \quad (2.7)$$

(2.3) can be rewritten as:

$$u_f^p = R_u^n - F_u^n (\zeta_2^p - \zeta_1^p), \quad (2.8)$$

with:

$$F_u^n = \frac{1}{1 + b^n \Delta t} \frac{g \Delta t}{\Delta x_u} \theta, \quad R_u^n = \frac{1}{1 + b^n \Delta t} \left( u_f^n + \Delta t e^n - \frac{g \Delta t}{\Delta x_u} (1 - \theta) (\zeta_2^n - \zeta_1^n) \right). \quad (2.9)$$

Substitution of (2.8) in (2.7) gives:

$$\begin{aligned} & \left( \frac{S_\zeta^{p-1}}{\Delta t} + \sum_{\text{cell faces}} A_f^n \theta F_u^n \right) \zeta_c^p - \sum_{\text{cell faces}} A_f^n \theta F_u^n \zeta_a^p - \Delta x_q q_c^p \\ &= \frac{S_\zeta^{p-1} \zeta_c^{p-1} - V_c^{p-1}}{\Delta t} + \frac{V_c^n}{\Delta t} - \sum_{\text{cell faces}} A_f^n s_{c,f} (1 - \theta) u_f^n - \sum_{\text{cell faces}} A_f^n s_{c,f} \theta R_u^n, \end{aligned} \quad (2.10)$$

with  $\zeta_c^p$  the value of  $\zeta^p$  at the grid cell/control volume under consideration, and with the  $\zeta_a^p$  the value of  $\zeta^p$  at the adjacent grid cells/control volumes.

Please recall that the above equations ((2.7), (2.8), (2.9), and (2.10)) have been formulated such that they represent the equations used in 2D simulations as well as in 1D simulations.

The equations (2.10) per control volume, together with the discretized boundary conditions, form the system of equations to be solved for the determination of the next iterative estimation  $\zeta^p$  of the solution  $\zeta^{n+1}$  that is sought.



**Note:** A couple of remarks on solving (2.10):

Linearization coefficient  $S_\zeta^{p-1}$  in the left-hand side of (2.10) as well as the first term in the right-hand side are to be updated at each nonlinear iteration. The first means that the matrix of the system of equations to be solved changes and hence has to be rebuilt at each nonlinear iteration. Keeping  $S_\zeta^{p-1}$  fixed at its first value  $S_\zeta^0 = S_\zeta^n$  inside each nonlinear iteration loop would prevent that, and would allow the reuse of the first matrix decomposition at the remaining iterations. This is not applied in D-Flow FM or SOBEK as it may be at the expense of quite some convergence speed. By keeping the value of  $S_\zeta^{p-1}$  fixed, the convergence speed changes

from quadratic (Newton linearization) to linear, which is generally considerably slower. This applies in particular to typical SOBEK applications where  $S_\zeta^{p-1} = W_\zeta^{p-1} \Delta x_\zeta$ . Because  $W_\zeta$  can be a strongly varying function of  $\zeta$ , the value of  $W_\zeta^{p-1}$  may change significantly within a nonlinear iteration loop. On the other hand, since both D-Flow FM and SOBEK use rather small time steps,  $S_\zeta^{p-1}$  will probably not vary much within the nonlinear iteration process per time step. It may be worth investigating if by keeping the linearization fixed, or by updating the matrix only every two or three iterations (or only the first couple of iterations, when the nonlinear changes of  $S_\zeta^{p-1}$  are the largest), a substantial decrease in computational time could be obtained.

In typical D-Flow FM applications, the water level will be largely above the bottom, so  $S_\zeta^{p-1}$  will generally be constant nearly everywhere anyway and the nonlinear iteration loop will converge very rapidly. However, in drying and flooding areas, typical for flooding applications, keeping  $S_\zeta^{p-1}$  fixed in D-Flow FM within each nonlinear iteration loop may have a negative effect on the nonlinear convergence speed. This *only* applies when the discrete approximation of the bathymetry is different from that of the water level, i.e., when it is not piecewise constant. Else, as mentioned before,  $S_\zeta^{p-1} = S_\zeta$  is always constant and hence system of equations (2.10) linear.

It needs to be mentioned here that investigations are going on to enhance the efficiency of D-Flow FM by a modification of the algorithm that allows the use of larger time steps. Efficiency issues related to any nonlinear behavior of  $V(\zeta)$  (variable  $S_\zeta^{p-1}$ ) will then become more pronounced. These issues are avoided by having  $V$  linear in  $\zeta$ , i.e., by approximating the bathymetry piecewise constant per grid cell.

When the  $S_\zeta^{p-1}$  and hence the matrix are updated, the  $A_f^n$  could be updated as well, making it effectively  $A_f^{p-1}$ . In particular, their upwind value could be adapted to the direction of the velocity approximation at the previous iteration  $\theta u_f^{p-1} + (1 - \theta) u_f^n$ . While upon convergence an  $A_f^n$  may have become a downwind value (because the sign of  $\theta u_f^{n+1} + (1 - \theta) u_f^n$  may be different from that of  $u_f^n$ , cf. Footnote 3), the  $A_f^{p-1}$  will always be upwind. This may improve both the accuracy and the stability of the discretization. However, it introduces a switch in the solution algorithm (a small change in some  $u_f^{p-1}$  may result in a large change in the  $A_f^{p-1}$  value at that location) that may hamper convergence. On the other hand, by definition that large change can only occur at a change in velocity direction and hence is always multiplied by a small velocity value. Just because this issue is only relevant at changes in the velocity direction normal to a cell face and hence small normal velocities, the gain in accuracy and stability that can be expected of this modification is likely to be small. That gain may *not* be small if  $u_f^{n+1}$  in (2.4) is multiplied by  $A_f^{n+1}$  instead of by  $A_f^n$ , with the  $A_f^{n+1}$  a function of both the  $u_f^{n+1}$  (for their upwind location) and the  $\zeta^{n+1}$  (for their value). NB, note that the iterative determination of the  $A_f^{n+1}$  by subsequent updates of their approximations  $A_f^{p-1}$  can conveniently be combined with the updates  $S_\zeta^{p-1}$  of that other geometry-dependent variable.

At each nonlinear iteration, linear system of equations (2.10) is to be solved. An iterative solver is used for this. As long as the outer nonlinear iteration loop has not converged ( $\zeta^p$  not yet a close approximation of  $\zeta^{n+1}$ ), full convergence of the inner linear iteration loop is not required. Exploiting this by making the convergence criterion of the inner iteration loop a small fraction of the convergence error of the outer iteration loop (inexact solvers) may give a nice reduction in computational time while having virtually no effect on the quality of the solution.

Strict mass conservation, independent of the number of nonlinear iterations, is obtained by

taking  $V_c^{n+1}$  equal to  $V_c^{p-1} + S_\zeta^{p-1}(\zeta_c^p - \zeta_c^{p-1})$ . This follows directly from (2.7). Strict mass conservation, independent of the number of nonlinear *and* linear iterations, is obtained by computing  $V_c^{n+1}$  directly from (2.4), using the most recent approximations of  $u_f^{n+1}$  and  $q_c^*$ :

$$V_c^{n+1} = V_c^n + \Delta t \left( \Delta x_q q_c^p - \sum_{\text{cell faces}} A_f^n s_{c,f} (\theta u_f^p + (1 - \theta) u_f^n) \right). \quad (2.11)$$

This may be a rather inaccurate approximation of the genuine solution of (2.4) if the nonlinear (and linear) iteration loop has reached an insufficient level of convergence. Moreover, solving (2.4) with limited accuracy weakens the implicit character of the time integration scheme and may have a negative effect on stability.

### 2.1.3.2 Embedded lateral horizontal 1D-2D coupling

The embedded horizontal 1D-2D coupling is currently under development and will become available within stand-alone D-Flow FM. For completeness sake a short and preliminary description of this coupling is given.

Across the interface additional momentum equations like (2.8) are applied (cf. Figure 2.4):

$$s_{c,I} u_{2D,I}^p = s_{c,I} R_I^n - F_I^n (\zeta_{1D}^p - \zeta_{2D,i}^p), \quad (2.12)$$

with the  $u_{2D,I}$  the values of additional 2D velocity components  $u_f$  along the interface, and with the  $R_I^n$  and  $F_I^n$  as in (2.9).

Similar to (2.5), directional switch  $s_{c,I}$  is set to 1 or  $-1$ , depending on whether  $u_{2D,I} > 0$  is directed from the 2D domain to the 1D domain or vice versa. The switch is included in (2.12) since here, unlike in (2.8) and (2.3) where the water-level difference  $\zeta_2 - \zeta_1$  is set in positive  $u_f$ -direction, the water-level difference is set from the 1D domain to the 2D domain, which may be either in positive  $u_{2D,I}$ -direction or in negative  $u_{2D,I}$ -direction.

The  $\Delta x_u$  in the  $R_I^n$  and  $F_I^n$  are taken equal to the local effective thickness of the interface. The  $b^n$  used in the  $R_I^n$  and  $F_I^n$  contain additional terms to model the losses across the interface due to, e.g., the presence of a bank or the sudden change in water depth. How to deal with the  $e^n$  in the  $R_I^n$  is a subject of investigation. They may contain special discretizations modeling the convection of normal momentum across the interface. Alternatively, those  $e^n$  may be set to zero. Since the complex flow across interfaces cannot be modeled in detail anyway (the variation of velocity and water level across interfaces is not included in the discretization), the effect of convection (and viscosity, Coriolis, wind force) across a 1D-2D interface may just as well be ignored. Since the 1D-2D interfaces form only a small part of the entire modeling area, this is a viable approach, especially when the net effect of the omitted terms across the interface is included in the  $b^n$  (subgrid modeling).

The mass flux through the 1D-2D interface is  $A_I^n s_{c,I} (\theta u_{2D,I}^p + (1 - \theta) u_{2D,I}^n)$ , cf. the second term in the left-hand side of (2.4), with  $A_I$  the surface of the relevant part of the flow area across the interface. So we have:

$$Q_{2D-1D}^p = A_I^n s_{c,I} (\theta u_{2D,I}^p + (1 - \theta) u_{2D,I}^n) \text{ and } Q_{1D-2D}^p = -A_I^n s_{c,I} (\theta u_{2D,I}^p + (1 - \theta) u_{2D,I}^n), \quad (2.13)$$

with  $Q_{2D-1D}^p$  and  $Q_{1D-2D}^p$  respectively the discharge from the 2D domain to the 1D domain and from the 1D domain to the 2D domain. These mass fluxes are added to the 2D and to the 1D model equations by setting  $\Delta x_q q_c^p$  in (2.7) or (2.10) equal to  $Q_{1D-2D}$  (mass flux from 1D to 2D) for the 2D grid cell where this flux is applied, and by setting  $\Delta x_q q_c^p$  in (2.7) or (2.10)

equal to  $Q_{2D-1D}$  (mass flux from 2D to 1D) for the 1D grid cell where this flux is applied. In both cases the flux represents a (sort of) lateral discharge.

Mass conservation (2.13) and normal momentum approximation (2.12) together define the embedded horizontal 1D-2D coupling. Its properties have been briefly discussed in Section 2.1.2.

Note that in this approach it is not required that the 2D domains and the 1D domains are adjacent. Equations (2.12) and (2.13) can also be applied when there is a gap in between the domains, connecting some 1D grid cell to some 2D grid cell that is at the boundary of a 2D domain. The orientation of the boundaries of both domains does not have to be the same either. Because of this flexibility, it is even possible to have the 2D domains overlapping the 1D domains. That latter way of modeling 1D-2D interfaces actually corresponds with an embedded vertical coupling (not presented in this document).

### 2.1.3.3 Lateral horizontal 1D-2D coupling with strict model separation

The approach that is used in SOBEK 3 is very similar to the one presented in Kuiry *et al.* (2010). The difference is their use of a quasi-2D horizontal flood inundation model, using a steady-state friction formulation instead of the full 2D horizontal shallow-water momentum equations, and solving the coupling between the 1D horizontal network flow model and the quasi-2D flood model implicitly. The applied 1D-2D coupling equations, however, are the same as the ones that will be used here.

The coupling equations are expressed in terms of the variables at the 1D-2D interface (cf. Figure 2.5):  $z_s$  is the height of the bank that separates the 1D and 2D domain,  $q_{2D-1D}$  is the lateral discharge per unit length from the 2D domain to the 1D domain,  $q_{1D-2D}$  the lateral discharge per unit length in the other direction, and  $\zeta_{2D,I}$  and  $\zeta_{1D}$  are the water level of respectively the 2D domain and the 1D domain at the interface. NB, no subscript  $I$  in  $\zeta_{1D}$ , because in 1D domains the water level is taken constant across the channel width. The water level at the banks (and at a 1D-2D interface) is the same as the one at the center axis of the channel and are all denoted by  $\zeta_{1D}$  (without subscript  $I$ ).

1D-2D interfaces are not modeled in detail<sup>4</sup> (by simulation) but globally (by parameterization) by modeling the flow across interfaces by means of a weir formulation. The procedure that is customary in the modeling of hydraulic structures is followed and any unsteady behavior across interfaces is neglected, i.e., the flow is locally assumed to be in equilibrium. Since the width of 1D-2D interfaces is very small compared to the length scales of typical 1D-2D applications, this is a valid assumption. Notice that, because the flow across interfaces is not discretized in detail (cf. Footnote 4), a meaningful time-dependent discretization of the flow equations at interfaces is not possible anyway.

Modeling the flow across the bank at an interface by means of a standard weir formulation, the conservation of mass and the transfer of normal momentum across interfaces are modeled

<sup>4</sup>Because the variation of velocity and water level across interfaces is not included in the discretization, a reasonably accurate detailed modeling of the flow across an interface is not even possible, cf. Section 2.1.3.2.

by:

$$q_{2D-1D} = -q_{1D-2D} , \quad (2.14a)$$

$$q_{2D-1D} = \begin{cases} 0 & \text{if } \zeta_{2D,I} - z_s \leq 0 \\ & \text{and } \zeta_{1D} - z_s \leq 0 , \\ c_e c_w 2/3 \sqrt{2g/3} (\zeta_{2D,I} - z_s)^{3/2} & \text{if } \zeta_{2D,I} - z_s > 0 \\ & \text{and } \zeta_{2D,I} - z_s \geq 3/2(\zeta_{1D} - z_s) , \\ c_e c_w (\zeta_{1D} - z_s) \sqrt{2g(\zeta_{2D,I} - \zeta_{1D})} & \text{if } 3/2(\zeta_{1D} - z_s) > \zeta_{2D,I} - z_s \\ & \text{and } \zeta_{2D,I} - z_s \geq \zeta_{1D} - z_s > 0 , \\ -c_e c_w 2/3 \sqrt{2g/3} (\zeta_{1D} - z_s)^{3/2} & \text{if } \zeta_{1D} - z_s > 0 \\ & \text{and } \zeta_{1D} - z_s \geq 3/2(\zeta_{2D,I} - z_s) , \\ -c_e c_w (\zeta_{2D,I} - z_s) \sqrt{2g(\zeta_{1D} - \zeta_{2D,I})} & \text{if } 3/2(\zeta_{2D,I} - z_s) > \zeta_{1D} - z_s \\ & \text{and } \zeta_{1D} - z_s \geq \zeta_{2D,I} - z_s > 0 . \end{cases} \quad (2.14b)$$

with  $c_e$  the discharge coefficient  $[-]$  and  $c_w$  the lateral contraction coefficient  $[-]$ .

The second and fourth line in (2.14b) specify the modeling of free-weir flow and the free-weir conditions when the flow is respectively from 2D to 1D and from 1D to 2D; the third and fifth line pertain to the drowned-weir flow regime. It has been verified that this weir formulation is a continuous and continuously differentiable function of  $\zeta_{1D}$  and  $\zeta_{2D,I}$ , *also* at the water levels where the weir flow changes regime or direction. Besides being essential for physically meaningful behavior, this is also essential for smooth numerical behavior.

If required,  $\zeta_{2D,I}$  in (2.14b) could be corrected for the energy head normal to the interface by adding  $u_{2D,I}^2/(2g)$ , with  $u_{2D,I}$  the normal velocity in the 2D domain at the interface. At present, this correction is assumed to be small enough to be negligible. Since 1D flow models do not include the modeling of the flow across 1D channels (and normal to 1D-2D interfaces), such a correction is not possible for  $\zeta_{1D}$ . Notice that an energy-head correction based on the flow velocity tangential to the interface should not be applied, since flow parallel to a hydraulic structure has an at most limited effect on the dynamics of the flow across a structure.

As before, discharge  $q_{2D-1D}$  (same for  $q_{1D-2D}$ ) is defined *per unit length*, i.e., no multiplication of the expressions in (2.14b) by the width  $W_s$  of the weir that here would be the length of a stretch of channel bank.

In view of the numerical implementation it is convenient to rewrite (2.14b) in the form of a space-discretized normal momentum equation (cf. (2.3)), adding a time derivative<sup>5</sup> to allow some (limited) modeling of the dynamic behavior of the flow at a 1D-2D interface or to improve its numerical performance (the convergence speed of the iterative solution procedure that will be applied to solve the interface equations, cf. Section 2.1.3.4 below). Restricting the presentation to the *drowned-weir* flow regime for the moment, i.e., to an interface where  $3/2(\zeta_{1D} - z_s) > \zeta_{2D,I} - z_s > 2/3(\zeta_{1D} - z_s) > 0$  or, equivalently,  $3/2(\zeta_{2D,I} - z_s) >$

<sup>5</sup>Convection terms and viscosity terms are not present in (2.15b). Due to the geometry variations and hence flow variations at 1D-2D interfaces, cf. the green braces in the Figures 2.3, 2.4 and 2.5, these terms may locally be quite large. Integration of the normal momentum equation in conservative form across an interface shows that the change of normal momentum across an interface is determined by friction losses at the bottom (modeled by the last term in the left-hand side of (2.15b)), by the overall water-level difference (modeled by the second term), and by the balance of incoming and outgoing convection and viscous fluxes at the faces of the integration volume. The effect of the latter is assumed to be small enough to be negligible compared to the effect of the bottom friction at an interface. This is a reasonable assumption, since at the faces of an integration volume across an interface the convection and viscosity fluxes are relatively small. Note that this is in agreement with the applicability of hydraulic structure formulas and confirms the discussion in Section 2.1.3.2.



$\zeta_{1D} - z_s > 2/3(\zeta_{2D,I} - z_s) > 0$  (generalizations later), the equations (2.14) become<sup>6</sup>:

$$A_{I s_{c,I}} u_{2D,I} = -\Delta x_I q_{1D-2D} , \quad (2.15a)$$

$$\Delta x_{1D-2D} s_{c,I} \frac{\partial u_{2D,I}}{\partial t} + \alpha_{SF} g(\zeta_{1D} - \zeta_{2D,I}) + \alpha_{SF} \Delta x_{u,I} b_{S,I} s_{c,I} u_{2D,I} = 0 , \quad (2.15b)$$

with  $b_{S,I}$  the friction coefficient for a submerged weir at the interface, with  $A_I$  the value of an  $A_f$  at the 1D-2D interface, i.e., the surface of a cell face at the interface, with  $u_{2D,I}$  the velocity component  $u_f$  normal to that face (and hence at the interface) normal to the interface) directed from the 2D domain to the 1D domain if  $s_{c,I} = 1$  and in the opposite direction if  $s_{c,I} = -1$  (cf. Section 2.1.3.2), with  $\Delta x_I$  the length of that cell face (the grid size *along* the interface), with  $\Delta x_{u,I}$  the value of a  $\Delta x_u$  at the interface (the grid size *normal* to the interface), and with  $\Delta x_{1D-2D}$  an additional model parameter that should normally be at most a fraction of the grid size near the interface, i.e.,  $\Delta x_{1D-2D} \ll \Delta x_{u,I}$ . By definition, the  $\Delta x_{u,I}$  are the distances between the points where the  $\zeta_{2D,i}$  and the  $\zeta_{2D,v}$  are located, i.e., the distances between the circumcenters of the 2D virtual grid cells outside the interface and those of the adjacent 2D grid cells inside the 2D domain, cf. Figure 2.5. Also by definition, i.e., because the 2D grid is orthogonal, the lines connecting  $\zeta_{2D,i}$  and  $\zeta_{2D,v}$  points are normal to the 1D-2D interface.

Normalization coefficient  $\alpha_{SF}$  has been introduced in (2.15b) to ensure a continuous formulation at the transition between drowned-weir flow and free-weir flow (at  $\zeta_{2D,I} - z_s = 3/2(\zeta_{1D} - z_s)$  and at  $\zeta_{1D} - z_s = 3/2(\zeta_{2D,I} - z_s)$ ) when the time derivative of  $u_{2D,I}$  is present. Since  $\alpha_{SF}$  is included in both the second term and the third term of (2.15b), its value is irrelevant when  $\Delta x_{1D-2D} = 0$ .

The choice for  $\Delta x_{u,I}$  in (2.15b) is arbitrary. A typical length scale normal to the interface is needed to enable recasting (2.14b) in the form of a space-discretized momentum equation like (2.3) with a friction coefficient  $b_{S,I}$  of dimension  $[1/s]$ .

Equation (2.15a) has been obtained by replacing  $q_{2D-1D}$  in (2.14a) by  $(A_f/\Delta x_I) s_{c,f} u_f = (A_I/\Delta x_I) s_{c,I} u_{2D,I}$  (cf. the mass fluxes in (2.4) and the first expression in (2.13)). The same substitution has been used to obtain (2.15b) from the square of (2.14b). Parameter  $\Delta x_{1D-2D}$  in (2.15b) sort of represents the effective thickness of the interface, i.e., the size of the green braces in the Figures 2.3, 2.4 and 2.5. It has merely been introduced as a modeling parameter; by increasing or decreasing  $\Delta x_{1D-2D}$ , the relative importance of the time derivative in (2.15b) can be increased or decreased. Apart from that time derivative, which provides a relaxation effect that may be physically realistic or that may be exaggerated for numerical purposes, (2.15b) is equivalent with the third and fifth line in (2.14b) (*drowned-weir* flow regime) when  $\alpha_{SF} = 1$  and when  $b_{S,I}$  is taken equal to:

$$b_{S,I} = \frac{A_I^2 \sqrt[3]{|u_{2D,I}|^k + u_\epsilon^k}}{2\Delta x_{u,I} (\Delta x_I c_e c_w (\zeta_{1D/2D,I} - z_s))^2} , \quad (2.16)$$

with  $\zeta_{1D/2D,I}$  equal to  $\zeta_{1D}$  if  $\zeta_{2D,I} \geq \zeta_{1D}$  and equal to  $\zeta_{2D,I}$  if  $\zeta_{1D} > \zeta_{2D,I}$ . Notice the division by  $\Delta x_{u,I}$  in (2.16) that compensates for the multiplication by  $\Delta x_{u,I}$  in the last term of (2.15b).

<sup>6</sup>Kernkamp (2008) adds a time derivative to structure equations like (2.14b) to obtain an equation of the form  $\partial u_{2D-1D}/\partial t + |u_{2D-1D}| u_{2D-1D}/\Delta x_{u,I} = |u_{2D-1D}|/(\Delta x_{u,I} b_{S,I}) \times g(\zeta_{2D,I} - \zeta_{1D})/\Delta x_{u,I}$ . The balance between the time derivative and the water-level gradient in this equation depends on the modeling of the friction loss across the structure, which is not in agreement with a momentum equation. In particular, for a very smooth weir modeled by a very small friction coefficient  $b_{S,I}$ , the effect of the time derivative in this equation vanishes. On the other hand, for a very large friction coefficient (and/or very small  $|u_{2D-1D}|$ ) the balance between water-level gradient and friction in (2.14b) is replaced by a balance between time derivative and friction. This may result in structures reacting unrealistically slow to the flow dynamics. In contrast, (2.15b) has the correct form of a momentum equation and hence the correct physical dependence on  $b_{S,I}$ .

Another important difference is that (2.15b) has been designed such that the transition between drowned-weir flow and free-weir flow is continuous and smooth, just like in structure equation (2.14b) (see the explanation on normalization coefficient  $\alpha_{SF}$ ). This is not the case in the Kernkamp formulation.

Small positive parameter  $u_\varepsilon > 0$  of dimension  $[m/s]$  has been added in (2.16) to stabilize the computations for small  $|u_{2D,I}| \lesssim u_\varepsilon$ , when equation (2.15b) would otherwise become highly nonlinear. The stabilization is required because of the explicit discretization in time of the coefficient  $b_{S,I}$  in (2.15b) (Picard linearization, see below). At present the stabilization is implemented for  $k = 1$ , i.e., the coefficient  $|u_{2D,I}|$  in (2.16) has been replaced by  $|u_{2D,I}| + u_\varepsilon$ , which gives a rather large perturbation of 1D-2D coupling equation (2.15b) at larger  $|u_{2D,I}|$ . Smaller perturbations are obtained for, e.g.,  $k = 2$  ( $\Rightarrow \sqrt[k]{|u_{2D,I}|^k + u_\varepsilon^k} = \sqrt{|u_{2D,I}|^2 + u_\varepsilon^2}$ ) or  $k \rightarrow \infty$  ( $\Rightarrow \sqrt[k]{|u_{2D,I}|^k + u_\varepsilon^k} \rightarrow \max(|u_{2D,I}|, u_\varepsilon)$ ). These two options are currently investigated. As an alternative to stabilization by means of the introduction of  $u_\varepsilon$ , coefficient  $b_{S,I}$  could be discretized implicitly in time. This would require an iterative solution procedure, which could very well be combined with the iterative solution procedure for the 1D-2D coupling as a whole. It may be an option worth considering in the future.

For free-weir flow across an interface the same equation (2.15b) may be used, but with  $\zeta_{1D}$  replaced by  $z_s$  if  $\zeta_{2D,I} > z_s$  and  $\zeta_{2D,I} - z_s \geq 3/2(\zeta_{1D} - z_s)$ , with  $\zeta_{2D,I}$  replaced by  $z_s$  if  $\zeta_{1D} > z_s$  and  $\zeta_{1D} - z_s \geq 3/2(\zeta_{2D,I} - z_s)$ , with  $\alpha_{SF} = 1/3$ , and with  $b_{S,I}$  replaced by  $b_{F,I}$ , the friction coefficient for *free-weir* flow across the interface:

$$b_{F,I} = \frac{A_I^2 \sqrt[k]{|u_{2D,I}|^k + u_\varepsilon^k}}{(2/3)^3 \Delta x_{u,I} (\Delta x_I c_e c_w (\zeta_{1D/2D,I} - z_s))^2}, \quad (2.17)$$

with  $\zeta_{1D/2D,I}$  equal to  $\zeta_{2D,I}$  if  $\zeta_{2D,I} \geq \zeta_{1D}$  and equal to  $\zeta_{1D}$  if  $\zeta_{1D} > \zeta_{2D,I}$ . This is *opposite* to the definition of  $\zeta_{1D/2D,I}$  in (2.16), whence the coefficient  $(2/3)^3$  instead of 2 in the denominator. This coefficient compensates for the sudden change in value of  $\zeta_{1D/2D,I} - z_s$  at the transition from drowned-weir flow to free-weir flow or vice versa at  $\zeta_{2D,I} - z_s = 3/2(\zeta_{1D} - z_s)$  or at  $\zeta_{1D} - z_s = 3/2(\zeta_{2D,I} - z_s)$ .

Summarizing, (2.15a) is always applied, in combination with:

IF  $\zeta_{2D,I} - z_s \leq 0$  AND  $\zeta_{1D} - z_s \leq 0$  THEN

! **no flow** across interface

$u_{2D,I} = 0$  (or, equivalently,  $q_{1D-2D} = 0$ )

ELSE IF  $\zeta_{2D,I} - z_s \geq 3/2(\zeta_{1D} - z_s)$  THEN

! **free-weir flow** from 2D to 1D

(2.15b) with  $\alpha_{SF} = 1/3$ , with  $\zeta_{1D} \Leftarrow z_s$ , and with  $b_{S,I} \Leftarrow b_{F,I}$  where  $\zeta_{1D/2D,I} \Leftarrow \zeta_{2D,I}$

ELSE IF  $\zeta_{1D} - z_s \geq 3/2(\zeta_{2D,I} - z_s)$  THEN

! **free-weir flow** from 1D to 2D

(2.15b) with  $\alpha_{SF} = 1/3$ , with  $\zeta_{2D,I} \Leftarrow z_s$ , and with  $b_{S,I} \Leftarrow b_{F,I}$  where  $\zeta_{1D/2D,I} \Leftarrow \zeta_{1D}$

ELSE IF  $\zeta_{2D,I} \geq \zeta_{1D}$  THEN

! **drowned-weir flow** from 2D to 1D

(2.15b) with  $\alpha_{SF} = 1$ , and with  $b_{S,I}$  where  $\zeta_{1D/2D,I} \Leftarrow \zeta_{1D}$

ELSE ! i.e. IF  $\zeta_{1D} > \zeta_{2D,I}$

! **drowned-weir flow** from 1D to 2D

(2.15b) with  $\alpha_{SF} = 1$ , and with  $b_{S,I}$  where  $\zeta_{1D/2D,I} \Leftarrow \zeta_{2D,I}$

ENDIF

As mentioned before, first the case of a *drowned-weir* flow across an interface will be considered, which is modeled by (2.15a) and (2.15b) 'as is'. The free-weir flow case will be considered afterwards.

The discretization of (2.15) in time must be in agreement with the discretizations (2.4) and



(2.3), but must also be in agreement with equation (2.14b):

$$A_I^n s_{c,I} (\theta u_{2D,I}^{n+1} + (1 - \theta) u_{2D,I}^n) = -\Delta x_I q_{1D-2D}^* , \quad (2.18a)$$

$$\Delta x_{1D-2D} s_{c,I} \frac{u_{2D,I}^{n+1} - u_{2D,I}^n}{\Delta t} + \alpha_{SF} g (\zeta_{1D}^{n+1} - \zeta_{2D,I}^{n+1}) + \alpha_{SF} \Delta x_{u,I} b_{S,I}^n s_{c,I} u_{2D,I}^{n+1} = 0 . \quad (2.18b)$$

The left-hand side of (2.18a) is the same discretization as presented in the first expression of (2.13). A backward Euler discretization ( $\theta = 1$ ) has been applied in (2.18b) to ensure that it is equivalent with the third and fifth line of (2.14b) evaluated at the next time level in the limit of  $\Delta x_{1D-2D} = 0$ .

It has been decided to evaluate  $b_{S,I}$  (and  $b_{F,I}$ ) explicitly, whence the superscript  $n$  of  $b_{S,I}^n$  in (2.18b). This makes the equation linear in the unknowns  $u_{2D,I}^{n+1}$ ,  $\zeta_{1D}^{n+1}$  and  $\zeta_{2D,I}^{n+1}$ , and therefore relatively easy to solve. It is also the procedure followed in SOBEK and D-Flow FM, cf. Kernkamp (2008). On the other hand, to ensure the best nonlinear performance (and, in consequence, the highest stability), the time-dependent variables  $|u_{2D,I}|$  and  $\zeta_{1D/2D}$  in  $b_{S,I}$  (and  $b_{F,I}$ ) should be evaluated at the next time level  $n + 1$ . Note that the time discretization of  $A_I$  in  $b_{S,I}$  (and  $b_{F,I}$ ) should be in agreement with that of the  $A_f$  in (2.4), hence  $A_I$  in  $b_{S,I}$  (and  $b_{F,I}$ ) is always to be evaluated at previous time level  $n$ . Of course, if  $b_{S,I}$  is (partially) evaluated at the next time level, (2.18b) becomes a nonlinear equation that is to be solved iteratively.

For slow variation of the flow near the interface or when a small time step  $\Delta t$  is used, there will be hardly any difference in the results obtained with  $b_{S,I}$  ( $b_{F,I}$ ) evaluated at  $n$  and those obtained with  $b_{S,I}$  ( $b_{F,I}$ ) at  $n + 1$ . At transient flow conditions near a 1D-2D interface, however, the differences may be large. This applies in particular to (free-weir!) flow at the onset of flooding, i.e., there may be noticeable temporary differences between results obtained with  $b_{F,I}$  evaluated at  $n$  and those with  $b_{F,I}$  at  $n + 1$ .

Replacing next time level  $n + 1$  by iteration index  $p$  and separating terms with variables at the next iteration level  $p$  (that are to be determined) from terms that only depend on known information at previous time level  $n$ , (2.18) becomes:

$$\begin{aligned} \theta A_I^n s_{c,I} u_{2D,I}^p + \Delta x_I q_{1D-2D}^p &= -(1 - \theta) A_I^n s_{c,I} u_{2D,I}^n , \\ \left( \frac{\Delta x_{1D-2D}}{\Delta t} + \alpha_{SF} \Delta x_{u,I} b_{S,I}^n \right) s_{c,I} u_{2D,I}^p + \alpha_{SF} g (\zeta_{1D}^p - \zeta_{2D,I}^p) &= \frac{\Delta x_{1D-2D}}{\Delta t} s_{c,I} u_{2D,I}^n . \end{aligned} \quad (2.19)$$

To get the coupling conditions formulated in the water-level variables at the cell centers of the 2D domain, the linear interpolation  $\zeta_{2D,I}^p = (\zeta_{2D,i}^p + \zeta_{2D,v}^p)/2$  is used and (2.8) is used at the cell faces along the interface to replace  $u_{2D,I}^p$ . The latter is obviously an equation very similar to (2.12) and reads:

$$s_{c,I} u_{2D,I}^p = s_{c,I} R_I^n - F_I^n (\zeta_{2D,v}^p - \zeta_{2D,i}^p) , \quad (2.20)$$

with  $R_I^n$  and  $F_I^n$  as in (2.9), and with  $\zeta_{2D,v}^p$  and  $\zeta_{2D,i}^p$  as in Figure 2.5. The result is:

$$-\theta A_I^n F_I^n (\zeta_{2D,v}^p - \zeta_{2D,i}^p) + \Delta x_I q_{1D-2D}^p = -A_I^n s_{c,I} \left( \theta R_I^n + (1 - \theta) u_{2D,I}^n \right) , \quad (2.21a)$$

$$\begin{aligned} & - \left( \frac{\Delta x_{1D-2D}}{\Delta t} + \alpha_{SF} \Delta x_{u,I} b_{S,I}^n \right) F_I^n (\zeta_{2D,v}^p - \zeta_{2D,i}^p) + \alpha_{SF} g \left( \zeta_{1D}^p - \frac{\zeta_{2D,i}^p + \zeta_{2D,v}^p}{2} \right) \\ & = \frac{\Delta x_{1D-2D}}{\Delta t} s_{c,I} u_{2D,I}^n - \left( \frac{\Delta x_{1D-2D}}{\Delta t} + \alpha_{SF} \Delta x_{u,I} b_{S,I}^n \right) s_{c,I} R_I^n . \end{aligned} \quad (2.21b)$$

Notice that these equations define an *implicit* coupling across the 1D-2D interfaces, since the unknowns of the 2D domain ( $\zeta_{2D,i}$ ,  $\zeta_{2D,v}$ ) and those of the 1D domain ( $q_{1D-2D}$ ,  $\zeta_{1D}$ ) are all at the next iteration level  $p$ . This may strongly complicate the implementation of the algorithm. It would require the construction of a system of equations composed of elements of both the 2D model and the 1D model, which is especially not obvious when dealing with separate implementations, as is the intention here (D-Flow FM as the 2D model, SOBEK as the 1D model). Nevertheless, as long as the 1D and 2D grids match at the interfaces<sup>7</sup> and the 1D and 2D models all use the same time step<sup>8</sup>, a direct implicit coupling, although still complex, might be feasible. However, a general and much more flexible 1D-2D coupling with non-matching grids at the interface and possibly the use of different time steps in the 2D and 1D model is virtually impossible with an implicit coupling; its implementation would be far too complex.

There is also a numerical reason for not applying an implicit coupling. When eliminating  $q_{1D-2D}^p$  in (2.21) (using (2.10) for the 1D channel with lateral discharge  $q_c^p$  equal to  $-q_{1D-2D}^p$ <sup>9</sup>, the resulting system of equations for the unknowns  $\zeta^p$  will have a positive-definite symmetric matrix, because of the skew-symmetry of the discretization of the water-level gradient in (2.3) (and in (2.8) and (2.20)) and in (2.15b) (and (2.18b)). Systems of equations with a positive-definite symmetric matrix are guaranteed to be well posed and to be always solvable using a (preconditioned) CG iterative method, which is why this method is applied in D-Flow FM and SOBEK.

The skew-symmetry in (2.15b) (and (2.18b)) is *only* because of the drowned-weir case that is being considered for the moment. When the flow across the 1D-2D interface is to be modeled by a *free weir* an expression similar to (2.15b) applies that, however, does *not* depend on either  $\zeta_{1D}$  or  $\zeta_{2D,I}$ , cf. the second and fourth line in (2.14b). Equations of the form (2.15b) and (2.18b), and hence of the form (2.21b), still apply, but with  $b_{S,I}^n$  replaced by  $b_{F,I}^n$ , with  $\alpha_{SF} = 1/3$  instead of  $\alpha_{SF} = 1$ , and, most importantly, with the water-level difference  $\zeta_{1D} - \zeta_{2D,I}$  replaced by either  $\zeta_{1D} - z_s$  or  $z_s - \zeta_{2D,I}$ , depending on whether the free-weir flow is from the 1D domain to the 2D domain or in the opposite direction. Such water-level differences destroy the skew-symmetry of the equations and hence the symmetry of the system of  $\zeta^p$  equations.

Non-symmetric systems of equations are avoided when the coupling equations (2.21) are not applied implicitly, but *explicitly*. This also makes it feasible to develop and implement (in the future) a 1D-2D coupling that can handle non-matching grids at the interface and possibly the use of different time steps in the 2D and in the 1D model.

An *explicit* coupling involves a solution procedure where the implicit coupling equations (2.21) are solved iteratively per nonlinear iteration  $p$ . This coupling iteration process is best combined with the nonlinear iteration loop. After all, the nonlinear iteration process per 1D and 2D model only needs to be solved up to (a fraction of) the convergence level of the coupling in between them. Solving the 1D and 2D models with a much higher precision than the coupling convergence error (a measure of  $|\zeta_{2D,I}^p - \zeta_{2D,I}^{p-1}|$  and  $|\zeta_{1D}^p - \zeta_{1D}^{p-1}|$ ) would be a waste of computational effort.

Although an explicit coupling can be realized by applying one of the coupling equations (2.21) in one direction and the other one in the other direction (the naive coupling that is usu-

<sup>7</sup>What is meant here is that the space discretizations should match. When the 1D models and 2D models use the same type of space discretizations (as is the case here) this is equivalent with the condition that the grids should match.

<sup>8</sup>Not only the time steps, but the applied time integration methods as a whole should match. When the 1D models and 2D models use the same type of time integration methods (as is the case here) this is equivalent with the condition that the time steps should match.

<sup>9</sup>Recall that  $q_{1D-2D}$  has been defined as the flux from the 1D domain to the 2D domain, cf. (2.13), while  $q_c$  has been defined as an incoming flux, here incoming to the 1D domain, cf. (2.4).

ally applied), a better performance is obtained by applying in each direction an optimized (and obviously different) combination. To determine this combination, first notice that for  $\Delta x_{1D-2D} = 0$  and no friction losses across the 1D-2D interface (i.e.,  $b_{S,I}^n = 0$ ), (2.21b) reduces to  $\zeta_{1D}^p = (\zeta_{2D,i}^p + \zeta_{2D,v}^p)/2$ , i.e., coupling condition (2.21b) essentially imposes a relation between the water levels at both sides of the interface (Dirichlet condition). The other coupling condition, (2.21a), obviously imposes a relation between the (lateral) velocities at both sides, cf. (2.18a) where this condition originates from. It is a Neumann condition for  $\zeta_{2D,I}$ , the water levels of the 2D domain.

A suitable combination of coupling equations for the transfer of information to a 2D domain is one based on the concept of absorbing boundary conditions, see, e.g., [Ye et al. \(2011\)](#). The simplest form is the one that specifies the incoming Riemann invariant in normal direction  $-h_{2D,I} s_{c,I} u_{2D-1D} + \sqrt{gh_{2D,I}} \zeta_{2D,I}^{10}$ , with  $h_{2D,I} = \zeta_{2D,I} + d_{2D,I}$  the total water depth of the 2D domain at the interface. This choice is equivalent with the Sommerfeld radiation condition. Formulated in the discretized water level this condition reads  $(\zeta_{2D,i} + \zeta_{2D,v})/2 + \sqrt{gh_{2D,I}} \Delta t / \Delta x_{u,I} (\zeta_{2D,v} - \zeta_{2D,i})$ . Because all flow dynamics in lateral direction is neglected in a 1D model, the concept of Riemann invariants cannot be used at a 1D-2D interface in the other direction for the transfer of lateral information to a 1D domain, so here it is necessary to come up with something different.

To allow a full optimization of the coupling, it is proposed to use a parameterized combination of  $-1/(\alpha_{SF} g)$  times (2.21b) and  $-1/(\theta A_I^n F_I^n)$  times (2.21a). The normalization is to get (2.21b) in the form of (almost) a Dirichlet condition for the water level of the 2D domain at the interface, and (2.21a) in the form of a Neumann condition. The combination is the Robin coupling condition:

$$\begin{aligned} & \alpha_{2D}^n \frac{\zeta_{2D,v}^p + \zeta_{2D,i}^p}{2} + (\beta_{2D}^n + \alpha_{2D}^n f_{S,I}^n F_I^n) (\zeta_{2D,v}^p - \zeta_{2D,i}^p) \\ &= \alpha_{2D}^n \zeta_{1D}^{p-1} + \beta_{2D}^n \frac{\Delta x_I}{\theta A_I^n F_I^n} q_{1D-2D}^{p-1} \\ &+ \alpha_{2D}^n s_{c,I} \left( f_{S,I}^n R_I^n - \frac{\Delta x_{1D-2D}}{\alpha_{SF} g \Delta t} u_{2D,I}^n \right) + \beta_{2D}^n \frac{s_{c,I}}{\theta F_I^n} \left( \theta R_I^n + (1 - \theta) u_{2D,I}^n \right), \end{aligned} \quad (2.22)$$

with (drowned-weir flow  $\rightarrow$  substitute  $\alpha_{SF} = 1$ ):

$$f_{S,I}^n = \left( \frac{\Delta x_{1D-2D}}{\alpha_{SF} \Delta x_{u,I}} + b_{S,I}^n \Delta t \right) \frac{\Delta x_{u,I}}{g \Delta t} = \left( \frac{\Delta x_{1D-2D}}{\Delta x_{u,I}} + b_{S,I}^n \Delta t \right) \frac{\Delta x_{u,I}}{g \Delta t}. \quad (2.23)$$

The coupling parameters  $\alpha_{2D}^n$  and  $\beta_{2D}^n$  (and the coupling parameters that will be introduced later) are allowed to vary in time, whence the superscript  $n$ . Like all other coefficients in the above equations (and like many terms and coefficients in the D-Flow FM and SOBEK time integration scheme) they are evaluated explicitly at the previous time level. For the moment the variation of coupling parameters inside the coupling iteration loop, evaluating them explicitly at the previous iteration level  $p-1$ , is not considered. In view of the strongly explicit nature of the solution algorithm as a whole, this is not expected to have a positive effect on the convergence properties of the 1D-2D coupling that is significant enough to be worth considering.

Obviously the scaling of the two coupling parameters  $\alpha_{2D}^n$  and  $\beta_{2D}^n$  is irrelevant. The multiplication of  $\alpha_{2D}^n$  and  $\beta_{2D}^n$  by any non-zero factor has no effect on the coupling, indicating that a single coupling parameter would have sufficed (to be obtained by replacing  $\alpha_{2D}^n$  by, e.g.,

<sup>10</sup>The minus sign of  $s_{c,I} u_{2D-1D}^p$  is because the positive direction at cell faces has been defined as the direction pointing outward of a cell. This applies to the 2D faces at the boundaries of a 2D domain as well, and hence to the 2D faces at a 1D-2D interface.

$1 - \beta_{2D}^n$ ). Nevertheless, two coupling parameters instead of one are considered, because it facilitates the implementation of the coupling. In particular, the use of two coupling parameters makes it easy to set either one of them to 0 or 1 and the other respectively to 1 or to some optimized value.

By choosing  $\alpha_{2D}^n = 1$  and  $\beta_{2D}^n = 1/2 - f_{S,I}^n F_I^n$ , coupling equation (2.22) only specifies  $\zeta_{2D,v}^p$ , which variable can then immediately be eliminated from the system of equations for the  $\zeta^p$  of the 2D domains. The simplicity and ease of implementation of this coupling seems to make this choice of  $\beta_{2D}^n$  (with  $\alpha_{2D}^n = 1$ ) attractive. The main concern, however, should be the convergence speed of the iterative explicit coupling per time step and the according optimization of  $\beta_{2D}^n$ .

For vanishing time derivative ( $\Delta x_{1D-2D} = 0$ ) and vanishing friction ( $b_{S,I}^n = 0$ ) at the 1D-2D interface ( $\rightarrow f_{S,I}^n = 0$ ), coupling equation (2.22) reduces to:

$$\begin{aligned} \alpha_{2D}^n \frac{\zeta_{2D,v}^p + \zeta_{2D,i}^p}{2} + \beta_{2D}^n (\zeta_{2D,v}^p - \zeta_{2D,i}^p) &= \alpha_{2D}^n \zeta_{1D}^{p-1} + \beta_{2D}^n \frac{\Delta x_I}{\theta A_I^n F_I^n} q_{1D-2D}^{p-1} \\ &+ \beta_{2D}^n \frac{s_{c,I}}{\theta F_I^n} \left( \theta R_I^n + (1 - \theta) u_{2D,I}^n \right). \end{aligned} \quad (2.24)$$

In the second line only terms at the previous time level that do not affect the convergence properties of the explicit 1D-2D coupling.

For  $\alpha_{2D}^n = 1$  and  $\beta_{2D}^n = 0$ , (2.24) reduces to  $(\zeta_{2D,v}^p + \zeta_{2D,i}^p)/2 = \zeta_{1D}^{p-1}$ , the discretization and iterative approximation of  $\zeta_{1D}^{n+1} - \zeta_{2D,I}^{n+1} = 0$ . For  $\alpha_{2D}^n = 0$  and  $\beta_{2D}^n = 1$ , one gets  $\zeta_{2D,v}^p - \zeta_{2D,i}^p = 1/(\theta F_I^n) (q_{1D-2D}^{p-1} \Delta x_I / A_I^n + s_{c,I} (\theta R_I^n + (1 - \theta) u_{2D-1D}^n))$ . Using (2.20), this can be written as  $s_{c,I} (\theta u_{2D,I}^p + (1 - \theta) u_{2D,I}^n) = -q_{1D-2D}^{p-1} \Delta x_I / A_I^n$ , showing that the other coupling contained in (2.24) is of course (2.18a), the equation ensuring mass conservation across the interface.

Equation (2.22) defines the coupling from the 1D domain to the 2D domain. The coupling in the other direction, from the 2D domain to the 1D domain, is similar:

$$\begin{aligned} \alpha_{1D}^n \zeta_{1D}^p - \beta_{1D}^n \frac{\Delta x_I}{\theta A_I^n F_I^n} q_{1D-2D}^p \\ = \alpha_{1D}^n \frac{\zeta_{2D,i}^{p-1} + \zeta_{2D,v}^{p-1}}{2} + (\beta_{1D}^n - \alpha_{1D}^n f_{S,I}^n F_I^n) (\zeta_{2D,i}^{p-1} - \zeta_{2D,v}^{p-1}) \\ - \alpha_{1D}^n s_{c,I} \left( f_{S,I}^n R_I^n - \frac{\Delta x_{1D-2D}}{\alpha_{SF} g \Delta t} u_{2D,I}^n \right) + \beta_{1D}^n \frac{s_{c,I}}{\theta F_I^n} \left( \theta R_I^n + (1 - \theta) u_{2D,I}^n \right). \end{aligned} \quad (2.25)$$

The minus sign of the second term in the left-hand side is because  $q_{1D-2D}^p$  is the *outgoing* flux from the 1D domain to the 2D domain, *not* a flux entering the 1D domain, like  $q_c^p$  in (2.7) and (2.10). NB, (2.25) and (2.22) are obviously equivalent. Apart from the iteration levels  $p$  and  $p - 1$  in the first and second line, the former can be obtained from the latter by setting  $\alpha_{1D}^n = \alpha_{2D}^n$  and  $\beta_{1D}^n = -\beta_{2D}^n$ . The change of sign in the latter takes account of the fact that quantities at an interface that are normal to that interface and hence have a direction with respect to the interface (like velocity, mass flux and water-level gradient across the interface) change sign when they are considered in opposite direction.

Equation (2.22) and (2.25) are for the case that the flow across the 1D-2D interface is modeled as a *drowned weir*. If the flow is to be modeled by a *free weir*, one of the water levels in (2.15b) ((2.18b)) is to be replaced by  $z_s$ . (Also  $b_{S,I}$  and  $b_{S,I}^n$  are to be replaced by  $b_{F,I}$  and  $b_{F,I}^n$ , while

$\alpha_{SF} = 1/3$  instead of  $\alpha_{SF} = 1$  is to be used.) For free-weir flow from the 2D domain to the 1D domain, this means replacement of  $\zeta_{1D}^p$  in (2.21b) by  $z_s$ , in which case the coupling equation becomes a boundary condition for the 2D domain:

$$\frac{\zeta_{2D,v}^p + \zeta_{2D,i}^p}{2} + f_{F,I}^n F_I^n (\zeta_{2D,v}^p - \zeta_{2D,i}^p) = z_s + s_{c,I} \left( f_{F,I}^n R_I^n - \frac{\Delta x_{1D-2D}}{\alpha_{SF} g \Delta t} u_{2D,I}^n \right), \quad (2.26)$$

with (free-weir flow  $\rightarrow$  substitute  $\alpha_{SF} = 1/3$ ):

$$f_{F,I}^n = \left( \frac{\Delta x_{1D-2D}}{\alpha_{SF} \Delta x_{u,I}} + b_{F,I}^n \Delta t \right) \frac{\Delta x_{u,I}}{g \Delta t} = \left( \frac{3 \Delta x_{1D-2D}}{\Delta x_{u,I}} + b_{F,I}^n \Delta t \right) \frac{\Delta x_{u,I}}{g \Delta t}. \quad (2.27)$$

The discharge determined at the boundary of the 2D domain is then simply imposed as *minus* a lateral discharge of the 1D domain (one-sided coupling from the 2D domain to the 1D domain). That is equivalent with applying (2.25) for  $\alpha_{1D}^n = 0$  and  $\beta_{1D}^n = 1$ .

Note that (2.26) is obtained from (2.22) by substituting  $\zeta_{1D}^{p-1} = z_s$ ,  $\alpha_{2D}^n = 1$  and  $\beta_{2D}^n = 0$ . In other words, coupling conditions (2.22) and (2.25) can be used for both the drowned-weir case and the free-weir case when the flow is from the 2D domain to the 1D domain.

Likewise, in the case of free-weir flow from the 1D domain to the 2D domain,  $(\zeta_{2D,i}^p + \zeta_{2D,v}^p)/2$  in (2.21b) is to be replaced by  $z_s$ . However, unlike the previous case, this does not lead to an equation with only variables defined in the 1D domain, because (2.15b) has been formulated in terms of the velocity  $u_{2D,I}$  at the 2D side of the interface. An equation independent of variables at the next time level in the 2D domain is obtained by eliminating  $u_{2D,I}^p$  from the equations (2.19) and substituting  $\zeta_{2D,I}^p = z_s$  in the result:

$$\zeta_{1D}^p - f_{F,I}^n \frac{\Delta x_I}{\theta A_I^n} q_{1D-2D}^p = z_s + s_{c,I} \left( f_{F,I}^n \frac{1 - \theta}{\theta} + \frac{3 \Delta x_{1D-2D}}{g \Delta t} \right) u_{2D,I}^n. \quad (2.28)$$

The discharge determined at the boundary of the 1D domain is then simply imposed as discharge boundary condition to the 2D domain (one-sided coupling from the 1D domain to the 2D domain). That is equivalent with applying (2.22) for  $\alpha_{2D}^n = 0$  and  $\beta_{2D}^n = 1$  (see interpretation of (2.24) directly after that equation).

Similar as before with free-weir flow from the 2D domain to the 1D domain, equation (2.28) is included in (2.25). It is obtained by replacing  $f_{S,I}^n$  by  $f_{F,I}^n$  and setting  $\alpha_{SF} = 1/3$  (for a free-weir formulation), and by substituting  $(\zeta_{2D,i}^{p-1} + \zeta_{2D,v}^{p-1})/2 = z_s$ ,  $\alpha_{1D}^n = 1$ , and  $\beta_{1D}^n = f_{F,I}^n F_I^n$ . So coupling conditions (2.22) and (2.25) can also be used for both the drowned-weir case and the free-weir case when the flow is from the 1D domain to the 2D domain.

Care should be taken in case of extremely small  $f_{F,I}^n$  (its value becomes zero for  $\Delta x_{1D-2D} = 0$  and  $b_{F,I}^n = 0$ ). For very small  $f_{F,I}^n$  (which implies very small  $\Delta x_{1D-2D}$ ) (2.28) reduces to the condition  $\zeta_{1D} = z_s$ . This means that the water level in the 1D channel would become independent of the flow dynamics, which does not make sense. The same applies to (2.26) by the way. That equation reduces for very small  $f_{F,I}^n$  (and hence very small  $\Delta x_{1D-2D}$ ) to the condition  $(\zeta_{2D,v}^p + \zeta_{2D,i}^p)/2 = z_s$ . Although physically incorrect, it does not pose a computational problem, so in that sense there is no reason for concern with a very small  $f_{F,I}^n$  when considering a free-weir flow from 2D to 1D. NB, the situation is different for a drowned weir. As shown before, for  $f_{S,I}^n$  very small that coupling reduces to  $(\zeta_{2D,v}^p + \zeta_{2D,i}^p)/2 = \zeta_{1D}^{p-1}$ , next to mass conservation (2.15a). This is the correct physical limit for a large water depth and hence very low friction losses at and across a 1D-2D interface.

### 2.1.3.4 Analysis of the lateral horizontal 1D-2D coupling

#### 2.1.3.4.1 Preliminaries

To analyse and optimize the performance of the explicit solution procedure with strict model separation for the implicit horizontal 1D-2D coupling, rectangular domains, uniform conditions, and uniform rectangular grids are considered:

- ◇ a straight 1D-2D interface, arbitrarily set at the location  $x = 0$ ;
- ◇ a straight 1D channel with uniform depth  $h_{1D}$ , width  $W_{1D}$  and friction coefficient  $b_{1D}$  at the side  $x > 0$  of the interface, numerically modeled using a uniform grid with cells of size  $\Delta y$ ;
- ◇ a 2D area with uniform depth  $h_{2D}$  and friction coefficient  $b_{2D}$  at the side  $x < 0$  of the interface, numerically modeled using a uniform grid with rectangular cells of size  $\Delta x$  by  $\Delta y$ ;
- ◇ uniform friction coefficient  $b_I$  at the interface of uniform thickness  $\Delta x_{1D-2D}$ , cf. equation (2.15b).

The uniform conditions make it possible to perform a normal-mode analysis.

The underlying idea is that the modeling near 1D-2D interfaces will generally be such that in the optimization of the coupling parameters  $\alpha_{2D}^n$ ,  $\beta_{2D}^n$ ,  $\alpha_{1D}^n$  and  $\beta_{1D}^n$  in (2.22) and (2.25), the conditions are smooth enough for the coefficients to be assumed locally constant, for the 1D-2D interface to be assumed locally straight, and for the grid to be assumed locally uniform. If the conditions are not smooth (strong variations of water depth or grid size near a 1D-2D interface, strong bends in a 1D-2D interface), the optimization is assumed to give reasonable approximations of the optimal coupling parameters, especially when non-smooth conditions occur in only a small number of locations. Note that the normal-mode analysis presented below is the only feasible way to arrive at reasonable and simply to use estimations of the optimal coupling parameters that will perform better than no optimization.

In the straight and uniform 1D domain with uniform grid, water-level equation (2.10) becomes:

$$(1 + 2\text{CFL}_{1D}^2)\zeta_j^p - \text{CFL}_{1D}^2(\zeta_{j-1}^p + \zeta_{j+1}^p) - q_{c,j}^p \Delta t / W_{1D} = \text{rhs}_{1D,j}^n, \quad (2.29)$$

with  $j$  the control volume index in  $y$ -direction and with  $\text{rhs}_{1D,j}^n$  all the known terms at the previous time level  $n$  (note that the term  $(S_\zeta^{p-1} \zeta_c^{p-1} - V_c^{p-1}) / \Delta t$  in (2.10) vanishes for the constant-coefficient case that is considered here). Variable  $\text{CFL}_{1D}$  represents the coefficient  $\Delta t A_f^n \theta F_u^n / S_\zeta^{p-1}$  in the  $y$ - or channel direction that for this uniform case becomes equal to:

$$\text{CFL}_{1D} = \frac{\theta \Delta t \sqrt{g h_{1D}}}{\Delta y \sqrt{1 + b_{1D} \Delta t}}. \quad (2.30)$$

In the uniform 2D domain with uniform rectangular grid, (2.10) becomes:

$$(1 + 2\text{CFL}_{2D,x}^2 + 2\text{CFL}_{2D,y}^2)\zeta_{i,j}^p - \text{CFL}_{2D,x}^2(\zeta_{i-1,j}^p + \zeta_{i+1,j}^p) - \text{CFL}_{2D,y}^2(\zeta_{i,j-1}^p + \zeta_{i,j+1}^p) = \text{rhs}_{2D,i,j}^n, \quad (2.31)$$

with  $i, j$  the control volume indices in  $x$ -,  $y$ -direction,  $\text{rhs}_{2D,i,j}^n$  all terms at time level  $n$ , and with  $\text{CFL}_{2D,x}$  and  $\text{CFL}_{2D,y}$  representing the coefficient  $\Delta t A_f^n \theta F_u^n / S_\zeta^{p-1}$  in the two coordinate directions that here become equal to:

$$\text{CFL}_{2D,x} = \frac{\theta \Delta t \sqrt{g h_{2D}}}{\Delta x \sqrt{1 + b_{2D} \Delta t}}, \quad \text{CFL}_{2D,y} = \frac{\theta \Delta t \sqrt{g h_{2D}}}{\Delta y \sqrt{1 + b_{2D} \Delta t}}. \quad (2.32)$$



Substituting  $F_I^n = 1/(1 + b_{2D}\Delta t) \times \theta g \Delta t / \Delta x$  (cf. (2.9)) and  $A_I^n = \Delta x_I h_{2D,I} = \Delta x_I h_{2D}$  (depth across 2D domain is uniform), equation (2.22) with (2.23) becomes (coupling from 1D to 2D for *drowned-weir* flow):

$$\begin{aligned} & \alpha_{2D}^n \frac{\zeta_{2D,v}^p + \zeta_{2D,i}^p}{2} + \left( \beta_{2D}^n + \alpha_{2D}^n \frac{\theta(\Delta x_{1D-2D}/\Delta x + b_I \Delta t)}{1 + b_{2D}\Delta t} \right) (\zeta_{2D,v}^p - \zeta_{2D,i}^p) \\ &= \alpha_{2D}^n \zeta_{1D}^{p-1} + \beta_{2D}^n \frac{\Delta x(1 + b_{2D}\Delta t)}{\theta^2 g h_{2D} \Delta t} q_{1D-2D}^{p-1} + \text{rhs}_{1D-2D}^n, \end{aligned} \quad (2.33)$$

with as before  $\Delta x_{1D-2D} \ll \Delta x$  the effective thickness of the interface, and with all known terms at previous time level  $n$  collected in  $\text{rhs}_{1D-2D}^n$ . Introducing non-dimensional parameter:

$$b'_I = \frac{\theta(\Delta x_{1D-2D}/\Delta x + b_I \Delta t)}{1 + b_{2D}\Delta t} \quad (2.34)$$

and substituting  $\text{CFL}_{2D,x}$  as defined in (2.32), (2.33) may be written as:

$$\begin{aligned} & \alpha_{2D}^n \frac{\zeta_{2D,v}^p + \zeta_{2D,i}^p}{2} + (\beta_{2D}^n + \alpha_{2D}^n b'_I) (\zeta_{2D,v}^p - \zeta_{2D,i}^p) \\ &= \alpha_{2D}^n \zeta_{1D}^{p-1} + \beta_{2D}^n \frac{\Delta t}{\Delta x \text{CFL}_{2D,x}^2} q_{1D-2D}^{p-1} + \text{rhs}_{1D-2D}^n. \end{aligned} \quad (2.35)$$

For  $\alpha_{2D}^n = 1$  and  $\beta_{2D}^n = 1/2 - b'_I$ , the contribution of  $\zeta_{2D,i}^p$  in the left-hand side of (2.35) vanishes and the coupling equation reduces to:

$$\zeta_{2D,v}^p = \zeta_{1D}^{p-1} + (1/2 - b'_I) \frac{\Delta t}{\Delta x \text{CFL}_{2D,x}^2} q_{1D-2D}^{p-1} + (\text{rhs}_{1D-2D}^n)_{\alpha_{2D}^n=1, \beta_{2D}^n=1/2-b'_I}. \quad (2.36)$$

This equation is not to be applied as such. As mentioned before, better coupling performance is obtained with (2.35) ((2.33)) and an optimized  $\beta_{2D}^n$ . However, a parameterized combination of (2.36) at different locations along the 1D-2D interface can be added to (2.35) to enhance the possibilities for optimizing the coupling performance. Since (2.35) and (2.36) are both valid coupling equations, any linear combination is a valid coupling as well. This generalization of couplings between domains is well known in the field of domain decomposition.

An interesting extension of coupling equation (2.35) applied along the interface at the indices  $j$  is to combine it with the coupling equation consisting of minus two times (2.36) at  $j$  plus (2.36) at  $j - 1$  and  $j + 1$ . That addition represents the finite difference discretization of the second derivative of (2.36) along the 1D-2D interface, which vanishes for a solution mode that is uniform along the interface (second-derivative discretization is zero for a constant) and is maximum for a highly oscillatory solution mode along the interface (second-derivative discretization is maximum for the wiggle mode). The extended coupling equation reads:

$$\begin{aligned} & \alpha_{2D}^n \frac{\zeta_{2D,v,j}^p + \zeta_{2D,i,j}^p}{2} + (\beta_{2D}^n + \alpha_{2D}^n b'_I) (\zeta_{2D,v,j}^p - \zeta_{2D,i,j}^p) \\ & - \delta_{2D}^n (\zeta_{2D,v,j-1}^p - 2\zeta_{2D,v,j}^p + \zeta_{2D,v,j+1}^p) \\ &= \alpha_{2D}^n \zeta_{1D,j}^{p-1} + \beta_{2D}^n \frac{\Delta t}{\Delta x \text{CFL}_{2D,x}^2} q_{1D-2D,j}^{p-1} \\ & - \delta_{2D}^n \left( \zeta_{1D,j-1}^{p-1} - 2\zeta_{1D,j}^{p-1} + \zeta_{1D,j+1}^{p-1} \right. \\ & \quad \left. + (1/2 - b'_I) \frac{\Delta t}{\Delta x \text{CFL}_{2D,x}^2} (q_{1D-2D,j-1}^{p-1} - 2q_{1D-2D,j}^{p-1} + q_{1D-2D,j+1}^{p-1}) \right) \\ & + \text{rhs}_{1D-2D,j}^n - \delta_{2D}^n (\text{rhs}_{1D-2D,j-1}^n - 2\text{rhs}_{1D-2D,j}^n + \text{rhs}_{1D-2D,j+1}^n)_{\alpha_{2D}^n=1, \beta_{2D}^n=1/2-b'_I}. \end{aligned} \quad (2.37)$$

Note the dependence of the  $\text{rhs}_{1\text{D}-2\text{D}}^n$  on  $\alpha_{2\text{D}}^n$  and  $\beta_{2\text{D}}^n$ .

Coupling equation (2.37) uses the same computational stencil (minus one unknown) as equation (2.10) and preserves (after a proper scaling) the symmetry of the system of the equations. For suitable choices of the coupling parameters ( $\alpha_{2\text{D}}^n = 1$ ,  $\beta_{2\text{D}}^n > -b'_I$ , and  $\delta_{2\text{D}}^n \geq 0$ ) the positive definiteness of the system is preserved as well.

Parameter  $\delta_{2\text{D}}^n$  and accompanying terms have been introduced in (2.37) to investigate the gain in performance that may be obtained with this extension of coupling (2.35), with the intention to figure out if implementation of it (somewhere in the future) may be worth considering. NB, the combination of (2.35) with the second difference of (2.35) for two different values of  $\beta_{2\text{D}}^n$  (taking  $\alpha_{2\text{D}}^n = 1$ ) will not be considered. Although in principle possible, it would destroy the symmetry of the matrix to be solved in 2D domains *and* would extend near 1D-2D interfaces the computational stencil of the  $\zeta^p$  equations to be solved (the left-hand side of (2.10)). Only the combination of (2.35) with the second difference of (2.35) for  $\alpha_{2\text{D}}^n = 1$  and  $\beta_{2\text{D}}^n = 1/2 - \theta b'_I$ , i.e., with the second difference of (2.36), is feasible enough to consider for implementation.

For  $\alpha_{2\text{D}}^n = 1$  and  $\beta_{2\text{D}}^n = -1/2 - b'_I$ , the contribution of  $\zeta_{2\text{D},v}^p$  in the left-hand side of (2.35) vanishes. The result is an equation totally unsuitable for the coupling of the 1D domain to the 2D domain, among other things because combination with the equations (2.10) destroys the positive definiteness of the system:

$$\zeta_{2\text{D},i}^p = \zeta_{1\text{D}}^{p-1} + (-1/2 - b'_I) \frac{\Delta t}{\Delta x \text{CFL}_{2\text{D},x}^2} q_{1\text{D}-2\text{D}}^{p-1} + (\text{rhs}_{1\text{D}-2\text{D}}^n)_{\alpha_{2\text{D}}^n=1, \beta_{2\text{D}}^n=-1/2-b'_I}.$$

However, the equation might be useful in combination with (2.35). The result is an equation similar to (2.37):

$$\begin{aligned} & \alpha_{2\text{D}}^n \frac{\zeta_{2\text{D},v,j}^p + \zeta_{2\text{D},i,j}^p}{2} + (\beta_{2\text{D}}^n + \alpha_{2\text{D}}^n b'_I) (\zeta_{2\text{D},v,j}^p - \zeta_{2\text{D},i,j}^p) \\ & - \delta_{2\text{D}}^n (\zeta_{2\text{D},i,j-1}^p - 2\zeta_{2\text{D},i,j}^p + \zeta_{2\text{D},i,j+1}^p) \\ & = \alpha_{2\text{D}}^n \zeta_{1\text{D},j}^{p-1} + \beta_{2\text{D}}^n \frac{\Delta t}{\Delta x \text{CFL}_{2\text{D},x}^2} q_{1\text{D}-2\text{D},j}^{p-1} \\ & - \delta_{2\text{D}}^n \left( \zeta_{1\text{D},j-1}^{p-1} - 2\zeta_{1\text{D},j}^{p-1} + \zeta_{1\text{D},j+1}^{p-1} \right. \\ & \quad \left. - (1/2 + b'_I) \frac{\Delta t}{\Delta x \text{CFL}_{2\text{D},x}^2} (q_{1\text{D}-2\text{D},j-1}^{p-1} - 2q_{1\text{D}-2\text{D},j}^{p-1} + q_{1\text{D}-2\text{D},j+1}^{p-1}) \right) \\ & + \text{rhs}_{1\text{D}-2\text{D},j}^n - \delta_{2\text{D}}^n (\text{rhs}_{1\text{D}-2\text{D},j-1}^n - 2\text{rhs}_{1\text{D}-2\text{D},j}^n + \text{rhs}_{1\text{D}-2\text{D},j+1}^n)_{\alpha_{2\text{D}}^n=1, \beta_{2\text{D}}^n=-1/2-b'_I}. \end{aligned} \quad (2.38)$$

The advantage of (2.38) over (2.37) is that it fits well within the current implementation of the solution procedure of (2.10), in which the virtual unknowns  $\zeta_{2\text{D},v}^p$  have been eliminated. Unlike (2.37) that has several unknowns  $\zeta_{2\text{D},v}^p$  in its left-hand side, (2.38) with only  $\zeta_{2\text{D},v,j}^p$  in its right-hand side does not require the extension of the current matrix solver with equations for the virtual unknowns. On the other hand, it is expected that the performance of (2.38) will not be as good as that of (2.37). In particular, it is expected that the demand for positive definiteness will impose a restriction on the choice of  $\delta_{2\text{D}}^n$  that will hamper full optimization.

Exactly the same procedure as for the coupling from the 1D domain to the 2D domain is applied to construct the coupling in the other direction, from the 2D domain to the 1D domain. Substitution of  $F_I^n = 1/(1 + b_{2\text{D}}\Delta t) \times \theta g \Delta t / \Delta x$  and  $A_I^n = \Delta x_I h_{2\text{D},I} = \Delta x_I h_{2\text{D}}$  in (2.25)



yields, using (2.23) (coupling from 2D to 1D for *drowned-weir* flow):

$$\begin{aligned} \alpha_{1D}^n \zeta_{1D}^p - \beta_{1D}^n \frac{\Delta x(1 + b_{2D}\Delta t)}{\theta^2 g h_{2D} \Delta t} q_{1D-2D}^p \\ = \alpha_{1D}^n \frac{\zeta_{2D,i}^{p-1} + \zeta_{2D,v}^{p-1}}{2} + \left( \beta_{1D}^n - \alpha_{1D}^n \frac{\theta(\Delta x_{1D-2D}/\Delta x + b_I \Delta t)}{1 + b_{2D}\Delta t} \right) (\zeta_{2D,i}^{p-1} - \zeta_{2D,v}^{p-1}) + \text{rhs}_{2D-1D}^n . \end{aligned} \quad (2.39)$$

Notice the similarity between this equation and (2.33).

Upon substitution of  $b'_I$  as defined in (2.34) and  $\text{CFL}_{2D,x}$  as defined in (2.32), (2.39) becomes:

$$\begin{aligned} \alpha_{1D}^n \zeta_{1D}^p - \beta_{1D}^n \frac{\Delta t}{\Delta x \text{CFL}_{2D,x}^2} q_{1D-2D}^p \\ = \alpha_{1D}^n \frac{\zeta_{2D,i}^{p-1} + \zeta_{2D,v}^{p-1}}{2} + (\beta_{1D}^n - \alpha_{1D}^n \theta b'_I) (\zeta_{2D,i}^{p-1} - \zeta_{2D,v}^{p-1}) + \text{rhs}_{2D-1D}^n , \end{aligned} \quad (2.40)$$

which is similar to (2.35).

The most useful simplified version of coupling (2.40) is the one that is obtained for  $\alpha_{1D}^n = 1$  and  $\beta_{1D}^n = 0$ :

$$\zeta_{1D}^p = \frac{\zeta_{2D,i}^{p-1} + \zeta_{2D,v}^{p-1}}{2} - b'_I (\zeta_{2D,i}^{p-1} - \zeta_{2D,v}^{p-1}) + (\text{rhs}_{2D-1D}^n)_{\alpha_{1D}^n=1, \beta_{1D}^n=0} . \quad (2.41)$$

The extended coupling obtained upon combining (2.40) and the second difference of (2.41) (minus two times (2.41) at  $j$  plus (2.41) at  $j-1$  and  $j+1$ ) reads:

$$\begin{aligned} \alpha_{1D}^n \zeta_{1D,j}^p - \beta_{1D}^n \frac{\Delta t}{\Delta x \text{CFL}_{2D,x}^2} q_{1D-2D,j}^p - \delta_{1D}^n (\zeta_{1D,j-1}^p - 2\zeta_{1D,j}^p + \zeta_{1D,j+1}^p) \\ = \alpha_{1D}^n \frac{\zeta_{2D,i,j}^{p-1} + \zeta_{2D,v,j}^{p-1}}{2} + (\beta_{1D}^n - \alpha_{1D}^n b'_I) (\zeta_{2D,i,j}^{p-1} - \zeta_{2D,v,j}^{p-1}) \\ - \delta_{1D}^n \left( (\zeta_{2D,i,j-1}^{p-1} + \zeta_{2D,v,j-1}^{p-1})/2 - (\zeta_{2D,i,j}^{p-1} + \zeta_{2D,v,j}^{p-1}) + (\zeta_{2D,i,j+1}^{p-1} + \zeta_{2D,v,j+1}^{p-1})/2 \right. \\ \left. + b'_I (\zeta_{2D,v,j-1}^{p-1} - \zeta_{2D,i,j-1}^{p-1} - 2(\zeta_{2D,v,j}^{p-1} - \zeta_{2D,i,j}^{p-1}) + \zeta_{2D,v,j+1}^{p-1} - \zeta_{2D,i,j+1}^{p-1}) \right) \\ + \text{rhs}_{2D-1D,j}^n - \delta_{1D}^n (\text{rhs}_{2D-1D,j-1}^n - 2\text{rhs}_{2D-1D,j}^n + \text{rhs}_{2D-1D,j+1}^n)_{\alpha_{1D}^n=1, \beta_{1D}^n=0} . \end{aligned} \quad (2.42)$$

Note again the dependence of the  $\text{rhs}_{2D-1D}^n$  on  $\alpha_{1D}^n$  and  $\beta_{1D}^n$ .

Equation (2.42) has only a single unknown  $q_{1D-2D}^p$  in its left-hand side. This makes it relatively easy to combine it with the  $\zeta^p$  equations (2.10) to be solved in 1D domains. By combining both equations such that  $q_{1D-2D}^p$  in the former and single variable  $q_c^p$  in the latter cancel (using  $q_c = -q_{1D-2D}$ ), a system of equation in only the  $\zeta_{1D,j}^p$  is obtained that has the same tridiagonal structure as (2.10). Implementation of (2.42) should therefore be feasible. It is for this reason that (2.41) has been considered for the extension of (2.40).

Similar to the coupling from 1D to 2D, parameter  $\delta_{1D}^n$  and accompanying terms have been introduced in (2.42) to investigate the gain in performance that may be obtained with this extension of coupling (2.40) from 2D to 1D, with the intention to figure out if implementation of it (somewhere in the future) may be worth considering. NB, the combination of (2.40) with the

second difference of (2.40) for two different values of  $\beta_{1D}^n$  (i.e.,  $\beta_{1D}^n = 0$  and a value  $\beta_{1D}^n \neq 0$ ) will not be considered. Although in principle possible, with an extension based on  $\beta_{1D}^n \neq 0$  one would get in the left-hand side of (2.42) three coupled  $q_{1D-2D}^p$  at the indices  $j-1$ ,  $j$  and  $j+1$  that cannot be easily eliminated from the equations. This would destroy the tridiagonal structure of the systems of equations to be solved in 1D domains. Only the combination of (2.40) with the second difference of (2.40) for  $\alpha_{1D}^n = 1$  and  $\beta_{1D}^n = 0$ , i.e., with the second difference of (2.41), is feasible enough to consider for implementation. NB, a proper choice of the coupling parameters  $\beta_{1D}^n$  and  $\delta_{1D}^n$  (taking  $\alpha_{1D}^n = 1$ ) is required to ensure the positive definiteness of the systems of equations.

#### 2.1.3.4.2 Normal-mode analysis

Because of the simplifications introduced (straight 1D-2D interface, uniform depths, rectangular domains, uniform grids, cf. the beginning of Section 2.1.3.4.1) and ignoring the effect of the conditions (far) upstream and downstream along the 1D-2D interface, the solution in the direction tangential to the 1D-2D interface can be expanded in linearly independent Fourier modes. For the convergence analysis and the subsequent optimization of the coupling parameters, it is convenient to consider the (convergence) errors per time step  $\Delta\zeta_j^p = \zeta_j^{n+1} - \zeta_j^p$  (in 1D) and  $\Delta\zeta_{i,j}^p = \zeta_{i,j}^{n+1} - \zeta_{i,j}^p$  (in 2D), and to expand them in Fourier modes. So consider convergence-error modes of the form:

$$\Delta\zeta_j^p = \Delta Z_{1D,k}^p \exp(iky_j) , \quad (2.43a)$$

$$\Delta\zeta_{i,j}^p = \Delta Z_{2D,k}^p \lambda_k^i \exp(iky_j) , \quad (2.43b)$$

with  $\Delta Z_{1D,k}^p$  and  $\Delta Z_{2D,k}^p$  the amplitude of the mode with tangential wave number  $k$  ( $0 \leq k\Delta y \leq \pi$ ) at iteration level  $p$  in respectively the 1D domain and the 2D domain, with  $\exp(iky_j)$  the behavior of the modes in the direction tangential to the 1D-2D interface (in 1D and 2D the same, and assumed to be periodic), and with  $\lambda_k^i$  the exponential behavior of the error mode in 2D normal to the 1D-2D interface. The 1D error mode is uniform in that direction, since the solution in 1D channels has been assumed uniform in crosswise direction.

Note that the  $i$  inside the  $\exp$  functions in (2.43) denotes the unit imaginary number  $\sqrt{-1}$  in the description of the oscillatory Fourier modes. The other occurrences of  $i$  (in (2.43b) only) denote the index in  $x$ -direction (the direction normal to the 1D-2D interface) of the cell centers, with superscript  $i$  in  $\lambda_k^i$  the power in the exponential amplitude behavior of  $\Delta\zeta_{i,j}^p$  normal to the interface.

It is easy to verify that, since  $\zeta_j^{n+1}$  and  $\zeta_{i,j}^{n+1}$  (and  $q_{1D-2D,j}^{n+1}$ ) are the converged solution of the equations (2.29), (2.31), (2.35) (or (2.37), or (2.38)) and (2.40) (or (2.42)),  $\Delta\zeta_j^p$  and  $\Delta\zeta_{i,j}^p$  (and  $\Delta q_{1D-2D,j}^p = q_{1D-2D,j}^{n+1} - q_{1D-2D,j}^p$ ) satisfy the homogeneous version of these equations. The homogeneous equations are obtained by omitting all terms at the previous time level  $n$ , i.e.,  $\text{rhs}_{1D,j}^n$ ,  $\text{rhs}_{2D,i,j}^n$ ,  $\text{rhs}_{1D-2D}^n$  and  $\text{rhs}_{2D-1D}^n$ .

The first step in the analysis is the determination of the normal-mode convergence-error behavior in the 2D domain (no normal mode in the 1D domain where the convergence error normal to a 1D-2D interface is uniform). Inserting (2.43b) in the homogenized (2.31), one obtains for the 2D domain the quadratic equation:

$$1 + 2\text{CFL}_{2D,x}^2 + 4\sin^2(k\Delta y/2)\text{CFL}_{2D,y}^2 - \text{CFL}_{2D,x}^2(\lambda_k^{-1} + \lambda_k) = 0 ,$$

whose two solutions are:

$$\begin{aligned} \lambda_{\pm k} &= 1/(2\text{CFL}_{2D,x}^2 + \Gamma + 1) \pm \sqrt{(1/(2\text{CFL}_{2D,x}^2 + \Gamma))(1/(2\text{CFL}_{2D,x}^2 + \Gamma + 2))} \\ &\approx \frac{1}{\text{CFL}_{2D,x}^{\pm 2}} \exp(\pm 2\text{CFL}_{2D,x}^2 \pm 4\sin^2(k\Delta y/2)\text{CFL}_{2D,y}^2), \end{aligned} \quad (2.44)$$

with  $\Gamma = 2\sin^2(k\Delta y/2)\text{CFL}_{2D,y}^2/\text{CFL}_{2D,x}^2$ . The approximate expansion in the second line is valid for small  $\text{CFL}_{2D,x}^2$  and  $\text{CFL}_{2D,y}^2$ , when terms of  $O(\text{CFL}_{2D,x}^4)$ ,  $O(\text{CFL}_{2D,x}^2\text{CFL}_{2D,y}^2)$  and  $O(\text{CFL}_{2D,y}^4)$  can be neglected. Note that for small  $k$  one can apply  $\sin^2(k\Delta y/2) \approx (k\Delta y)^2/4$ , neglecting terms of  $O((k\Delta y)^4)$ .

The two solutions (2.44) describe the behavior in  $x$ -direction of two modes  $\Delta\zeta_{i,j}^p$  per Fourier mode  $k$  that roughly speaking correspond with a left-going and a right-going error wave in the 2D domain. Because of the symmetry of (2.31) it turns out that these modes are the inverse of each other, i.e.,  $\lambda_{-k}\lambda_{+k} = 1$ .

The larger  $\text{CFL}_{2D,x}$ , i.e., the larger the non-dimensional time step, the closer  $\lambda_{-k}$  and  $\lambda_{+k}$  are to 1 and the larger the penetration distance into the domain, while the larger  $k$ , i.e., the larger the non-dimensional angle of the error wave with respect to the normal direction, the more that penetration is tangential to the boundary. This behavior is recognized in Figure 2.6 that shows the normalized normal behavior of the two modes  $\Delta\zeta_{i,j}^p$  per wave number  $k$  (one left-going, one right-going) (right-going mode  $\lambda_{-k}$  and left-going mode  $\lambda_{+k}$ ) for a number of combinations of  $\text{CFL}_{2D} = \text{CFL}_{2D,x} = \text{CFL}_{2D,y}$  and  $k\Delta y$ .

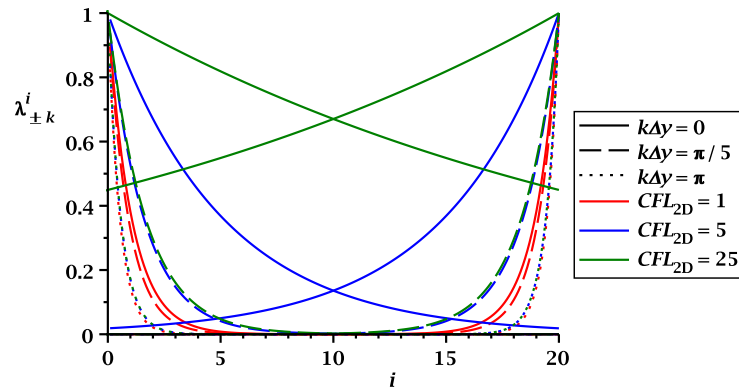


**Figure 2.6:** Behavior of normal-mode solutions of (2.31) for 3 different tangential modes  $k\Delta y$  (solid, dashed and dotted lines) and 3 different values of  $\text{CFL}_{2D} = \text{CFL}_{2D,x} = \text{CFL}_{2D,y}$  (red, blue and green lines).

For  $4\sin^2(k\Delta y/2)\text{CFL}_{2D,y}^2 \ll 1$  and  $\text{CFL}_{2D,x} \gg 1$ , expression (2.44) can be approximated by  $\lambda_{\pm k} \approx 1 \pm 1/\text{CFL}_{2D,x}$ , from which  $\ln(\lambda_{\pm k}) \approx \pm 1/\text{CFL}_{2D,x}$  can be obtained. This shows in particular that for the constant mode tangential to a 1D-2D interface ( $k\Delta y = 0$ ) the exponential decay or increase in normal direction per grid cell  $\ln(\lambda_{\pm k})$  is about inversely proportional to  $\text{CFL}_{2D,x}$  and hence can be rather small, as can also be observed in Figure 2.6: the larger  $\text{CFL}_{2D,x}$ , the further a constant tangential-mode perturbation (convergence error) at a 1D-2D interface (which is a boundary for the 2D domain) penetrates into the 2D domain.

The situation is completely different for the shortest (wiggle) mode  $k\Delta y = \pi$  along the 1D-2D interface. Assuming equal  $\text{CFL}_{2D,x}$  and  $\text{CFL}_{2D,y}$  for the moment,  $\Gamma = 2$  and hence  $\lambda_{\pm k} \approx 3 \pm 2\sqrt{2}$  for  $\text{CFL}_{2D,x}$  sufficiently larger than 1. In fact, for  $k\Delta y = \pi$ , for all  $\text{CFL}_{2D,y} =$

$\text{CFL}_{2\text{D},x} > 1$  the large exponential decay or increase per grid cell  $\ln(\lambda_{\pm k}) \approx \ln(3 \pm 2\sqrt{2}) = \pm 1.763$ . In other words, for the wiggle mode tangential to a 1D-2D interface ( $k\Delta y = \pi$ ) the exponential decay or increase per grid cell  $\ln(\lambda)$  is large and virtually independent of  $\text{CFL}_{2\text{D},x}$ , cf. Figure 2.6.

The large range in normal-mode behavior for large  $\text{CFL}_{2\text{D},x}$  complicates the optimization of the interface coupling for maximum convergence speed, but also makes this optimization important.

It is now assumed that the optimization of the coupling at a 1D-2D interface can be considered as a problem that is independent of the coupling optimization at other interfaces. This assumption is obviously not true, but is expected to hold reasonably well. The reason for this is the exponential normal-mode decay. Figure 2.6 shows that when there are 20 grid cells between the 1D-2D interfaces present at both sides of a 2D domain, the effect of the solution at one interface on the solution at the other is less than 50% at a  $\text{CFL}_{2\text{D}}$  value as high as 25. The effect that the presence of an opposite interface at a distance of 20 grid cells has on the behavior of the coupling at a 1D-2D interface has twice that attenuation factor, i.e., it has an effect of about 20% at  $\text{CFL}_{2\text{D}} = 25$ . Since 20 2D grid cells between 1D-2D interfaces is not a large number, but especially because in practice  $\text{CFL}_{2\text{D}}$  will usually be (much) smaller than 25, the mutual influence between 1D-2D interfaces will generally be small.

An important exception is the situation that occurs when 1D channels are close together, such as in a braided river system as illustrated in Figure 2.1. The narrow 2D areas that are in between 1D channels may in that case be only a few grid cells wide. Also near nodes connecting branches at different angles there may be a mutual influence of the coupling at different 1D-2D interfaces. Because of the complexity of this problem it is not feasible to include the interdependence of couplings at different 1D-2D interfaces in the optimization, so this aspect will be ignored. Likewise, because of the simplifications introduced, the effect of (strongly) curved 1D-2D interfaces, non-uniform depths, varying grid sizes, varying 1D channel widths, and varying friction coefficients will be ignored.

Concerning the optimization strategy it is first noticed that, because 1D solutions are uniform in crosswise direction, all 1D normal convergence-error modes are constant. See also expression (2.43a) that is independent of  $x$ , hence constant in  $x$ -direction. As a result, 1D convergence-error modes are 'global', in the sense that they depend equally on the convergence error at the 1D-2D interface at either side of the 1D channel. This creates an interdependency between the 1D-2D couplings at each of the two lateral boundaries of a 1D channel. Insight in the strength of that interdependency can be obtained from a normal-mode analysis where the 1D-2D couplings at both lateral boundaries of a 1D channel are considered simultaneously. Pending such an analysis, it is presently not known how strong that interdependency is.

In contrast to the 1D domains, the 2D domains have normal modes that decay exponentially with the distance from the boundaries, cf. (2.43b), (2.44), and Figure 2.6. Assuming that this decay is large enough<sup>11</sup>, the solution imposed at a boundary will within one time step hardly affect the solution at the opposite boundary.

---

<sup>11</sup> This requires a sufficiently large number of grid cells across the width of a 2D domain and a sufficiently small CFL number, cf. figure 2.6.

### 2.1.3.5 Properties of the horizontal 1D-2D coupling

Expected properties of the SOBEK 3 1D-2D coupling:

- ◇ Works well for sufficiently small Courant number CFL or sufficiently wide 2D areas in between the 1D channel sections, hence may not work that well if large CFL *and* narrow 2D areas (as in between two parallel 1D channels that are close together, cf. Figure 2.1).
- ◇ Large CFL may be a problem because then large spreading in exponential behavior of normal modes, cf. Figure 2.6, while the optimization of the coupling is for a single 'average' mode. In consequence, the optimization is not optimal for the full range of modes.  
NB, a better optimization for the full range of modes requires consideration of the proposed extended couplings.  
IMPORTANT: large CFL are in particular a problem when the 1D grids and the 2D grids are conformal, i.e., match along an interface (the 1D and 2D grid size in tangential direction along the 1D-2D interfaces are equal). This is the current restriction; the presently available coupling has been developed with this grid restriction. Required is a coupling for 1D and 2D models as they are used in practice, where the grid size applied in the 1D channels is usually (much) larger than the grid size applied in the 2D areas. This (strongly) reduces the number of relevant Fourier modes, hence the spreading in normal-mode exponential behavior, and therefore improves the applicability of the applied single-mode optimization of the 1D-2D coupling. This is something to take into account when testing the coupling for the current conformal-grid limitation.
- ◇ Optimization of the coupling is based on the assumption of constant coefficients and straight 1D-2D interfaces, hence may not work that well in case of large variation in 2D depth or 2D friction coefficient along an interface, if large curvature of a 1D-2D interface, if corners in an interface at intersections of 1D channel sections, ...



### 3 Numerical concepts (1D)

#### 3.1 Staggered grid

For the numerical solution of the flow equations a so-called “staggered grid” (Stelling and Duinmeijer, 2003; Stelling and Verwey, 2006) is used. A channel network is discretized in

- ◇ water level points (also called h-points, grid points or calculation points) and
- ◇ velocity points<sup>1</sup> (also called u-points or v-points).

Figure 3.1 shows a schematic view of a staggered grid. Water level points form the basis of the computational grid, velocity points are located half between two h-points. At h-points the continuity equation is solved, while the momentum equation is solved at u-points. Consequently, for h-points a water level is computed, while for u-points the simulation result is the velocity. Table 3.1 summarizes which output parameter is located on which discretization point type.

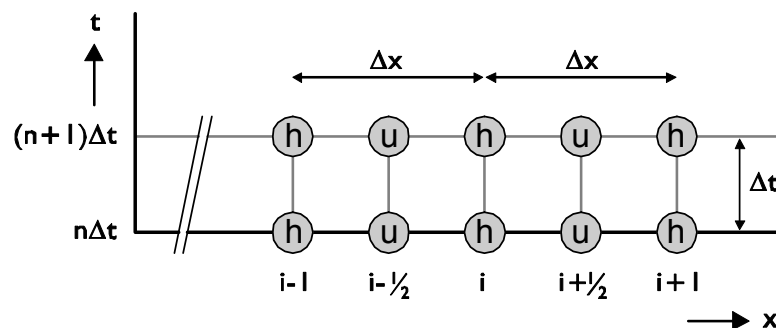


**Figure 3.1:** Equidistant staggered grid for unsteady channel flow (after Stelling and Verwey, 2006).  $h$  represents the water level,  $u$  the velocity.  $\Delta x$  the distance between two grid points (or calculation points) in space and  $\Delta t$  the time step size.  $i$  and  $n$  represent a point in the spatial or temporal discretization, respectively. Velocity points ( $u$ -points) are located on  $i - \frac{1}{2}$  and  $i + \frac{1}{2}$  between the grid points (i.e. on the reach segments that connect the grid points), water level points ( $h$ -points) are located on the grid points  $i - 1$ ,  $i$ , and  $i + 1$ .

**Table 3.1:** Overview on the equation solved for the two different grid elements of a staggered grid and the corresponding output parameters

grid object	equation	flow parameter (selection)
grid point, calculation point	continuity	water level $h$ , salinity, total width
reach segment	momentum	velocity $u$ , discharge $Q$ , flow width

The mathematical formulations of the shallow water flow and transport (only salinity) model SOBEK-RUR were presented in the previous chapters. To solve these partial differential equations the equations should be transformed to the discrete space. In this chapter the space discretization and the time integrations methods in SOBEK-RUR will be briefly presented.

To understand the algorithms in SOBEK-RUR it is important to know something about the history of the software package. The first version of SOBEK-RUR was developed and programmed by G.S. Stelling for the simulation of unsteady flows in sewer systems. The hy-

<sup>1</sup> In the Sobek 2 user interface  $u$ -points are displayed as reach segments. However, strictly speaking, simulation results assigned to a reach segment are only valid for the center point of a reach segment, because the velocity points do not represent a cell or a volume.

draulics in such systems can be very complicated e.g. the flows can locally be supercritical. Therefore, numerical stability and robustness were major factors for the choice of a numerical method. It was therefore decided to apply in SOBEK-RUR a **Finite Volume** approximation of the conservation laws on a **staggered grid** and for an implicit time integration of the hydrostatic pressure term. In SOBEK-RUR, the final system of difference equations is solved with a Conjugate Gradient algorithm. The discretizations of the equations are made in such a way that the resulting system of equations is symmetric.

### 3.2 Computational grid and definitions

SOBEK-RUR is a numerical model is applied that is based on finite volumes. The arrangement of the flow variables in presented in Figure 3.2. Let  $x$  be the longitudinal coordinate, which follows the channel axis. The channel may be a reach of a river network. To discretise the balance equations in space, we introduce a so-called staggered grid with  $m$  the grid index

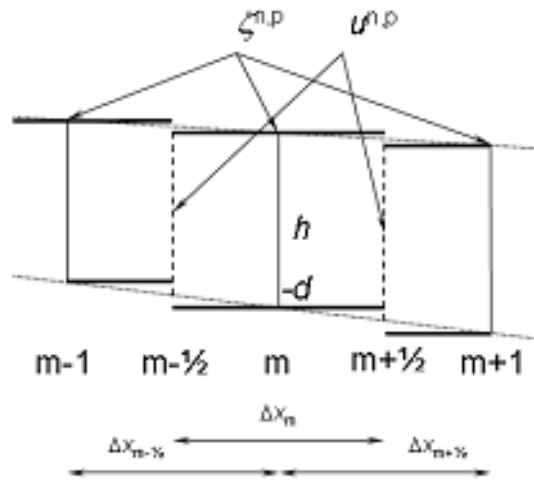


Figure 3.2: Staggered flow grid

along the main axis, see the Figure 3.2. The water level points (pressure points) are defined in the centre of a (continuity) cell. The velocity components are defined at grid cell faces.

The grid of the pressure (water level) points is given by  $x_m$  and the velocity points by  $x_{m+\frac{1}{2}}$ . We approximate the river (channel or pipe) by Finite Volumes  $V_m$  around the so-called pressure (or water level points). In SOBEK-RUR these Finite Volumes in the water level points for the mass balance are the total volume, the combination of the flow and the storage area. SOBEK-RUR is a one-dimensional flow model. We assume that the independent variables in our one-dimensional model the waterlevel  $\zeta(x, t)$ , the velocity  $U(x, t)$  and discharge  $Q(x, t)$  are constant (independent of  $y$ ) for a cross section. The water in the storage area is assumed to be stagnant. This assumption is important for the derivation of the advection terms in the following sections.

The length of the box along the river axis is  $\Delta x_m = [x_{m-\frac{1}{2}}, x_{m+\frac{1}{2}}]$  and the Volume

$$V_m^Z(\zeta_m(t)) = \int_{x_{m-\frac{1}{2}}}^{x_{m+\frac{1}{2}}} \int_{-d(x')}^{z=\zeta(x',t)} W_t(x', z') dz' dx' \quad (3.1)$$

Noted that the vertical integral is from the bottom until the free surface) with  $W_t(x, z)$  the



total width of the river at cross section  $x$  at level  $z$ . Let  $H(x, y, t) = \zeta(x, t) + d(x, y)$  be the total water depth.

River cross-sections often consist of a main channel through which the discharge is conveyed and shallow flood plains which are mainly functioning as storage areas, particular when groynes are present for channel regulation.

Instead of taking an integral over the vertical coordinate  $z$ , we can also take an integral of the total water depth  $H$  over the width of the river in the transverse coordinate  $y$ , from the left bank of the river  $y = -b_l(x)$  until the right bank  $y = b_r(x)$ .

$$Z(\zeta_m(t)) = \int_{x_m - \frac{1}{2}}^{x_m + \frac{1}{2}} \int_{-d(x')}^{z=\zeta(x',t)} W_t(x', z') dz' dx' \quad (3.2)$$

$$= \int_{x_m - \frac{1}{2}}^{x_m + \frac{1}{2}} \int_{-b_l(x')}^{-b_r(x')} H(x', y', t) dy' dx' \quad (3.3)$$

The total area (flow and storage area together) of the cross section in the pressure point is defined as:

$$A_t(\zeta(t))_m = \int_{-d(x_m)}^{z=\zeta_m(t)} W_t(x_m, z') dz' \quad (3.4)$$

$$= \int_{-b_l(x_m)}^{-b_r(x_m)} H(x_m, y', t) dy' \quad (3.5)$$

Because we assume that the average velocity component in the direction of the river axis for the storage area is almost zero, we can split this integral over the total area of a cross section in the integral over the flowing part and the storage part. When the depths of the main channel and the flood plains are very different and the discharge through the flood plain can not be neglected, it is better to schematize the cross sections in a 1D-model into two parallel channels: one main channel or conveyance channel and one for the flood plain.

$$A_t(x, \zeta(t)) = (\text{flow}) \int_{y', u(x,y,t) > 0} [\zeta(x, t) + dp(x, y')] dy' \quad (3.6)$$

$$+ (\text{storage}) \int_{y', u(x,y,t) = 0} [\zeta(x, t) + dp(x, y')] dy' \quad (3.7)$$

The flow area is defined as:

$$A_f(x, \zeta(t)) = \int_{y', u(x,y,t) > 0} [\zeta(x, t) + dp(x, y')] dy' \quad (3.8)$$

The total volume in a water level point is approximated by:

$$V_m^Z(H_m(t)) = A_t(H_m(t)) \Delta x_m \quad (3.9)$$

### 3.3 Upwinding

Due to the staggered grid the water levels and the depths are missing at the grid point  $x_{m+\frac{1}{2}}$ . These values  $\tilde{\zeta}_{m+\frac{1}{2}}$  and  $d_{m+\frac{1}{2}}$  should be approximated by some kind of interpolation from the values in the water level points.

In SOBEK-RUR, the flow area and the wet perimeter are specified at input in water level points. To determine the flow area in a velocity point an upwind approach is used to determine the total waterdepth  $H$  at the velocity point. The bottom depth  $d$  is defined positive downwards.

$$\tilde{H}_{m+\frac{1}{2}}(t) = \begin{cases} \zeta_m(t) + d_m & u_{m+\frac{1}{2}} > 0 \\ \zeta_{m+1}(t) + d_{m+1} & u_{m+\frac{1}{2}} < 0 \\ \max(\zeta_m(t), \zeta_{m+1}(t)) + \min(d_m, d_{m+1}) & u_{m+\frac{1}{2}} = 0 \end{cases} \quad (3.10)$$

The approximation of the flow area in the cross section  $x_{m+\frac{1}{2}}$  is given by:

$$A_f\left(x_{m+\frac{1}{2}}, \tilde{\zeta}_{m+\frac{1}{2}}(t)\right) = \int_{y', u(x_{m+\frac{1}{2}}, y, t) > 0} \left[ \tilde{H}_{m+\frac{1}{2}}(x_{m+\frac{1}{2}}, y') \right] dy' \quad (3.11)$$

with  $A_f(x, z)$  the area of the flowing part of the river (representative conveyance cross section) at location  $x$ . Like the water levels we assume that the velocity in a one dimensional model is independent of the coordinate  $y$ . The average flow velocity in the cross section  $U_{m+\frac{1}{2}}(x, t)$  along the river axis, is defined as:

$$U_{m+\frac{1}{2}}\left(x_{m+\frac{1}{2}}, t\right) = \frac{\int_{-d(x_{m+\frac{1}{2}})}^{\tilde{\zeta}_{m+\frac{1}{2}}(t)} u(x_{m+\frac{1}{2}}, y', t) \tilde{H}(x_{m+\frac{1}{2}}, y') dy' dz'}{A_f\left(x_{m+\frac{1}{2}}, \tilde{\zeta}_{m+\frac{1}{2}}(t)\right)} = \left[ \frac{Q}{A_f} \right] \left(x_{m+\frac{1}{2}}, t\right) \quad (3.12)$$

The water level and the velocity (discharge) characterise the flow in a one-dimensional network model.

### 3.4 Time integration

In this section the time integration of SOBEK-RUR is explained. A subdivision is made between the time integration of the continuity equation and for the momentum equation.

#### 3.4.1 Time integration of the continuity equation

The rate of change of the mass in a Finite Volume approach at the water level point (volume of channel flow and volume of off-channel storage together) is given by:

$$\frac{dV_m^Z}{dt} = \frac{dV_m^f}{dt} + \frac{dV_m^S}{dt} \quad (3.13)$$

The fluxes through the interfaces of the Finite Volume at the water level point  $m$  are given by

$$Q_{m+\frac{1}{2}} - Q_{m-\frac{1}{2}} \quad (3.14)$$

so the balance equation for the conservation of mass

$$\frac{dV_m^Z}{dt} + Q_{m+\frac{1}{2}} - Q_{m-\frac{1}{2}} = q_m \quad (3.15)$$

with  $q_m$  is the sum of the lateral discharges, which are volumes of water entering or leaving the Control Volume from the outside world at a specified location. It may be a point source (pump, discharge) or an incoming flow across a specified branch (for instance rainfall or groundwater seepage). An incoming volume of water can also be supplied by a hydraulic structure.

In most of the 1D network branches, the volume of the Control Volume for mass is a non-linear function of the water level in the central water level point  $V_m^Z(\zeta(t))$ . The momentum equations and the continuity equation are integrated in time with a so-called  $\theta$ -scheme, leading to the discrete equation:

$$\frac{V_m^Z(\zeta^{n+1}) - V_m^Z(\zeta^n)}{\Delta t} + Q_{m+\frac{1}{2}}^{n+\theta} - Q_{m-\frac{1}{2}}^{n+\theta} = q_m \quad (3.16)$$

with

$$\begin{aligned} Q_{m+\frac{1}{2}}^{n+\theta} &= \theta Q_{m+\frac{1}{2}}^{n+1} + (1 - \theta) Q_{m+\frac{1}{2}}^n \\ &= \theta A_f \left( x_{m+\frac{1}{2}}, \tilde{\zeta}_{m+\frac{1}{2}}^n \right) u_{m+\frac{1}{2}}^{n+1} + (1 - \theta) A_f \left( x_{m+\frac{1}{2}}, \tilde{\zeta}_{m+\frac{1}{2}}^n \right) u_{m+\frac{1}{2}}^n \end{aligned} \quad (3.17)$$

To solve this equation for the water level  $\zeta_m^{n+1}$  at the new time level, it should be linearised. This is done by a Newton iteration procedure with index  $i$  on the storage term. This leads to the equation:

$$V_m^Z(\zeta^{n+1,i+1}) = V_m^Z(\zeta^{n+1,i}) + (\zeta^{n+1,i+1} - \zeta^{n+1,i}) \frac{dV_m^Z(\zeta^{n+1,i})}{d\zeta} \quad (3.18)$$

from [Equation 3.13](#) it follows that the change of the Control Volume with the water level is the total horizontal area of the Control Volume:

$$V_m^Z(\zeta^{n+1,i+1}) = V_m^Z(\zeta^{n+1,i}) + (\zeta^{n+1,i+1} - \zeta^{n+1,i}) W_t(x_m, \zeta^{n+1,i}) \Delta x \quad (3.19)$$

If we take the limit to zero for the length of the Control Volume the continuity equation becomes:

$$\frac{\partial A_f}{\partial t} + \frac{\partial Q}{\partial x} + \frac{\partial (A_t - A_f)}{\partial t} = q(x, t) \quad (3.20)$$

The total horizontal area is the sum of the area of the flowing part and the off-channel storage area. The wet surface area and discharge are related to the element length  $\Delta x_m$  associated with velocity:  $A_{\zeta;m}^n = W_{\zeta;m}^n \Delta x_m$  and  $Q_m^n = q_m^n \Delta x_m$ : Substituting [Equation 3.19](#) into [Equation 3.16](#) and applying a so-called the  $\theta$ -method, yields

$$\begin{aligned} &A_{\zeta;m}^n \frac{\zeta_m^{n+1} - \zeta_m^n}{\Delta t} + \\ &\theta \left( A_{f;m+\frac{1}{2}}^n u_{m+\frac{1}{2}}^{n+1} - A_{f;m-\frac{1}{2}}^n u_{m-\frac{1}{2}}^{n+1} \right) + (1 - \theta) \left( A_{f;m+\frac{1}{2}}^n u_{m+\frac{1}{2}}^n - A_{f;m-\frac{1}{2}}^n u_{m-\frac{1}{2}}^n \right) = Q_m^n \end{aligned} \quad (3.21)$$

After separating the major and minor indices we arrived at:

$$\frac{A_{\zeta;m}^n}{\Delta t} \zeta_m^{n+1} - \theta A_{f;m-\frac{1}{2}}^n u_{m-\frac{1}{2}}^{n+1} = \frac{A_{\zeta;m}^n}{\Delta t} \zeta_m^n - (1 - \theta) A_{f;m+\frac{1}{2}}^n u_{m+\frac{1}{2}}^n + Q_m^n \quad (3.22)$$

### 3.4.2 Time integration of the momentum equation

The momentum equation is derived from a momentum balance for a 3D Control Volume around a velocity point  $x_{m+\frac{1}{2}}$ . The Volume of a Control Volume in a velocity point is defined as the integral over the flowing part of the cross section:

$$V_{m+\frac{1}{2}}^U \left( \tilde{\zeta}_{m+\frac{1}{2}}(t) \right) = \int_{x_m}^{x_m+\Delta x} \int_{y', u(x', y', t) > 0} \left[ \tilde{H}_{m+\frac{1}{2}}(x', y') \right] dy' dx' \quad (3.23)$$

with  $W_f(x, z)$  the width of the flow area at cross section  $x$  at level  $z$  (the integral is from the bottom until the free surface). We assume that outside the flow area  $W_f$  the water is stagnant in the storage area, so the horizontal velocity for that part of the cross section is zero and does not contribute to the discharge.

The volume of the Control Volume for the momentum balance, situated in a velocity point is approximated by:

$$V_{m+\frac{1}{2}}^U \left( \tilde{\zeta}_{m+\frac{1}{2}}(t) \right) = A_f \left( \tilde{\zeta}_{m+\frac{1}{2}}(t) \right) \Delta x_m \quad (3.24)$$

The rate of change of the momentum in a Finite Volume

$$\frac{d \left( \rho V_{m+\frac{1}{2}}^U U_{m+\frac{1}{2}} \right)}{dt} \quad (3.25)$$

should be the sum of in- and outflowing momentum fluxes through the cross sections at the pressure points  $x_m$  and  $x_{m+1}$ . These convective momentum fluxes are given by:

$$\tilde{Q}_{m+1} \rho \tilde{U}_{m+1} - \tilde{Q}_m \rho \tilde{U}_m \quad (3.26)$$

If we take the limit to zero for the length of the Control Volume the continuity equation becomes:

$$\frac{dV_m^Z(\zeta(t))}{dt} + \frac{\partial Q}{\partial x} = q(x_m, t) - \frac{dV_m^S(\zeta(t))}{dt} \quad (3.27)$$

and if we take into account the definitions of total area and flow area, we get for the momentum equations:

$$\frac{\partial u}{\partial t} + u \frac{\partial u}{\partial x} + g \frac{\partial \zeta}{\partial x} + \frac{gu|u|}{C^2 R} = \frac{\partial (A_t - A_f)}{\partial t} (u_b - u) \quad (3.28)$$

Due to the staggered grid the discharge  $\tilde{Q}_m$  and  $\tilde{Q}_{m+1}$  should be approximated in the pressure points  $x_m$  and  $x_{m+1}$ . In SOBEK-RUR in the water level points the average discharge is used, so:

$$\tilde{Q}_m = \frac{Q_{m+\frac{1}{2}} + Q_{m-\frac{1}{2}}}{2} \quad (3.29)$$

The transport term due to convection is in most rivers and channels of minor importance. Only in river sections with a strongly varying conveyance area, this term generates an energy loss, which should be taken into account accurately. For nodal points in 1D networks where more than two branches come together, only the incoming fluxes are taken into account.

The flow is accelerated due to the external forces the pressure force related to the free surface gradient and decelerated by the bottom friction. For the bottom friction a quadratic friction law is assumed with friction coefficient  $c_f$  and  $S_f$  the surface area where the bottom friction acts on the flowing fluid volume. We divide the momentum equation by the constant density  $\rho$ , we get

$$\frac{d \left( V_{m+\frac{1}{2}}^U U_{m+\frac{1}{2}} \right)}{dt} + \tilde{Q}_{m+1} \tilde{U}_{m+1} - \tilde{Q}_m \tilde{U}_m + \tilde{A}_f \left( \tilde{\zeta}_{m+\frac{1}{2}}(t) \right) g \frac{\zeta_{m+1} - \zeta_m}{\Delta x} + c_f U_{m+\frac{1}{2}} \left| U_{m+\frac{1}{2}} \right| S_{f_{m+\frac{1}{2}}} = 0 \quad (3.30)$$

Assuming a constant density, the equation is simplified. We use the chain rule to expand the first term:

$$\frac{d \left( V_{m+\frac{1}{2}}^U U_{m+\frac{1}{2}} \right)}{dt} = U_{m+\frac{1}{2}} \frac{dV_{m+\frac{1}{2}}^U}{dt} + V_{m+\frac{1}{2}}^U \frac{dU_{m+\frac{1}{2}}}{dt} \quad (3.31)$$

The Control Volume in a velocity point differs from the Control Volume in a waterlevel point. We can write:

$$\frac{dV_m^Z}{dt} = \frac{dV_m^U}{dt} + \frac{dV_m^S}{dt} \quad (3.32)$$

so,

$$\frac{dV_m^U}{dt} + Q_{m+\frac{1}{2}} - Q_{m-\frac{1}{2}} = q_m - \frac{dV_m^S}{dt} \quad (3.33)$$

This difference in the definition of the Control Volumes for the continuity and the momentum balance introduces an additional lateral discharge. For rising water levels there is a Flow from the flowing part to the storage area and for the falling water levels there is a flow from the storage area to the flowing area. For the momentum balance this introduces a term:

$$q_b = - \frac{dV_m^S}{dt} u_b \quad (3.34)$$

$u_b$  is the velocity of the water that is exchanged between these two areas, so

$$u_b = \begin{cases} u_b = U_m & \frac{dV_m^S}{dt} > 0 \\ u_b = 0 & \frac{dV_m^S}{dt} < 0 \end{cases} \quad (3.35)$$

If we multiply the continuity equation with the velocity  $U_{m+\frac{1}{2}}^n$  and we subtract it from [Equation 3.31](#) we get

$$\begin{aligned} \frac{dU_{m+\frac{1}{2}}}{dt} + \frac{\tilde{Q}_{m+1}}{V_{m+\frac{1}{2}}^U} \left[ \tilde{U}_{m+1} - U_{m+\frac{1}{2}} \right] + \frac{\tilde{Q}_m}{V_{m+\frac{1}{2}}^U} \left[ U_{m+\frac{1}{2}} - \tilde{U}_m \right] + g \frac{\zeta_{m+1} - \zeta_m}{\Delta x} + \frac{c_f U_{m+\frac{1}{2}} \left| U_{m+\frac{1}{2}} \right|}{\frac{V_{m+\frac{1}{2}}^U}{S_{f_{m+\frac{1}{2}}}}} \\ = \left( q_m - \frac{dV_m^S}{dt} \right) \left( u_b - U_{m+\frac{1}{2}} \right) \end{aligned} \quad (3.36)$$

Equation 3.13 is discretised using the  $\vartheta$ - method as:

$$\frac{u_{m+\frac{1}{2}}^{n+1} - u_{m+\frac{1}{2}}^n}{\Delta t} + \frac{g}{\Delta x_{m+\frac{1}{2}}} \left\{ \theta (\zeta_{m+1}^{n+1} - \zeta_m^{n+1}) + (1 - \theta) (\zeta_{m+1}^n - \zeta_m^n) \right\} + B_{m+\frac{1}{2}}^n u_{m+\frac{1}{2}}^{n+1} = D_{m+\frac{1}{2}}^n \quad (3.37)$$

After separating the mMajor and minor indices, we arrive at:

$$u_{m+\frac{1}{2}}^{n+1} \left( \frac{1}{\Delta t} + B_{m+\frac{1}{2}}^n \right) + \frac{g\theta}{\Delta x_{m+\frac{1}{2}}} (\zeta_{m+1}^{n+1} - \zeta_m^{n+1}) = \frac{u_{m+\frac{1}{2}}^n}{\Delta t} - \frac{g(1-\theta)}{\Delta x_{m+\frac{1}{2}}} (\zeta_{m+1}^n - \zeta_m^n) + D_{m+\frac{1}{2}}^n \quad (3.38)$$

A relation between major velocity and water level terms is obtained with coefficients depending on minor velocity and water level terms:

$$u_{m+\frac{1}{2}}^{n+1} = R_{m+\frac{1}{2}}^n - F_{m+\frac{1}{2}}^n (\zeta_{m+1}^{n+1} - \zeta_m^{n+1})$$

$$F_{m+\frac{1}{2}}^n = \frac{\frac{g\theta}{\Delta x_{m+\frac{1}{2}}}}{\frac{1}{\Delta t} + B_{m+\frac{1}{2}}^n} \quad R_{m+\frac{1}{2}}^n = \frac{\frac{u_{m+\frac{1}{2}}^n}{\Delta t} - \frac{g(1-\theta)}{\Delta x_{m+\frac{1}{2}}} (\zeta_{m+1}^n - \zeta_m^n) + D_{m+\frac{1}{2}}^n}{\frac{1}{\Delta t} + B_{m+\frac{1}{2}}^n} \quad (3.39)$$

In a numerical simulation, smaller high-frequency spurious modes may be generated, which depend on the size of the timestep. To prevent these modes from becoming large and important one should use a value of  $\theta$  that is larger than 0.5 to introduce a numerical dissipation mechanism. For most applications the recommended value of  $\theta$  is 0.55. This gives usually sufficient dissipation without decreasing the accuracy too much.

### 3.4.3 Time integration of the combined continuity and momentum equation

The discretised continuity Equation 3.22 and momentum Equation 3.16 form a linear system with the two unknowns, water level and flow velocity. From these equations the velocity may be eliminated. The velocities are copied from Equation 3.16:

$$u_{m-\frac{1}{2}}^{n+1} = R_{m-\frac{1}{2}}^n - F_{m-\frac{1}{2}}^n (\zeta_m^{n+1} - \zeta_{m-1}^{n+1}) \quad u_{m+\frac{1}{2}}^{n+1} = R_{m+\frac{1}{2}}^n - F_{m+\frac{1}{2}}^n (\zeta_{m+1}^{n+1} - \zeta_m^{n+1}) \quad (3.40)$$

Substitution into Equation 3.22 leads to:

$$\frac{A_{\zeta;m}^n \zeta_m^{n+1}}{\Delta t} + \theta A_{f;m+\frac{1}{2}}^n \left\{ R_{m+\frac{1}{2}}^n - F_{m+\frac{1}{2}}^n (\zeta_{m+1}^{n+1} - \zeta_m^{n+1}) \right\} - \theta A_{f;m-\frac{1}{2}}^n \left\{ R_{m-\frac{1}{2}}^n - F_{m-\frac{1}{2}}^n (\zeta_m^{n+1} - \zeta_{m-1}^{n+1}) \right\} = \frac{A_{\zeta;m}^n \zeta_m^n}{\Delta t} + (1 - \theta) A_{f;m+\frac{1}{2}}^n u_{m+\frac{1}{2}}^n - (1 - \theta) A_{f;m-\frac{1}{2}}^n u_{m-\frac{1}{2}}^n + Q_m^n \quad (3.41)$$

Or, after moving the known terms to the right side:

$$\frac{A_{\zeta;m}^n \zeta_m^{n+1}}{\Delta t} - \theta A_{f;m+\frac{1}{2}}^n F_{m+\frac{1}{2}}^n (\zeta_{m+1}^{n+1} - \zeta_m^{n+1}) + \theta A_{f;m-\frac{1}{2}}^n F_{m-\frac{1}{2}}^n (\zeta_m^{n+1} - \zeta_{m-1}^{n+1}) = \frac{A_{\zeta;m}^n \zeta_m^n}{\Delta t} - (1 - \theta) A_{f;m+\frac{1}{2}}^n u_{m+\frac{1}{2}}^n - \theta A_{f;m+\frac{1}{2}}^n R_{m+\frac{1}{2}}^n + (1 - \theta) A_{f;m-\frac{1}{2}}^n u_{m-\frac{1}{2}}^n + \theta A_{f;m-\frac{1}{2}}^n R_{m-\frac{1}{2}}^n + Q_m^n \quad (3.42)$$

This is a tridiagonal system of equations for the water level, which is solved by forward and backward elimination.

### 3.4.4 Numerical method for the transport equation

The time integration of the transport equation for salinity is an explicit Forward Euler methode. For the space discretization of the advective terms the first-order upwind method is applied. This can be written into:

$$V_i^{n+1} s_i^{n+1} = V_i^n s_i^n + \Delta t \left( \sum_{k \in K_{in}} |q_k^n| s_{i_k}^n - \sum_{k \in K_{out}} |q_k^n| s_i^n + \sum_{k \in K} A_k^n D_k^n \frac{s_{i_k}^n - s_i^n}{\Delta x_k} \right) \quad (3.43)$$

$$+ s_i^n \left( V_i^{n+1} - V_i^n + \Delta t \left( \sum_{k \in K_{out}} |q_k^n| - \sum_{k \in K_{in}} |q_k^n| \right) \right) \quad (3.44)$$

$$= V_i^{n+1} s_i^n + \Delta t \left( \sum_{k \in K_{in}} |q_k^n| (s_{i_k}^n - s_i^n) + \sum_{k \in K} A_k^n D_k^n \frac{s_{i_k}^n - s_i^n}{\Delta x_k} \right), \quad (3.45)$$

with  $K$  the collection of all links of computational cell  $i$ ,  $K_{in}$  the collection of link with inflow, and  $K_{out} = K - K_{in}$  therefore the collection of links with outflow. For the remainder we have that  $V_i > 0$ , which is de volume of cell  $i$  (at different time levels),  $A_k \geq 0$  is the wetted cross-section oflink  $k$ ,  $D_k^n \geq 0$  is the dispersion coefficient at link  $k$ , and  $\Delta x_k > 0$  is the mesh size over link  $k$  (the distance between unknowns  $s_i^n$  of cell  $i$  and its neighbour  $s_{i_k}^n$  in the cell at the other side of link  $k$ ).

For monotonicity of the numerical solution, thus yielding positive salinity concentrations, the following condition should be satisfied:

$$A_k^n D_k^n = \min \left( \frac{\Delta x_k}{2} \left( \frac{V_{i_1}^{n+1}}{\Delta t} - \sum_{k \in K_{in}^1} |q_k^n| \right), \frac{\Delta x_k}{2} \left( \frac{V_{i_2}^{n+1}}{\Delta t} - \sum_{k \in K_{in}^2} |q_k^n| \right) \right), \quad (3.46)$$

in which the sub-/superscripts 1 and 2 represent the computational cells at both sides of link  $k$ . In simplified form, this can be rewritten to

$$D_k^n \leq \frac{1}{2} \frac{\min(V_{left}, V_{right})}{A_k^n} \frac{\Delta x_k}{\Delta t}, \quad (3.47)$$

In SOBEK the factor 1/2 is replaced by parameter DispMaxFactor. The default value is set to 0.45. SOBEK checks whether this condition is satisfied. If this is not the case and the dispersion coefficient, which is specified on input, is too large, then the dispersion coefficient is reduced and is set to it maximum value. Then, in the SOBEK.LOG file a message is generated, so that the user can verify whether a reduction of the dispersion coefficient has been applied.

### 3.4.5 Open boundary conditions for the transport equation

The horizontal transport of dissolved substances in rivers, estuaries, and coastal seas is dominated by advection. The horizontal diffusion in flow direction is of secondary importance. The consequence is that the transport equation is advection dominated, has a wave character, and from a mathematical point of view is of hyperbolic type. The equation has only one characteristic, which is parallel to the flow. Without diffusion, an observer moving with the flow, experiences a constant concentration. As described before, open boundaries have to

limit the computational area. At an open boundary during inflow (flood) a boundary condition is needed. During outflow (ebb) the concentration must be free. At inflow we have to specify the concentration which may be determined by the concentration at outflow of the former ebb period. Because usually only the background concentration is known from measurements or from a larger model area, a special boundary condition based on the concentration in the interior area in combination with a return time is used, which does not completely fix the concentration at the background value. This is the so-called Thatcher-Harleman boundary condition ([Thatcher and Harleman, 1972](#)), which is discussed in the next section.

The transport of dissolved substances such as salt is described by the advection-diffusion equation. The horizontal transport is advection dominated and the equation is of hyperbolic type. At inflow, one boundary condition is needed and the concentration is specified. At outflow, no boundary condition is allowed. The concentration is determined by pure advection from the interior area:

$$\frac{\partial C}{\partial t} + \frac{U}{\sqrt{G_{\xi\xi}}} \frac{\partial C}{\partial \xi} = 0 \quad (3.48)$$

In SOBEK the dispersive fluxes through the open boundaries at both inflow and outflow can be switched on or off. This is done via parameter DiffusionAtBoundaries. If the dispersive fluxes are switched off, we have:

$$\frac{D_H}{\sqrt{G_{\xi\xi}}} \frac{\partial C}{\partial \xi} = 0 \quad (3.49)$$

#### 3.4.5.1 Thatcher Harleman time lag

If the concentration at outflow differs from the boundary condition at inflow, there is a discontinuity in the concentration at the turn of the flow. The transition of the concentration at the boundary from the outflow value to the inflow value may take some time. This depends on the refreshment of the water in the boundary region. The transition time is called the return time. The functional relationship describing the variation in concentration from the slack-water value to the present value is arbitrary. In SOBEK a half-cosine variation is used. After the return time, the boundary value remains constant until outward flow begins ([Thatcher and Harleman, 1972](#)). The mathematical formulation of this memory effect is given as follows:

$$C(t) = C^{out} + \frac{1}{2}(C^{bnd} - C^{out}) \left[ \cos \left\{ \pi \frac{T_{ret} - t_{out}}{T_{ret}} \right\} + 1 \right], \quad 0 \leq t_{out} \leq T_{ret} \quad (3.50)$$

where

$C^{out}$	is the computed concentration at the open boundary at the last time of outward flow,
$C^{bnd}$	is the background concentration described by you,
$t_{out}$	is the elapsed time since the last outflow and
$T_{ret}$	$t$ is the constituent return period.

When the flow turns inward ( $t_{out} = 0$ ), the concentration is set equal to  $C^{out}$ . During the interval  $0 \leq t_{out} \leq T_{ret}$  the concentration will return to the background concentration  $C^{bnd}$ . After that period, the concentration will remain  $C^{bnd}$ . The mechanism is illustrated in [Figure 3.3](#).



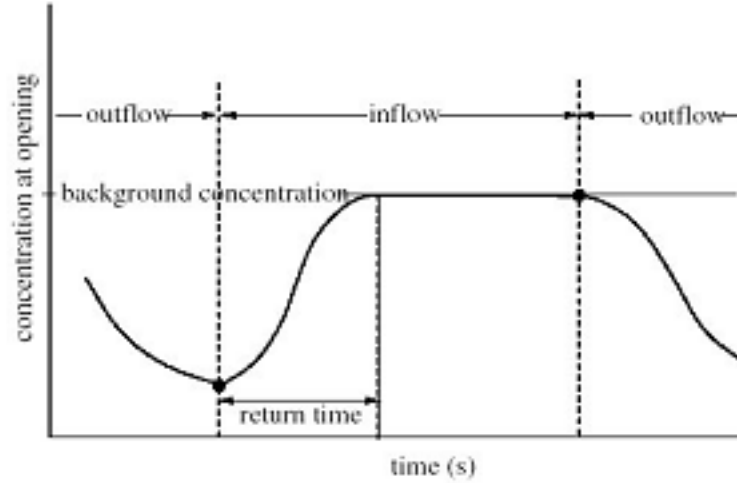


**Figure 3.3:** Figure: Illustration of memory effect for open boundary

### 3.4.5.2 Density

The water flow is influenced by the density of the salt water, so the concentration must be translated into a density of the water. This is done using the Eckert formula: This empirical relation derived by (Eckart, 1958) is based on a limited number of measurements dating from 1910 (only two salinities at five temperatures). In the original equation the pressure is present, but at low pressures the effect on density can be neglected. The Eckart formulation is given by:

$$\rho = \frac{1000P_0}{\lambda + \alpha_0 P_0} \quad (3.51)$$

where:

$$\lambda = 1779.5 + 11.25 T - 0.0745 T^2 - (3.80 + 0.01 T) S, \quad (3.52)$$

$$\alpha_0 = 0.6980, \quad (3.53)$$

$$P_0 = 5890 + 38 T - 0.375 T^2 + 3 S. \quad (3.54)$$

with the salinity  $S$  in ppt and the water temperature  $T$  in °C. The range is:  $0 < S < 40$  ppt,  $0 < T < 40$  °C.

### 3.4.5.3 Dispersion coefficient

In the advection-diffusion equation to compute the salinity transport, a dispersion coefficient is used. The user should define the dispersion coefficient  $D$ . Two options are available in SOBEK:

- 1 A time-constant but possibly space-varying dispersion coefficient:

$$D = f_1(x, t) \quad (3.55)$$

- 2 Thatcher-Harleman dispersion formula of the form:

$$D = f_1(x, t) + f_3(x, t) H(x, t) \frac{\sqrt{g}}{C(x)} |u(x, t)| \quad (3.56)$$

in which:

$C(x)$	Chézy coefficient [ $\text{m}^{\frac{1}{2}}/\text{s}$ ]
$H(x, t)$	water depth [m]
$f_1(x, t)$	function to be defined by the user [ $\text{m}^2/\text{s}$ ]
$f_3(x, t)$	function to be defined by the user [-]

#### 3.4.5.4 Salinity intrusion and baroclinic term

When one of the boundaries of a river or estuary is in contact with the sea, salt water may enter the system. This effect is important for the water flow, because salt water has a higher density than fresh water. Salt intrusion into a river or estuary is truly a two- or even three-dimensional phenomenon. The dense sea water flows under the fresh water in a so-called salt wedge (see [Figure 3.4](#)).

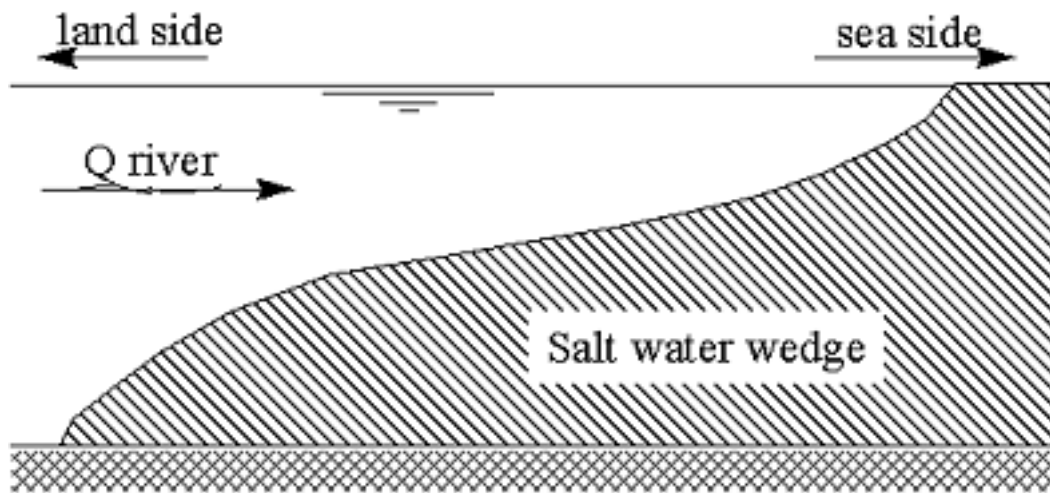


**Figure 3.4:** Salt wedge

In SOBEK, the density in a cross-section is assumed uniform. The effect on the water flow is represented in the momentum equation through the density term:

$$-\frac{1}{2} \frac{g}{\rho_0} \frac{\partial \rho}{\partial x} H^2 \quad (3.57)$$

in which:

$g$	acceleration of gravity [ $\text{m}/\text{s}^2$ ]
$\rho_0$	reference density [ $\text{kg}/\text{m}^3$ ]
$\rho$	density of salt water [ $\text{kg}/\text{m}^3$ ]
$H$	water depth [m]

This so-called baroclinic pressure term is added to the momentum equation. We will now explain how this term has been derived.

Starting with the 3D Navier Stokes equations we have:

$$\frac{\partial u}{\partial t} = -\frac{1}{\rho_0} \frac{\partial p}{\partial x} \quad (3.58)$$

$$\frac{\partial p}{\partial z} = -g\rho_0 \quad (3.59)$$

By integration from the bottom  $z = -d(x, y)$  to the free water surface  $z = -\zeta(x, y, t)$  we obtain:

$$\int_{z=-d}^{z=-\zeta} \left( \frac{\partial u}{\partial t} \right) dz' = -\frac{1}{\rho_0} \int_{z=-d}^{z=-\zeta} \left( \frac{\partial p}{\partial x} \right) dz' \quad (3.60)$$

By integration at the free water surface we obtain for the pressure:  $z' = z$  to  $z' = \zeta(x, y, t)$  (with  $z$ -axis upward positive):

$$p(x, y, z, t) = P_{atm} + \rho_0 g (\zeta(x, y, t) - z) \quad (3.61)$$

As boundary condition we assume that the pressure at the free water surface is equal to the atmospheric pressure  $P_{atm}$ , which we assume to be 0. Substitution of Equation 3.61 into Equation 3.60 yields:

$$\frac{\partial(HU)}{\partial t} - U \frac{\partial H}{\partial t} = -\frac{g}{\rho_0} \int_{z=-d}^{z=-\zeta} \left( \frac{\partial \rho}{\partial x} \right) (\zeta(x, y, t) - z) dz' - g \int_{z=-d}^{z=-\zeta} \left( \frac{\partial \zeta}{\partial x} \right) dz' \quad (3.62)$$

$$= -\frac{g}{\rho_0} \left( \frac{\partial \rho}{\partial x} \right) \int_{z=-d}^{z=-\zeta} (\zeta(x, y, t) - z) dz' - gH \left( \frac{\partial \zeta}{\partial x} \right) \quad (3.63)$$

$$= -\frac{g}{\rho_0} \left( \frac{\partial \rho}{\partial x} \right) \left[ \zeta z - \frac{1}{2} z^2 \right]_{z=-d}^{z=-\zeta} - gH \left( \frac{\partial \zeta}{\partial x} \right) \quad (3.64)$$

$$= -\frac{g}{\rho_0} \left( \frac{\partial \rho}{\partial x} \right) \left[ \frac{1}{2} \zeta^2 + \frac{1}{2} d^2 + \zeta d \right] - gH \left( \frac{\partial \zeta}{\partial x} \right) \quad (3.65)$$

$$= -\frac{1}{2} \frac{g}{\rho_0} \left( \frac{\partial \rho}{\partial x} \right) [(\zeta + d)^2] - gH \left( \frac{\partial \zeta}{\partial x} \right) \quad (3.66)$$

$$= -\frac{1}{2} \frac{g}{\rho_0} \left( \frac{\partial \rho}{\partial x} \right) [H^2] - gH \left( \frac{\partial \zeta}{\partial x} \right) \quad (3.67)$$

The first term in the right-hand side corresponds to the additional baroclinic term.



## 4 Numerical concepts (1D2D)

### 4.1 1D-2D coupling

#### 4.1.1 General

The implementation of the 1D-2D coupling is based on the equations derived in chapter 2.

Equation (2.22) for the transfer of information from 1D to 2D:

$$\begin{aligned} & \alpha_{2D}^n \frac{\zeta_{2D,v}^p + \zeta_{2D,i}^p}{2} + (\beta_{2D}^n + \alpha_{2D}^n f_I^n F_I^n)(\zeta_{2D,v}^p - \zeta_{2D,i}^p) \\ &= \alpha_{2D}^n \zeta_{1D}^{p-1} + \beta_{2D}^n \frac{\Delta x_I}{\theta A_I^n F_I^n} q_{1D-2D}^{p-1} \\ &+ \alpha_{2D}^n s_{c,I} \left( f_I^n R_I^n - \frac{\Delta x_{1D-2D}}{\alpha_{SF} g \Delta t} u_{2D,I}^n \right) + \beta_{2D}^n \frac{s_{c,I}}{\theta F_I^n} \left( \theta R_I^n + (1 - \theta) u_{2D,I}^n \right), \end{aligned} \quad (4.1)$$

with  $n$  denoting variables at the previous time level  $t^n$ , and  $p$  and  $p - 1$  denoting variables at the current and previous iteration level of the solution at the next time level  $t^{n+1}$ . Variables without a superscript are time independent.

Equation (2.25) for the transfer of information from 2D to 1D:

$$\begin{aligned} & \alpha_{1D}^n \zeta_{1D}^p - \beta_{1D}^n \frac{\Delta x_I}{\theta A_I^n F_I^n} q_{1D-2D}^p \\ &= \alpha_{1D}^n \frac{\zeta_{2D,i}^{p-1} + \zeta_{2D,v}^{p-1}}{2} + (\beta_{1D}^n - \alpha_{1D}^n f_I^n F_I^n)(\zeta_{2D,i}^{p-1} - \zeta_{2D,v}^{p-1}) \\ &- \alpha_{1D}^n s_{c,I} \left( f_I^n R_I^n - \frac{\Delta x_{1D-2D}}{\alpha_{SF} g \Delta t} u_{2D,I}^n \right) + \beta_{1D}^n \frac{s_{c,I}}{\theta F_I^n} \left( \theta R_I^n + (1 - \theta) u_{2D,I}^n \right). \end{aligned} \quad (4.2)$$

The different flow regimes across the interface, the conditions at which they apply, and the way they are modeled, are (pseudo code, with  $\zeta_{2D,I}^n = (\zeta_{2D,i}^n + \zeta_{2D,v}^n)/2$ ):

IF  $\zeta_{2D,I}^n - z_s \leq 0$  AND  $\zeta_{1D}^n - z_s \leq 0$  THEN  
! **no flow** across interface

$$u_{2D,I}^n = 0 \quad \text{and} \quad q_{1D-2D}^n = 0$$

ELSE IF  $\zeta_{2D,I}^n - z_s \geq 3/2(\zeta_{1D}^n - z_s)$  THEN  
! **free-weir flow** from 2D to 1D

(4.1) with  $\alpha_{SF} = 1/3$ ,  $\zeta_{1D}^{p-1} \leftarrow z_s$ ,  $\alpha_{2D}^n = 1$ ,  $\beta_{2D}^n = 0$ ,

(4.2) with  $\alpha_{1D}^n = 0$  ( $\Rightarrow$  value of  $\alpha_{SF}$  and  $\zeta_{1D}^p$  irrelevant),  $\beta_{1D}^n = 1$ ,

$$\text{and with } f_I^n = f_{F,I}^n = \left( \frac{3\Delta x_{1D-2D}}{\Delta x_{u,I}} + \frac{(A_I^n)^2 |u_{2D,I}^n| \Delta t}{(2/3)^3 \Delta x_{u,I} (\Delta x_I c_e c_w (\zeta_{2D,I}^n - z_s))^2} \right) \frac{\Delta x_{u,I}}{g \Delta t}.$$

ELSE IF  $\zeta_{1D}^n - z_s \geq 3/2(\zeta_{2D,I}^n - z_s)$  THEN  
! **free-weir flow** from 1D to 2D

$$\begin{aligned}
(4.2) \text{ with } \alpha_{SF} &= 1/3, \quad \frac{\zeta_{2D,i}^{p-1} + \zeta_{2D,v}^{p-1}}{2} \Leftarrow z_s, \quad \alpha_{1D}^n = 1, \quad \beta_{1D}^n = f_I^n F_I^n, \\
(4.1) \text{ with } \alpha_{2D}^n &= 0 \quad (\Rightarrow \text{value of } \alpha_{SF} \text{ and } \zeta_{1D}^{p-1} \text{ irrelevant}), \quad \beta_{2D}^n = 1, \\
\text{and with } f_I^n &= f_{F,I}^n = \left( \frac{3\Delta x_{1D-2D}}{\Delta x_{u,I}} + \frac{(A_I^n)^2 |u_{2D,I}^n| \Delta t}{(2/3)^3 \Delta x_{u,I} (\Delta x_I c_e c_w (\zeta_{1D}^n - z_s))^2} \right) \frac{\Delta x_{u,I}}{g \Delta t}.
\end{aligned}$$

ELSE

! **drowned-weir flow** across interface

(4.1) with  $\alpha_{SF} = 1$ ,  $\alpha_{2D}^n = 1$ ,  $\beta_{2D}^n = \dots$  (optimized value, see below)

(4.2) with  $\alpha_{SF} = 1$ ,  $\alpha_{1D}^n = 1$ ,  $\beta_{1D}^n = \dots$  (optimized value, see below)

$$\text{and with } f_I^n = f_{S,I}^n = \left( \frac{\Delta x_{1D-2D}}{\Delta x_{u,I}} + \frac{(A_I^n)^2 |u_{2D,I}^n| \Delta t}{2 \Delta x_{u,I} (\Delta x_I c_e c_w (\zeta_{1D/2D,I}^n - z_s))^2} \right) \frac{\Delta x_{u,I}}{g \Delta t},$$

where IF  $\zeta_{2D,I}^n \geq \zeta_{1D}^n$  THEN  $\zeta_{1D/2D,I}^n \Leftarrow \zeta_{1D}^n$  ELSE  $\zeta_{1D/2D,I}^n \Leftarrow \zeta_{2D,I}^n$  ENDIF

ENDIF

with:

$F_I^n$  = first order term in linearization of momentum equation at the interface

$R_I^n$  = zeroth order term in linearization of momentum equation at the interface

$\Delta x_I$  = length of the 2D cell face (along the interface)

$\Delta x_{u,I}$  = grid size of the 2D cell at the interface (normal to the interface)

$\Delta x_{1D-2D}$  = sort of represents the effective thickness of the interface

$A_I^n$  = Flow area at the 1D-2D interface

$$Q_{2D-1D}^p = -Q_{1D-2D}^p = s_{c,I} A_I^n u_I^p$$

$$s_{c,I} u_{2D-1D}^p = s_{c,I} R_I^n - F_I^n (\zeta_{2D,v}^p - \zeta_{2D,i}^p)$$

$z_s$  = crest level of the interface

#### 4.1.2 Optimization of the coupling parameters

A normal-mode analysis has been used to analyse and optimize the performance of the explicit solution procedure for the implicit horizontal 1D-2D coupling by considering rectangular domains, uniform conditions, and uniform rectangular grids:

- ◇ a straight 1D-2D interface of uniform thickness and with a uniform friction coefficient between
- ◇ a straight 1D channel with uniform depth, width, friction coefficient and grid at one side, and
- ◇ a 2D area with uniform depth, friction coefficient and grid consisting of rectangular cells at the other side.

This implies that all coefficients in (4.1) and (4.2) relevant to the coupling, i.e.,  $f_I^n$ ,  $F_I^n$ ,  $\Delta x_I$ , and  $A_I^n$ , are considered to be constant, both in time and in space.

The uniform conditions are required to perform a normal-mode analysis. It is a reasonable assumption when the coefficients can locally be assumed constant, when the 1D-2D interface can locally be assumed straight, and when the grids can locally be assumed uniform. If the conditions are not smooth (e.g., strong variations in water depth or grid size near a 1D-2D interface, strong bends in a 1D-2D interface), the optimization is assumed to give a reasonable

approximation of the optimal coupling parameters, especially when non-smooth conditions occur in only a small number of locations.

In addition to the uniform conditions, it has been assumed for the time being that the solution procedure of each 1D-2D coupling can be considered independently. In reality, the iterative performance of the 1D-2D coupling at one side of a 1D channel (only relevant if drowned-weir flow) can be *strongly* affected by the coupling at the other side. It is easy to see that this applies in particular when we have drowned-weir flow or free-weir flow from 1D to 2D at that other side<sup>1</sup>. Taking the effect of a coupling at the other side of a channel into account in the optimization is p.m. There may also be some mutual influence between the 1D-2D couplings at either side of a 2D area, especially if the distance between the two interfaces is small (small 2D strip between two 1D channels). Taking this effect into account in the optimization of the couplings is not feasible.

A normal-mode analysis of the 1D-2D coupling shows that the optimal value of  $\beta_{2D}^n$  and  $\beta_{1D}^n$  for a Fourier-mode perturbation with wave number  $k$ ,  $0 \leq k \leq \pi/\Delta x_I$ , are:

$$\beta_{2D}^{n,opt} = \frac{\Delta x_{u,I} \text{CFL}_{2D,n}^2}{W(1 + 4(\sin(k\Delta x_I/2)\text{CFL}_{1D}^n)^2)}, \quad (4.3)$$

$$\beta_{1D}^{n,opt} = f_I^n F_I^n + \frac{\sqrt{1 + 4(\sin(k\Delta x_I/2)\text{CFL}_{2D,s}^n)^2 + 4(\text{CFL}_{2D,n}^n)^2}}{2\sqrt{1 + 4(\sin(k\Delta x_I/2)\text{CFL}_{2D,s}^n)^2}}, \quad (4.4)$$

with  $W$  the width of the 1D channel, with  $\text{CFL}_{1D}$  the CFL number in the 1D domain (along the interface), and with  $\text{CFL}_{2D,n}$  and  $\text{CFL}_{2D,s}$  the CFL number in the 2D domain normal to and along the interface.

NOTE: when (4.3) is inserted in (4.1) with CFL as specified below in (4.6), the coefficient of  $q_{1D-2D}^{p-1}$  in the right-hand side would become:

$$\beta_{2D}^{n,opt} \frac{\Delta x_I}{\theta A_I^n F_I^n} = \frac{\Delta t}{W(1 + 4(\sin(k\Delta x_I/2)\text{CFL}_{1D}^n)^2)}.$$

This shows that in an *optimal* 1D-2D coupling the terms in (4.1) at the previous iteration level  $p-1$  (first and second term in the right-hand side) *only* depend on variables of the 1D domain. Likewise, inserting (4.4) in (4.2) (with  $\alpha_{1D}^n = 1$ ) to obtain:

$$\beta_{1D}^{n,opt} - f_I^n F_I^n = + \frac{\sqrt{1 + 4(\sin(k\Delta x_I/2)\text{CFL}_{2D,s}^n)^2 + 4(\text{CFL}_{2D,n}^n)^2}}{2\sqrt{1 + 4(\sin(k\Delta x_I/2)\text{CFL}_{2D,s}^n)^2}},$$

we see that in an optimal coupling in the other direction, the terms at the previous iteration level  $p-1$  (again the first and second term in the right-hand side) only depend on variables of the 2D domain. The part in the coefficient of  $\zeta_{2D,v}^p - \zeta_{2D,i}^p$  that depends on  $f_I^n$ , a factor depending on parameters and variables pertaining to the weir formulation applied at the 1D-2D interface, vanishes.

The above is true in general. It has been verified that the convergence speed of an implicit-coupling solver consisting of the iterative explicit update of coupling information is always

<sup>1</sup> In the case of free-weir flow from 2D to 1D at that other side, an additional lateral discharge is imposed to the 1D channel that does not depend on the 1D flow solution and hence will have little or no effect on the convergence speed of the 1D-2D coupling at this side of the 1D channel.

maximized by minimizing the transfer of information. Since information to be transferred (by definition at a previous iteration level) is determined by the numerics of the domain it is coming from, it is these numerics that determine the optimal information. In consequence, optimal information that is transferred can only depend on variables and parameters defined in a single domain. This fact may be used to simplify the implementation of the coupling.

The general expression of the CFL number in a certain direction is obtained from (2.10):

$$\text{CFL}^n = \sqrt{\theta \Delta t A_f^n F_u^n / S_\zeta^n} . \quad (4.5)$$

This expression can be used to estimate the value of all three CFL numbers<sup>2</sup>  $\text{CFL}_{1D}$ ,  $\text{CFL}_{2D,n}$  and  $\text{CFL}_{2D,s}$ . In case of a (fairly regular) 2D unstructured grid,  $\text{CFL}_{2D,s}$  can be taken equal to  $\text{CFL}_{2D,n}$ . Alternatively, the values obtained from the cell faces touching the 1D-2D interface can be used. To reduce a possibly strong variation of  $\text{CFL}_{1D}$ ,  $\text{CFL}_{2D,n}$  and  $\text{CFL}_{2D,s}$  along the interface (after all, in the optimization these values are assumed constant), the application of a simple explicit space filter is recommended, e.g., a  $1/4 - 1/2 - 1/4$  weighing.

Expressions (4.3) and (4.4) are for a single Fourier mode only. To obtain expressions that can be used for all modes, the value of (4.3) and (4.4) for some ‘average’  $k$  can be used, or some average of (4.3) and (4.4) evaluated at the smallest and largest wave number  $k = 0$  and  $k = \pi / \Delta x_I$  can be used. A combination of these options, e.g., the use of weighted averages of (4.3) and (4.4) evaluated at different  $k$ , is possible as well. There is not much difference between these options. The analysis indicates that a good convergence performance of the 1D-2D coupling for a wide variety of conditions can be obtained by using (4.3) and (4.4) evaluated at well-selected  $k$ -values. So we propose to use (for the time being):

$$\beta_{2D}^n = \beta_{2D}^{n,opt}(k\Delta x_I = \delta_{2D}^n\pi) , \quad \beta_{1D}^n = \beta_{1D}^{n,opt}(k\Delta x_I = \delta_{1D}^n\pi) , \quad (4.7)$$

with:

$$\delta_{2D}^n = 1/16 , \quad \delta_{1D}^n = 3/8 . \quad (4.8)$$

Figure 4.1 shows the convergence speed that is obtained with this setting, as predicted by the analysis. Note that the solution procedure is ‘exact’ (full convergence in a finite number of iterations) for  $k\Delta x_I = \pi/16$  and  $k\Delta x_I = 3\pi/8$ . These values are set by the choice of  $\delta_{2D}^n$  and  $\delta_{1D}^n$ . The values specified in (4.8) have been chosen such that a high convergence speed is obtained over the full range of Fourier modes.

We recall that (4.7) with (4.8) is just a rough optimization ‘by hand’, given the limitations of the current iterative 1D-2D solution procedure and its analysis. The assumption underlying the analysis that locally the conditions are smooth enough to be considered uniform is obviously not valid in practice, but may be acceptable. A more significant drawback of the current analysis is that it does not take into account the presence of a 1D-2D coupling at the other

<sup>2</sup> If the bottom of a 2D grid cell is fully submerged, its surface  $S_\zeta$  is constant and can, for a quadrilateral 2D cell near a 1D-2D interface, be approximated by  $S_{\zeta,I} \approx \Delta x_I \Delta x_{u,I}$ . So for quadrilateral cells we have:

$$\text{CFL}_{2D,n}^n \approx \sqrt{\theta \Delta t A_I^n F_I^n / \Delta x_I / \Delta x_{u,I}} , \quad (4.6)$$

as well as  $\text{CFL}_{2D,s}^n \approx \text{CFL}_{2D,n}^n \Delta x_{u,I} / \Delta x_I$ . These may be more suitable expressions for  $\text{CFL}_{2D,n}^n$  and  $\text{CFL}_{2D,s}^n$  than (4.5) in case of quadrilateral 2D cells near the interface. However, these expressions do not seem to be suitable for triangular 2D grid cells, where we have  $S_{\zeta,I} \approx 1/2 \Delta x_I \Delta x_{u,I}$ . Moreover, because of the use of  $S_{\zeta,I}^n$ , (4.5) automatically includes the effect of the shape of the grid cell (not included in the analysis where the optimized expressions of  $\beta_{2D}^n$  and  $\beta_{1D}^n$  were obtained), which may be advantageous. On the other hand, expression (4.6) is more convenient for implementation.

Since the variables that are required are already computed in SOBEK, the evaluation of  $\text{CFL}_{1D}$  should be straightforward. The same applies to  $\text{CFL}_{2D,n}$  and  $\text{CFL}_{2D,s}$ , whether computed using (4.5) or using (4.6).



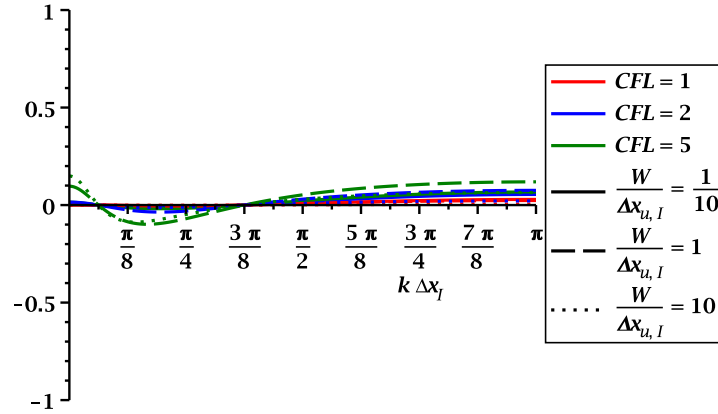


**Figure 4.1:** Predicted reduction factor per 1D-2D iteration as a function of dimensionless wave number  $k\Delta x_I$  for several ratios between channel width  $W$  and normal 2D grid size  $\Delta x_{u,I}$  and several CFL-values, taking all CFL numbers equal ( $CFL_{1D} = CFL_{2D,s} = CFL_{2D,n} = CFL$ ).

side of a 1D channel. The good news is that it seems to be possible to extend the analysis of the 1D-2D coupling for this case. Extensions of the coupling for better overall performance across the entire range of Fourier modes are possible as well. Pending such developments, one must be aware of a 1D-2D coupling not yet performing well in difficult applications. This is largely a temporary situation.

#### 4.1.3 Implementation of the 1D-to-2D coupling into the 2D system of equations

Rewrite (4.1) as:

$$b_{2D,v}^n \zeta_{2D,v}^p + b_{2D,i}^n \zeta_{2D,i}^p = d_{2D}^{p-1}, \quad (4.9)$$

with

$$\begin{aligned} b_{2D,v}^n &= \frac{\alpha_{2D}^n}{2} + (\beta_{2D}^n + \alpha_{2D}^n f_I^n F_I^n), \\ b_{2D,i}^n &= \frac{\alpha_{2D}^n}{2} - (\beta_{2D}^n + \alpha_{2D}^n f_I^n F_I^n), \\ d_{2D}^{p-1} &= \alpha_{2D}^n \zeta_{1D}^{p-1} + \beta_{2D}^n \frac{\Delta x_I}{\theta A_I^n F_I^n} q_{1D-2D}^{p-1} \\ &\quad + \alpha_{2D}^n s_{c,I} \left( f_I^n R_I^n - \frac{\Delta x_{1D-2D}}{\alpha_{SF} g \Delta t} u_{2D,I}^n \right) + \beta_{2D}^n \frac{s_{c,I}}{\theta F_I^n} \left( \theta R_I^n + (1 - \theta) u_{2D,I}^n \right). \end{aligned}$$

In general we have for each control volume the equation:

$$\begin{aligned} &\left( \frac{S_\zeta^{p-1}}{\Delta t} + \sum_{\text{cell faces}} A_f^n \theta F_u^n \right) \zeta_c^p - \sum_{\text{cell faces}} A_f^n \theta F_u^n \zeta_a^p - Q_{\text{lat},c}^p \\ &= \frac{S_\zeta^{p-1} \zeta_c^{p-1} - V_c^{p-1}}{\Delta t} + \frac{V_c^n}{\Delta t} - \sum_{\text{cell faces}} s_{c,f} A_f^n (1 - \theta) u_f^n - \sum_{\text{cell faces}} s_{c,f} A_f^n \theta R_u^n, \end{aligned} \quad (4.10)$$

with  $Q_{\text{lat},c}$  the discharge *into* the grid cell.

Rewrite (4.10) as:

$$\left(\frac{S_\zeta^{p-1}}{\Delta t} + bb_c^n\right)\zeta_c^p - \sum_{\text{cell faces}} cc_{c,f}^n \zeta_a^p - Q_{\text{lat},c}^p = \frac{S_\zeta^{p-1}\zeta_c^{p-1} - V_c^{p-1}}{\Delta t} + \frac{V_c^n}{\Delta t} + dd_c^n, \quad (4.11)$$

with:

$$\begin{aligned} bb_c^n &= \sum_{\text{cell faces}} \theta A_f^n F_u^n, \\ cc_{c,f}^n &= -\theta A_f^n F_u^n, \\ dd_c^n &= - \sum_{\text{cell faces}} s_{c,f} (\theta A_f^n R_u^n + (1 - \theta) Q_f^n). \end{aligned} \quad (4.12)$$

The coefficients (4.12) are used in SOBEK and D-Flow FM to define the system of equations.

At the 1D2D interface we have the equations (4.11) and (4.9). Rewriting (4.9) in such a way that the system is symmetrical results in:

$$cc_{c,2D,I}^n \frac{b_{2D,v}^n}{b_{2D,i}^n} \zeta_{2D,v}^p + cc_{c,2D,I}^n \zeta_{2D,i}^p = cc_{c,2D,I}^n \frac{d_{2D}^{p-1}}{b_{2D,i}^n},$$

Using this equation in the matrix coefficients, we get:

$$\begin{aligned} bb_{v,2D,I}^n &= cc_{c,2D,I}^n \frac{b_{2D,i}^n}{b_{2D,i}^n}, \\ dd_{v,2D,I}^{p-1} &= cc_{c,2D,I}^n \frac{d_{2D}^{p-1}}{b_{2D,i}^n}. \end{aligned} \quad (4.13)$$

#### 4.1.4 Implementation of the 2D-to-1D coupling into the 1D system of equations

(4.2) is rewritten as:

$$b_{1D,s}^n \zeta_{1D}^p + b_{1D,Q}^n Q_{1D-2D}^p = d_{1D}^{p-1},$$

with

$$\begin{aligned} b_{1D,s}^n &= \alpha_{1D}^n, \\ b_{1D,Q}^n &= -\beta_{1D}^n \frac{1}{\theta A_I^n F_I^n}, \\ d_{1D}^{p-1} &= \alpha_{1D}^n \frac{\zeta_{2D,i}^{p-1} + \zeta_{2D,v}^{p-1}}{2} + (\beta_{1D}^n - \alpha_{1D}^n f_I^n F_I^n) (\zeta_{2D,i}^{p-1} - \zeta_{2D,v}^{p-1}) \\ &\quad - \alpha_{1D}^n s_{c,I} \left( f_I^n R_I^n - \frac{\Delta x_{1D-2D}}{\alpha_{SF} g \Delta t} u_{2D,I}^n \right) + \beta_{1D}^n \frac{s_{c,I}}{\theta F_I^n} \left( \theta R_I^n + (1 - \theta) u_{2D,I}^n \right), \end{aligned}$$

which results in:

$$Q_{1D-2D}^p = -\frac{b_{1D,s}^n}{b_{1D,Q}^n} \zeta_{1D}^p + \frac{d_{1D}^{p-1}}{b_{1D,Q}^n}, \quad (4.14)$$

where  $-Q_{1D-2D}^p = -\Delta x_I q_{1D-2D}^p$  (notice the *minus* signs) is the lateral discharge *into* the 1D cell over the current time step.

Substituting (4.14) into (4.11) results in:

$$\begin{aligned}
 bb_{c,1D,I}^n &= -\frac{b_{1D,s}^n}{b_{1D,Q}^n} + \sum_{\text{cell faces}} \theta A_f^n F_u^n, \\
 cc_{c,1D,I}^n &= -\theta A_f^n F_u^n, \\
 dd_{c,1D,I}^{p-1} &= -\frac{d_{1D}^{p-1}}{b_{1D,Q}^n} - \sum_{\text{cell faces}} s_{c,f} (\theta A_f^n R_u^n + (1 - \theta) Q_f^n).
 \end{aligned} \tag{4.15}$$

Notice that  $cc_{c,1D,I}^n = cc_{c,f}^n$ , i.e., this coefficient remains unchanged.

## 4.2 Incorporation of boundary conditions in SOBEK

For a simple 1D channel with a discharge boundary condition at one end and a water-level boundary condition at the other end, the system of equations looks like:

$$\begin{pmatrix}
 1 & 0 & & & & \\
 0 & b_2 & c_2 & & & \\
 & c_2 & b_3 & c_3 & & \\
 & & c_3 & \ddots & \ddots & \\
 & & & \ddots & b_{n-2} & c_{n-2} \\
 & & & & c_{n-2} & \tilde{b}_{n-1} & 0 \\
 & & & & & 0 & 1
 \end{pmatrix} \cdot \begin{pmatrix} \zeta_1 \\ \zeta_2 \\ \zeta_3 \\ \vdots \\ \zeta_{n-2} \\ \zeta_{n-1} \\ \zeta_n \end{pmatrix} = \begin{pmatrix} d_1 \\ d_2 \\ d_3 \\ \vdots \\ d_{n-2} \\ \tilde{d}_{n-1} \\ d_n \end{pmatrix} \tag{4.16}$$

A boundary condition at grid point  $b$  with interior point  $i$  connected by link  $l$

- 1 All coefficients on row  $n$  and column  $b$  in the system matrix are set to 0, except for the diagonal coefficient  $b_b$ .
- 2 The diagonal coefficient  $b_b$  is set to 1.
- 3 For a water-level boundary condition: the right-hand side coefficient  $d_b$  is set to the boundary value  $\zeta_{bnd}$ :

$$d_b = \zeta_{bnd} \tag{4.17}$$

- 4 For a discharge boundary condition:

$$d_b = \zeta_i^n \tag{4.18}$$

$$\tilde{b}_i = b_i + dir \cdot Q_{bnd} \tag{4.19}$$

where  $dir$  denotes the direction of the flow at the boundary with respect to the orientation of the link.

- 5 The momentum equation is then substituted into the equation for the interior point:

$$\tilde{d}_i = d_i + A_u(l) \cdot (dir \cdot R_u(l) + F_u(l) * d_b) \tag{4.20}$$

$$\tilde{b}_i = b_i + A_u(l) F_u(l) \tag{4.21}$$

### 4.3 Interface requirements for SOBEK and D-Flow FM

In SOBEK and D-Flow FM the user-defined time step can be reduced. In this chapter we observe the inner loop for the computation of one sub time step.

For the computation of a coupled of SOBEK (1D flow) and D-Flow FM (2D/3D flow), we suggest the following work flow:

In the computational core of both SOBEK and D-Flow FM the computation of a time step has to be split up in parts, in order to allow for iterative computation. As a result the following interface is required:

- ◇ *InitializeTimestep*
- ◇ *ComputeTimeStep*
- ◇ *FinalizeTimestep*

For now we are restricting ourselves to 1D-2D interfaces where the D-Flow FM grids and SOBEK grids match, i.e., to 1D-2D interfaces where there is a single connection that is (close to) normal to the interface between consecutive D-Flow FM water levels and consecutive SOBEK water levels along the interface. We also impose for now the restriction that the time step in both models is to be identical. However, we anticipate the development of a 1D-2D coupling for non-matching spatial discretizations and time steps in the future. So although the transfer of data from 1D to 2D and vice versa is trivial at present, it will not be trivial in the future. For this reason we have defined the two separate subroutines `MapDataFromSOBEK2DFlowFM()` and `MapDataFromDFlowFM2SOBEK()` for the implementation of the required mappings in space and in time from 1D to 2D and from 2D to 1D.

In addition to this:

- ◇ The computation of the 1D-2D interface formulation for the 2D side has to be implemented in D-Flow FM.
- ◇ D-Flow FM requires the 1D water levels and the SOBEK lateral discharge at the 1D-2D interfaces.
- ◇ The computation of the 1D-2D interface formulation for the 1D side has to be implemented in SOBEK.
- ◇ SOBEK requires the water levels in the 2D virtual grid cells and 2D inner grid cells at the 1D-2D interfaces.
- ◇ A number of coefficients that are computed in D-Flow FM have to be transferred to SOBEK.
- ◇ A 1D-2D interface convergence check needs to be implemented.
- ◇ Each time step a final SOBEK computation with imposed lateral discharge from the 2D domains has to be performed to enforce mass conservation.

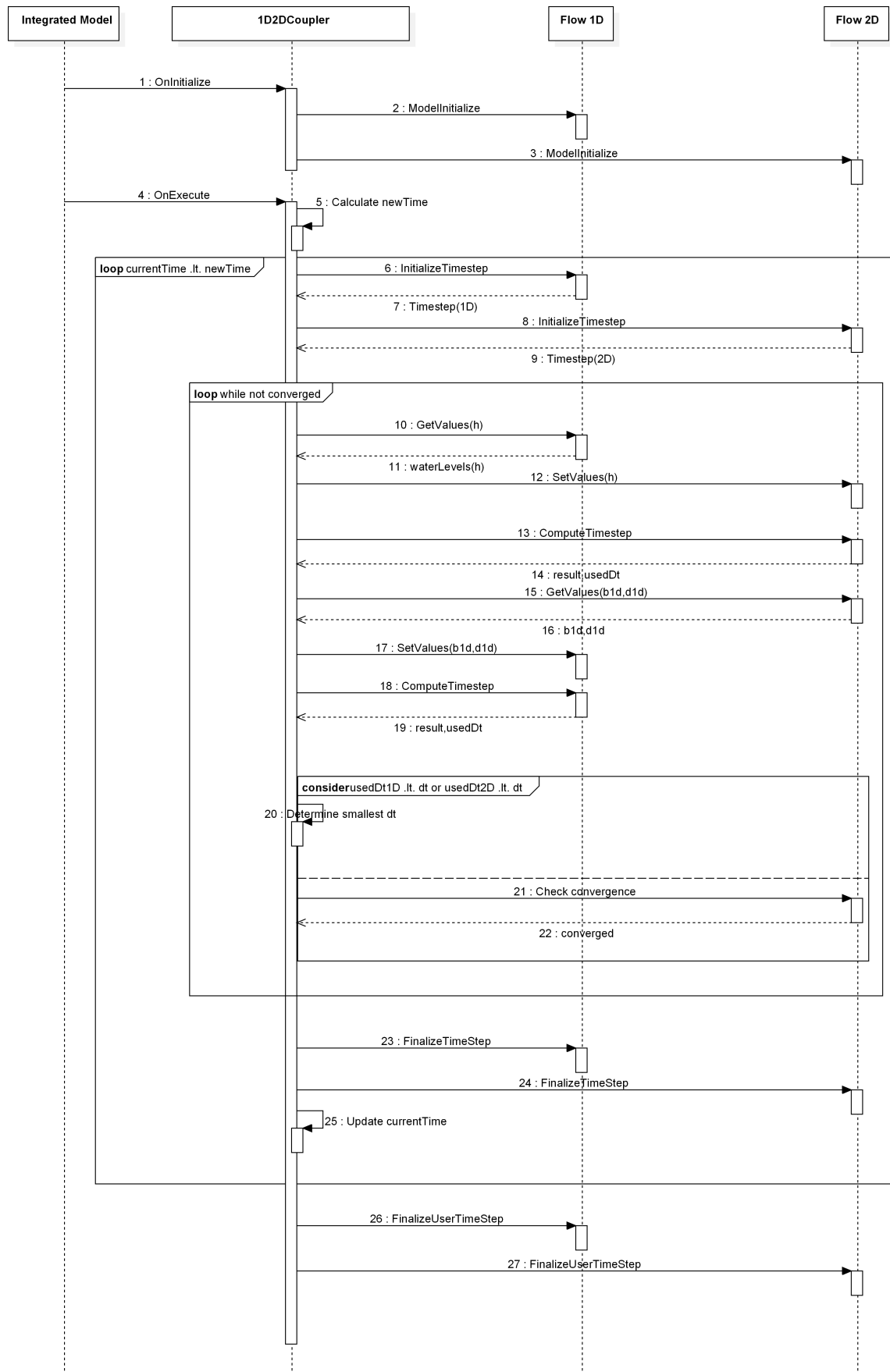


**Figure 4.2:** workflow of coupled time step computation.



## References

- Ackers, P., W. White, J. Perkins and A. Harrison, 1978. *Weirs and Flumes for Flow Measurement*. John Wiley & Sons Ltd.
- Begnudelli, L., B. F. Sanders and S. F. Bradford, 2008. "Adaptive Godunov-based model for flood simulation." *J. Hydraul. Eng.* 134 (6): 714–725.
- Bos, 1989. *Discharge Measuring Structures*. International Institute for Land Reclamation and Improvement/ILRI, Wageningen, The Netherlands.
- Bradford, S. F. and B. F. Sanders, 2002. "Finite-volume model for shallow-water flooding of arbitrary topography." *J. Hydraul. Eng.* 128 (3): 289–298.
- Chen, W.-B., W.-C. Liu and C.-Y. Wu, 2013. "Coupling of a one-dimensional river routing model and a three-dimensional ocean model to predict overbank flows in a complex river–ocean system." *Appl. Math. Model.* 37 (9): 6163–6176.
- Chen, Y., Z. Wang, Z. Liu, and D. Zhu, 2012. "1D–2D coupled numerical model for shallow-water flows." *J. Hydraul. Eng.* 138 (2): 122–132.
- Deltares, 2014. *D-Flow Flexible Mesh Technical Reference Manual – Draft*. Tech. rep., Deltares.
- Eckart, C., 1958. "Properties of water, Part II. The equation of state of water and sea water at low temperatures and pressures." *American Journal of Science* 256: 225–240.
- Ellis, B. and J. Bertrand-Krajewski, 2010. *Assessing infiltration and exfiltration on the Performance of Urban Sewer Systems (APUSS)*. IWA Publishing, London, UK. ISBN: 978-1-84-339149-4.
- Engelund, F. and E. Hansen, 1967. *A monograph on Sediment Transport in Alluvial Streams*. Teknisk Forlag, Copenhagen.
- Gallegos, H. A., J. E. Schubert and B. F. Sanders, 2009. "Two-dimensional, high-resolution modeling of urban dam-break flooding: A case study of Baldwin Hills, California." *Adv. Water Resour.* 32 (8): 1323–1335.
- Karpf, C., J. Traenckner and P. Krebs, 2008. "Hydraulic modelling of sewage exfiltration." In *11th International Conference on Urban Drainage*. Edinburgh, Scotland, UK.
- Kernkamp, H., 2008. "Stellings time integration in Sobek and Unstruc." Memo.
- Kim, J., A. Warnock, V. Y. Ivanov and N. D. Katopodes, 2012. "Coupled modeling of hydrologic and hydrodynamic processes including overland and channel flow." *Adv. Water Resour.* 37: 104–126.
- Kuiry, S. N., D. Sen and P. D. Bates, 2010. "Coupled 1D–quasi-2D flood inundation model with unstructured grids." *J. Hydraul. Eng.* 136 (8): 493–506.
- Rutsch, J., M., J. Rieckermann, C. J.B., J. Ellis, Vollertsen and P. Krebs, 2008. "Towards a better understanding of sewer exfiltration,." In *Water Research*, vol. 42, pages 2385–2394.
- Sanders, B. F., J. E. Schubert and R. L. Detwiler, 2010. "ParBreZo: A parallel, unstructured grid, Godunov-type, shallow-water code for high-resolution flood inundation modeling at the regional scale." *Adv. Water Resour.* 33 (12): 1456–1467.
- Schmidt, 1955. "Unknown."



- Seyoum, S. D., Z. Vojinovic, R. K. Price and S. Weesakul, 2012. "Coupled 1D and noninertia 2D flood inundation model for simulation of urban flooding." *J. Hydraul. Eng.* 138 (1): 23–34.
- Stelling, G. S. and S. P. A. Duinmeijer, 2003. "A staggered conservative scheme for every Froude number in rapidly varied shallow water flows." *International Journal Numerical Methods In Fluids* 43: 1329-1354.
- Stelling, G. S. and A. Verwey, 2006. "Numerical flood simulation." In *Encyclopedia of Hydrological Sciences*. John Wiley & Sons.
- Thatcher, M. L. and D. R. F. Harleman, 1972. *A mathematical model for the prediction of unsteady salinity intrusion in estuaries*. Report no. 144, MIT School of Engineering Massachusetts Institute of Technologie, Department of Civil Engineering.
- Ye, Q., R. Morelissen, E. De Goede, M. Van Ormondt and J. Van Kester, 2011. "A new technique for nested boundary conditions in hydrodynamic modeling." In J. H.-W. Lee and C.-O. Ng, eds., *Proc. 6th Int. Conf. Asian and Pacific Coasts (APAC 2011)*, pages 1368–1377. World Scientific.







*Photo's by: BeeldbankVenW.nl, Rijkswaterstaat / Joop van Houdt.*

# Deltares **systems**

PO Box 177  
2600 MH Delft  
Rotterdamseweg 185  
2629 HD Delft  
The Netherlands

T +31 (0)88 335 81 88  
F +31 (0)88 335 81 11

[sales@deltaressystem.nl](mailto:sales@deltaressystem.nl)  
[www.deltaressystem.nl](http://www.deltaressystem.nl)